

# **Influence of Large Conductance $\text{Ca}^{2+}$ - and Voltage-Activated $\text{K}^{+}$ Channels (BK) on Synaptic Plasticity in Young and Aged Mice**

## **Dissertation**

der Mathematisch-Naturwissenschaftlichen Fakultät  
der Eberhard Karls Universität Tübingen  
zur Erlangung des Grades eines  
Doktors der Naturwissenschaften  
(Dr. rer. nat.)

vorgelegt von  
M. Sc. Thomas Huy Phu Pham  
aus Werne

Tübingen  
2023



Gedruckt mit Genehmigung der Mathematisch-Naturwissenschaftlichen Fakultät der Eberhard Karls Universität Tübingen.

Tag der mündlichen Qualifikation:

11.01.2024

Dekan:

Prof. Dr. Thilo Stehle

1. Berichterstatter/-in:

Prof. Dr. Peter Ruth

2. Berichterstatter/-in:

Prof. Dr. Robert Lukowski

3. Berichterstatter/-in:

Prof. Dr. Norbert Klugbauer



# INDEX

<b>INDEX</b> .....	<b>I</b>
<b>FIGURES</b> .....	<b>V</b>
<b>TABLES</b> .....	<b>VII</b>
<b>ABBREVIATIONS</b> .....	<b>IX</b>
<b>1. Introduction</b> .....	<b>1</b>
1.1. Learning and memory .....	1
1.1.1. Long-term potentiation .....	1
1.1.2. Long-term depression .....	3
1.2. Age-dependent cognitive decline .....	3
1.3. Cognitive decline in neurodegenerative disease.....	4
1.4. K <sup>+</sup> channels .....	6
1.4.1. Significance of K <sup>+</sup> channels in synaptic plasticity .....	6
1.4.2. KIR channels.....	6
1.4.3. Two pore-forming channels.....	7
1.4.4. Voltage-gated K <sup>+</sup> channels (K <sub>V</sub> ) .....	7
1.4.5. Ca <sup>2+</sup> -activated K <sup>+</sup> channels .....	7
1.5. BK channel.....	8
1.5.1. Structure.....	9
1.5.2. Associated auxiliary subunits .....	10
1.5.3. BK channel in the central nervous system .....	11
1.6. Further important ion channels for synaptic plasticity .....	12
1.6.1. Glutamate receptors.....	12
1.6.1.1. Ionotropic Glutamate receptors .....	13
1.6.1.2. Metabotropic glutamate receptors.....	16
1.6.2. Voltage gated Ca <sup>2+</sup> channels .....	17
<b>2. Aims</b> .....	<b>21</b>
<b>3. Material and methods</b> .....	<b>23</b>
3.1. Mouse breeding .....	23
3.1.1. Animal husbandry .....	23
3.1.2. Conditional and global BK mouse model .....	23
3.2. Culturing primary hippocampal neurons .....	24
3.2.1. Coating of cell culture dishes with poly-L-lysine.....	24
3.2.2. Dissociation and culture of primary hippocampal neurons.....	25
3.3. Immunofluorescence.....	26
3.3.1. Tissue fixation and cryosectioning .....	26
3.3.2. Immunofluorescent staining of brain sections .....	27

3.3.3.	Immunofluorescence staining of cultured neurons.....	28
3.4.	Genotyping.....	28
3.4.1.	DNA Isolation .....	29
3.4.2.	Amplification of PCR products .....	29
3.4.3.	DNA detection by agarose gel electrophoresis .....	30
3.5.	Protein biochemical methods.....	31
3.5.1.	Protein extraction .....	32
3.5.2.	Determination of protein concentration .....	32
3.5.3.	SDS-polyacrylamide gel electrophoresis (SDS-PAGE) .....	33
3.5.4.	Polyacrylamide gel reparation.....	33
3.5.5.	Western Blot.....	34
3.5.6.	Protein detection .....	35
3.5.7.	cLTP induction in acute hippocampal brain slices .....	36
3.6.	Electrophysiology.....	37
3.6.1.	Acute brain slices .....	37
3.6.2.	fEPSP recordings.....	37
3.7.	Behavioral tests.....	38
3.7.1.	Open field.....	38
3.7.2.	Beam walk.....	38
3.7.3.	Water-Maze.....	39
3.8.	Single cell live imaging.....	41
3.8.1.	K <sup>+</sup> sensitive imaging.....	41
3.8.2.	Ca <sup>2+</sup> imaging .....	43
3.8.3.	DiBAC <sub>4</sub> (3) imaging .....	43
3.8.4.	Software used .....	43
<b>4.</b>	<b>Results .....</b>	<b>45</b>
4.1.	T29.1-Cre specifically removes BK from CA1.....	45
4.2.	cKO display normal anxiety and locomotor behavior .....	47
4.3.	Hippocampal BK supports memory acquisition and retrieval.....	51
4.4.	Learning and memory during the process of aging.....	54
4.4.1.	Aged cKO mice display normal anxiety levels .....	54
4.4.2.	Locomotor activity of aged cKO mice is unaltered .....	56
4.4.3.	Aged cKO display learning behavior comparable to CTRL.....	59
4.5.	cKO shows deficient hippocampal LTP.....	61
4.6.	cKO display unaltered subunit composition of hippocampal iGluR.....	64
4.7.	Impaired AMPAR phosphorylation in cKO after cLTP induction in acute hippocampal slices	66
4.8.	BK supports neuronal K <sup>+</sup> outflow during cLTP induction.....	67
4.9.	BK sustains neuronal Ca <sup>2+</sup> oscillations during cLTP induction .....	70
4.10.	cLTP-associated, BK-mediated neuronal Ca <sup>2+</sup> oscillations depend on NMDAR and LTCC	71

4.11.	Unaltered membrane potential during cLTP .....	72
<b>5.</b>	<b>Discussion .....</b>	<b>75</b>
5.1.	T29.1-Cre-mediated hippocampal CA1 pyramidal neuron-restricted conditional BK knockout 75	
5.2.	<i>In vivo</i> characterization of the BK channel .....	75
5.2.1.	Characterization of BK in anxiety behavior and locomotor activity .....	75
5.2.2.	Function of BK in memory acquisition and retrieval .....	76
5.2.3.	Impact of BK on learning and memory in aged mice .....	76
5.3.	<i>Ex vivo</i> characterization of synaptic plasticity in cKO .....	77
5.3.1.	Lack of LTP in BK-deficient mice .....	77
5.4.	<i>In vitro</i> characterization of BK in synaptic plasticity .....	78
5.4.1.	In search of BK's molecular contribution to LTP induction .....	78
5.4.2.	BK-mediated effects on Ca <sup>2+</sup> and K <sup>+</sup> dynamics during cLTP induction .....	79
5.4.3.	BK and other K <sup>+</sup> channels in synaptic plasticity .....	82
5.5.	Putative role of BK in pathologies of the CNS.....	82
5.5.1.	BK in epilepsy .....	82
5.5.2.	Synaptic plasticity as an early marker of impaired cognitive performance.....	83
5.5.3.	BK as a therapy for impaired synaptic plasticity.....	84
5.6.	Limitations and subsequent experiments.....	86
<b>6.</b>	<b>Summary .....</b>	<b>91</b>
<b>7.</b>	<b>Zusammenfassung .....</b>	<b>93</b>
<b>8.</b>	<b>References.....</b>	<b>95</b>
<b>9.</b>	<b>Supplemental Tables .....</b>	<b>111</b>
<b>10.</b>	<b>Publications and congress contributions .....</b>	<b>125</b>
10.1.	Publications.....	125
10.2.	Congress contributions .....	126
<b>11.</b>	<b>Curriculum Vitae .....</b>	<b>127</b>
<b>12.</b>	<b>Acknowledgements .....</b>	<b>129</b>



# FIGURES

Figure 1: Expression mechanism of LTD and LTP in the postsynapse. ....	2
Figure 2: Schematic illustration of a BK channel with its subunit variants. ....	10
Figure 3: Overview of glutamate receptor families. ....	13
Figure 4: Experimental set-up of the open field test. ....	38
Figure 5: Experimental set-up of the beam walk test. ....	39
Figure 6: Experimental set-up of the Morris Water Maze. ....	40
Figure 7: Simplified model of FRET-based biosensors. ....	42
Figure 8: Hippocampal CA1 region-specific Cre-mediated BK recombination verified at transcriptional and protein level. ....	46
Figure 9: Comparable anxiety and locomotor activity in CTRL and cKO. ....	48
Figure 10: Comparable locomotor ability between both genotypes. ....	50
Figure 11: cKO display impaired memory acquisition and retrieval in the MWM. ....	53
Figure 12: Comparable locomotor activity and anxiety behavior of aged CTRL and cKO mice. ...	56
Figure 13: No differences in locomotor ability of aged CTRL and cKO. ....	58
Figure 14: Memory acquisition and retrieval in the MWM is unaltered in aged cKO. ....	60
Figure 15: Impaired LTP, but unaltered basal synaptic transmission in cKO. ....	63
Figure 16: Composition of hippocampal ionotropic glutamate receptors in CTRL and cKO was not different before and after MWM. ....	65
Figure 17: BK deficiency prevents phosphorylation of GluA1-S845 after cLTP induction. ....	67
Figure 18: cLTP provokes a strong and sustained K <sup>+</sup> efflux. ....	69
Figure 19: cLTP increases Ca <sup>2+</sup> oscillation frequencies depending on BK, NMDAR and LTCC. ...	71
Figure 20: cLTP does not influence membrane potential. ....	73
Figure 21: Proposed mechanism of BK's contribution to synaptic plasticity. ....	81



## TABLES

Table 1: Exemplary loading order on 96-well plate for BCA assay .....	33
Table 2: Mouse deployment locations for acquisition and reversal training during MWM .....	40
Table 3: Values and statistics for Figure 8 .....	111
Table 4: Values and statistics for Figure 9 .....	111
Table 5: Values and statistics for Figure 10 .....	112
Table 6: Values and statistics for Figure 11 .....	113
Table 7: Values and statistics for Figure 12 .....	115
Table 8: Values and statistics for Figure 13 .....	116
Table 9: Values and statistics for Figure 14 .....	117
Table 10: Values and statistics for Figure 15 .....	119
Table 11: Values and statistics for Figure 16 .....	121
Table 12: Values and statistics for Figure 17 .....	122
Table 13: Values and statistics for Figure 18 .....	122
Table 14: Values and statistics for Figure 19 .....	122
Table 15: Values and statistics for Figure 20 .....	123



## ABBREVIATIONS

[Ca <sup>2+</sup> ] <sub>i</sub>	Intracellular Ca <sup>2+</sup> concentration
[K <sup>+</sup> ] <sub>i</sub>	Intracellular K <sup>+</sup> levels
%	Percent
3xTg	Triple transgenic
aa	amino acids
ACSF	Artificial cerebrospinal fluid
AD	Alzheimer's disease
AHP	Afterhyperpolarization
am	Before noon
AMPA	α-amino-3-hydroxy-5-methyl-4-isoxazole propionic acid
AMPA	Amino-3-hydroxy-5-methyl-4-isoxazolepropionic acid receptor
AP	Action potential
AP5	DL-2-Amino-5-Phosphonovaleric acid
APS	Ammonium peroxydisulfate
Aβ	Amyloid-beta
BB	Blocking buffer
BBB	blood-brain barrier
BCA	Bicinchoninic acid
BK	Large-conductance Ca <sup>2+</sup> - and voltage-activated K <sup>+</sup> channel
bp	Base pairs
BSA	Bovine serum albumin
BWR	Beam walk test
Calcineurin	Protein phosphatase 2B
CaMKII	Ca <sup>2+</sup> -/calmodulin-dependent protein kinase II
CDR-SB	Clinical Dementia Rating-Sum of Boxes
CFP	Cyan fluorescent protein
cGKI	cGMP-dependent protein kinase I
CICR	Ca <sup>2+</sup> induced Ca <sup>2+</sup> release
cKO	Conditional BK-KO
cLTP	chemical LTP
cm	Centimeter
CNS	Central nervous system
CP-AMPA	Ca <sup>2+</sup> permeable AMPAR
CSD	Ca <sup>2+</sup> sensor domain
CTRL	Control
DAG	Diacylglycerol
DiBAC <sub>4</sub> (3)	Bis-(1,3-dibutylbarbituric acid)trimethine oxonol dye
DIV	Days <i>in vitro</i>
DL-AP5	DL-2-Amino-5-Phosphonovaleric acid
DM	Dissociation medium
DNase I	Deoxyribonuclease I
ELPHOR	Electrophoresis buffer

EPSP	Excitatory postsynaptic potentials
fAHP	Fast phase of afterhyperpolarization
fEPSP	Field potentials
FRET	Förster resonance energy transfer
FRP	Forskolin, 0.1 $\mu$ M Rolipram and 50 $\mu$ M Picrotoxin
GABA	Gamma-aminobutyric acid
GEPII	Genetically encoded potassium ion indicator
HFS	High frequency stimulus
Ig11	Immunoglobulin lambda locus 1
iGluR	Ionotropic glutamate receptor
IK	Intermediate conductance $Ca^{2+}$ activated $K^+$ channel
IP <sub>3</sub>	Inositol triphosphate
K2P	Two-pore-domain $K^+$ channel
K <sub>Ca</sub>	$Ca^{2+}$ -activated $K^+$ channels
KIR	Inward-rectifier $K^+$ channel
K <sub>v</sub>	Voltage-gated $K^+$ channel
Ic-LysM	Low-charge LysM
LRRC	Leucine-rich repeat-containing
LTCC	L-type $CaV_1$ channel
LTD	Long-term depression
LTP	Long-term potentiation
mA	Milliampere
mg	Milligram
mGluR	Metabotropic glutamate receptor
min	Minute
mL	Milliliter
mm	Millimeter
MM	Maintenance medium
ms	Millisecond
MWM	Morris water maze
ND	Neurodegenerative disease
NE	Northeast
NIFE	Nifedipine
nm	Nanometer
NMDA	N-Methyl-D-aspartic acid
NMDAR	N-Methyl-D-Aspartate receptor
NO-GC	Nitric oxide sensitive guanylate cyclase
NW	Northwest
OFT	Open field test
PAX	Paxilline
PBS	Phosphate-buffered saline
PCR	Polymerase chain reaction
PD	Parkinson's disease

PFA	Paraformaldehyde
pGC	Particulate guanylate cyclase
PGD	Pore gated domain
PIP <sub>2</sub>	phosphatidylinositol-4,5-bisphosphate
PKA	Protein kinase A
PKC	Protein kinase C
PLL	Poly-L-lysine
pm	After noon
PM	Plating medium
P <sub>o</sub>	Open probability
PP1	Phosphatase 1
pS	Picosiemens
PSD	Postsynaptic density
PVDF	Polyvinylidene fluoride
RCK	regulators of K <sup>+</sup> conductance
RIPA	Radioimmunoprecipitation assay
rpm	revolutions per minute
RT	Room temperature
s	Second
S818	Serine 818
S831	Serine 831
S845	Serine 845
sACSF	Sucrose artificial cerebrospinal fluid
SCA7	Spinocerebellar ataxia type 7
SCN	Suprachiasmatic nucleus
SE	Southeast
SK	Small-conductance channel
Slack	Sodium-activated sequence like a Ca <sup>2+</sup> -activated K <sup>+</sup> channel
Slo	Slowpoke
SNc	Substantia nigra pars compacta
SNP	Single nucleotide polymorphism
SW	Southwest
TBE	Tris-Borate-EDTA
TBST	Tris-buffered saline with Tween 20
TEMED	Tetramethylethylenediamine
tg	Transgenic
TM	Transmembrane domain
VGCC	Voltage gated Ca <sup>2+</sup> channel
VSD	Voltage sensor domain
µm	Micrometer
µM	micromolar



# 1. Introduction

## 1.1. Learning and memory

Acquiring new knowledge and abilities, retaining acquired knowledge, and recalling, adjusting, or discarding these memories are vital in order to adjust an individual's behavior to a dynamic environment. As early as 1949, Donald Hebb hypothesized about the growth of neural connections in the brain and the conditions under which such growth might occur. He described synaptic connections as activity-dependent, dynamically adjusting the effectiveness of synaptic transmission according to the frequency and intensity of activity (Morris, 1999).

Experimental proof indicating that synapses in the mammalian brain are plastic, came approximately two-decades later with the discovery of long-term potentiation (LTP). LTP was unveiled as result of intense stimulation, known as tetanus. Applied to hippocampal mossy fibers, it causes a long-lasting increase in synaptic transmission (Bliss & Lomo, 1973). Shortly thereafter, long-term depression (LTD) was found to cause an activity-related decrease in synaptic transmission efficiency. These long-lasting adaptations to synaptic transmission efficiency were summarized under the term *synaptic plasticity*. Although synaptic plasticity may be the physiological correlate of learning and memory from a mechanistic perspective, it was initially difficult to unambiguously link the two processes. To show that synaptic plasticity is one major principle underlying learning and memory, N-Methyl-D-Aspartate receptor (NMDAR), which was already known to be important for LTP, was inhibited by *DL*-2-Amino-5-Phosphonovaleric acid (*DL*-AP5, AP5) infusion in the hippocampus. This did indeed lead to memory impairment in behavioral tests.

Synaptic plasticity occurs in both physiological and pathological conditions. Under physiological conditions, it includes developmental plasticity, learning and memory, and repair in the adult brain. Under pathological conditions, it includes, for example, plasticity i.e., recovery of function following injury and removal of a brain tumor, stroke, epilepsy and neurodegenerative diseases (ND) (Dorszewska et al., 2020). The single most important model for the study of synaptic plasticity is the hippocampus, a part of the limbic system that helps to form memory by associating cortical engrams. In the hippocampus, cells are organized into distinct layers, allowing reproducible examination of synaptic connections in acute tissue slices. In most classical experiments, synaptic transmission was recorded in the so-called Schaffer collateral synapses connecting hippocampal pyramidal neurons in the CA3 to the CA1 area. Here, excitatory postsynaptic potentials (EPSP), can be recorded as field potentials (fEPSP) by using extracellular recording electrodes (Johnston & Amaral, 2004).

### 1.1.1. Long-term potentiation

LTP is usually divided into the following phases: Induction, Expression and Maintenance. Potentiation can directly be induced with a high frequency stimulus (HFS, 100 Hz for 1s).

This results in a potentiated fEPSP which corresponds to a higher synaptic transmission efficiency and is also referred to as LTP expression. Once transmission efficiency is increased, this potentiated state is maintained (Hayashi, 2022).

During LTP induction, stimulation of fibers projecting from the CA3 area to the CA1 area provokes glutamate release into the synapses leading to a depolarization of the postsynaptic neurons. Due to stimulation at a frequency of 100 Hz for 1s, which is a strong stimulus, overlapping and cumulative depolarization may occur (Herron et al., 1986).

Despite the causal relationship between glutamate release and depolarization, it is experimentally possible to separate them and show that both glutamate release and depolarization are required for the induction of LTP (Gustafsson et al., 1987). Thus, if the postsynaptic membrane is hyperpolarized LTP cannot be induced by HFS (Malinow & Miller, 1986).

NMDAR are the reason why LTP requires both glutamate release and depolarization, because this  $\text{Ca}^{2+}$ -conducting channel is only opened after glutamate binding, when the postsynaptic membrane potential is depolarized above about -40 mV which leads to the ejection of the  $\text{Mg}^{2+}$  ion blocking the conducting pore (Nowak et al., 1984).

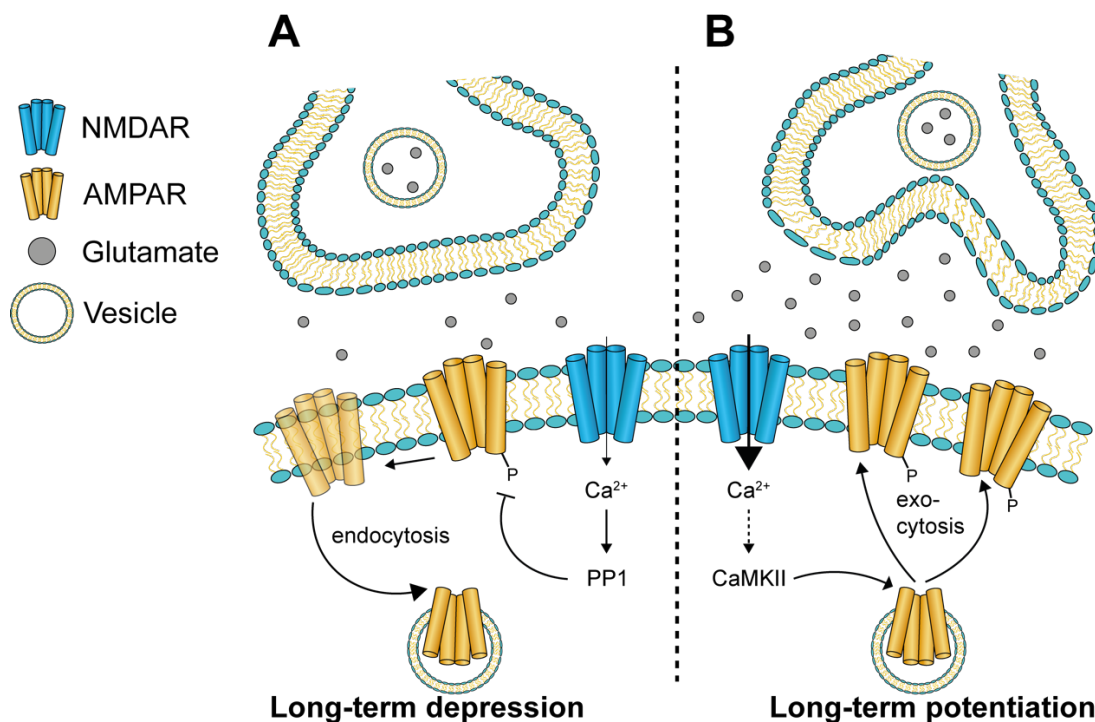


**Figure 1: Expression mechanism of LTD and LTP in the postsynapse. (A)** Following a weak stimulus reaching the presynapse, low-level glutamate release occurs. Postsynaptically, this leads to a weak  $\text{Ca}^{2+}$  influx. Since phosphatase 1 (PP1) is very  $\text{Ca}^{2+}$  sensitive, it is primarily activated and subsequently dephosphorylates the GluA1 subunit of  $\alpha$ -amino-3-hydroxy-5-methyl-4-isoxazolepropionic acid receptor (AMPA), which promotes its endocytosis and therefore a reduction of AMPAR in the postsynapse (Collingridge et al., 2010). This chain of events is also referred to as long-term depression. **(B)** Strong stimulation of the presynapse is followed by a strong release of glutamate, resulting in a strong  $\text{Ca}^{2+}$  influx postsynaptically. The strong increase in  $[\text{Ca}^{2+}]_i$  drives activation of  $\text{Ca}^{2+}$ /calmodulin-dependent protein kinase II (CaMKII), which consequently

phosphorylates AMPAR at GluA1, facilitating its exocytosis and thus incorporation into the postsynapse. This process is called long-term potentiation.

Consequently, the inhibition of NMDAR hampers LTP at the CA3-CA1 synapse and impairs hippocampus dependent learning. After NMDAR activation, increased intracellular  $Ca^{2+}$  concentration ( $[Ca^{2+}]_i$ ) leads to the activation of calmodulin (Giese et al., 1998) and subsequently to an increase in  $Ca^{2+}$ -calmodulin-dependent protein kinase II (CaMKII) activity (see **Figure 3**). CaMKII autophosphorylates itself at T286, whereby it is constitutively activated (Miller & Kennedy, 1986) and translocates into the postsynaptic density (PSD) (Shen & Meyer, 1999). CaMKII activation is less  $Ca^{2+}$ -sensitive than protein phosphatase 2B (calcineurin) (**1.1.2**), however CaMKII dominates in function over calcineurin when activated. In the PSD, CaMKII enhances AMPAR mediated transmission in two ways. First, GluA1 is phosphorylated at Serine 831 (S831), resulting in an enhanced conductance of the corresponding AMPAR (Barria et al., 1997; Lee et al., 2003). In addition, CaMKII phosphorylates the AMPAR-binding protein TARP, allowing it to bind to PSD-95, which stabilizes AMPAR in the PSD to increase its postsynaptic abundance (Opazo et al., 2010; Tomita et al., 2005). Both effects contribute to increased synaptic transmission strength.

### **1.1.2. Long-term depression**

LTD is characterized by an persistently reduced strength of AMPAR-mediated synaptic transmission (Collingridge et al., 2010). Hippocampal LTD can result from NMDAR-, metabotropic glutamate receptors- (mGluR) or endocannabinoid receptor stimulation. Best characterized, however, are forms of LTD that depend on NMDAR and mGluR. One way to elicit NMDAR-dependent LTD experimentally is either by low-frequency stimulation or by brief N-Methyl-D-aspartic acid (NMDA) application (Collingridge et al., 2010). Opening of the NMDAR results in activation of calcineurin by binding  $Ca^{2+}$ /calmodulin following a moderate  $Ca^{2+}$  influx. Its function is to dephosphorylate protein phosphatase 1 (PP1), which is thereby activated. The substrates of PP1 include Serine 295 of PSD-95 (Kim et al., 2007) and Serine 845 (S845) of the AMPAR subunit GluA1 (Heo et al., 2018; Mulkey et al., 1993). Affected AMPAR lose their PSD-95 mediated anchoring in the PSD, making internalization more likely and thereby leading to LTD (Collingridge et al., 2010).

## **1.2. Age-dependent cognitive decline**

Approximately twenty percent (%) of people over age 65 have cognitive problems that affect their quality of life and are not the result of dementia (Roberts & Knopman, 2013).

The process of aging is characterized by a gradual decline in the body's overall functioning, resulting in decreased quality of life. One common complaint associated with aging is cognitive decline, which includes memory deficiency and changes in brain functions such as processing speed and executive functions (Richardson et al., 2013). Certain memory

parameters, like spatial recollection, long-term episodic memory and working memory, tend to decline with growing age (Harada et al., 2013; Park & Festini, 2017; Ward et al., 2013). Age dependent cognitive decline, however, is not based on massive neuronal loss seen in dementias like Alzheimer's disease (AD) (Gomez-Isla et al., 1996; Pannese, 2011; West et al., 1994; Yankner et al., 2008). Despite extensive research, knowledge about the precise mechanisms underlying age-related cognitive decline is still very limited.

One of the mechanisms responsible for reduced synaptic plasticity in the adult brain could be developmental changes in gene expression (Kondo et al., 1996; Styren et al., 1997). Scientists have demonstrated that the levels of certain postsynaptic proteins like PSD95 and synaptophysin decrease as individuals grow older, but the specific process behind this decline remains unclear (Canas et al., 2009; Liu et al., 2008; VanGuilder et al., 2010). It is worth noting that a recent study involving older individuals revealed a connection between cognitive abilities and the quantities of these proteins as well (Honer et al., 2012).

Also the large-conductance  $Ca^{2+}$ - and voltage-activated  $K^+$  channel (BK) could play such a role as it demonstrated that its activity in suprachiasmatic nucleus (SCN) neurons varies with age (Farajnia et al., 2015). In aged SCN neurons, it was observed that BK currents no longer increase during nighttime. This loss of nighttime enhancement in BK channel activity leads to alterations in action potential (AP) waveform and increased  $[Ca^{2+}]_i$ . These changes have the potential to disrupt behavioral rhythms and contribute to the development of  $Ca^{2+}$ -related disfunctions in aged adults (Farajnia et al., 2015).

### **1.3. Cognitive decline in neurodegenerative disease**

AD and Parkinson's disease (PD) are common ND manifesting as the gradual deterioration of cognitive and motor functions, respectively. These conditions are defined by the progressive deterioration of nerve cells in certain regions of the brain. Such deterioration in the hippocampus is linked to memory impairment in AD (Barnes et al., 2009) while in the substantia nigra pars compacta (SNc), it is associated with motor dysfunction in PD (Sako et al., 2014). The compromised synaptic plasticity observed in the affected brain areas and networks is believed to be a fundamental pathological mechanism that contributes to progressively declining cognitive and motor abilities observed in these ND.

Disruptions in synaptic function have emerged as a primary contributor to cognitive impairment observed in various neurological disorders (Baudouin et al., 2012; Wang et al., 2004; Zoghbi & Bear, 2012). In the studies mentioned before synaptic vesicles responsible for releasing neurotransmitters and facilitating signal transmission between neurons were of particular interest. Any dysregulation or malfunctioning of the synaptic vesicle release machinery can have profound effects on information transfer within the brain, leading to significant deficits.

Therefore, compromised synaptic plasticity may represent a critical cellular process that underlies the gradual cognitive and motor decline witnessed in individuals with AD and

PD. Should this hypothesis hold true, assessing synaptic plasticity and its impairment in the human brain could yield valuable quantitative biomarkers to aid in the diagnosis and prognosis of patients afflicted by these conditions (Colom-Cadena et al., 2020; Olsson et al., 2011). Furthermore, targeting and treating impaired synaptic plasticity could potentially decelerate or even reverse the progression of these diseases.

Over the last decade,  $\text{Ca}^{2+}$ -activated  $\text{K}^+$  channels ( $\text{K}_{\text{Ca}}$ ) have gained recognition as promising tools for neuroprotection (Malinska et al., 2010; Su et al., 2017; Sugunan et al., 2016). In this context, BK turned out to be a particularly important player.

Several genome-wide association studies have suggested a possible link between AD pathology, such as age at onset or disease duration and a specific single nucleotide polymorphism (SNP) in the gene that encodes the pore-forming  $\alpha$ -subunit of BK channels. In addition, another SNP in the gene which encodes the modulatory  $\beta 2$  subunit of BK channels has been linked to the hippocampal sclerosis, a neuropathological comorbidity of AD (Beecham et al., 2014; Beecham et al., 2009; Burns et al., 2011).

The activity of BK channels is significantly impaired in the presence of amyloid-beta ( $\text{A}\beta$ ) aggregates. Research conducted on rodent neurons has demonstrated that  $\text{A}\beta$  reduces BK-mediated currents both at the plasma membrane and within the mitochondrial fraction (Jafari et al., 2015). Injection of  $\text{A}\beta$  (1-42) into neocortical pyramidal neurons results in decreased BK channel activity. This phenotype is also observed in triple transgenic (3xTg) mice, an established and widely used model for AD, which carries three mutated proteins associated with familial AD, namely amyloid precursor protein, presenilin (M146V) and human tau MAPT (P301L) (Wang et al., 2015; Yamamoto et al., 2011).

Furthermore, the administration of isopimaric acid, a BK channel activator, into the ventricular-subarachnoid system has been shown to improve cognitive performance as assessed by novel object recognition and Morris water maze (MWM) tests (Wang et al., 2015). Consistent with these findings, mice lacking the BK  $\alpha$  subunit display impaired spatial learning (Typlt et al., 2013). In a fragile X syndrome knockout model, treatment with the BK activator BMS-204352 normalizes dendritic spike patterns, glutamate homeostasis, social recognition and interaction, non-social anxiety, and spatial memory (Hebert et al., 2014).

In addition, dysfunction of both BK and small-conductance channels (SK) has been associated with the characteristic spiking irregularity seen in spinocerebellar ataxia type 7 (SCA7). Reduced expression of BK channels contributes to SCA7 pathology. Notably, the overexpression of BK channels in the deep cerebellar nucleus of SCA7 mice restores spike regularity, underscoring the significance of BK channel expression for mitochondrial function, neuronal network integrity and neuromuscular interactions (Stoyas et al., 2020).

## 1.4. K<sup>+</sup> channels

Ion channels, specifically K<sup>+</sup> channels, play important roles in multiple cellular processes and physiological events, such as the transmission of nerve impulses and communication between neurons. Additionally, these channels contribute to the control of cognitive functions like thinking, memory, and other important functions of the brain (Fenyves et al., 2021).

The initial observation of Na<sup>+</sup> and K<sup>+</sup> currents being distinct was first documented in squid neurons (Hodgkin & Huxley, 1952). Subsequently, the identification of the first voltage-gated K<sup>+</sup> channel (K<sub>V</sub>), known as the Shaker gene, was accomplished by Papazian et al. (1987) through the use of *Drosophila*. This breakthrough led to the subsequent discovery of numerous other K<sup>+</sup> channels (Jan & Jan, 2012). To date, ninety different K<sup>+</sup> channels have been identified, divided into families depending on their number of transmembrane domains (TM) and their respective activation mechanisms along with their specific pharmacological properties (Capera et al., 2019; Kaczmarek et al., 2017). These families are inwardly rectifying (KIR) channels with 2 TM, two/tandem-pore domain (K2P) channels with 4 TM, K<sub>V</sub> channels with 6 TM and K<sub>Ca</sub> channels with 7 TM.

### 1.4.1. Significance of K<sup>+</sup> channels in synaptic plasticity

The storage and retrieval of information by the central nervous system (CNS) involves physical changes in the neural substrate that modulate the activity and communication of neurons (Voglis & Tavernarakis, 2006). These changes can take many forms. In addition to structural changes, there are also sophisticated changes in the function of individual neurons, such as the adjustment of neuronal excitability and the regulation of synaptic strength (Voglis & Tavernarakis, 2006) by LTP and LTD. Several studies have shown that specific ion channels localized at synapses facilitate synaptic plasticity (Voglis & Tavernarakis, 2006).

K<sup>+</sup> channels in excitable cells help to throttle membrane excitability as K<sup>+</sup> ion flux across the neuronal membrane generates a hyperpolarized reversal potential. In neurons, K<sup>+</sup> channels establish the resting membrane potential, counteract depolarizations from the resting state and repolarize APs. The great diversity of K<sup>+</sup> channels allows for a wide range of firing patterns in different neuron types and within a single neuron type under different conditions.

### 1.4.2. KIR channels

Within the 2 TM KIR channel group, there are two distinct subtypes: First, the ATP-sensitive K<sup>+</sup> channels, which consist of KIR 6.1–6.2 subunits and their associated obligatory sulfonylurea receptor subunits for regulation of cellular metabolism. Second, the G-protein-coupled KIR channels, comprising of KIR 3.1–3.4 subunits, which rely on G-proteins for activation. KIR channels, are essential for the proper functioning throughout

the body, in organs and tissues such as the kidney, pancreas, blood vessels, heart, skeletal and smooth muscles, parietal cells of the stomach, brain, inner ear and retina (Hibino et al., 2010; Kubo et al., 2005).

### **1.4.3. Two pore-forming channels**

The 4 TM K<sup>+</sup> channels have a particular feature: rather than the usual one, they possess two pore-forming loops, and operate as dimers, not tetramers. These channels are further divided into 15 subfamilies (Goldstein et al., 2005). They have a crucial role in the generation of neuronal leak currents, which are present at rest. These leak currents help maintain the plasma membrane potential beneath the threshold for firing and facilitate repolarization (Goldstein et al., 2005; Shieh et al., 2000). Normally, K<sup>+</sup> channel gating is regulated by a gate located on the inside of the pore called the helical crossing gate. In 4 TM channels, however, this gate appears to be permanently open. It is likely that the gating of these channels is regulated by the selection filter or by the adjacent regions in close proximity to it (Piechotta et al., 2011).

### **1.4.4. Voltage-gated K<sup>+</sup> channels (K<sub>v</sub>)**

The largest family of K<sup>+</sup> channels is formed by the K<sub>v</sub> channels, which are encoded by 40 genes. These channels can be divided into 12 subfamilies (Gutman et al., 2005; Shieh et al., 2000). Each mammalian K<sub>v</sub> channel consists of four α-subunits, containing six transmembrane (6 TM) regions each, which collectively create a single pore (Gutman et al., 2005; Sharman et al., 2011; Shieh et al., 2000). In certain subfamilies like K<sub>v</sub>1, the α-subunits have the ability to combine in various ways, resulting in a wide range of heteromeric tetramers with distinct biophysical and pharmacological properties. The characteristics of K<sub>v</sub> channel α-subunit complexes can also be modified through interaction with auxiliary β-subunits. Furthermore, among the K<sub>v</sub> channel families, K<sub>v</sub>5, K<sub>v</sub>6, K<sub>v</sub>8, and K<sub>v</sub>9 are unique in that they are not functional on their own. Instead, they co-assemble with K<sub>v</sub>2 subunits to modify the overall function of the resulting channels (Gutman et al., 2005).

### **1.4.5. Ca<sup>2+</sup>-activated K<sup>+</sup> channels**

There are two distinct groups of Ca<sup>2+</sup>-activated K<sup>+</sup> channels known as K<sub>Ca</sub> channels, consisting of either 6 TM or 7 TM structures (Wei et al., 2005). The first groups encompass 6 TM channels and are called SK (K<sub>Ca</sub> 2.1–2.3) and intermediate-conductance (IK) K<sub>Ca</sub> channels (K<sub>Ca</sub>3.1). These channels are not influenced by voltage but are instead activated by low levels of [Ca<sup>2+</sup>]<sub>i</sub>. SK and IK channels play crucial roles in various Ca<sup>2+</sup>-dependent signaling processes. These channels do not directly bind Ca<sup>2+</sup>, but Ca<sup>2+</sup>/calmodulin, which serves as a Ca<sup>2+</sup> sensor to regulate channel gating.

The second group consists of BK channels with 7 TM ( $K_{Ca}1.1$ ), where the N-terminus extends through the membrane to terminate on the extracellular side. These channels are expressed in a wide range of cells, including in the brain, muscle, cochlea, pancreas, kidney, heart, uterus, small intestine, testes, and lungs (Shieh et al., 2000; Wei et al., 2005). Unlike SK and IK, BK channels do not require association with calmodulin for binding to  $Ca^{2+}$ . Instead,  $Ca^{2+}$  is believed to directly bind three distinct sites on the channel's intracellular C-terminal tail. Additional channels, such as 6TM  $K_{Ca}4.1/4.2$  and 7TM  $K_{Ca}5.1$ , have been included in the  $K_{Ca}$  classification due to structural similarities. However,  $K_{Ca}4.1/4.2$  channels are activated by internal  $Na^+$  and  $Cl^-$  concentrations, while  $K_{Ca}5.1$  channels are activated by internal alkalization. Hence, these three channels cannot be accurately described as " $Ca^{2+}$ -activated" (Wei et al., 2005).

## 1.5. BK channel

BK, also known as big  $K^+$  (MaxiK) channel, is named due to its single channel conductance, which typically ranges from 100 to 300 pS. BK activation occurs in response to two main factors: membrane depolarization and the intracellular binding of  $Ca^{2+}$  ions. BK opening effectively repolarizes the cell membrane (Marty, 1981).

By repolarizing the membrane, BK channels play a crucial role in controlling cellular excitation. They contribute to maintaining the balance of  $Ca^{2+}$  ions within the cell, which is essential for proper cellular function. This regulation of  $Ca^{2+}$  homeostasis by BK channels is important for various physiological processes and is vital for the overall stability and function of cells.

In the 1970s, the presence of a  $Ca^{2+}$ -activated conductances in cells was first identified in Helix and Aplysia (Meech, 1972, 1974). Researchers observed that when  $Ca^{2+}$  was injected into neurons or when  $[Ca^{2+}]_i$  increased due to metabolic poisoning, there was a subsequent increase in  $K^+$  conductance. Meech (1978) proposed that this  $Ca^{2+}$ -activated conductance played a crucial role in connecting cell metabolism to electrical activity.

Significant progress was made in the early 1980s with the improvement of the patch-clamp technique (Hamill et al., 1981), which allowed for the detailed examination of single channels activated by voltage and internal  $Ca^{2+}$ . These observations were reported in chromaffin cells and in cultured muscle cells. Around this time, the same channels were incorporated into lipid bilayers derived from a muscle membrane preparation enriched with t-tubules (Latorre et al., 2017). Strikingly, these channels exhibited nearly identical properties to those observed in cells.

The gene, originally named slowpoke (*Slo*), was identified in *Drosophila melanogaster*. In this species, mutations in *Slo* result in the elimination of BK-analogue currents which hinder the ability to fly (Elkins et al., 1986). The mouse and human counterparts of this gene exhibit over 50 % sequence homology to *Drosophila Slo* (Butler et al., 1993; Pallanck & Ganetzky, 1994).

BK is expressed in a variety of tissues where it either increases or restricts membrane excitability (Kyle & Braun, 2014). BK thus performs different tasks in different tissues. This remarkable diversity is achieved for one by either the considerable number of alternative mRNA splice variants (Tseng-Crank et al., 1994; Xie & McCobb, 1998), second, by association with regulatory subunits, and third, by post-translational modification such as phosphorylation of key elements in the pore-forming alpha subunit. Most of these mechanisms are regulated by various upstream signaling pathways that alter either open probability or conductance.

Briefly, phosphorylation of BK by cGMP-dependent protein kinase I (cGKI) (Alioua et al., 1998) leads to activation of the channel by increasing voltage and  $\text{Ca}^{2+}$  sensitivity. Two of the most important phosphorylation sites are S691 and S873, as their mutation to alanine reduces cGKI-mediated phosphorylation by up to 50% (Kyle & Braun, 2014). In the case of protein kinase A (PKA), phosphorylation behaves in an activating or inactivating manner depending on the splice variant (Zhou et al., 2001). In most cases, phosphorylation by protein kinase C (PKC) predominantly leads to inhibition of channel activity (Schubert & Nelson, 2001; Shipston & Armstrong, 1996). Thus, phosphorylation at S1151 in the C-terminus with subsequent phosphorylation at S695 that lies between the RCK1 and RCK2 leads to inhibition of channel activity by PKC. If only S1151 is phosphorylated by PKC, this ensures that only cGKI, but no longer PKA can activate BK, whereas phosphorylation of S695 prevents activation by both PKA and cGKI (Zhou et al., 2010).

BK channels play a critical role in the CNS by acting as an "emergency brake" that prevents hyperexcitability and associated cellular toxicity caused by neurotransmitters (Bentzen et al., 2014). Recent studies have linked genetic variations in BK channels to conditions such as mental retardation, autism, and schizophrenia, which are characterized by severe cognitive impairments (Laumonier et al., 2006). BK channel deficiency result in slower training success, indicating that BK channels play a crucial role in learning (Typlt et al., 2013).

Studies on knockout mice lacking the BK $\alpha$  subunit have demonstrated impaired motor coordination and ataxia (Sausbier et al., 2004). Similar results have been observed in transgenic (tg) mice with selective deletion of BK channels specifically in the Purkinje cells of the cerebellum. In a mouse model of ataxia type 1, Dell'Orco et al. (2015) showed that neuronal atrophy is caused by reduced expression of BK channels and subthreshold-activated  $\text{K}^+$  channels, leading to neuron depolarization and subsequent cell loss.

### **1.5.1. Structure**

The  $\alpha$ -subunit of the BK channel consists of approximately 1,200 amino acids (aa) and is made up of seven membrane-spanning domains (S0-S6), these come to a combined total of around 330 aa (Wallner et al., 1999). Among these domains, S4 is a conserved region containing positive charges that acts as a voltage sensor, similar to what is observed in  $\text{K}_v$  channels (Liman et al., 1991; Logothetis et al., 1993; Lopez et al., 1991; Seoh et al., 1996).

The pore-gated domain, comprised of the transmembrane segments S5 and S6 (**Figure 2**), forms the central part of the BK channel and functions as a selective filter for  $K^+$  ions. This domain is responsible for allowing  $K^+$  ions to pass through. Moreover, the  $\alpha$ -subunit contains a sizable cytosolic region at the C-terminal end, spanning around 840 aa. Within this region, there are four hydrophobic segments (S7-S10) that include two distinct domains known as regulators of  $K^+$  conductance RCK1 and RCK2. These domains serve as regulators for the  $K^+$  conductance of the channel.

Each RCK domain contains a binding site with high affinity for  $Ca^{2+}$ , as well as multiple regulatory domains that can interact with various ligands (Jiang et al., 2002; Sweet & Cox, 2009; Xia et al., 2002) or divalent cations such as  $Mg^{2+}$  (Shi et al., 2002; Xia et al., 2002; Yang et al., 2008). The tetramer's gating ring is formed by these four RCK1-RCK2 arrangements (Tao et al., 2017).

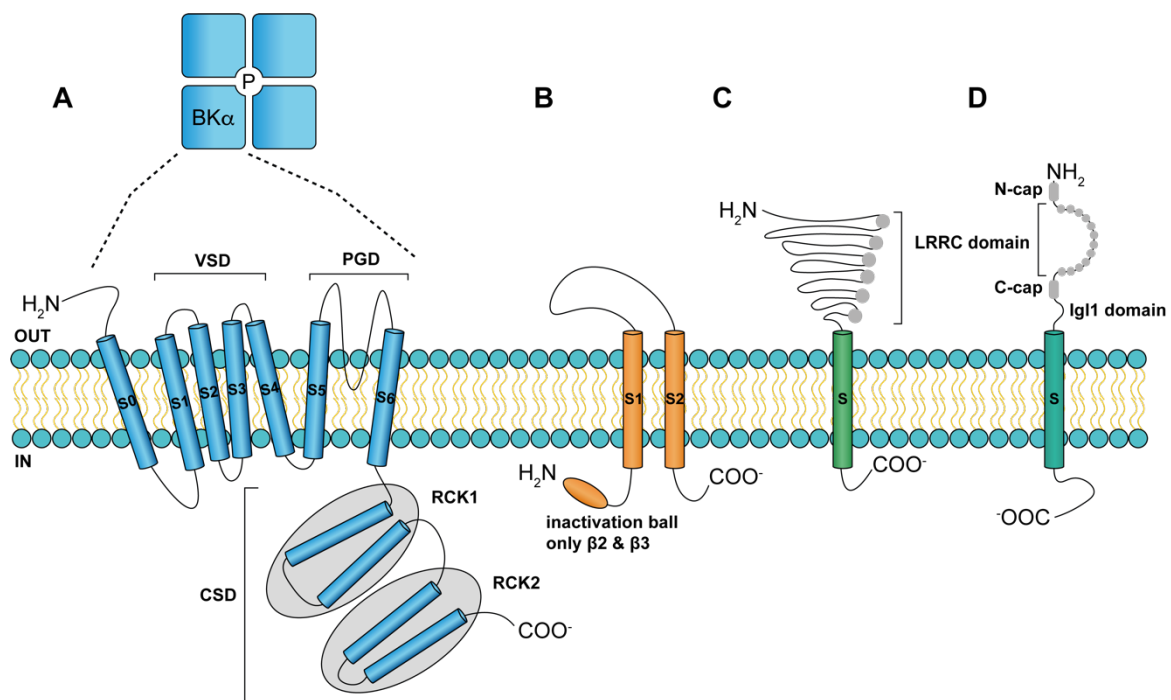


**Figure 2: Schematic illustration of a BK channel with its subunit variants. (A)** BK channels are homotetramers of BK $\alpha$  subunits. Each BK $\alpha$  subunit contains a voltage sensor domain (VSD), a pore-gated domain (PGD), and a  $Ca^{2+}$  sensor domain (CSD). The CSD consists of two non-identical regulators of  $K^+$  conductance domains (RCK), RCK1 and RCK2 (bottom). They contain high affinity  $Ca^{2+}$  binding sites. **(B)** There are 4 distinct  $\beta$ -subunit subtypes ( $\beta 1 - \beta 4$ ). They possess two transmembrane segments (S1 and S2) connected by an extracellular loop of 100 aa, along with short intracellular C- and N-termini. At the N-terminus  $\beta 2$  and  $\beta 3$  have an additional inactivation ball. **(C)** The  $\gamma$ -subunit family consists of 4 distinct members ( $\gamma 1 - \gamma 4$ ). The  $\gamma$  subunit possesses a single transmembrane segment (S), a large extracellular N-terminus containing a leucine-rich repeat containing (LRRC) domain and a short intracellular C-terminal end. **(D)** Lingo1 possesses a single transmembrane segment with an intracellular C-terminus and an extracellular N-Terminus consisting of an immunoglobulin lambda locus 1 (Ig1) and a LRRC domain, which is flanked by a C-cap and a N-Cap.

## 1.5.2. Associated auxiliary subunits

### $\beta$ – subunit

The presence of auxiliary subunits in BK channels contributes to significant functional diversity in various tissues and cell types of large mammals. By associating with tissue-specific auxiliary subunits, the BK channel  $\alpha$ -subunit generates a wide range of channel variations in terms of function (Li & Yan, 2016).

Two families of auxiliary proteins,  $\beta$  and  $\gamma$  subunits, have undergone extensive characterization. The  $\beta$  subunits consist of four distinct subtypes ( $\beta 1 - \beta 4$ ), sharing a similar structural arrangement. They possess two TMs (TM1 and TM2) connected by an extracellular loop of 100 aa, along with short intracellular C- and N-terminals. Each  $\beta$  subunit differently affects  $\text{Ca}^{2+}$  sensitivity, voltage dependence and gating mechanisms of BK channels to varying degrees. Due to their diverse expression patterns, their impact is individually tissue-specific (Brenner et al., 2000). Moreover,  $\beta$  subunits can modify the sensitivity of BK channels to regulatory molecules, including hormones and lipids (Hoshi et al., 2013; Mohr et al., 2022). B-1 subunits are primarily found in vascular smooth muscle, urinary bladder, and certain brain regions. B-2 subunits are highly expressed in chromaffin cells of the adrenal gland, pancreas, kidney, and hippocampal neurons.  $\beta$ -3 subunits are predominantly present in chromaffin cells, kidney, heart, liver, and lung; and  $\beta$ -4 subunits are primarily localized in the brain but may also be found in smooth muscle (Contreras et al., 2013).

#### **$\gamma$ – subunit**

The  $\gamma$ -subunit family also consists of four distinct members ( $\gamma 1 - \gamma 4$ ), encoded by different genes. Structurally, the  $\gamma$  subunit possesses a single transmembrane segment, a large extracellular domain containing leucine-rich repeat proteins, and a short intracellular C-terminal domain. The leucine-rich repeat proteins play a critical role in modifying the activation profile of BK channels (Yan & Aldrich, 2010). Recently, a new putative regulatory subunit called LINGO1 was identified. It shares structural similarities with  $\gamma 1$ -4 subunits. Ongoing studies focus on LINGO1, which has been associated with motor disorders and tremors such as PD and essential tremor. Notably, LINGO1 has been found to closely associate with BK channels and reduce BK channel activity in culture models and human cerebellar tissues, contributing to further understanding its role in these conditions (Dudem et al., 2020).

### **1.5.3. BK channel in the central nervous system**

In the CNS, BK channels are mainly present in axons as well as synaptic terminals (Trimmer, 2015) where they were implicated in neurotransmitter release (Yazefian et al., 2000). They play a role in repolarizing AP (Kimm et al., 2015) and mediating the fast phase of afterhyperpolarization (fAHP) (Gu et al., 2007). In specific neuron types like Purkinje, vestibular, and cerebral Golgi cells, inhibiting BK channels leads to increased AP firing speed accompanied by reduced afterhyperpolarization (AHP) (Hull et al., 2013). Conversely, in hippocampal CA1 pyramidal, gamma-aminobutyric acid (GABA), and

intracardiac autonomic neurons, inhibiting BK channels results in decreased firing rates (Perez et al., 2013). Recent research demonstrated that inhibiting BK channels in dopaminergic neurons of the SNc leads to significant broadening of APs, a more negative AHP, and an increased AP firing rate (Kimm et al., 2015). The study revealed that the increase in AP duration is caused by enhanced activation of the slowly deactivating  $K_v2$  current, which is hindered when the fast-activating BK channels are present (Latorre et al., 2017). Therefore, when analyzing the functional role of BK channels, it is important to consider their interaction with other ion conductances in the cell (Latorre et al., 2017).

In the CNS, there is a close spatial association between BK and  $Ca_v$  (Berkefeld & Fakler, 2008; Grunnet & Kaufmann, 2004). This co-localization is believed to be vital for achieving sufficient levels of  $Ca^{2+}$  concentration to activate BK channels at membrane voltages ranging from -50 to 0 mV, where their open probability ( $P_o$ ) reaches significant values (Berkefeld et al., 2010). Studies have found that BK channels in rat brain tissue are closely associated with L-, P/Q-, and N-type  $Ca_v$  channels (Berkefeld & Fakler, 2008). Further experiments with co-expression of BK and N-type  $Ca_v$  channels under conditions mimicking physiological settings revealed that BK channels function as ligand-activated channels gated by  $[Ca^{2+}]_i$  (Berkefeld & Fakler, 2013). P/Q- and N-type  $Ca_v$  channels are primarily localized in the pre- and postsynaptic compartments of cerebral Purkinje cells and cholinergic interneurons, whereas L-type  $Ca_v1$  channels (LTCCs) are predominantly found in the cell soma and dendrites of hippocampal pyramidal neurons (Latorre et al., 2017). Consequently, the functional properties of BK channels are expected to vary due to the co-assembly of BK channels with different  $Ca_v$  channel partners in different types of neurons (Berkefeld et al., 2010). Detailed electron microscopy studies on rat cerebellar Purkinje cells have quantified the distribution of P/Q-type  $Ca_v$  channels and BK channels, revealing clusters of P/Q channels in the protoplasmic face of soma and primary dendrites that co-localize with BK channels, with an average nearest neighbor distance of approximately 40 nm (Indriati et al., 2013).

## **1.6. Further important ion channels for synaptic plasticity**

### **1.6.1. Glutamate receptors**

Different neurotransmitters are employed by the CNS for the purpose of intercellular communication between synaptic membranes. Two prominent neurotransmitters for distinct functions are glutamate, responsible for excitatory processes, and GABA, which performs inhibitory functions. In the cerebral cortex, around 70% to 80% of neurons are glutamatergic (Micheva et al., 2010), while the remaining neurons are GABAergic interneurons (Hendry et al., 1987). Therefore, it becomes clear that the fundamental neural networks, particularly in the cortex, consist mainly of glutamatergic and GABAergic neurons. In the cerebral cortex, pyramidal neurons have approximately 30,000 synapses, with around 95% of them being excitatory synapses (Megias et al., 2001). This underlines that glutamate serves as the primary neurotransmitter for excitatory functions in the brain.

Strict control of extracellular glutamate concentration is crucial in the CNS due to its potential neurotoxic effects when present in high concentrations (Danbolt, 2001; Ehinger et al., 2021). Various mechanisms contribute to the regulation of glutamatergic signals, including glutamate transporters, inhibitory autoreceptors, and desensitization of postsynaptic receptors (Danbolt, 2001; Lau & Tymianski, 2010). Although it is known that direct activation of glutamate receptors can trigger seizures, the specific pathological functions of each glutamate receptor in epilepsy are not fully understood. Glutamate receptors can be categorized into two main subclasses: ionotropic glutamate receptors (iGluR) and mGluR. iGluR function as ligand-gated ion channels, while mGluR are G-protein-coupled receptors that activate second messengers (Lodge, 2009; Reiner & Levitz, 2018).

L-glutamate is recognized at postsynaptic terminals by both mGluR and iGluR. iGluRs are divided into three main types: AMPA-, NMDA- and kainite receptors (see **Figure 3**). All three bind glutamate with high affinity, but have different preferences for other agonists, including AMPA, NMDA and kainite (Reiner & Levitz, 2018).

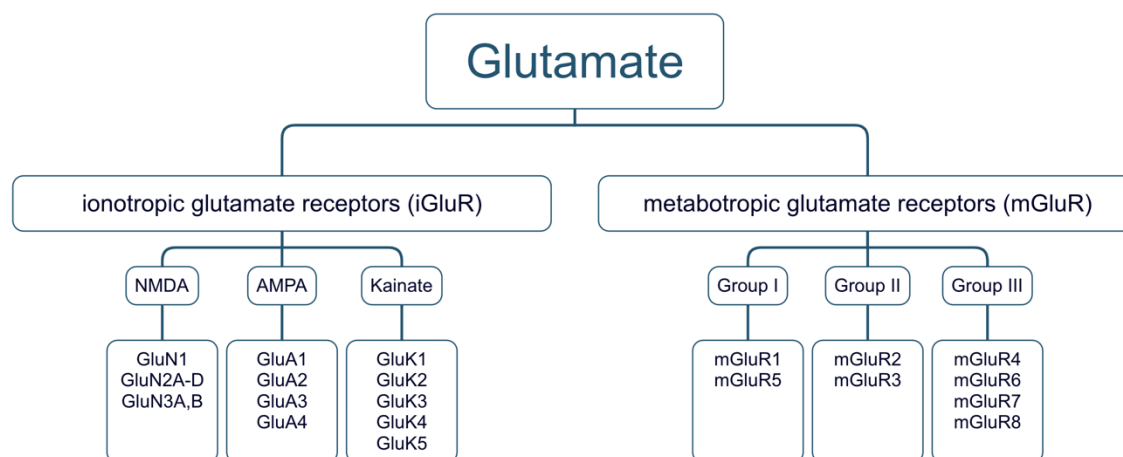


**Figure 3: Overview of glutamate receptor families.** Glutamate receptors can be classified into ionotropic (iGluR) and metabotropic glutamate receptors (mGluR) based on their structural makeup as well as their signal transduction mechanisms. The iGluRs include NMDA, AMPA, and kainite receptors. These ligand-gated ion channels were each composed of four different  $\alpha$ -subunits. The class of mGluRs can be divided into three subfamilies, group I-III. The representatives of group I are  $G_q$  protein-coupled receptors, whereas the receptors of group II and III are  $G_i$ -coupled. All mGluR are composed of seven transmembrane domains each.

### 1.6.1.1. *Ionotropic Glutamate receptors*

Due to their well-documented physiological functions, NMDAR and AMPAR have received significant attention in research and their roles within the body were extensively studied.

## NMDAR

Among the iGluR, NMDARs are of great interest for their role in synaptogenesis, synaptic plasticity, learning and memory, and in the pathogenesis of several disorders of the CNS (Lau & Tymianski, 2010; Sanz-Clemente et al., 2013). Functional NMDARs are composed of several subunits that form a heterotetrameric complex. Conventional NMDARs consist of two obligatory glycine-binding GluN1 and two glutamate-binding GluN2 (A-D) subunits. A GluN2 subunit can alternatively be replaced by a GluN3 (A-B) subunit (S. F. Traynelis et al., 2010). Although all NMDAR subunits share many common features and structural similarities, the specific composition confers biophysical and functional properties, such as conductance, kinetics, synaptic or extrasynaptic localization, protein-protein interaction and membrane trafficking as it is the case with AMPARs (Sanz-Clemente et al., 2013). A particular difference is that GluN2A-containing NMDARs are less mobile and more restricted in their localization in the synaptic membrane than their GluN2B counterpart (Bard et al., 2010; Groc et al., 2006). Whether NMDARs are composed of GluN2A or 2B subunits is developmentally regulated. While GluN2A is a component of the NMDAR only in the late postnatal phase, GluN2B is already expressed in the early phases of development (Monyer et al., 1994; Sheng et al., 1994). The subunits bind directly with the PDZ domains of membrane-associated guanylate kinase family scaffold proteins (Walikonis et al., 2000) through their C-terminal ESDV motif, with particularly high affinity for PSD-95 and SAP102 (Lim et al., 2002). These protein-protein interactions are essential for the stabilization of NMDAR in the postsynaptic density (Gardoni et al., 2006).

NMDA receptors are involved in both the induction and maintenance of LTP at postsynaptic neurons of the hippocampus. The opening of the NMDAR and the resulting mediated permeability to  $\text{Na}^+$ ,  $\text{K}^+$  and  $\text{Ca}^{2+}$  ions, occurs partly through the binding of a ligand, e.g., glutamate. However, the channel pore is blocked in a voltage-dependent manner by an  $\text{Mg}^{2+}$  ion. This blockade is lifted when the postsynaptic cell is simultaneously depolarized by concomitant AMPAR activation. NMDAR-mediated  $\text{Ca}^{2+}$  influx initiates a variety of signaling mechanisms including the activation of CaMKII, that can lead to changes in synaptic transmission and contribute to the maintenance of LTP through subsequent  $\text{Ca}^{2+}$ -induced synaptic changes. One such change involves the regulation of AMPA receptor gating and transport (see 1.1.1).

## **AMPA**

The activation of AMPAR occurs through the direct binding of glutamate or by the synthetic agonist  $\alpha$ -amino-3-hydroxy-5-methyl-4-isoxazole propionic acid (AMPA). As of now, no other naturally occurring ligand has been identified. These receptors are primarily found in the postsynaptic neuronal membrane and are responsible for facilitating fast excitatory neurotransmission within the brain's network.

AMPA are tetrameric ion channels consisting of the GluA1-4 subunits (Hollmann & Heinemann, 1994). The kinetic and conductance properties of AMPAR are determined during their biogenesis and regulated by post-transcriptional RNA modification, splice

variation, post-translational modification, and subunit composition. While NMDARs, with their slow kinetics, are primarily responsible for generating long-term synaptic potentiation and depression, AMPARs possess fast kinetics that allow rapid depolarization of the postsynaptic membrane and are thus critical for the expression of plasticity (Greger et al., 2017).

In the immature hippocampus, AMPAR are composed of GluA4/GluA2 (Zhu et al., 2000), whereas in adult animals there is a shift to GluA3/GluA2 and GluA1/GluA2. The latter accounts for 80% of all synaptic and more than 95% of all extrasynaptic AMPAR (Lu & Roche, 2012; Wenthold et al., 1996). AMPAR composition has received considerable attention in the past as it determines trafficking as well as biophysical properties (Malinow & Malenka, 2002; Shepherd & Huganir, 2007).

For example, the presence of the GluA2 subunit is crucial in determining the permeability of  $\text{Ca}^{2+}$ . GluA2 containing AMPAR are considered  $\text{Ca}^{2+}$ -impermeable and are primarily found in excitatory projection neurons (Lodge, 2009). On the other hand, AMPAR that lack the GluA2 subunit are  $\text{Ca}^{2+}$ -permeable and are predominantly expressed in inhibitory interneurons (Cull-Candy & Farrant, 2021). Additionally, the expression of  $\text{Ca}^{2+}$ -permeable AMPA receptors has been observed in excitatory neuronal synapses during synaptic plasticity, which includes both physiological plasticity and in response to pathological insult (Ceprian & Fulton, 2019; Liu et al., 2006).

Hence, understanding the mechanisms of AMPAR trafficking and synaptic plasticity requires a crucial molecular assessment of synaptic AMPAR subunit composition. Recent findings indicate that specific forms of synaptic plasticity not only impact the number of AMPARs but also alter the content of GluA2 subunits (Hanley, 2018).

NMDAR-dependent signal transduction modulates AMPAR activity through two primary mechanisms: direct phosphorylation of receptor subunits and changes in receptor density at the postsynaptic membrane (Voglis & Tavernarakis, 2006). In hippocampal pyramidal neurons, various kinases, including CaMKII and PKA, are activated during LTP. These kinases respond to  $\text{Ca}^{2+}$  signals and facilitate the induction of enhanced synaptic transmission by phosphorylating specific AMPAR subunits (Lee et al., 2003). Phosphorylation enhances receptor opening probability and membrane insertion during LTP. Dephosphorylation on the other hand occurs during LTD to reduce receptor  $P_0$  and membrane localization.

The transport of AMPAR to and from the synapse is also critical for synaptic plasticity. Following the induction of LTP, the concentration of AMPAR at the synapse increases, whereas it decreases during LTD (Lu et al., 2001). The insertion of AMPAR into the postsynaptic membrane and their turnover are regulated by phosphorylation of specific receptor subunits triggered by synaptic  $\text{Ca}^{2+}$ -fluctuations (Malenka, 2003; Malinow & Malenka, 2002).

The GluA1-4 subunits can be phosphorylated at multiple serine, threonine, and tyrosine residues by various kinases, including CaMKII, PKA, PKC, and cGKI (Lu & Roche, 2012; Shepherd & Huganir, 2007).

Regarding GluA1 C-terminal domain phosphorylation, three specific sites have been identified as crucial for controlling receptor activity and trafficking: Serine 818 (S818), S831, and S845. PKC-mediated phosphorylation of S818 enhances single channel conductance and promotes surface expression and synaptic uptake of GluA1 (Diering & Huganir, 2018). Both CaMKII and PKC phosphorylate S831, which may increase single channel conductance and regulates receptor transport and synaptic engagement (Summers et al., 2019). Phosphorylation of GluA1 S845 by PKA and cGKI is involved in regulating the opening probability of the receptor (Banke et al., 2000) and plays a role in receptor recycling between intracellular endosomes and the extrasynaptic plasma membrane (Stephen F. Traynelis et al., 2010), preventing their degradation in the lysosome and facilitating their delivery to the extrasynaptic membrane (Fernandez-Monreal et al., 2012; He et al., 2009; Yang et al., 2008; Yang et al., 2010). Notably, studies have revealed that approximately 15% of receptors are phosphorylated at S831 and S845 in their resting state (Diering et al., 2016; Hosokawa et al., 2015). These phosphorylation events are of utmost importance in regulating receptor transport and function during various forms of synaptic plasticity, including LTP, LTD and homeostatic synaptic plasticity.

#### **1.6.1.2. Metabotropic glutamate receptors**

As mentioned above, in addition to iGluR another group of receptors called mGluR were discovered later. In the 1980s, Sladeczek et al. demonstrated that glutamate causes an elevation in the intracellular second messenger inositol triphosphate (IP<sub>3</sub>) (Sladeczek et al., 1985). Two years later, a novel class of receptors, the mGluR was found (Sugiyama et al., 1987). Subsequently, eight different genes encoding mGluR1-8 receptors have been identified, along with numerous splice variants. All mGluR possess seven TM domains, an extracellular N-terminus, and an intracellular C-terminus. It is important to note that mGluR do not share sequence similarities with other G protein-coupled receptors.

Within the CNS, mGluR serve various functions. They mediate slow excitatory potentials and inhibitory postsynaptic potentials (IPSPs). They also participate in the regulation of Ca<sup>2+</sup>, K<sup>+</sup>, and nonselective ion channels, as well as modulation of presynaptic neurotransmitter release. Moreover, they contribute to the induction of LTP and LTD by regulating the transport of iGluR. Additionally, mGluR modulate NMDAR-mediated synaptic transmission and influence neuronal development. On the flip side, they are implicated in the development of various neurological disorders for example fragile X syndrome, exocytotic cell death and epilepsy.

mGluR can be categorized into three subfamilies based on their sequence homologies, pharmacological properties, and downstream signal transduction pathways. Group I of

mGluR consists of two subtypes, mGluR1 and mGluR5, along with numerous splice variants. Both mGluR1 and mGluR5 are predominantly located in the postsynapse and are coupled to the  $G_q$  protein. Activation of these receptors leads to the stimulation of phospholipase C (PLC), which triggers the hydrolysis of phosphatidylinositol-4,5-bisphosphate ( $PIP_2$ ). Cleavage of  $PIP_2$  results in increased intracellular concentrations of  $IP_3$  and diacylglycerol (DAG).

Within the endoplasmic reticulum (ER),  $IP_3$  binds its corresponding receptor, leading to  $Ca^{2+}$  release. Subsequently, DAG and  $Ca^{2+}$  activate PKC. This activation results in the phosphorylation of various target proteins, including AMPAR and NMDAR. Through this phosphorylation, mGluR can influence neuronal activity. Group II of mGluRs consists of two subtypes, mGluR2 and mGluR3, while Group III includes mGluR4, mGluR6, mGluR7, and mGluR8. Receptors in these two groups are coupled to  $G_i$ , leading to the inhibition of adenylate cyclase activity. As a result, intracellular cyclic adenosine monophosphate (cAMP) levels decrease, resulting in increased  $K^+$  currents, decreased  $Ca^{2+}$  currents and subsequent hyperpolarization of the cell membrane. mGluRII/III receptors are predominantly located presynaptically and modulate neurotransmitter release.

In the context of ND, mGluR1 and mGluR5 contribute to cell death by generating slow excitatory potentials and modulating ion channels. Conversely, studies by Lee et al. suggest a protective effect of mGluR2 on neuronal cell survival in AD (Lee et al., 2003). Activation of mGluR2 leads to the activation of the ERK signaling pathway, increased phosphorylation of tau protein, and a reduction in oxidative stress, among other effects.

However, not only do the various mGluR subtypes differ in their functions, but their expression patterns in the CNS also vary. In adult rat brain, studies using in situ hybridization and immunohistochemistry have revealed distinct expression patterns for different mGluR subtypes. Specifically, mGluR1 are predominantly expressed in the cerebellum, mitral cells of the olfactory bulb, hippocampus, thalamus, and substantia nigra. In contrast, mGluR5 transcripts are detected in the cerebral cortex, hippocampus, subiculum, olfactory bulb, striatum, and other brain structures. It should be noted that mGluR5s are believed to be absent in the cerebellum based on the work of (Ferraguti et al., 2005).

### **1.6.2. Voltage gated $Ca^{2+}$ channels**

LTP can be triggered by  $Ca^{2+}$  entry into the postsynaptic cell via either NMDAR,  $Ca^{2+}$ -permeable AMPAR or voltage gated  $Ca^{2+}$  channels (VGCC) (Raymond & Redman, 2002). VGCCs are a diverse group of heteromultimeric ion channels that respond to changes in membrane potential (Voglis & Tavernarakis, 2006). VGCCs are divided into six classes L-, N-, P-, Q-, R-, and T-types, according to their sensitivity to pharmacological blockade, single channel conductance, kinetics, and voltage dependence (Reuter, 1996). T-type channels have a low voltage threshold for activation, whereas L-, N-, P-, Q-, and R-type channels are activated with a high voltage threshold (Voglis & Tavernarakis, 2006).

LTCC are localized in non-neuronal excitable tissues such as skeletal and cardiac muscle as well as in presynaptic and postsynaptic structures of neurons and where they are required for excitation-contraction coupling (Hell et al., 1993; Obermair et al., 2004).

Neuronal LTCC are known to mediate cellular  $\text{Ca}^{2+}$  entry and play key roles in activity-dependent processes such as neurotransmission, gene transcription, and intracellular signaling cascades (Lipscombe et al., 2004). Several studies indicate that specific channel types are involved in different forms of synaptic plasticity.

For example Nifedipine (NIFE), which specifically inhibits LTCC, has been used to show that LTCC are critical for the expression of a variety of forms of neuroplasticity (Lei et al., 2003). One of the distinct forms of neuroplasticity is NMDAR-independent LTP (Manabe, 2017). The pyramidal cells of the hippocampus and neocortex were targeted in a mouse model utilizing the Cre/loxP technique and NEX-Cre (Goebbels et al., 2006), resulting in the knockout of  $\text{Ca}_v1.2$  ( $\text{Ca}_v1.2^{\text{HCKO}}$ ). Subsequent induction of NMDAR-independent LTP was induced in the acute brain slices through combined application of DL-AP5, a specific NMDAR inhibitor and a LTP stimulus either by 200 Hz tetanus, several 100 Hz tetanus or by perfusion of 25  $\mu\text{M}$  tetraethylammonium (Moosmang et al., 2005). For all three paradigms, potentiation was lower in the  $\text{Ca}_v1.2^{\text{HCKO}}$  compared to the control group, thus confirming the importance of LTCC for hippocampal LTP in a mouse model.

Chronic nimodipine treatment improves memory loss, suggesting that excessive  $\text{Ca}^{2+}$  influx through LTCC impairs learning and memory (Veng et al., 2003). It is interesting to note that patients with AD have higher expression of LTCC in the hippocampus compared to healthy individuals (Coon et al., 1999). This association suggests that aberrant levels of LTCC may contribute to the memory deficits in AD patients.

Nevertheless, the function of VGCC in LTP is not properly understood to date. LTP relies on the entry of  $\text{Ca}^{2+}$  into cells, which is an essential step in many types of synaptic plasticity involved in learning. Therefore, it is reasonable to speculate that VGCCs play a role in mediating  $\text{Ca}^{2+}$  entry during LTP and hence contribute to learning. However, multiple studies have found that VGCC-dependent LTP occurs in the hippocampus only when NMDA receptors are blocked and with extremely high-frequency pathway stimulation (at least 200 Hz), which is unlikely to happen naturally. In contrast, in the amygdala, a more physiologically plausible combination of postsynaptic depolarization and presynaptic stimulation of the thalamo-amygdala pathway has been shown to induce VGCC-dependent LTP. Various protocols have also demonstrated VGCC-dependent LTP in different pathways of the amygdala. This raises the question of whether VGCC-dependent LTP is present anywhere other than the amygdala or whether it is not experimentally challenging to stimulate VGCC-LTP by a more physiological stimulus.

However, the importance of these channels for learning can be better assessed in behavioral experiments, particularly in classically conditioned fear, a type of learning known to depend on the amygdala. Classically conditioned fear involves associating a neutral stimulus (conditioned stimulus), such as a tone or a contextual cue, with an

intrinsically aversive unconditioned stimulus, like a footshock. Conditioned fear can be diminished or suppressed by repeatedly presenting the conditioned stimulus without the unconditioned stimulus, a process called extinction. Fear extinction learning is entirely reliant on LTCC, as the process fails to occur when training takes place in the presence of LTCC inhibitors (Langwieser et al., 2010; McKinney & Murphy, 2006).

Experiments using  $Ca_v1.2$  knockout mice revealed that their genetic mutation disrupted NMDA-independent late LTP in the mossy fiber-CA1 pathway of the hippocampus, which was induced by a 200-Hz tetanus. Additionally, the mutation impaired spatial learning in those mice (Moosmang et al., 2005).

In another study the focus shifted to investigating the role of the  $Ca_v1.3$  subtype of LTCC in fear learning using knockout mice lacking this specific subtype. Interestingly, despite being deaf, the  $Ca_v1.3$  knockout mice displayed overall normal neurological and behavioral functioning, as evidenced by their comparable performance to wild-type littermate controls in measures of activity and general anxiety in an open-field setting (McKinney & Murphy, 2006).

Given the hearing impairment in  $Ca_v1.3$  knockout mice (Platzer et al., 2000) and the fact that most cue-based fear conditioning relies on auditory stimuli, contextual fear was rather evaluated than cue fear (McKinney & Murphy, 2006). To induce contextual conditioned fear, the mice were placed in a novel environment for an acclimatization period and then subjected to a single mild footshock. This protocol elicits fear responses when the animals are later returned to that context, as measured by freezing behavior ("Frontiers in Neuroscience," 2009).

Comparing the  $Ca_v1.3$  knockout mice to their wild-type littermates, the  $Ca_v1.3$  subtype of LTCCs seemed to be essential for the consolidation phase of conditioned fear toward the context, but not for its initial formation. Specifically, knockout mice exhibited fear responses similar to their littermates at 1 and 6 hours after fear conditioning but displayed significantly less fear than their littermates after 24 hours (McKinney & Murphy, 2006). Notably, this temporal pattern of  $Ca_v1.3$  dependence in conditioned fear aligns with findings from a separate study that examined cue-conditioned fear after administering a LTCC inhibitor into the basolateral amygdala (Bauer et al., 2002). Interestingly, it also corresponds with the time course of  $Ca_v1.2$  dependence in long-term spatial memory (Moosmang et al., 2005).



## 2. Aims

Although BK (Meredith et al., 2004; Sausbier et al., 2004) was intensively researched for many years, little is known about its role hippocampal synaptic plasticity or hippocampus-dependent learning and memory. So far, a single paper suggests reduced learning of global BK<sup>-/-</sup> (Typlt et al., 2013). As global BK<sup>-/-</sup> mice suffer from cerebellar ataxia (Sausbier et al., 2004), the results from these behavioral learning tests could be influenced by abnormal movement patterns and reduced motor coordination (Chen et al., 2010) and might therefore be viewed extremely critical.

To re-examine these findings and to further study mechanistically BK's role in synaptic plasticity, a CA1 pyramidal cell-specific conditional BK-KO (cKO) mouse was generated for this study.

In this dissertation, the specificity and efficiency of deleting the BK from CA1 pyramidal neurons will be examined first. Then, locomotor activity and motor capabilities of cKO were tested to evaluate the suitability of the mouse model for the MWM test for learning and memory performance. Subsequently, BK's role in synaptic plasticity was analyzed using electrophysiological and biochemical tools. As a last step, optical real-time image capturing and processing tools were used for a detailed mechanistic and molecular analysis of BK's influence on intracellular K<sup>+</sup> ([K<sup>+</sup>]<sub>i</sub>) and [Ca<sup>2+</sup>]<sub>i</sub> levels during LTP.



## 3. Material and methods

### 3.1. Mouse breeding

#### 3.1.1. Animal husbandry

All animal experiments performed were approved by the responsible animal welfare authority (Regierungspräsidium Tübingen) in compliance with German animal welfare laws. Mice were kept in an open specified pathogen-free SPF housing system with a room temperature (RT) of  $22 \pm 2$  °C at 50-60 % relative humidity and a 12 h light-dark cycle (light from 6 am to 6 pm). Animals were kept in groups of 2 to 3 mice per cage (macrolon type II), while breeding was done in type III cages. Cages were enriched with coarse wooden bedding (also for gnawing) and nesting material as well as small plastic houses (only for females and individually kept males).

Animals were fed *ad libitum* with drinking water and a standard commercial natural ingredient diet. For behavioral experiments, animals were separated and kept individually. Separation was done one week before start of experiments to allow the animals to acclimatize. Individual housing was performed to prevent hierarchy struggles after reintroduction of individual experimental animals into the group after the experiment. At least 1 day before and during the duration of behavioral experiments, subject animals were kept in the experimental room. This allows them to become accustomed to the experimental room and avoids additional stress from transport from the animal facility to the experimental room. The housing conditions in the experimental room were analogous to the existing animal housing facility and met the requirements for animal housing.

#### 3.1.2. Conditional and global BK mouse model

CA1 pyramidal neuron-selective BK knockout mice were generated using tg mice of the genotype B6.Cg-Tg(CaMKIIa-cre)T29-1Stl/J (T29.1-Cre; JAX Strain 005359) expressing Cre recombinase under control of the CaMKII-promotor selectively in hippocampal CA1 pyramidal neurons (Tsien, Chen, et al., 1996). Tg mice (T29.1-Cre<sup>tg/+</sup>; BK<sup>+/+</sup>) were cross-bred with heterozygous BK knockout mice (BK<sup>+/-</sup>). F1 filial double hemi-/heterozygous (T29.1-Cre<sup>tg/+</sup>;BK<sup>+/-</sup>) mice were subsequently mated with mice carrying floxed BK alleles (BK<sup>fl/fl</sup>) to yield both controls (CTRL; T29.1-Cre<sup>tg/+</sup> x BK<sup>fl/+</sup>) and conditional knockouts (cKO; T29.1-Cre<sup>tg/+</sup> x BK<sup>fl/-</sup>) in the F2 generation.

Experiments that were performed with primary hippocampal cells derived from BK<sup>+/+</sup> and global constitutive BK channel-deficient mice (BK<sup>-/-</sup>) to ensure BK removal from all hippocampal neurons in the latter case and not to obtain a mixed culture because whole hippocampi were used, although T29.1-Cre specificity is focused on the CA1 population (4.1). To generate BK<sup>-/-</sup>, exon 7 of the KCNMA1 gene was deleted by homologous recombination as previously described (Sausbier et al., 2004). This exon encodes the pore-forming region of the  $\alpha$ -subunit and a segment of the S6 segment of the BK channel.

Deletion of the corresponding gene sequence subsequently leads to a complete loss of channel function. BK<sup>+/+</sup> offspring were obtained by homozygous matings of parents of the identical genotype. Since male BK<sup>-/-</sup> mice are not fertile and homozygous BK<sup>-/-</sup> can therefore not be bred, BK<sup>-/-</sup> mice were obtained by heterozygous mating of BK<sup>+/-</sup> mice.

### 3.2. Culturing primary hippocampal neurons

Reagent/Resource	Reference or Source	Identifier (Cat#)
20% (wt/vol) glucose solution	Thermo Fisher Scientific	A2494001
200 mM GlutaMax (100x)	Thermo Fisher Scientific	35050038
B-27	Thermo Fisher Scientific	17504044
BME	Thermo Fisher Scientific	21010046
70 µm Cell Strainer	Corning	431751
DNase I	Sigma-Aldrich	DN25
Fetal Calf Serum	Thermo Fisher Scientific	26140
HBSS (Ca <sup>2+</sup> and Mg <sup>2+</sup> free)	Thermo Fisher Scientific	14175095
HEPES	Carl Roth	9105
Neubauer counting chamber	Millipore	MDH-2N1-50PK
Neurobasal medium	Thermo Fisher Scientific	21103049
Penicillin-Streptomycin (10.000 U/mL)	Thermo Fisher Scientific	15140122
Poly-L-Lysine (PLL)	Sigma-Aldrich	P2636
Sodium pyruvate solution (100x)	Thermo Fisher Scientific	11360070
Trypan blue solution	Sigma-Aldrich	T8154
Trypsin-EDTA (0.5%)	Thermo Fisher Scientific	15400054
Coverslip 18x18 mm Thickness No. 1	Marienfeld Superior	0111580
Coverslip 30x30 mm Thickness No. 1	Marienfeld Superior	0111700
12-well plate	Sarstedt	83.3921
6-well plate	Sarstedt	83.3920
Dumont #5 - Fine Forceps	Fine Science Tools	11254-20
Dumont #3 Forceps	Fine Science Tools	11231-30
Iris Spatulae	Fine Science Tools	10093-13

#### 3.2.1. Coating of cell culture dishes with poly-L-lysine

Coverslips used for culturing primary hippocampal neurons were coated with poly-L-lysine (PLL) to allow for better adhesion. For IF staining or single cell live imaging, individual 18 mm and 30 mm coverslips were placed in the 12- and 6-well plates, respectively, prior to coating with 0.5 mg/mL PLL in borate buffer overnight. To prevent contamination or drying of the tubes during coating, the plate dishes were sealed with parafilm and incubated overnight at RT under aseptic conditions in the laminar flow bench.

On the second day, PLL solution was carefully aspirated with a pasteur pipette and coverslips were washed 3x with sterile ddH<sub>2</sub>O. Care has been taken to ensure that the surfaces of the coverslips do not dry out. After the washing procedure, maintenance

medium (MM) was added to the wells. The cell culture plates were pre-incubated in the incubator for at least 2 h before the hippocampal neurons were seeded.

### **3.2.2. Dissociation and culture of primary hippocampal neurons**

Primary hippocampal neuron cultures with BK<sup>+/+</sup> and BK<sup>-/-</sup> genotypes were generated from homozygous BK WT and heterozygous BK<sup>+/-</sup> matings, respectively (3.1.2). For this purpose, mice were sacrificed by decapitation with scissors on the day of birth (P0) or at the latest one day after birth (P1) and hippocampi were subsequently isolated. No anesthesia with CO<sub>2</sub> was performed, as newborn mice are resistant to hypoxia. Three young animals per litter remained with the maternal animal until weaning at 21 days of age to avoid excessive stress. For BK<sup>+/+</sup> hippocampi, all hippocampi were collected in a petri dish and processed together. After isolation, hippocampal culturing procedures were performed in a tissue culture hood. Non-sterile hippocampi were transferred to a sterile 15 mL reaction tube and washed 3x with sterile dissociation medium (DM). From that moment on, work was performed exclusively under sterile conditions. After the last washing step, hippocampi were resuspended in 4.5 mL DM, combined with 0.5 mL trypsin and incubated for 20 min in a 37 °C water bath. During incubation, tissue should be occasionally inverted to allow for uniform digestion. After 20 min, 0.5 mL of Deoxyribonuclease I (DNase I) was added to the hippocampi for another 5 min incubation at RT. Hippocampi were subsequently washed 2x with DM and 2x with pre-warmed plating medium (PM) before resuspension in 2 mL of pre-warmed PM. Hippocampi were triturated using a fire-polished pipette. The diameter of the pipette opening and the length of the trituration should be chosen to allow efficient dissociation of the tissue so that there is no more tissue accumulation in the medium to ensure a high yield of live neurons. If the pipette opening is too large or trituration is too short, the percentage of live neurons will be increased but the yield greatly decreased. Too small pipette openings or too long trituration increases both the overall yield but also the percentage of neurons that perish. Thus, trituration should be performed slowly and carefully, while avoiding air bubbles. All this will prevent excessive damage to dissociated neurons. The solution should be cloudy but homogeneous at the end of trituration due to the dissociated neurons. Persisting tissue pieces can be removed using a tissue sieve with a mesh size of 70 µm. To determine cell density and viability, 10 µL of the cell suspension was taken and mixed with 50 µL PM and 40 µL trypan blue. 10 µL of this solution was pipetted into a hemocytometer. Intact neurons appear shiny round, while the defective neurons appear dark due to the trypan blue applied. After cell density is determined and corrected for the defective neurons, neurons can be seeded. After cells are settled, though no more than 2 h later, the PM is replaced with MM. Until the experiment at DIV 9, the cultivation medium is renewed by removing half of the volume and replacing it with the same volume of freshly prepared MM every 3 to 4 days.

DM		MM	
HBSS	97.5 %	Neurobasal medium	96 %
100 mM sodium pyruvate	1 mM	B-27 (50×)	1x
20% (wt/vol) glucose	0.1%	200 mM glutamax	2 mM
1 M HEPES (pH 7.3)	10 mM	Penicillin/streptomycin	1x

PM	
BME	86.55 %
FCS	10 %
20% (wt/vol) glucose	0.45 %
100 mM sodium pyruvate	1 mM
200 mM glutamax	2 mM
Penicillin/streptomycin	1x

### 3.3. Immunofluorescence

Reagent/Resource	Reference or Source	Identifier (Cat#)
Mouse Monoclonal IgG <sub>2A</sub> Anti-Slo1 Maxi-K <sup>+</sup> Channel (clone L6/60) 1:1000	NeuroMab	AB5849
Mouse Monoclonal IgG <sub>2A</sub> Anti-beta-III Tubulin Antibody 1:1000	R&D Systems	MAB1195
Goat anti-Mouse IgG <sub>2a</sub> Alexa Fluor 488 1:2500	Thermo Fisher	A-21131
Paraformaldehyd	Carl Roth	0335.1
Phosphate-buffered saline	Thermo Fisher	14190144
Permafluor	Fisher Scientific	TA-030-FM
Neg-50 Frozen Section Medium	Epredia	6502
SuperFrost Plus	Epredia	10149870
ImmEdge Hydrophobic Barrier Pen	Vector Laboratories	H-4000
Boric acid	Carl Roth	5935.1
Sodium tetraborate	Carl Roth	4403.1
Normal Goat Serum (NGS)	Biozol	ENG9010
Triton X-100	Carl Roth	3051.2
Bovine serum albumin (BSA)	Sigma Aldrich	7906-50G

#### 3.3.1. Tissue fixation and cryosectioning

To obtain tissue, adult mice were euthanized using CO<sub>2</sub>. For this purpose, CO<sub>2</sub> was slowly introduced into the closed holding cage of the mice. The speed of the CO<sub>2</sub> feed was selected for the gas concentration inside the cage to increase as fast as possible in order to rapidly induce unconsciousness. Care was taken, however, to ensure that animals were not subjected to stress by the sound or sensation of the incoming gas. To ensure euthanasia, the absence of eyelid and inter-toe reflexes were tested. Following

euthanization of the mouse, thorax was opened, and the mediastinum exposed. After opening the pericardium, the right atrium was opened by incision to allow pressure relief. A wing cannula 21G was inserted into the left ventricle so that both phosphate-buffered saline (PBS) and 4 % paraformaldehyde (PFA) in PBS could be perfused through the mouse via a three-way valve using a gravity-based perfusion system. First, all mouse blood was displaced and flushed out by perfusion with 20 mL of PBS. After proteins were fixed by 20 mL of 4 % PFA, perfusion was performed with an additional 20 mL of PBS to rinse out remaining PFA. The brain was then immediately isolated and snap frozen in isopentane cooled to -40 °C by liquid nitrogen. Brains were stored at -80 °C until the day of sectioning. Before sectioning, brain tissue was stored at -20 °C for at least 1 h to adjust to a temperature similar to that of the cryotome. To make cryosections, frozen brain tissue was fixed on the stage with a small amount of NEG-50. The cutting temperature of the cryotome was thereby set to -20 °C tissue temperature and -18 °C blade temperature. 8 µm thick sections were made and mounted on SuperFrost Plus slide. The sections were air dried for 30 min and subsequently preserved for immunofluorescence staining by storage at -20 °C.

4 % (wt/vol) PFA	
PBS supplemented with paraformaldehyd	4 % wt/vol
Adjust pH to 7.4	

### 3.3.2. Immunofluorescent staining of brain sections

Prior to staining, brain sections were thawed at RT for at least 30 min. The sections were surrounded by a hydrophobic barrier using an ImmEdge pen to facilitate staining on the slide. After curing of the hydrophobic barrier, sections were rehydrated in PBS for 5 min and incubated with blocking buffer (BB) for 2 h at RT. Primary antibodies were incubated overnight in BB. On the following day, samples were washed 2x 5 min and 1x 15 min with 0.01 % Triton-X-100 in PBS at RT. After another 1 h incubation with BB at RT, the corresponding secondary antibodies and 5 µg/mL Hoechst 33342 in BB were added to the sections for 2 h at RT. Due to the photosensitivity of the fluorophores, incubation of the tissue with diluted fluorophore-coupled secondary antibody solution was performed in the absence of light. Subsequent washing steps were also performed with as little light exposure as possible. Thereafter, sections were washed with 2x 5 min 0.01 % Triton-X-100 in PBS and 1x 15 min, then 1x 5 min with PBS and a final time with H<sub>2</sub>O for 5 min before mounting with Permafluor. After hardening at RT overnight, images could be taken on a fluorescence microscope (Axioimager Z1, Zeiss) with a 20x or 63x objective.

BB	
PBS supplemented with	
Glycerol	2 %
Normal Goat Serum (NGS)	5 %
Triton-X-100	0.3 %
Bovine Serm Albumin	2 % (wt/vol)
NH <sub>4</sub> Cl	50 mM

### 3.3.3. Immunofluorescence staining of cultured neurons

For immunostaining, primary hippocampal neurons were cultured in 12-well plates on 18 mm PLL-coated coverslips. For coating, sterile coverslips were transferred to the 12-well plates and each covered with 0.5 mL of a 0.5 mg/mL PLL in borate buffer. On the following day, coverslips were briefly washed 3x with 1 mL ddH<sub>2</sub>O. Hippocampal neurons were isolated and cultured according to procedures described in section 3.2.2. Immunostaining of hippocampal neuronal cultures was performed on 9 days *in vitro* (DIV) by carefully removing the MM of one well and replacing it with 0.5 mL of 4 % PFA/4 % sucrose solution in PBS at 37 °C. Subsequent staining procedures were performed analogous to brain sections (3.3.2).

Borate buffer 1 M	
boric acid	1.24 g
sodium tetraborate	1.90 g
ddH <sub>2</sub> O	in 400 mL
Adjust pH to 8.5 and filter sterilize	

## 3.4. Genotyping

Reagent/Resource	Reference or Source	Identifier (Cat#)
T29.1-Cre forward 5'-CGT CCA TCT GGT CAG AAA AG-3'	The Jackson Laboratory	
T29.1-Cre reverse 5'-TCT TCT TCT TGG GCA TGG TC-3'	The Jackson Laboratory	
BK forward1 5'-TGG TCT TCT TCA TCC TCG GG-3'	Sausbier et al., 2004	
BK forward2 5'-AAG GGC CAT TTT GAA GAC GTC-3'	Sausbier et al., 2004	
BK reverse 5'-CCA GCC ACG TGT TTG TTG G-3'	Sausbier et al., 2004	
2-Log DNA Ladder	N3200S	New England Biolabs

Agarose	Genaxxon	M3044.0500
DMSO	D8418	Sigma-Aldrich
Ethidium bromide solution 1 %	Carl Roth	2218.2
EDTA	Carl Roth	#8043.1
Ear hole punch	3104605	Zoonlab
Forceps mini straight	11200-12	Fine Science Tools
KAPA Mouse Genotyping Kit	Roche	KK7301
Mastercycler gradient		Eppendorf

### 3.4.1. DNA Isolation

First, biopsies were incubated in a 1.5 mL reaction tube containing 100  $\mu$ L master mix (containing per extraction reaction in  $\mu$ L; 2 extraction enzyme, 10 extraction buffer and 88 ddH<sub>2</sub>O) at 75 °C and 500 revolutions per minute (rpm) for 10 min in a thermal shaker. After shaking at 95 °C and 500 rpm for 5 min to inactivate the enzyme activity, samples were briefly centrifuged. The supernatant containing the DNA was then removed and transferred to a fresh reaction tube (1.5 mL). Samples were stored for a short time until further use at 4 °C.

### 3.4.2. Amplification of PCR products

All genotyping polymerase chain reactions (PCR) were pipetted according to the same scheme into 500  $\mu$ L micro reaction tubes (see table below). The PCR was performed by a thermal cycler (Mastercycler gradient, Eppendorf). In this approach, 24  $\mu$ L of master mix is initially provided and 1  $\mu$ L of DNA was added. During each PCR cycle, due to a specific temperature protocol, the following 3 phases were run: Denaturation, primer hybridization and elongation. Since the DNA polymerase included in the KAPA kit is a hot start DNA polymerase, it must be activated at a temperature of 94 °C before starting the actual PCR. It started with the denaturation phase, in which the samples are heated to 95 °C. Subsequently, the sample is cooled to 64 °C. This allows the attachment of the two primers to the nucleotide sequence of the single-stranded DNA segment to be amplified. During the subsequent elongation phase at 72 °C, the DNA polymerase (KAPA2G Fast Hot Start DNA Polymerase) synthesized a complementary strand to the primer-flanked sequence in the 5' - 3' direction using the available deoxynucleosidtriphosphate. A total of 30 such cycles were run. The temperature protocol for the thermal cycler is shown in the table below.

PCR mix	BK	CaMKII-Cre
ddH <sub>2</sub> O	8 µL	10.5 µL
2x KAPA2G Fast (HotStart)	12.5 µL	12.5 µL
Primer F1	1.5 µL	1 µL
Primer F2	1 µL	-
Primer R		1 µL
DMSO	1 µL	-
DNA	1.2 µL	1.2 µL

General PCR temperature protocol		
Heat activation (hot start)	94 °C	3 min
Denaturation	94 °C	30 s
Annealing	64 °C	30 s
Elongation	72 °C	30 s
Repeat denaturation, annealing and elongation for further 29 steps		
Final elongation	72 °C	5 min
Keep at 4 °C before long-term storage at -20 °C		

### 3.4.3. DNA detection by agarose gel electrophoresis

In the following, amplified DNA fragments were separated by agarose gel electrophoresis according to their size in an electric field. A 2 % agarose gel was used to separate the DNA fragments. To prepare the gel, the appropriate amount of agarose was dissolved in 1x Tris-Borate-EDTA (TBE) buffer by heating in a microwave. Subsequently, this agarose solution was stirred on a magnetic stirrer until it cooled down to RT. Just before casting the gel, 0.1 µg/mL of the fluorescent dye ethidium bromide was added to the agarose solution. After pouring the gel into the designated gel casting chamber, special combs were used to create the sample pockets as the gel solidified. After complete gel polymerization, specimens as well as 6 µL length standard (2-log DNA ladder) were applied to gel pockets. Separation was initially performed for about 15 min at a voltage of 80 V to run samples out of the gel pockets. Then, the voltage was increased to 120 V. The total duration of electrophoresis was approximately 1 to 2 h, depending on gel size. Following gel electrophoretic separation, DNA bands could be visualized using a UV gel detection device due to the intercalated ethidium bromide. The wild-type allele (+), the floxed BK allele (fl) and the recombined null allele (-) were expected at 466 base pairs (bp), 577 bp and 132 bp, respectively.

10x TBE buffer		0.5 M EDTA pH 8.0	
TRIS	108 g	EDTA	40 mL
boric acid	55 g	dH <sub>2</sub> O	add to 1 L
0.5 M EDTA pH 8.0	40 mL	→ adjust pH to 8.0	
dH <sub>2</sub> O	add to 1 L		
→ 1x TBE buffer: 1:10 dilution in dH <sub>2</sub> O			

### 3.5. Protein biochemical methods

Reagent/Resource	Reference or Source	Identifier (Cat#)
20 % (wt/vol) glucose solution	Thermo Fisher Scientific	A2494001
Leupeptin	Carl Roth	CN 33.2
Pepstatin A	Carl Roth	2936.1
Phenylmethylsulfonyl fluoride (PMSF)	Carl Roth	6367.2
Tris(hydroxymethyl)-aminomethan (Tris)	Carl Roth	5429.3
NaCl	Carl Roth	9265
EDTA	Carl Roth	8043.1
EGTA	Carl Roth	3054.1
NP-40	Sigma-Aldrich	I3021
Sodium dodecyl sulfate pellets (SDS)	Carl Roth	8029.3
deoxycholic acid (DOC)	Carl Roth	3484.2
Glycerol	Carl Roth	3738.1
Phosphatase Inhibitor-Cocktail 2	Sigma-Aldrich	P5726
Phosphatase Inhibitor-Cocktail 3	Sigma-Aldrich	P0044
Bromphenol blue	Serva	15375.01
Glycine	Carl Roth	3908.3
Acrylamid (AA) 30 % / Bisacrylamid (Bis AA) 0.2 % (Rotiphorese <sup>®</sup> )	Carl Roth	3029.2
Tetramethylethylenediamine (TEMED)	Carl Roth	2367.2
Ammonium persulfate (APS) 30 %	Carl Roth	9592.2
Aminocaproic acid	Sigma-Aldrich	A2504-100G
Methanol	Carl Roth	4627.5
KH <sub>2</sub> PO <sub>4</sub> ·1H <sub>2</sub> O	Carl Roth	3904.1
MgSO <sub>4</sub>	Carl Roth	P027.2
NaHCO <sub>3</sub>	Carl Roth	S5761-500g
CaCl <sub>2</sub> ·2H <sub>2</sub> O	Carl Roth	5239.1
Pierce <sup>™</sup> BCA Protein Assay Kit	Thermo Fisher	23225

### 3.5.1. Protein extraction

After euthanization (3.3.1) and isolation of hippocampi, tissue was transferred to a 2 mL reaction tube, mixed with radioimmunoprecipitation assay (RIPA) buffer and homogenized by a hand dispenser. Protein lysates were incubated for 20 min at 4 °C on a shaker, allowing proteins to solubilize. Cell debris was separated by subsequent centrifugation at 4 °C and 20.000 g for 20 min. The supernatant was transferred to a fresh reaction tube. The extracted protein lysates could be stored at -80 °C for a maximum of one week until further processing.

RIPA buffer	
Tris pH 7.4	50 mM
NaCl	150 mM
EGTA	5 mM
EDTA	10 mM
NP-40	1 %
SDS	0.05 % (wt/vol)
DOC	0.4 %
Glycerol	10 %
ddH <sub>2</sub> O	Add to 100 mL
Add directly before use	
PepA 2 mM	1:1000
PMSF 200 mM	1:1000
L/A 2 mM / 50 mM	1:10000
Phosphatase Inhibitor Cocktail 2	1:100
Phosphatase Inhibitor Cocktail 3	1:100

### 3.5.2. Determination of protein concentration

Protein concentration was determined using the Pierce™ bicinchoninic acid (BCA) Protein Assay Kit and performed according to the manufacturer's instructions. An internal standard curve consisting of increasing volumes of albumin standard (2 mg/mL) were pipetted together with protein samples into a 96-well plate in triplicates (**Table 1**). BCA reaction solution A and B were mixed at a ratio of 1:50 according to the manufacturer's instructions and 200 µL were then added to each well. The 96-well plate was incubated at 37 °C for 30 min and measured photometrically by a TECAN Sunrise plate reader at a wavelength of 492 nm. Raw data were then transferred to an Excel file. Polynomial regression of the mean values of albumin standard absorbance were used to generate calibration curve to determine protein concentration in µg/µL from the mean absorbance values of the samples. When possible, absolute protein levels were adjusted to 80 µg per

lane. If this was not possible due to low protein concentration, all samples were brought to the same highest possible protein concentration.

**Table 1: Exemplary loading order on 96-well plate for BCA assay**

	1	2	3	4	5	6	7	8	9	10	11	12
A	0	μL BSA		2 μL Sample 1			2 μL Sample 9			2 μL Sample 17		
B	0.25	μL BSA		2 μL Sample 2			2 μL Sample 10			2 μL Sample 18		
C	0.5	μL BSA		2 μL Sample 3			2 μL Sample 11			2 μL Sample 19		
D	1	μL BSA		2 μL Sample 4			2 μL Sample 12			2 μL Sample 20		
E	2.5	μL BSA		2 μL Sample 5			2 μL Sample 13			2 μL Sample 21		
F	5	μL BSA		2 μL Sample 6			2 μL Sample 14			2 μL Sample 22		
G	10	μL BSA		2 μL Sample 7			2 μL Sample 15			2 μL Sample 23		
H				2 μL Sample 8			2 μL Sample 16			2 μL Sample 24		

### 3.5.3. SDS-polyacrylamide gel electrophoresis (SDS-PAGE)

By adding the appropriate amounts of ddH<sub>2</sub>O and sample buffer (4x Laemmli in combination with dithiothreitol), protein lysates were adjusted to the calculated concentrations. Afterwards, the samples were heated to 95 °C for 5 min in a thermoblock.

4x Laemmli	
Tris	1.2 g
SDS	2.25 g
Glycerol	20 mL
Bromphenol blue	6 mg
ddH <sub>2</sub> O	ad 50 mL

### 3.5.4. Polyacrylamide gel preparation

10% polyacrylamide gels were used to separate protein lysates (prepared from Rotiphorese 30 containing 30 % of a 37.5:1 acrylamide/bisacrylamide mixture). Ammonium peroxodisulfate (APS) was used as radical to initiate polymerization while tetramethylethylenediamine (TEMED) served as a catalyst. Gels were poured into a special gel casting apparatus consisting of two glass plates separated by a small gap. The separating gel was pipetted into the gap using a 10 mL serological pipette and care was taken to ensure that all gels were filled to the same level (approximately 75 % of the glass plates height). The gel was then layered with 100% isopropanol to achieve a smooth surface without bubbles and to protect the polymerization radicals from atmospheric oxygen. After 1 h, the gel completely polymerized, and isopropanol was removed. The collection gel (3.5 %) was poured onto the separation gel and a sample comb was inserted while avoiding the formation of bubbles. To allow for complete polymerization, gels were

usually poured the day before and stored overnight at 4 °C wrapped in moist towels. For electrophoresis, glass plates containing the gels were clamped in the inner module of the electrophoresis chamber and the outer module was filled with electrophoresis buffer (ELPHOR) only to cover the electrode-connecting wire. Samples were loaded into the gel pockets using a 50 µL hamilton syringe. and a protein marker was placed in the two pockets to the right and left of the samples. All empty pockets were filled with 20 µL 1x Laemmli to achieve a uniform running front of proteins. Electrophoresis was started at 80 V and after the samples ran out of the collection gel, the voltage was increased to 120 V. Duration of electrophoresis depended on the size of the proteins to be separated.

10x Elphor buffer		10 % separation gel	
Tris	30 g	dH <sub>2</sub> O	8.5 mL
Glycine	144 g	4x Resolving Buffer	5 mL
SDS	10 g	Rotiphorese 30	6.5 mL
ddH <sub>2</sub> O	add to 1 L	Add directly before casting gel	
→ adjust pH to 8.3		TEMED	10 µL
→ 1x Elphor buffer: 1:10 dilution in dH <sub>2</sub> O		30 % APS	100 µL
3.5 % stacking gel			
dH <sub>2</sub> O	6.3 mL		
4x stacking buffer	2.5 mL		
Acrylamid 30%	1.2 mL		
Add directly before casting gel			
TEMED	10 µL		
30 % APS	100 µL		
4x resolving buffer		4x stacking buffer	
Tris	181.72 g	Tris	30.3 g
SDS	4 g	SDS	2 g
ddH <sub>2</sub> O	add to 1 L	ddH <sub>2</sub> O	add to 1 L

### 3.5.5. Western Blot

Western blot was performed in the so-called Semi Dry configuration. Before starting, filter papers and membrane had to be cut to the appropriate size first (depending on the gel size). The polyvinylidene fluoride (PVDF) membrane was briefly soaked in methanol to reduce hydrophobicity of the PVDF membrane and to achieve better saturation with transfer buffer. 3 filter papers were then soaked in anode buffer 1 and 2 filters as well as the membrane were soaked in anode buffer 2 until fully saturated. Another 5 filter papers were soaked in cathode buffer until fully saturated. After sufficient soaking and subsequent

wetting of the platinum-coated anode plate with anode buffer, the blot assembly was stacked in a sandwich-like manner. For this purpose, a stack of filter papers soaked in anode buffers 1 and 2 were placed in the center of the anode plate on top of each other. The PVDF membrane was placed on top of the filter papers soaked in anode buffer 2, while avoiding trapping air bubbles between filter papers and membrane. Collecting gel was separated from the separating gel under running water with the aid of a plastic scraper and placed on the membrane, again without trapping air bubbles in between. Gel was then covered with the stack of filter papers soaked in cathode buffer. Finally, the cathode plate, well-watered and wetted with cathode buffer, was then placed on top. The whole apparatus is weighted down with a filled 2 L glass bottle and connected to the power source. Protein transfer was performed at 110 mA for 60 min. If 2 Western blots were performed simultaneously in a blotting apparatus, current was increased to 220 mA.

Anodenpuffer 1		cathode buffer 2	
Tris	36.3 g	Tris	3.0 g
Methanol	200 mL	6-Aminocaprinsäure	5.8 g
ddH <sub>2</sub> O	add to 1 L	Methanol	200 mL
Adjust pH to 10.4		ddH <sub>2</sub> O	add to 1 L
Anode buffer 2		Adjust pH to 7.6	
Tris	3.6 g		
Methanol	200 mL		
ddH <sub>2</sub> O	add to 1 L		
Adjust pH to 10.4			

### 3.5.6. Protein detection

Membranes were incubated on a shaker for 1 h in tris-buffered saline with Tween 20 (TBST) containing 5 % BSA. After washing 3x for 5 min in 1x TBST buffer, the membrane was cut with a scalpel. This allowed parallel detection of proteins of different sizes. When cutting the membrane, the bands of the protein marker served as an orientation. The individual protein-loaded membrane strips were incubated in the respective primary antibody dilutions in 5 % BSA in TBST in 50 mL centrifuge tubes overnight at 4 °C on a test tube rotator. During this process, the primary antibodies bind to specific epitopes of the protein of interest. On the following day, nonspecifically bound as well as unbound antibodies were removed by washing 3 x 5 min with 1x TBST buffer. Subsequently, membrane pieces were incubated for 2 h in secondary antibody solution consisting of secondary antibody at the respective dilution in 5 % BSA in TBST at RT on the test tube rotator. Due to the photosensitivity of fluorescently labeled secondary antibodies, incubation was performed in 50 mL centrifugation tubes wrapped in aluminum foil. The

subsequent washing steps 3 x 5 min in TBST were also performed in the dark. Before proteins detection, membrane sections were completely dried between lint-free cloth. Protein detection was performed using an Amersham Imager 600 and ImageJ was used to evaluate and quantify the protein bands.

10x TBST	
Tris	12.1 g
NaCl	82.3 g
Tween® 20	5 mL
ddH <sub>2</sub> O	Add to 1 L
→ 1x TBST buffer: 1:10 dilution in dH <sub>2</sub> O	

### 3.5.7. cLTP induction in acute hippocampal brain slices

The mouse was euthanized (3.3.1) and the brain isolated and immediately transferred to ice-cold sucrose artificial cerebrospinal fluid (sACSF) buffer. Hippocampi were removed and cut into 400 µm thick sections with a McIlwain tissue chopper. All sections from one genotype were first collected in a Petri dish containing carbogen saturated artificial cerebrospinal fluid (ACSF). Next, an equal number of sections were distributed into a non-stimulated control group and a chemical LTP (cLTP) stimulated group for transfer to the respective cell culture inserts, each located in one well of a 24-well plate. Acute hippocampal slices of both experimental groups were first incubated in ACSF for 30 min at RT. The 24-well plate has attachments to enable the buffer to be aerated with carbogen during the whole time to maintain a stable pH due to carbonate buffering while ensuring oxygenation. In the experimental group, cLTP was induced by replacing regular ACSF with one supplemented with 20 µM Forskolin, 0.1 µM Rolipram and 50 µM Picrotoxin (FRP). In the control group, ACSF was replaced with fresh regular ACSF only. After 10 min of stimulation, the buffer was replaced with regular ACSF in both groups and incubated for an additional 10 min to wash out the drugs and therefore to terminate cLTP induction, if necessary. Finally, the acute hippocampal sections were transferred in 1.5 mL reaction tubes, briefly pelleted and the supernatant decanted so that they could undergo intermediate storage until sample preparation after snap freezing in liquid nitrogen at -80 °C. Sample preparation for protein detection by Western blot was performed as described in 3.5.5.

Sucrose ACSF		ACSF	
Sucrose	254 mM	NaCl	127 mM
KCl	1.9 mM	KCl	1.9 mM
KH <sub>2</sub> PO <sub>4</sub>	1.2 mM	KH <sub>2</sub> PO <sub>4</sub>	1.2 mM
NaHCO <sub>3</sub>	26 mM	NaHCO <sub>3</sub>	26 mM
D-glucose	10 mM	D-glucose	10 mM

MgSO <sub>4</sub>	2 mM	MgSO <sub>4</sub>	1 mM
CaCl <sub>2</sub>	1.1 mM	CaCl <sub>2</sub>	2.2 mM
saturated with 5 % CO <sub>2</sub> and 95 % O <sub>2</sub>		saturated with 5 % CO <sub>2</sub> and 95 % O <sub>2</sub>	
final pH 7.4		final pH 7.4	

## 3.6. Electrophysiology

### 3.6.1. Acute brain slices

The mouse was euthanized (3.3.1) and the brain immediately transferred to ice-cold cutting buffer. The cerebellum was separated from the forebrain using a scalpel. An adhesive strip was attached to the specimen holder plate, to which the forebrain was attached at the cut edge using cyanoacrylate glue and clamped into the vibratome. The brain was trimmed to the beginning of the hippocampus. Acute brain slices with 400  $\mu\text{m}$  thickness were made across the entire thickness of the hippocampus. Hemispheres were separated using a scalpel and transferred to a container of ACSF at RT using the wide end of a broken-off and flame-polished pasteur pipette. Brain sections were incubated in ACSF at 30 °C for 1 h before measurements and were stored at RT for the remainder of the day.

### 3.6.2. fEPSP recordings

Extracellular fEPSP were recorded as previously described (Matt et al., 2021). Slices were transferred to a recording chamber continuously perfused with oxygenated and 30 °C warm ACSF (3.5.7). Stimulating (bipolar concentric, TM53CCINS, WPI) and measuring (ACSF-filled glass pipettes, 2-3 M $\Omega$ ) electrodes were placed in the stratum radiatum to measure Schaffer collateral fEPSPs. Signals were amplified using an Axopatch 200B amplifier, digitized using a LIH 8+8 (HEKA) and recorded using WinWCP. A stimulus isolator (WPI) generated the stimuli (100  $\mu\text{s}$ ). A HFS was used to induce LTP at the same intensity used for baseline. The potentiation of LTP induced by HFS was determined by comparing the mean initial slope of fEPSP measured between 45 and 60 min after HFS with the mean initial slope of baseline fEPSP. Prior to each LTP measurement, both the input-output ratio was measured for stimulation intensities between 25-150  $\mu\text{A}$  and paired-pulse facilitation at interstimulus intervals of 10, 20, 50, 100, 200 and 500 ms was assessed for each slice at the same stimulation intensity used for the LTP measurements. Four recorded traces were averaged for each data point. Data were retrieved and analyzed using Clampfit and Excel respectively. Statistics and graphs were generated using GraphPad Prism. Two-way ANOVA was used to compare results between conditions.

### 3.7. Behavioral tests

#### 3.7.1. Open field

The open field test (OFT) was conducted in a circular arena with 112 cm in diameter and about 50 cm wall height (**Figure 4**). The area was illuminated by general ceiling lamps without any additional bright illumination. After habituation to the conditions in the test room, mice placed in the center of the open area were free to explore their surroundings without any disturbance or manipulation. Animals were left there for a maximum of 30 min while their behavior was recorded using a camera system. Walking paths were then evaluated using a video tracking system. Following the test, animals were transferred back to their home cage. After test completion, the arena was cleaned with 80% ethanol and allowed to dry for 15 min. Test were always performed at the same time of day to minimize fluctuations caused by endogenous rhythms.

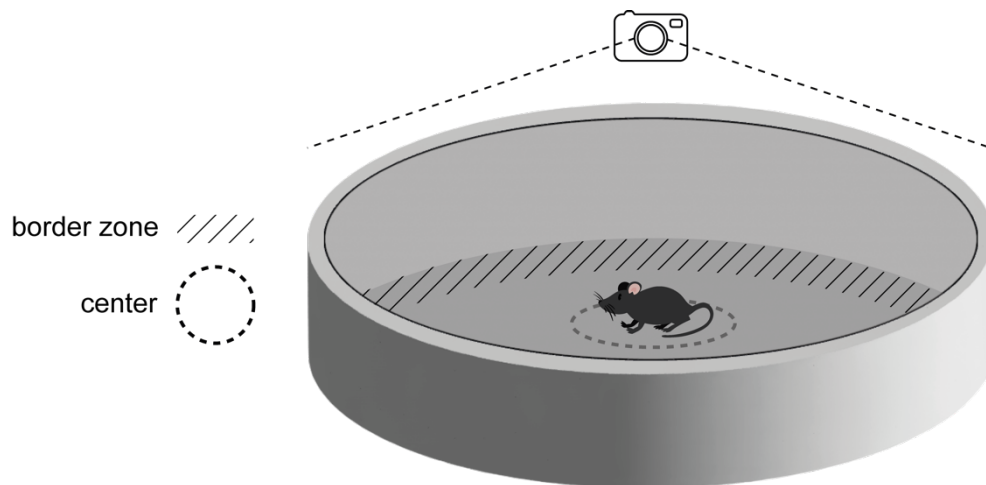


**Figure 4: Experimental set-up of the open field test.** Mice were placed in the center of a circular arena with a diameter of 112 cm and recorded for 30 min with a camera located perpendicular to the center of the arena. The arena was virtually divided into a border zone and a center. Using a video tracking software, the recorded material was analyzed, evaluating time in the center, time to enter the border zone, time in rest, distance traveled and mean speed.

#### 3.7.2. Beam walk

The beam walk test (BWT) represents a simple method to assess motor coordination and balance abilities. In this test, mice balanced 50 cm above the ground over a beam to enter a dark enclosure ("house") (**Figure 5**).

Three square beams of 28 mm, 12 mm and 5 mm in diameter and three round beams of 28 mm, 17 mm and 11 mm in diameter, each with a length of 100 cm, were used to test the mice. Markers were drawn at a distance of 10 cm from the beginning as well as from the end of the bar to indicate the evaluation range of 80 cm.

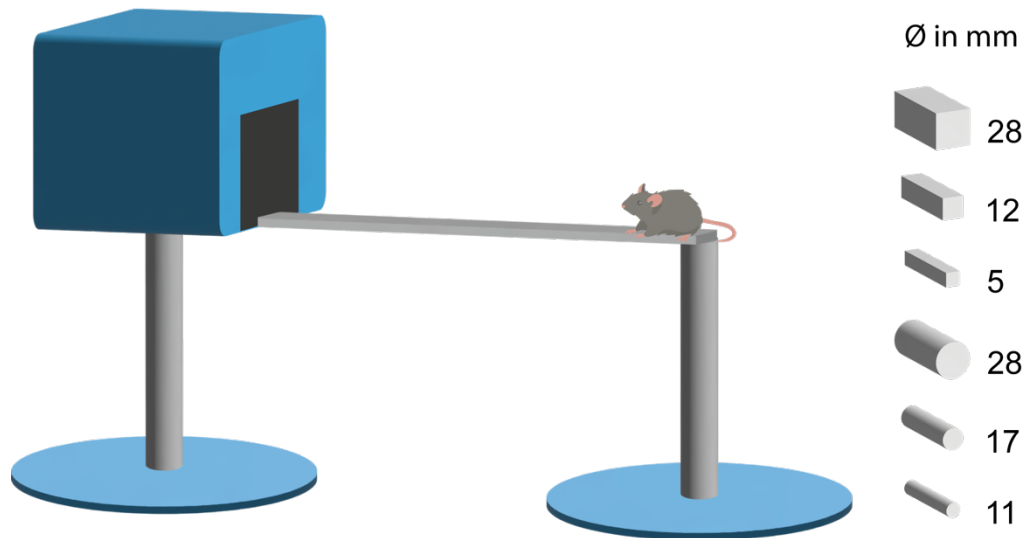


**Figure 5: Experimental set-up of the beam walk test.** Mice have to balance 50 cm above the ground over a beam to enter a dark enclosure. Three square beams of 28 mm, 12 mm and 5 mm in diameter and three round beams of 28 mm, 17 mm and 11 mm in diameter, each with a length of 100 cm, were used to test the mice. Markers were drawn at a distance of 10 cm from the beginning as well as from the end of the bar to indicate the evaluation range of 80 cm.

**Training phase:** Each mouse was trained for three days with four consecutive trials per day on the square beam of 12 mm in diameter. After the first trial, the mouse was given a slightly longer rest period in the house so that it could register it as a safe hiding place. On each trial, the animal had a maximum of 60 s to cross the bar. If the animal did not succeed in reaching the house in time, the trial was aborted and the mouse was placed in the house for a short time. After the fourth run, the mouse was placed back in its cage. Beam and house were cleaned with 80 % ethanol.

**Test phase:** Mice performed two trials for each of the six different beams. These were presented in order of decreasing diameter and thus increasing difficulty. Trials began with square beams, as these are easier for the mice to pass (Carter et al., 2001). After each square beam was crossed twice, trials were started with the round bars in order of decreasing size. Beams contaminated during runs were cleaned with 80 % ethanol.

For each mouse, time to cross the 80 cm evaluation range was measured. In parallel, the number of times the mouse slips off the beam with its hind legs (footslips) as well as failed trials were counted.

### 3.7.3. Water-Maze

A 112 cm diameter pool was virtually divided into four quadrants (northeast (NE), southeast (SE), southwest (SW) and northwest (NW)) (**Figure 6**). The pool was filled to a level of 30 cm with  $25 \pm 1$  °C warm water which was made opaque with skimmed milk powder (Millipore #70166). A transparent cylinder of 12 cm diameter was placed 0.5 cm

below the water surface and served as a platform for the mice to rest on. During the 5-day acquisition phase with 4 trials per day, experimental animals learned and remembered the hidden platform location in the SW quadrant by using visual cues in the room. Care was taken to release the mice into the pool from different, pseudorandomized deployment locations (**Table 2**). The probe trial was performed on the 6<sup>th</sup> experimental day. For this, the platform was removed and the mouse was released in the SE quadrant opposite of the platform. The percentage of time the mouse spent in the target quadrant compared to the other quadrants was evaluated for 30 s. The probe trial of the acquisition phase was immediately followed by the reversal phase on the 6<sup>th</sup> experimental day to assess memory flexibility. The quadrant of the hidden platform as well as the deployment locations were mirrored. The procedure of the entire reversal phase as well as the subsequent probe trial was conducted analogous to the acquisition phase.

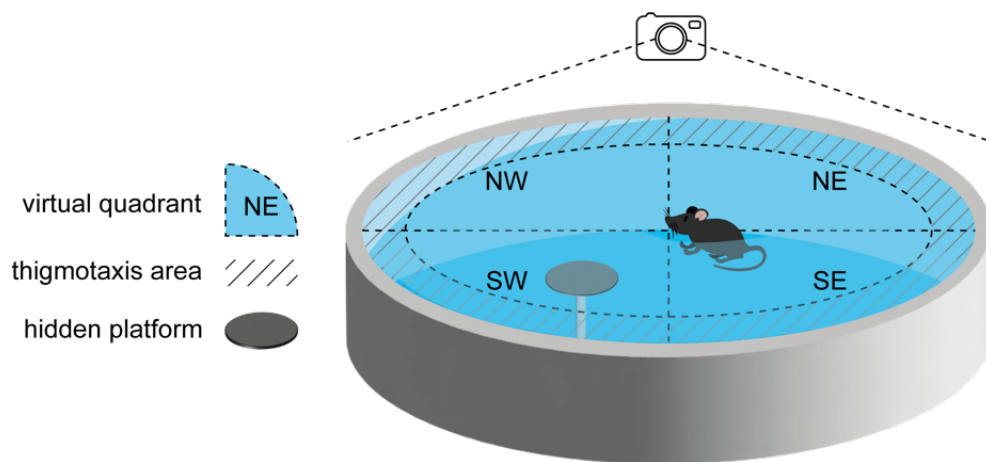


**Figure 6: Experimental set-up of the Morris Water Maze.** A pool with a diameter of 112 cm was filled with  $25 \pm 1$  °C warm water at a water level of 30 cm. The water was made opaque with skimmed milk powder. The pool was virtually divided into four quadrants. A transparent cylinder was placed 0.5 cm below the water surface in the SW quadrant during the acquisition phase and in the NE quadrant during the relearn phase. Mice were released into the pool from different, pseudorandomized deployment locations. During the probe trials, the cylinder was removed and mice were placed in the opposite quadrant of the initial target quadrant. The thigmotaxis area was located at the edge of the pool. Mice were recorded with a camera placed perpendicular to the center of the pool. The recorded material was analyzed using a video tracking software,

**Table 2: Mouse deployment locations for acquisition and reversal training during MWM**

<b>Acquisition</b>				
<b>Day</b>	<b>Trial 1</b>	<b>Trial 2</b>	<b>Trial 3</b>	<b>Trial 4</b>
1	N	E	SE	NW
2	SE	N	NW	E
3	NW	SE	E	N
4	E	NW	N	SE
5	N	SE	E	NW
6 (Probe)	NE			

## Reversal

Day	Trial 1	Trial 2	Trial 3	Trial 4
1	S	W	NW	SE
2	NW	S	SE	W
3	SE	NW	W	S
4	W	SE	S	NW
5	S	NW	W	SE
6 (Probe)	SW			

### 3.8. Single cell live imaging

Reagent/Resource	Reference or Source	Identifier (Cat#)
20 % (wt/vol) glucose solution	Thermo Fisher Scientific	A2494001
DiBAC <sub>4</sub> (3)	Thermo Fisher Scientific	B438
Forskolin	Tocris	1099
Fura-2AM	AAT Bioquest	21022
MgCl <sub>2</sub> *6H <sub>2</sub> O	Carl Roth	A537
NaCl	Carl Roth	9265
Paxilline	Tocris	2006
Picrotoxin	Sigma-Aldrich	P1675
Rolipram	Sigma-Aldrich	R6520
Nifedipine	Sigma-Aldrich	N7634
DL-AP5	Tocris	0105
Sodium pyruvate	Sigma-Aldrich	P2256
HEPES	Carl Roth	9105
D-Glucose	Sigma-Aldrich	G7528
L-Glutaminsäure	Sigma-Aldrich	G1251
KCl	Carl Roth	6781
CaCl <sub>2</sub> *2H <sub>2</sub> O	Carl Roth	5239

#### 3.8.1. K<sup>+</sup> sensitive imaging

Förster resonance energy transfer (FRET) describes a process in which the energy of the excited fluorophore (donor) is directly transferred to a second fluorophore of longer wavelength (acceptor) in spatial proximity ( $\leq 10$  nm) without radiation (**Figure 7**), i.e. not by emission and absorption (Förster, 2006). (FRET) -based recordings of  $[K^+]_i$  were performed as previously described (Ehinger et al., 2021).

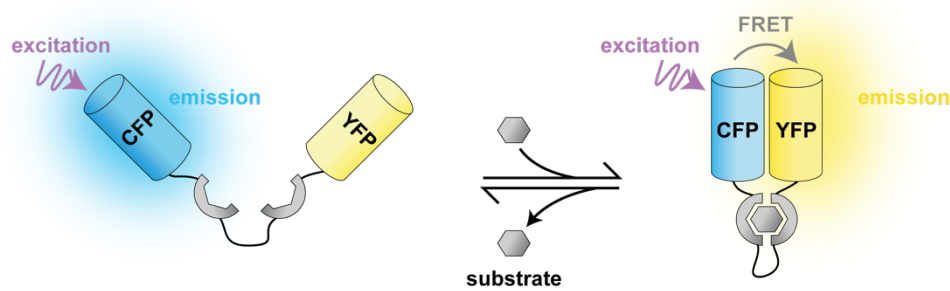


**Figure 7: Simplified model of FRET-based biosensors.** FRET-based biosensors consist of a donor fluorophore and an acceptor fluorophore. In this example, the donor is CFP and the acceptor is YFP. Donor and acceptor flank the binding site by using linkers. In the unbound state, the donor is excited and subsequently emits light. When the ligand binds to the binding site, a conformational change occurs, which leads to spatial approximation of the donor to the acceptor. This results in a radiation-free energy transfer from donor to acceptor and the emission wavelength of the acceptor is now detectable.

Neurons were seeded onto 30 mm coverslips. A cytosol targeted  $K^+$  sensitive low-charge LysM (Ic-LysM) the genetically encoded potassium ion indicator (GEPII) 1.0 FRET-based biosensor (Bischof et al., 2017) was introduced after DIV 7 into the neurons by transducing at a multiplicity of infection of 100 with an adeno associated virus -DJ/8 vector system under control of a CAG promoter, which was kindly provided by Prof. Dr. Plesnila (Ludwig-Maximilians-University Munich). After DIV 9, coverslips were mounted in a perfusion chamber (PC30, NGFI GmbH, Graz, Austria), perfused with imaging buffer through a gravity-based perfusion which was also used for drug application. Single cell live imaging was conducted on a Zeiss Observer Z.1 (Wetzlar, Germany) connected to an external light source (2200114 LED-Hub, Omicron Laserage, Rodgau-Dudendorf, Germany) and a Plan-Neofluar 40x/1.30 Oil immersion. Using an Optosplit II (Cairn Research, Faversham, UK) emissions were simultaneously collected at 480 and 535 nm. Emissions were recorded using a 459/526/596 dichroic with a 475/543/702 emission filter (AHF Analysentechnik, Tuebingen, Germany). The LED hub (Omicron Laserage, Rodgau-Dudendorf, Germany) contained a 340 nm, 380 nm and 455 nm, LED with 340x, 380x and 427/10 bandpass filters, respectively (AHF Analysentechnik, Tübingen, Germany). Images were recorded using a pco.panda 4.2 bi sCMOS camera (pco., Kelheim, Germany). To control the microscope and acquire images VisiView software (Visitron Systems, Puchheim, Germany) was used. If drugs were used to modulate cLTP, neurons were incubated with the drug at RT for 10 min before the start of the actual measurement. Emission signals from FRET and cyan fluorescent protein (CFP) were background corrected and used to calculate the FRET/CFP ratio, which is proportional to  $[K^+]_i$ . The first 5 min of measurements were used to determine basal ratios and for normalization.

Imaging buffer	
NaCl	126.5 mM
KCl	5 mM

Sodium pyruvate	10 mM
HEPES	10 mM
D-Glucose	30 mM
MgCl <sub>2</sub>	2 mM
CaCl <sub>2</sub>	2 mM

---

final pH 7.4

---

### 3.8.2. Ca<sup>2+</sup> imaging

DIV 9 neurons were loaded with 2.5 µM of the ratiometric dye Fura-2AM for 20 min at 37 °C in IB. This was followed by a wash step for 10 min at RT in IB. Using the same setup as for 3.8.1, induced emissions were recorded at 340 nm (Ca<sup>2+</sup> bound to Fura-2) and 380 nm (free Ca<sup>2+</sup>). Spikes of at least 10 % of the height of the glutamate peak were included in the analysis.

### 3.8.3. DiBAC<sub>4</sub>(3) imaging

DIV 9 neurons were loaded with a 1:40,000 dilution of a 10 mg/mL stock of a slow-response membrane potential-sensitive probe Bis-(1,3-dibutylbarbituric acid)trimethine oxonol dye (DiBAC<sub>4</sub>(3)) for 30 min at RT in IB. Every buffer used during measurement was supplemented with the indicated concentration of DiBAC<sub>4</sub>(3) as well. Using the same setup as for 3.8.1, induced emissions were recorded at 516 nm.

### 3.8.4. Software used

Software	Company	Source
Office 365	Microsoft	<a href="https://www.office.com">https://www.office.com</a>
Illustrator 27.0	Adobe	<a href="https://www.adobe.com/de/products/illustrator.html">https://www.adobe.com/de/products/illustrator.html</a>
ImageJ 1.53v	NIH	<a href="https://imagej.nih.gov/ij/index.html">https://imagej.nih.gov/ij/index.html</a>
Origin Pro	OriginLab	<a href="https://www.originlab.com/origin">https://www.originlab.com/origin</a>
Panlab Smart 3.0	Harvard Apparatus	<a href="https://www.panlab.com/en/products/smart-video-tracking-software-panlab">https://www.panlab.com/en/products/smart-video-tracking-software-panlab</a>
pCLAMP 10.7	Molecular Devices	<a href="http://www.moleculardevices.com/products/software/pclamp.html">http://www.moleculardevices.com/products/software/pclamp.html</a>
Prism 9.5.1	GraphPad	<a href="https://www.graphpad.com/scientific-software/prism/">https://www.graphpad.com/scientific-software/prism/</a>
VisiView	Visitron Systems	<a href="https://www.visitron.de/products/visiviewr-software.html">https://www.visitron.de/products/visiviewr-software.html</a>
WinWCP 5.7.1	University of Strathclyde Glasgow	<a href="https://spider.science.strath.ac.uk/sipbs/software_ses.htm">https://spider.science.strath.ac.uk/sipbs/software_ses.htm</a>
Zen Lite 2.6	Zeiss	<a href="https://www.zeiss.de/mikroskopie/produkte/mikroskopsoftware/zen-lite.html">https://www.zeiss.de/mikroskopie/produkte/mikroskopsoftware/zen-lite.html</a>



## 4. Results

### 4.1. T29.1-Cre specifically removes BK from CA1

Impaired memory acquisition was previously described in global BK<sup>-/-</sup> (Typlt et al., 2013) which are known to suffer from debilitating cerebellar ataxia (Sausbier et al., 2004). To ensure that the impaired memory acquisition is indeed due to reduced cognitive performance and not to impaired motor abilities caused by cerebellar ataxia, conditional BK knockout mice were generated. In these the pore-forming BK $\alpha$  subunit is specifically ablated in CA1 pyramidal cells using the T29.1-Cre driver mouse (Tsien, Chen, et al., 1996). In this context, the transgenic subline in which the Cre recombinase is expressed under control of the CaMKII $\alpha$  promoter was crossed with mice possessing floxed BK $\alpha$  (BK<sup>fl/fl</sup>) (Sausbier et al., 2004) or BK null (BK<sup>+/-</sup>) alleles to obtain controls (T29.1-Cre<sup>tg/+</sup>; BK<sup>fl/+</sup>; CTRL) and conditional knockouts (T29.1-Cre<sup>tg/+</sup>; BK<sup>fl/-</sup>; cKO) in the F2 generation. To verify that BK expression is normal in CTRL and to show that BK ablation in cKO is efficient and restricted to hippocampal CA1 pyramidal cells, genotyping, Western blot and immunofluorescence staining was employed.

Genotyping PCR was used in T29.1-Cre<sup>tg/+</sup>; BK<sup>fl/+</sup> animals to check whether recombination of the floxed BK (BK<sup>fl</sup>) to the BK knockout (BK<sup>-</sup>) allele occurred exclusively in the hippocampus. First, DNA was isolated from different organs and amplified using PCR and primers specific for BK<sup>fl</sup>, BK wildtype (BK<sup>+</sup>) and BK<sup>-</sup>. After separation of the amplified DNA by a 2% agarose gel electrophoresis, recombination of the BK<sup>fl</sup> allele (577 bp) to a BK<sup>-</sup> allele (132 bp) was clearly observed in the hippocampus (**Figure 8A**). Faint additional recombination could also be detected in the cortex. As expected, no recombination was detected in cerebellar and heart tissue where only the BK<sup>fl</sup> and BK<sup>+</sup> alleles were detected (**Figure 8A**). This confirms hippocampus specific Cre activity.

To check whether this finding on the DNA level was also reflected on the protein level, whole hippocampi were lysed and examined for BK expression by Western blot. Compared to CTRL, cKO showed a significant reduction of BK immunoreactivity in whole hippocampal lysates (**Figure 8B and C**). To verify the specificity of the antibody, BK<sup>+/+</sup> and BK<sup>-/-</sup> hippocampi were co-analyzed in the same gel. As expected, strong expression was found in the BK<sup>+/+</sup> samples, but completely absent in the BK<sup>-/-</sup> samples. The antibody thus proved to be of suitable specificity for this type of analysis. Since only whole hippocampal lysates could be analyzed by Western blot, no conclusions could be drawn whether the BK recombination exclusively happens in the CA1 region. Thus, to achieve a cellular resolution of BK expression, immunofluorescence staining against the channel was carried out in brain cryosections. In the CA1 region, complete ablation of the pore-forming BK $\alpha$  in the cKO could be observed (**Figure 8D**), while in CA3 and DG only a slight decrease in BK $\alpha$  protein levels was detectable. As expected, all three regions showed strong fluorescence signals for BK in samples obtained from CTRL. No expression could be detected in the global BK<sup>-/-</sup>, again confirming the specificity of the present immune-based analysis.

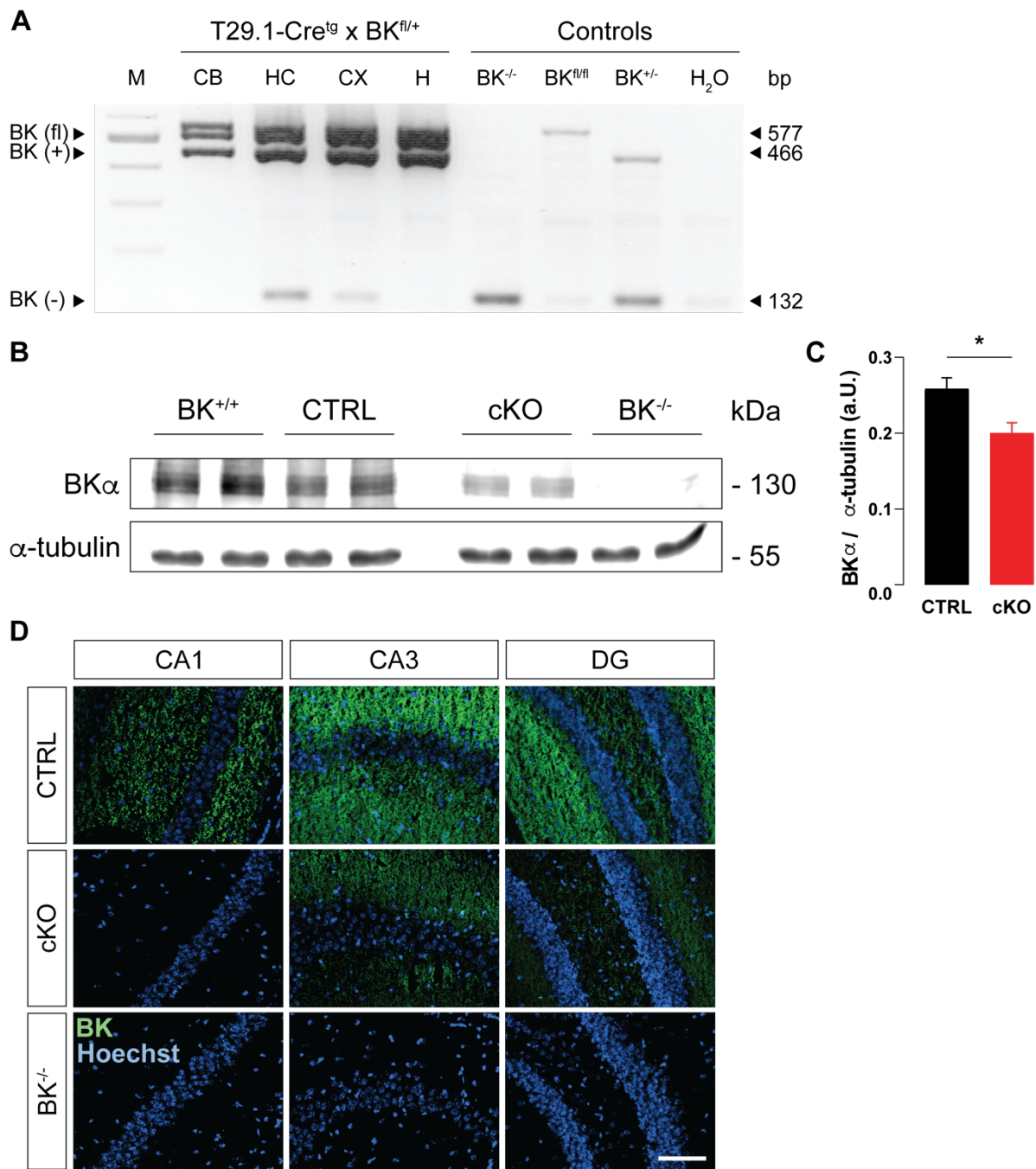


**Figure 8: Hippocampal CA1 region-specific Cre-mediated BK recombination verified at transcriptional and protein level.** Hippocampal tissue samples were collected from CTRL and cKO. Specificity of recombination of floxed BK alleles by T29.1-Cre was evaluated at transcriptional and protein levels by PCR, Western blot and immunofluorescence analysis. **(A)** DNA from different tissues of T29.1-Cre<sup>tg/+</sup>, BK<sup>fl/+</sup> was isolated, amplified by PCR and separated by agarose gel electrophoresis. As expected, the BK WT allele was detected at 466 bp in all samples. Recombination from the floxed ([fl], 577 bp) to the null allele ([-], 132 bp) was observed mainly in the hippocampus (HC) and to a minor extent in the cortex (CX). No recombination was detected in the cerebellum (CB) or heart (H). Respective tissues obtained from BK<sup>-/-</sup>, BK<sup>fl/fl</sup> and BK<sup>+/-</sup> as well as water served as internal controls. N = 3 independent experiments from N = 3 animals. PCR was performed by Stefanie Simonsig (M.Sc., Experimental pharmacology, University of Tübingen). **(B)** Western blot analysis of BK $\alpha$  abundance in 80  $\mu$ g total protein of whole hippocampal lysates. BK $\alpha$  expression is visibly lower in cKO compared to CTRL. Co-analysis of BK<sup>+/+</sup> and BK<sup>-/-</sup> samples verified primary antibody specificity.  $\alpha$ -Tubulin is used as a loading control. Western blot was

performed and quantified by Daniel Kalina (M.Sc., Experimental pharmacology, University of Tübingen). **(C)** Densitometric quantification of BK band intensity in B normalized to  $\alpha$ -tubulin. **(D)** Representative immunofluorescence images of CTRL, cKO and BK<sup>-/-</sup> cryosections stained against the pore-forming subunit BK $\alpha$  (green). Nuclei were counterstained with Hoechst (blue). No BK $\alpha$  expression was detected in the CA1 region of cKO, while its expression was reduced in CA3 and DG. The suitability of the primary antibody is confirmed by the immunoreactivity in all three regions in BK<sup>+/+</sup> and its absence in BK<sup>-/-</sup>. Scale bar: 100  $\mu$ m. Immunofluorescence staining was performed by Stefanie Simonsig (M.Sc., Experimental pharmacology, University of Tübingen). Statistics: Unpaired Student's t-test. All bar diagrams presented as means  $\pm$  SEM. See also **Table 3: Values and statistics for Figure 8**. Adapted from (Pham et al., 2023).

## 4.2. cKO display normal anxiety and locomotor behavior

Fear behavior and locomotor abilities can influence murine learning behavior. The MWM is a behavior-based learning experiment that depends on the assessment of movement parameters. Therefore, alteration of movement behavior (either by anxiety or by locomotor impairment) can lead to differences that might incorrectly be interpreted as changes in cognitive performance. Anxiety triggers stress, which has additional negative effects on cognitive functions such as learning and memory (Nascimento et al., 2022). In the case of altered locomotor activity, swimming could be disturbed due to uncoordinated and thus slower swimming movements. To exclude both possibilities, CTRL and cKO were first evaluated in the OFT. For this purpose, mice were released in the middle of a round arena (**3.7.1**). The entire procedure was recorded for 30 min with a camera positioned perpendicularly above the center of the arena. By analyzing the video material with PanLab, mice can be followed virtually. On the one hand, the OFT is used to analyze fear behavior; on the other hand, it is also a simple test for assessing motor performance. The OFT makes use of the mice's instinct to avoid large, open and well-lit areas in order to avoid predators. However, they also explore the environment to forage for food sources and to be prepared for possible dangers (Ennaceur, 2014). In the beginning, the mouse's behavior is dominated by the novelty of the environment. The longer the test persists, the more the general activity is tested. To better represent the two phases of the OFT, data were divided into different observation intervals, 0 – 5 and 5.01 – 30 min (Gould et al., 2009). For completeness, the data were also presented for the entire 30 min. Both the percentage of time spent in the central zone (**Figure 9A**) and the first entry into the peripheral zone (**Figure 9B**) do not differ between the two genotypes. This indicates similar exploratory drive and fear behavior. The rearings (**Figure 9E**) which correspond to exploratory drive are also comparable in both genotypes. Measures for general activity like time in rest (**Figure 9C**), total distance travelled (**Figure 9D**) and mean movement speed (**Figure 9F**) did not differ either.

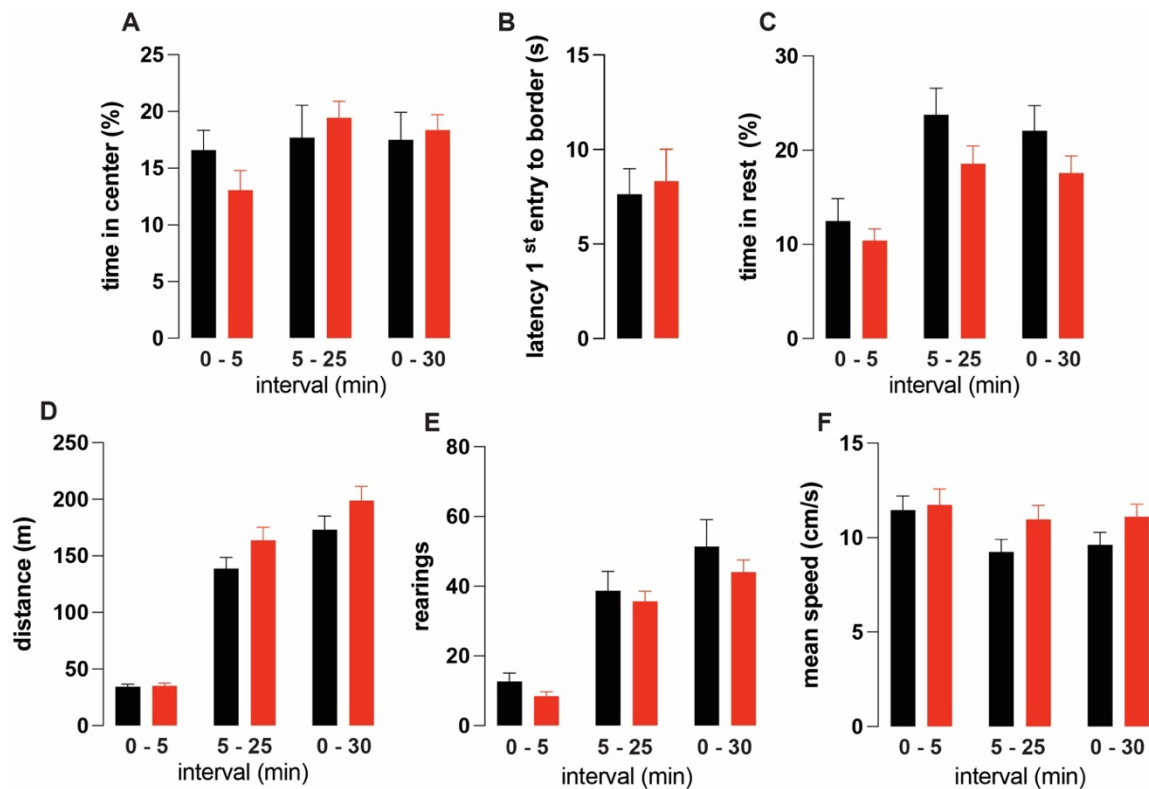


**Figure 9: Comparable anxiety and locomotor activity in CTRL and cKO.** Anxiety-related behavior and locomotor activity of cKO (N = 15) were investigated in comparison to CTRL (N = 14) using OFT and beam walk. During the 30-minute observation period, no differences were found in (A) time in center, (B) latency of 1<sup>st</sup> entry to border (C) time in rest (D) distance travelled, (E) rearings and (F) mean speed. OFT was performed by Stefanie Simonsig (M.Sc., Experimental pharmacology, University of Tübingen). Statistics: Two-way ANOVA with Sidak's multiple comparison test. All bar diagrams presented as means  $\pm$  SEM. See also **Table 4: Values and statistics for Figure 9.** Adapted from (Pham et al., 2023).

So far, these data do not indicate that lack of BK in CA1 causes abnormal anxiety behavior and motor abilities. Therefore, we continued our examination of cKO locomotor abilities in additional detail using the more demanding BWT with the mice. In this test, mice have to balance a distance of 80 cm over three beams of a square and three of a round cross-section, which are presented in descending order of difficulty (3.7.2). Each beam was crossed twice and the resulting values were averaged. The values were presented for each bar individually (Figure 10A – C) as well as averaged for all square or all round bars respectively (Figure 10D – F). Across all beams, CTRL and cKO exhibit comparable number of falls. Only on the square beam with 28 mm edge length did the cKO fall more often than the CTRL. These falls, however, did not amount to a statistically significant difference (Figure 10A). Looking at summary values, the CTRL fell less often from the square bars, while the cKO fell less from the round bars (Figure 10D). By not reaching statistical significance, this trend is negligible, especially since there is no difference after both bars are combined. Also for foot slips, there was no difference between the two genotypes for most bars and diameters, except for the smallest square bar, 5 mm in diameter, where the cKO slipped significantly more often (Figure 10B). This effect can be

neglected as this is only the second most difficult bar. At the most difficult bar, the round bar of 11 mm diameter, again no difference was detectable between both genotypes. Accordingly, the summarized data confirmed no difference in multiple beam crossing parameters for cKO vs CTRL mice (**Figure 10F**). A slight tendency towards faster performance of the cKO was noted when the latency to cross the bars were assessed (**Figure 10C**). Accordingly, for the most difficult two bars, 5 mm square and 11 mm round, did the cKO take a slightly longer time to cross. This is also confirmed in the summarized data set on the time that it took to pass the test (**Figure 10E**). However, none of the small differences observed were statistically significant. The more complex beam walking test also confirms comparable fine motor coordination and balance ability, as there were no differences in the frequency of falls and slips (**Figure 9E and F**).

Thus, both the OFT and BWT results confirm that cKO mice display comparable anxiety levels and motor controls as CTRL and thus are suitable for the MWM behavioral learning experiment.

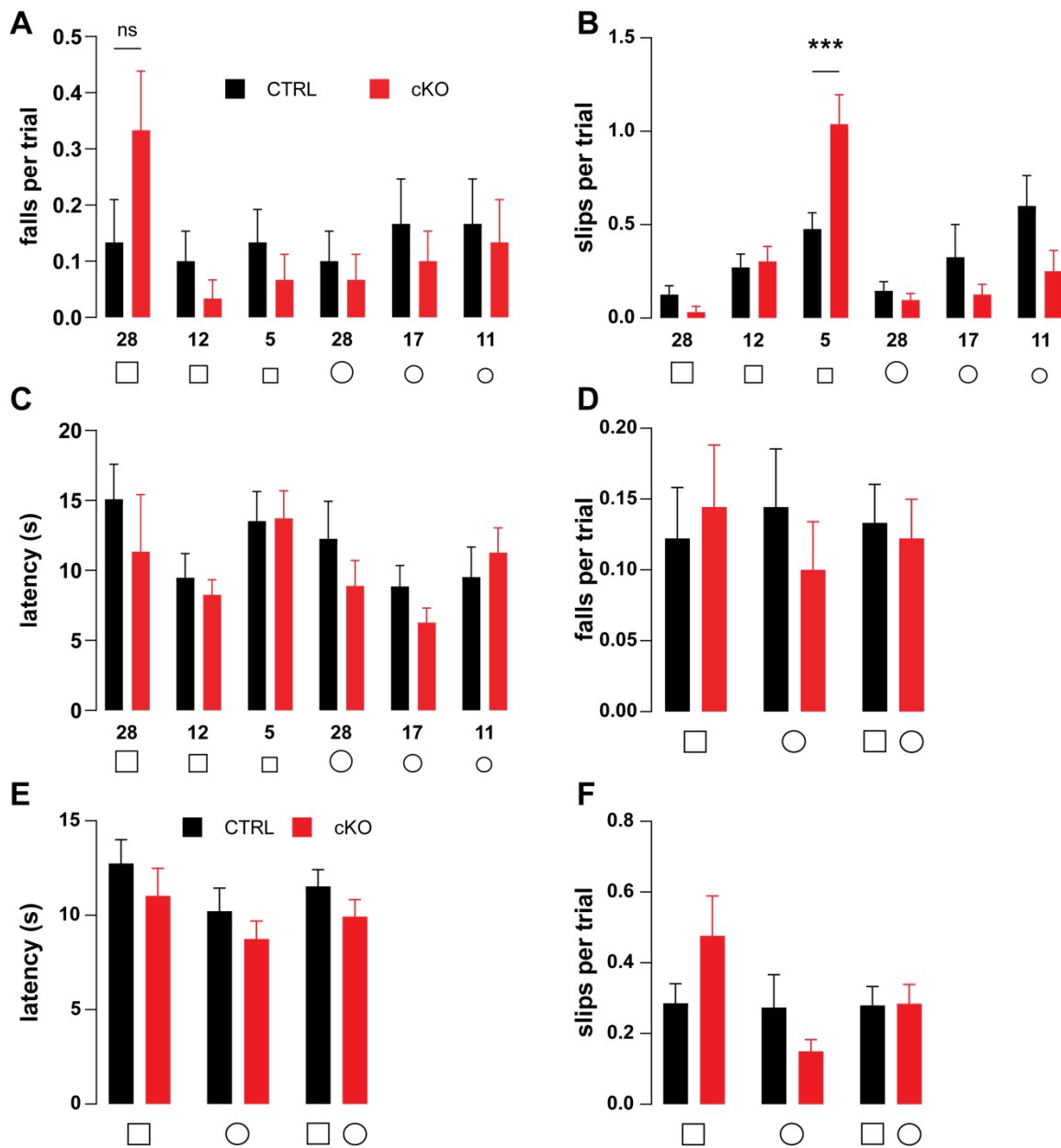


**Figure 10: Comparable locomotor ability between both genotypes.** Detailed data for individual bars (A-C) as well as mean values for all diameters of the square bar (28, 12, 5 mm), the round bar (28, 17, 11 mm) or both bar types (D-F). When crossing an 80 cm square or round cross-section bar, no differences were found in (A) falls per trials. (B) Slips per trial for the 5 mm square bar was significantly increased in cKO, while for the other bars slips per trial were comparable for both genotypes including the more difficult 12 mm round bar. (C) Latency was comparable between genotypes for all bars. When the data for the square, round and both bar types are combined, no difference could be found in (D) falls per trial (E) latency (F) slips per trial. BWT was performed by Stefanie Simonsig (M.Sc., Experimental pharmacology, University of Tübingen). Statistics: N = 8 – 15, Two-way ANOVA with Sidak's multiple comparison test. All bar diagrams presented as means  $\pm$  SEM. See also **Table 5: Values and statistics for Figure 10.** Adapted from (Pham et al., 2023).

### 4.3. Hippocampal BK supports memory acquisition and retrieval

As already stated several times, a delayed learning phenotype was previously demonstrated in global  $BK^{-/-}$  who tried to solve the MWM task (Typlt et al., 2013).  $BK^{-/-}$  exhibited a longer latency to reach the hidden platform during the 5-day acquisition phase. However, these results may be biased due to the cerebellar ataxia of global  $BK^{-/-}$  (Sausbier et al., 2004) which leads to abnormal locomotion and pronounced motor coordination deficits in the mice. The conditional knockout of BK in the spatial learning center, the hippocampus, with unchanged expression of BK in the cerebellar purkinje cells was designed to ensure that results from behavioral learning experiments, such as the MWM, were indeed related to the role of BK in the learning performance of the mice. Over the 5 training days of the acquisition phase with 4 learning trials per day (3.7.3), latency from entering the pool to reaching the platform decreased in both CTRL and cKO, indicating functional memory acquisition (Figure 11A). However, already on the first day over 4 runs, cKO required 5 s more to reach the platform. This delayed learning in comparison to CTRL continued to the end of the acquisition period on day 5. The subsequent probe trial served to test the stability of the memory formed during the training period. To this end, the platform was removed and the time the mice spent in the 4 different quadrants, especially the target quadrant was quantified (Figure 11B). Although latency to the original platform location was reached by both genotypes in a comparable latency (Figure 11C, left), time of stay in the virtual quadrants was different. While CTRL spent most of their time in the target quadrant, cKO spend similar amounts of time in all quadrants. Consistently, CTRL stayed significantly longer in the northeastern target quadrant, in contrast to cKO which stayed significantly longer in the opposite southwestern quadrant (Figure 11B). Interestingly, the CTRL preferred the northeastern target quadrant over all others, in contrast to the cKO which do not seem to prefer any particular quadrant. This generally suggests that the cKO have greater difficulty in recalling what they have learned than CTRL. This assumption is again confirmed by the representative swimming paths during the probe trial, as the swimming path of the CTRL is mostly located in the target quadrant, but that of the cKO is evenly distributed throughout the arena (Figure 11D). In addition to time in quadrant, target crossings and thigmotaxis were evaluated during probe trial as well. Like time in quadrant, target crossings and thigmotaxis are alternative measures for memory retrieval (Brooks et al., 2017; Gehring et al., 2015). Thigmotaxis describes the behavior of the mouse to swim close to the edge of the pool while circling the perimeter and is often reported as percentage of time. Thigmotaxis often occurs at the beginning of the training phase and is considered a passive search strategy that should decrease towards the end of the probe trial when a proactive, goal-oriented search strategy is developed (Gehring et al., 2015). Thus, increased thigmotaxis indicates impaired memory consolidation. Indeed, a slight tendency towards less frequent crossing of the virtual platform (Figure 11C, center) and increased thigmotaxis (Figure 11C, right) could be detected in the cKO, which is consistent with the constrained memory retrieval. None of these differences, however, was statistically significant.

Another  $K^+$  channel important for synaptic plasticity, also like BK, is the sodium-activated sequence like a  $Ca^{2+}$ -activated  $K^+$  channel (Slack), which was shown to play an essential role in physiological memory flexibility (Bausch et al., 2015). In the work of Typlt et al. the global  $BK^{-/-}$  were tested only for memory acquisition. This led to the postulation that BK channel may also support memory flexibility, which is why a reversal phase was conducted, directly subsequent to the acquisition phase. Memory flexibility supports the cognitive process of adaptation to new circumstances. To replicate this in the MWM, the hidden platform and the pseudorandomized deployment sites were moved to the opposite side of the pool. This requires mice to adapt to the fact that the already learned location is no longer the target and to adjust by developing a new search strategy to locate the new target quadrant under unchanged conditions. Although the new location of the target quadrant is now in the opposite south-western quadrant, mice of both genotypes are able to find the platform equally fast on all days (**Figure 11E**). It is noticeable that the learning curve is no longer as steep as in the acquisition phase. This is probably due to the fact that mice have already become accustomed to the experiment and know immediately from the previous probe trial that the platform is no longer necessarily located in the north-eastern quadrant. In the subsequent probe trial, both CTRL and cKO reached the virtual platform in a similar latency (**Figure 11G, left**) stayed significantly longer in the southwestern target quadrant than in the opposite northeastern quadrant (**Figure 11F**), indicating successful adaptation of platform relocation and thus correct execution of the protocol. However, in contrast to the acquisition phase, no significant difference in learning performance between the genotypes was observed in either the reversal phase or the subsequent probe trial. This observation matches with the comparable virtual target crossings (**Figure 11G, center**) and thigmotaxis (**Figure 11G, right**) as both were comparable as well. In brief, memory acquisition and retrieval are impaired in cKO but cognitive flexibility of both genotypes is comparable.

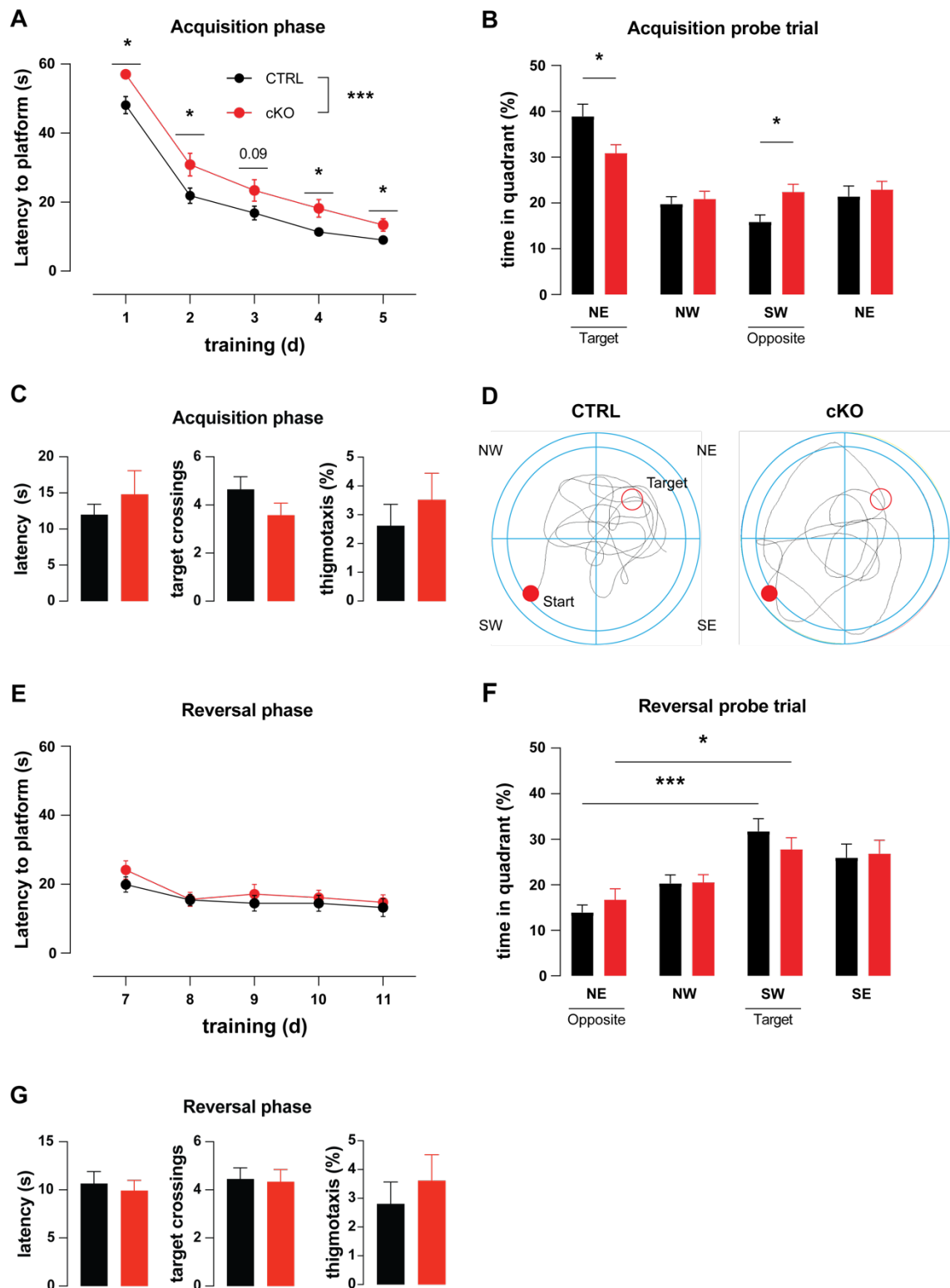


**Figure 11: cKO display impaired memory acquisition and retrieval in the MWM. (A)** Over 4 trials per day, cKO (N = 21) consistently required more time than CTRL (N = 20) to find the hidden platform in the NE quadrant. **(B)** The hidden platform was removed to determine memory retrieval performance in a probe trial of acquisition. cKO remained significantly shorter in the target quadrant and longer in the opposite quadrant compared to the CTRL. **(C)** During probe trial acquisition, latency to virtual platform (left), target crossings (center) over the virtual platform and time spent in the virtual border zone (thigmotaxis, right) were comparable between CTRL and cKO. **(D)**

Representative swim trajectories during the probe trial show that CTRL developed a goal-directed search strategy (red empty circle), whereas cKO kept randomly swimming through the arena after deployment (red filled circle). **(E)** Memory flexibility was determined by changing the hidden platform location and adjusting the pseudorandomized insertion points. No difference in latency to the platform was found. **(F)** In a probe trial for the reversal phase, both CTRL and cKO spent significantly more time in the target quadrant than in the opposite quadrant. However, the time spent in the target and opposite quadrants was comparable between genotypes. **(G)** During the reversal probe trial, latency to virtual platform (left), target crossings (center) over the virtual platform and time spent in the virtual border zone (thigmotaxis, right) were comparable. MWM was performed by Stefanie Simonsig and Daniel Kalina (M.Sc., Experimental pharmacology, University of Tübingen). Statistics: Two-way ANOVA with Sidak's multiple comparison test (**A, B, E, F**), unpaired Student's t-test (**C and G**). All diagrams presented as means  $\pm$  SEM. See also **Table 6: Values and statistics for Figure 11**. Adapted from (Pham et al., 2023).

#### 4.4. Learning and memory during the process of aging

In general, old age is associated with a decline in cognitive performance and is the main risk factor for various forms of dementia. The hippocampus is a brain region essential for normal functioning memory. During aging, the number of primary hippocampal glutamatergic neurons counted stereologically in humans, monkeys or rats does not change significantly (Morrison & Hof, 1997). It is therefore consensus that the age-related impairment of memory is probably due to impaired synaptic plasticity.

Previous studies have shown that the expression of BK channels and their regulatory  $\beta 1$ -subunit in coronary arteries declines dramatically in an age-dependent manner (Marijic et al., 2001; Nishimaru et al., 2004). Age-related decline in BK activity in neurons of the suprachiasmatic nucleus (Farajnia et al., 2015) and dorsal spinal ganglia (Yu et al., 2015) furthermore correlates with age-related deficits. It therefore stands to reason that there is also an age-related reduction in BK activity in hippocampal neurons.

##### 4.4.1. Aged cKO mice display normal anxiety levels

Since age can influence anxiety behavior and locomotor abilities, the suitability for the MWM test must also be tested for the aged mice in the OFT and BWT. Again, the results of the MWM can only be correlated with learning behavior if anxiety behavior and locomotor activity are comparable between the two genotypes.

Time in rest, total distance, and mean speed (**Figure 12A-C**) are activity markers and, as previously mentioned, indicate the locomotor characteristics of the mouse. Time in rest indicates that mice show increased activity during the first 5 min of the trial compared to the following 25 min. This represents a higher exploratory behavior at the beginning of the trial, as the arena represents new territory for the mouse and therefore the mouse's interest to explore the new environment is aroused. Since the arena could already be explored in the first 5 min, the interest is not as high in the next 25 min which is represented in the increased percentual time in rest for the 5 – 25 min interval. No difference between the two genotypes can be detected, neither in the first 5 min, nor in the next 25 min or if the

whole interval is considered. This indicates a comparable explorative behavior. What also correlates with increased activity and exploratory behavior besides the decreased resting time in the first 5 min is the average speed (**Figure 12E**). Thus, a higher mean speed can also be observed in the first 5 min compared to the subsequent 25 min. Considering all three intervals, a trend toward higher mean velocity of cKO became apparent. However, the difference is not statistically significant, leading to a comparable exploratory behavior between the two genotypes. Analogous to mean speed, a trend toward longer distance traveled in the cKO compared with the CTRL can be observed (**Figure 12D**). Again, the trend does not reach statistical significance, so this also indicates comparable locomotor activity of aged cKO vs CTRL mice. Since in the OFT all parameters point to similar locomotor activity and anxiety behavior, this suggests that advanced age does not lead to changes, at least in the OFT. This enabled us to evaluate the aged mice in the more complex BWT.

Comparing the performance of the aged animals with that of the young animals), the reduced time spent in the center and the reduced latency to first entry into the border zone were surprisingly lower in the aged cohort (**Figure 12A and B**) than in the young (**Figure 9A and B**), indicating reduced anxiety behavior. As expected, the time in rest was almost twice as high in the aged cohort (**Figure 12C and Figure 9C**), and the distance (**Figure 12D and Figure 9D**) and mean speed (**Figure 12E and Figure 9F**) correspondingly lower. With advanced age, this could either be due to a limited locomotor system, a reduced motivation to move or a reduced explorative behavior. As there are no significant differences between the two genotypes in the aged cohort, the observed differences affect both genotypes equally and are not relevant for further experiments.

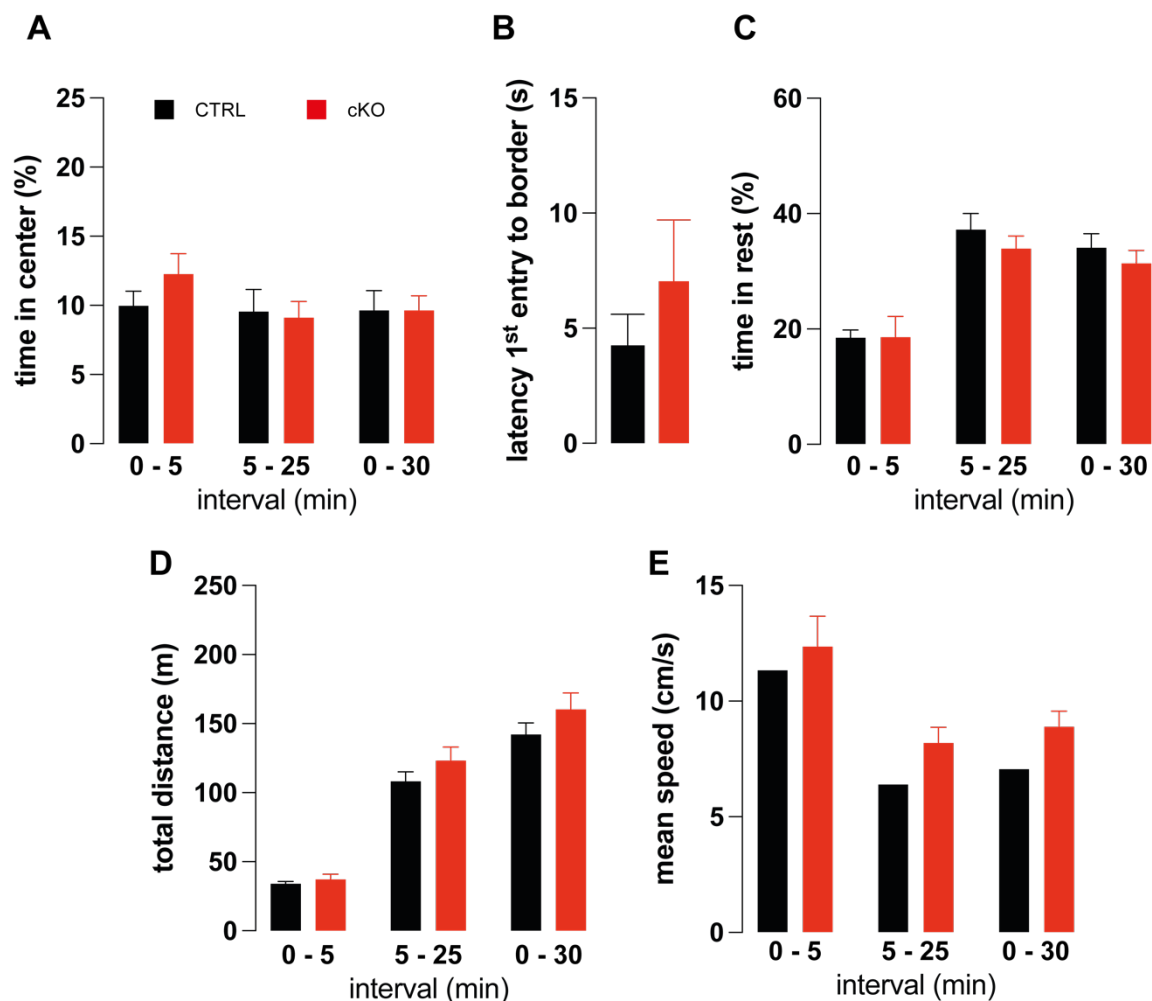


**Figure 12: Comparable locomotor activity and anxiety behavior of aged CTRL and cKO mice.** The fear behavior and locomotor activity of aged cKO (N = 5) compared to aged CTRL (N = 10) was investigated using OFT and BWT. During the 30-minute observation period, no differences were found in (A) time in center, (B) latency of 1<sup>st</sup> entry to border (C) time in rest (D) distance travelled and (E) mean speed. Statistics: Two-way ANOVA with Sidak's multiple comparison test (A, C, D, E), Unpaired Student's t-test (B). All bar diagrams presented as means ± SEM. See also **Table 7: Values and statistics for Figure 12.**

#### 4.4.2. Locomotor activity of aged cKO mice is unaltered

To test whether advanced age has an influence on the ability to balance and thus on locomotor skills, 12-month-old mice had to complete the BWT. The procedure is performed analogous to young animals (3.7.2). While it appears that cKO produce, per trial, more falls from the 28 mm and 12 mm square bar, CTRL fell more frequently from the 5 mm square and 28 mm round bar (Figure 13A). However, differences were not sufficient to reach statistical significance for any of the aforementioned comparisons. No cases occurred with the 17 mm and 11 mm round bars. No trend was discernible in the summarized data (Figure 13D) either. Also slips per trial were equally distributed between genotypes (Figure 13B). CTRL slipped less frequently on the 28 mm round and square

bars and on the 12 mm square and 11 mm round bars. In contrast, the cKO performed better on the 5 mm square and 17 mm round bars. However, there was no statistical significance here either, which can also be observed in the summarized data (**Figure 13F**), as for once the CTRL performed better on the square bars and the cKO on the round bars. If both bar types are combined, number of slips are identical between genotypes. For cKO a tendency towards shorter latency times could be observed for the individual values (**Figure 13C**) for all bar types and sizes as well as for the combined values. Since differences in consolidated data were not statistically significant as well (**Figure 13E**), it can be concluded that the locomotor activity of the two genotypes is comparable despite the test subject's advanced age.

When comparing the aged cohort (**Figure 13**) with the younger one (**Figure 10**), it was found that the aged animals fell less frequently during the BWT (**Figure 13D and Figure 10D**) and crossed the bar in a shorter time (**Figure 13E and Figure 10E**), whereby the slips were comparable (**Figure 13F and Figure 10F**). However, since there were no significant statistical differences between the two genotypes within the aged cohort, there is no evidence of bias in learning performance in the MWM.

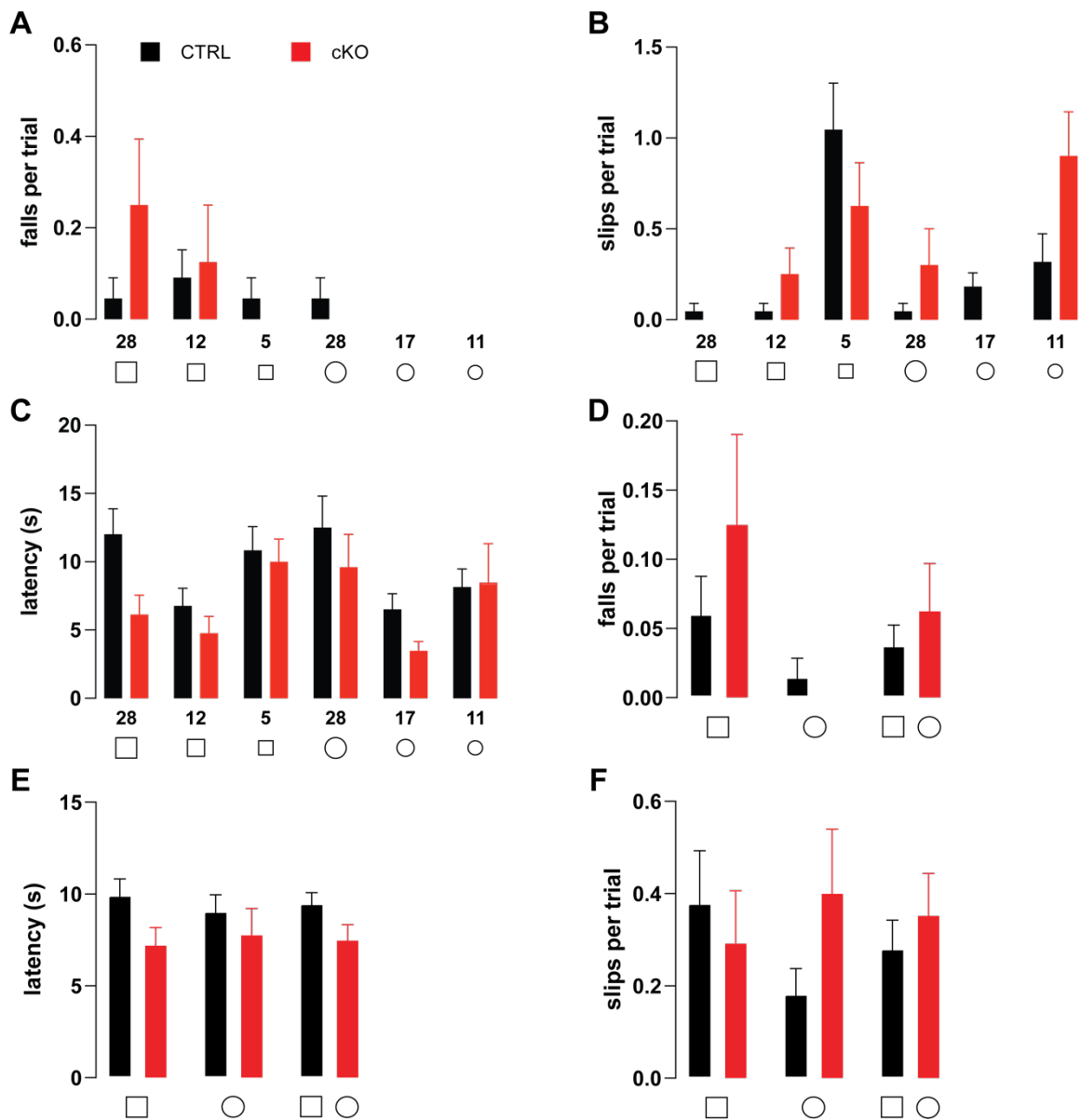


**Figure 13: No differences in locomotor ability of aged CTRL and cKO.** Detailed data for individual bars (A - C) as well as categorized means for all diameters of the square bar (28, 12, 5 mm), the round bar (28, 17, 11 mm) or both bar types (D - F). When crossing an 80 cm square or round cross-section bar, no differences were found in (A) falls per trials. (B) Slips per trial for the 5 mm square bar were significantly increased in cKO (N = 4) compared to CTRL (N = 11), while for the other bar types, slips per trial were comparable for both genotypes including the more difficult 12 mm round bar. (C) Latency was comparable between genotypes for all bars. When the data for the square, round and both bar types are combined, no difference could be found in (D) falls per trials, (E) latency (F) slips per trial. Statistics: Two-way ANOVA with Sidak's multiple comparison test. All diagrams presented as means  $\pm$  SEM. See also **Table 8: Values and statistics for Figure 13.**

#### 4.4.3. Aged cKO display learning behavior comparable to CTRL

Next, we tested whether age has an influence on the phenotype observed in younger animals (**4.3**). To this end, aged mice were introduced into the MWM from pseudorandom locations to learn the path to the hidden platform. Since memory performance of mice may decrease with age, and we suspected a smaller difference in learning performance in both CTRL and cKO as a result, we wanted to make the MWM more difficult to improve measurement of smaller differences. Therefore, in contrast to the young mice, which were trained 4 times per day, we trained the aged mice only twice per day. While the two genotypes initially took a similar amount of time to reach the platform, CTRL showed a slight tendency towards shorter latencies throughout day 2 - 5, which was not statistically significant (**Figure 14A**). On the following 6<sup>th</sup> day, successful memory formation was examined by removing the hidden platform and testing how long the mice stay in the virtual quadrants. Both CTRL and cKO needed the same amount of time to reach the virtual platform and spent significantly more time in the target quadrant, indicating successful memory retrieval in both genotypes (**Figure 14B**). In addition to latency (**Figure 14C**, left), target crossings (**Figure 14C**, center) and thigmotaxis (**Figure 14C**, right) were assessed during the trial. As expected, target crossings and thigmotaxis did not differ, since time in quadrant and latency did not differ between genotypes.

Next, we tested whether advanced age alters memory flexibility, which was similar in young CTRL and cKO (**Figure 11E**). Therefore, the hidden platform was relocated to the opposite quadrant, analogous to **4.3**, and the insertion points were now mirrored. Initially, CTRL took slightly longer to detect the hidden platform than cKO (**Figure 14D**). Interestingly, mean latency for both experimental groups is significantly lower than the one observed on the first day of the acquisition phase (**Figure 14A**). On day 2 and 3, the latencies of the two experimental groups converged, with both groups being faster than on the first day. On day 4 and 5, latencies did not change in both CTRL and cKO, with cKO now showing slightly, but not significant, higher latency than CTRL. In general, however, it can be noted that memory flexibility took place similarly well for both experimental groups, with the latency no longer reducing as rapidly, meaning that the learning curve is no longer as steep during the reversal phase as it was during the acquisition phase. This is explained by the fact that, in contrast to the first day, the novelty factor is no longer present for the mouse, which has already understood that a hidden platform is present and must be searched for. During the subsequent probe trial, in which the hidden platform was removed to test memory retrieval, no differences were observed in time in quadrant (**Figure 14E**) neither in latency between genotypes (**Figure 14F**, left). The similarity in memory flexibility and retrieval between the two genotypes is further confirmed by comparable numbers of target crossings and thigmotaxis (**Figure 14F**, center and right, respectively).

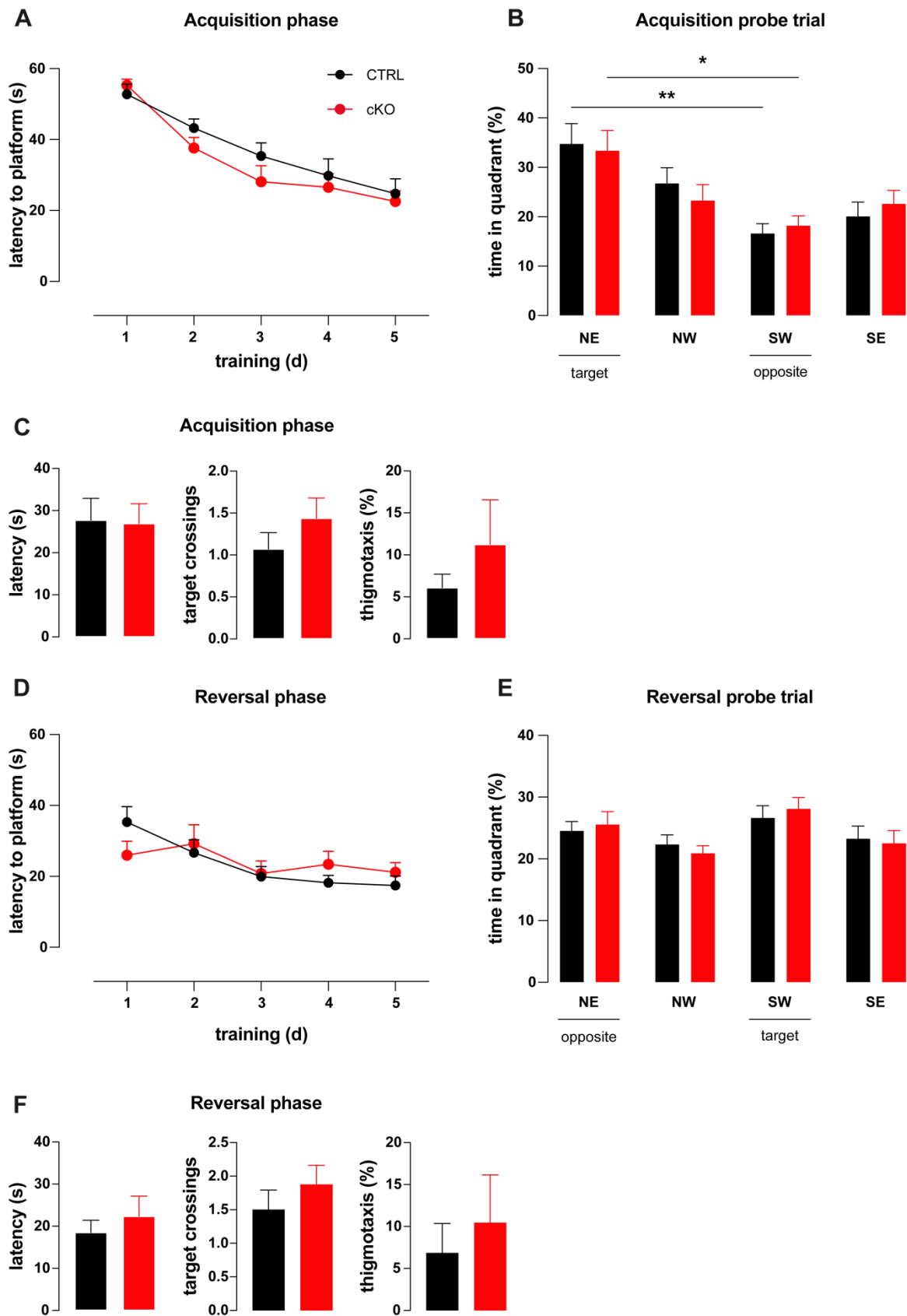


**Figure 14: Memory acquisition and retrieval in the MWM is unaltered in aged cKO.** (A) Over 2 trials per day, latency to find the hidden platform in the NE quadrant of CTRL (N = 11 – 14) and cKO (N = 13 – 16) was comparable. (B) During the probe trial, the hidden platform was removed to determine memory retrieval performance. Both CTRL and cKO spent significantly more time in the

target than in the opposite quadrant indicating a comparable memory retrieval. **(C)** During the probe trial of the acquisition phase, latency to virtual platform (left), target crossings over the virtual platform (center) and time spent in the virtual border zone (thigmotaxis, right) did not differ. **(D)** Memory flexibility was determined by changing the hidden platform location and pseudorandomized placement of insertion. No difference in latency to the platform was found. **(E)** Time spent in the target and opposite quadrant was comparable between the two genotypes. **(F)** During the probe trial of the reversal phase, latency (left), target crossings (center) and thigmotaxis (right) were not different. Statistics: Two-way ANOVA with Sidak's multiple comparison test (**A, B, E, F**), unpaired Student's t-test (**C and F**). All diagrams presented as means  $\pm$  SEM. See also **Table 9: Values and statistics for Figure 14**.

#### 4.5. cKO shows deficient hippocampal LTP

Activity-dependent plasticity of glutamatergic synapses in the hippocampus, particularly NMDA receptor (NMDAR)-dependent LTP, has been identified as a primary cellular substrate for learning and memory (Martin et al., 2000). Accordingly, memory acquisition in MWM can be impaired by inhibition of NMDAR activation through either pharmacological or genetic approaches (Morris et al., 1986; Sakimura et al., 1995; Tsien, Huerta, & Tonegawa, 1996). To confirm the *in vivo* findings of impaired memory acquisition in the MWM *ex vivo*, we measured LTP in our mouse model by recording fEPSP from acute brain slices (**3.6.2**). After a 10 min continuous baseline, LTP was induced by a high-frequency stimulus (HFS) of 100 Hz in 1 s (**Figure 15A**). As expected, this led to a potentiation of fEPSP in both genotypes. Surprisingly, the fEPSP slope in the cKO slowly but steadily decreased after 20 min to return back to baseline levels within 60 min. The potentiation of the fEPSP slope in the CTRL remained stable even after 60 min of measurement and was thus significantly above the level of the cKO.

It is well established in the literature that FRP induces LTP in a NMDAR-dependent (Otmakhov et al., 2004), so both the previously electrically induced and the chemically induced LTP most likely share the same signaling pathway and are therefore comparable. This provided a good opportunity to reconfirm the genotype-specific disadvantage of BK-deficient cKO acute brain slices by an alternative approach. Analogous to the electrical LTP induction, fEPSP were measured prior and after LTP induction, which this time was provoked by a 10-minute perfusion of FRP (**Figure 15B**). Indeed, FRP treatment resulted in a stable potentiation of fEPSP in both CTRL and cKO, which was higher than respective fEPSP induced by an HFS. This might be accounted for by the fact that FRP could penetrate more easily throughout the 400  $\mu$ m-thick brain slice and reach more neurons, whereas the recruitment of neurons by the HFS stimulus of electrical nature decreased with increasing distance of the stimulus pipette with the concomitant increase in resistance. Importantly, potentiation was again significantly lower in the cKO than in the CTRL, and therefore the result was similar to electrical LTP, reconfirming the genotype-specific disadvantage of BK-deficient cKO brain slices.

Impaired capacity for LTP expression may be due to, among other things, altered presynaptic transmitter release probability or altered postsynaptic synaptic transmission.

Both functions can be evaluated by paired-pulse facilitation (PPF) or by input-output relationship (IOR), respectively. Stimulation by two rapid consecutive pulses leads to presynaptic  $\text{Ca}^{2+}$  accumulation triggering the amount of synaptic vesicles to fuse with the presynaptic membrane in response to the second stimulus. The different interstimulus intervals of 10-500  $\mu\text{s}$  are chosen to examine this so-called short-term plasticity. Comparing the fEPSP slopes from the second to the first pulse of the two genotypes, we find that the PPF ratios do not differ (**Figure 15B**). The IOR is the dependence of the fEPSP slope to the respective stimulation current strengths of 25 – 150  $\mu\text{A}$ . It indicates whether the number of synaptic connections or the postsynaptic receptor density is altered. No differences in IOR could be detected between CTRL and cKO (**Figure 15C**). In conclusion, LTP could not be expressed in cKO, confirming the *in vivo* findings of reduced memory acquisition in the acute brain slices. However, this defect is not due to fundamental pre- or postsynaptic dysfunctions.

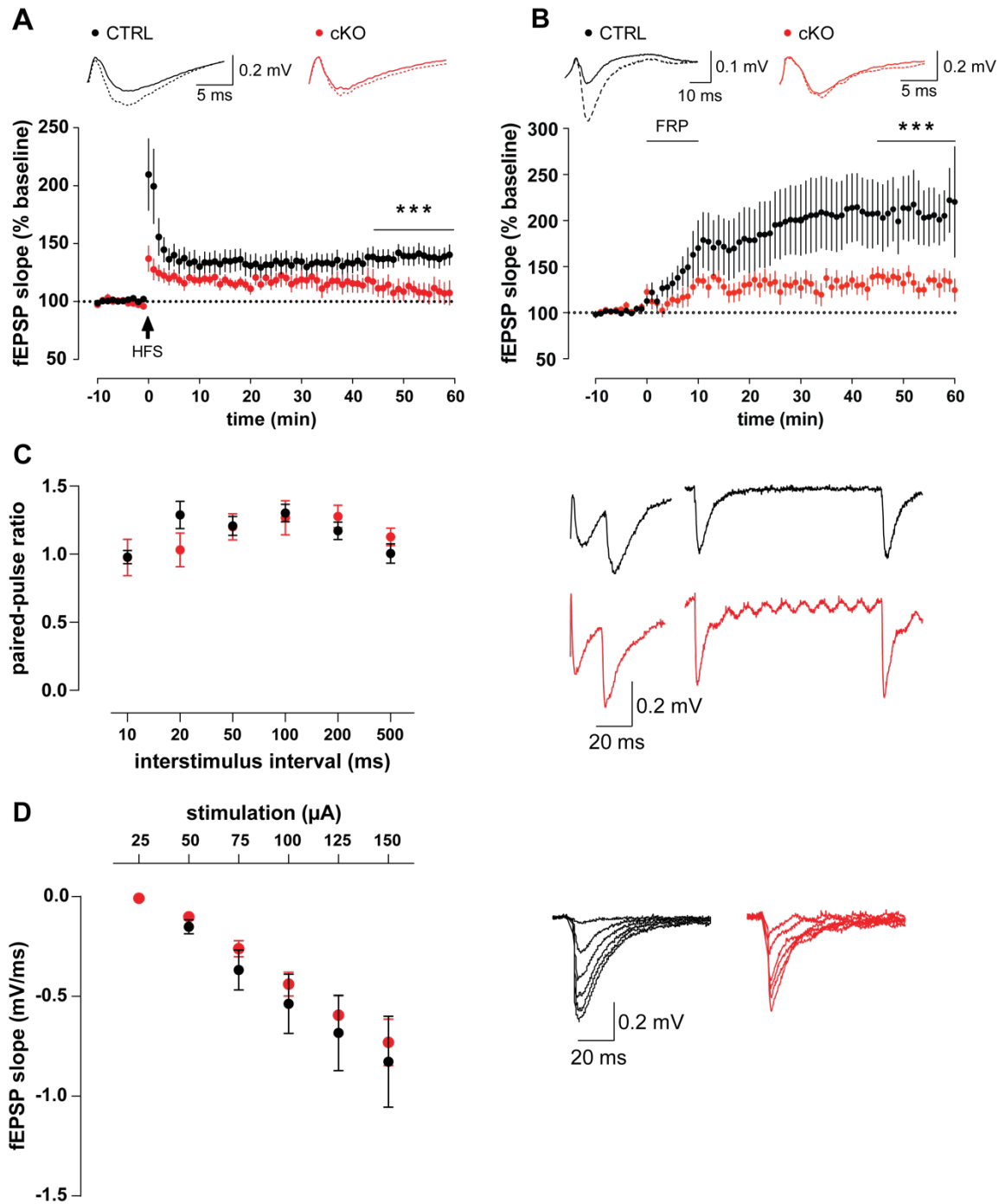


**Figure 15: Impaired LTP, but unaltered basal synaptic transmission in cKO.** (A and B) fEPSP recorded from the hippocampal CA1 *stratum radiatum* in response to electrical or chemical stimulation of Schaffer collateral axons. LTP was elicited by either HFS or FRP after 10-minute baseline. (A) HFS led to stable potentiation of fEPSP in CTRL (black,  $n = 7$  slices from  $N = 4$  animals), fEPSP of cKO dropped back to baseline level after initial potentiation, the (red,  $n = 8$  slices from  $N = 4$  animals) leading to a significant difference at the end of the measurement. Representative fEPSP of traces from CTRL and cKO before (solid) and after HFS (dotted) are shown on top. (B) FRP provoked a stable potentiation in CTRL (black,  $n = 8 - 10$  slices from  $N = 4$  animals) and cKO (red,  $n = 10$  slices from  $N = 5$  animals). However, potentiation in cKO was significantly decreased in comparison to CTRL. Representative fEPSP of traces from CTRL and cKO before (solid) and after HFS (dotted) are shown on top. cLTP induction during fEPSP

measurement was performed and analyzed by Dila Calis (M.Sc., Department of Otolaryngology, Head and Neck Surgery, University of Tübingen). **(C)** The mean PPF ratio of all interstimulus intervals is comparable ( $n = 6$  slices from  $N = 3$  animals). Representative PPF curves for the 20 ms and 200 ms interstimulus intervals are shown on the right. **(D)** No differences between CTRL ( $n = 8$  slices from  $N = 4$  animals) and cKO ( $n = 9$  slices from  $N = 5$  animals) in the mean IOR could be measured for stimulus strengths ranging from 25 – 150  $\mu\text{A}$  in 25  $\mu\text{A}$  increments. Representative IOR curves for all stimulation strengths are shown on the right. Statistics: Two-way ANOVA with Sidak's multiple comparison test. All bar diagrams presented as means  $\pm$  SEM. See also **Table 10: Values and statistics for Figure 15**. Adapted from (Pham et al., 2023).

#### 4.6. cKO display unaltered subunit composition of hippocampal iGluR

Modulation of the number of postsynaptic AMPAR by LTP NMDAR is well established (Luscher & Malenka, 2012). First, learning-naive mice were studied. To determine the number of AMPARs and NMDARs, whole hippocampal lysates were tested for their obligate GluA1 and GluN1 subunits, respectively, by Western blot (**Figure 16A**). In both CTRL and cKO, neither GluA1 nor GluN1 expression differed (**Figure 16B**). The functional properties of postsynaptic glutamate receptors not only depend on their number, but also their exact subunit composition (Diering & Huganir, 2018; Wong & Gray, 2018). Although NMDAR and AMPAR subunits share many common features and structural similarities, the specific composition confers biophysical and functional properties such as conductance, kinetics, synaptic or extrasynaptic localization, protein-protein interaction as well as membrane transport (Sanz-Clemente et al., 2013) is thus also involved in the expression of LTP. AMPAR not containing GluA2, for example, were shown to be  $\text{Ca}^{2+}$  permeable (CP-AMPAR). As a result, CP-AMPAR contribute to  $\text{Ca}^{2+}$  influx during LTP induction (Cull-Candy & Farrant, 2021). No differences were detected, however, when whole hippocampal lysates were examined for GluA2 expression (**Figure 16B**). It was previously reported that animals lacking the closely related  $\text{Na}^+$ -activated  $\text{K}^+$  channel Slack show reduced GluN2B expression in favor of GluN2A in the hippocampus and impaired synaptic plasticity in the hippocampus (Matt et al., 2021). Therefore, CTRL and cKO were tested for GluN2A and N2B, but did not differ in expression (**Figure 16B**). In conclusion, the number of AMPARs and NMDARs and their composition in learning-naive mice are not different between CTRL and cKO. This is in accordance with the previous electrophysiological finding of unaltered IORs (**Figure 15D**). There, transmission strength also indicated unchanged numbers of postsynaptic glutamatergic receptors and a similar functional receptor composition.

Since learning-naïve mice show no changes in the expression and composition of NMDAR and AMPAR, it was hypothesized that LTP might alter their expression or composition. Indeed, current knowledge strongly suggests that upon synaptic plasticity induction or memory consolidation, more GluN2A-containing NMDARs are formed, probably utilizing GluN2A from local translation and GluN1 from local ER (Baez et al., 2018). Later in the process, NMDARs are mobilized from other pools and *de novo* syntheses occurs in the

soma (Baez et al., 2018). To examine these processes in the present model, whole hippocampal lysates were obtained from mice that were sacrificed immediately after performing the reversal probe trial of the MWM. These were subsequently analyzed for GluA1, GluN2A and GluN2B, due to lower sample availability (**Figure 16C**). Also, after the MWM, however, no differences in glutamate receptor subunit expression could be detected between CTRL and cKO (**Figure 16D**).

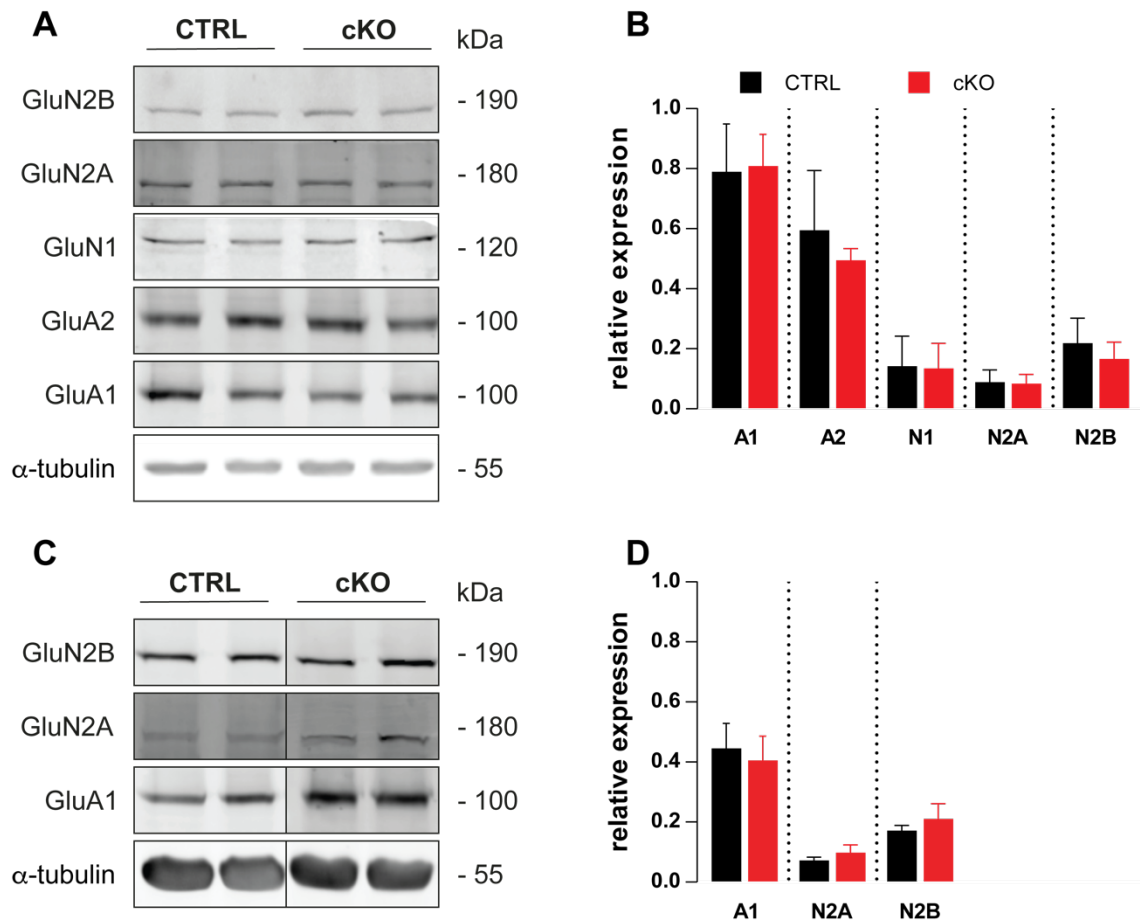


**Figure 16: Composition of hippocampal ionotropic glutamate receptors in CTRL and cKO was not different before and after MWM.** (A) Whole hippocampal lysates were obtained from 8-12-weeks-old learn-naive mice. No differences were detected in AMPAR (GluA1 N = 3 and GluA2 N = 3) or NMDAR (GluN1 N = 3, GluN2A N = 3 and GluN2B N = 3) subunit composition Western blot.  $\alpha$ -Tubulin served as loading control. Left: Representative blots; Right: Densitometric quantification of each subunit normalized to  $\alpha$ -tubulin. (B) After MWM, whole hippocampal lysates were used for Western blot analysis. No difference in AMPAR (GluA1 N = 5-7) or NMDAR (GluN2A N = 5-7 and GluN2B N = 5-7) subunit composition of was detected.  $\alpha$ -Tubulin served as a loading control. Left: Representative blots; Right: Densitometric quantification of each subunit normalized to  $\alpha$ -tubulin. Western blot was performed and quantified by Daniel Kalina (M.Sc., Experimental pharmacology, University of Tübingen). Statistics: Two-way ANOVA with Sidak's multiple comparison test. All bar diagrams presented as means  $\pm$  SEM. See also **Table 11: Values and statistics for Figure 16**. Adapted from (Pham et al., 2023).

#### 4.7. Impaired AMPAR phosphorylation in cKO after cLTP induction in acute hippocampal slices

Since neither presynaptic nor postsynaptic functions differ between genotypes and glutamate receptor expression and composition are similar, one of the most likely causes remains the incorporation of AMPAR into the postsynapse induced by NMDAR-dependent LTP. Different forms of behavior and synaptic plasticity in different brain regions, including hippocampal/cortical LTP and LTD require phosphorylation of the GluA1 subunit at S845 or S831 (Diering et al., 2016). We therefore used phosphorylation of GluA1 S845 and S831 detected by Western blot as surrogate parameters for physiological LTP (3.5.7). Since a large amount of tissue is required for Western blotting and electrical field stimulation using HFS is not an efficient method for this purpose, LTP was induced in bulk by pharmacological means. Since it has already been demonstrated that chemically induced LTP behaves similarly to electrically induced LTP by an HFS (Figure 15B) (Otmakhov et al., 2004), except that the former efficiently reaches more neurons in the tissue slices, we decided to also induce LTP in acute 400  $\mu\text{m}$  thick hippocampal slices by FRP .

After cLTP induction, phosphorylation levels as well as total GluA1 expression were determined by Western blot, quantified by densitometric measurement, and put into relation. In CTRL, a significant increase in phosphorylation of S845 could be detected after cLTP induction (Figure 17A). This is relevant, as phosphorylation of GluA1 at S845 was shown to promote GluA1 cell surface insertion and synaptic retention, increase channel opening probability and facilitate induction of LTP, while dephosphorylation of S845 was associated with receptor endocytosis and LTD (Diering et al., 2016). In the cKO, however, no significant increase in GluA1-S845 phosphorylation was detected after cLTP induction, which is consistent with their impaired memory acquisition and retrieval in the MWM (4.3) as well as the lack of electrophysiologically detected LTP in acute slices.

Aa residue S831 of GluA1 was used as another read-out for LTP induction. Its phosphorylation is thought to increase channel conductance and thereby to regulate LTP (Diering et al., 2014). No cLTP-induced differences in the degree of S831 phosphorylation, however, could be detected in either CTRL or cKO (Figure 17B). These results suggest that memory acquisition and LTP are due to a lack of phosphorylation of S845 and thus a reduced incorporation of GluA1 into the postsynapse.

To test whether GluA1-S845 phosphorylation is BK-dependent, the same protocol was performed in the presence of 5  $\mu\text{M}$  paxilline (PAX), a BK-specific inhibitor (Figure 17C). After BK blockade, the phosphorylation levels of GluA1-S845 in CTRL and cKO remained at basal levels despite cLTP induction. Similarly, phosphorylation levels of GluA1-S831 remained unchanged after cLTP induction with concomitant BK blockade (Figure 17D). In conclusion, GluA1-S845 phosphorylation appears to promote AMPAR incorporation into the postsynapse after LTP induction. This impacts expression of physiological LTP as well as memory acquisition, *ex vivo* and *in vivo* respectively. Interestingly, cLTP-induced

GluA1-S845 phosphorylation seems to be BK-dependent while GluA1-S831 does not seem to play a role in this model.

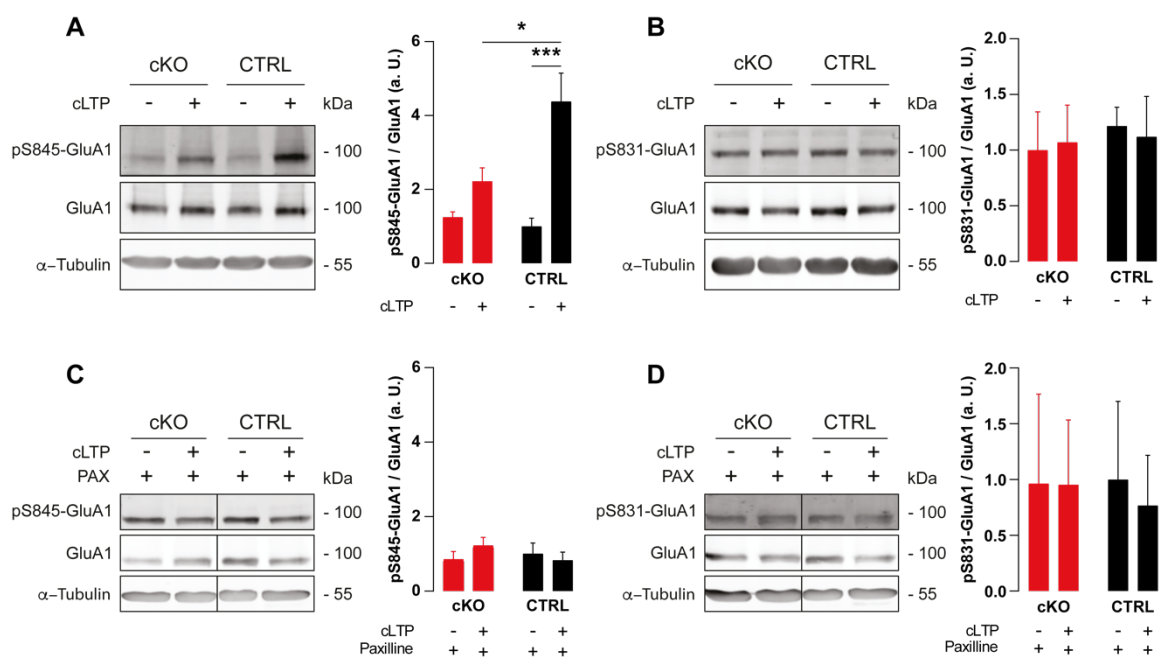


**Figure 17: BK deficiency prevents phosphorylation of GluA1-S845 after cLTP induction.** In acute hippocampal slices from 8–12-weeks-old animals, cLTP was induced by FRP with or without the BK inhibitor paxilline (PAX). Acute slices were subsequently lysed and tested by Western blot for increased phosphorylation of GluA1 at residues S845 and S831 as surrogate parameters for successful LTP induction. Representative blots are shown on the left. Densitometric quantification is shown on the right. **(A)** cLTP elicited significantly increased phosphorylation of GluA1 S845 in CTRL (N = 4 animals) but not cKO (N = 4). **(B)** cLTP did not change in GluA1 S831 phosphorylation in CTRL and cKO (N = 4 animals). **(C)** BK inhibition by PAX prevented the increased phosphorylation of GluA S845 after cLTP induction in CTRL (N = 3 animals). **(D)** PAX did not alter GluA1 S831 phosphorylation levels in either genotype (N = 3 animals). cLTP induction and western blot were performed and quantified by Daniel Kalina (M.Sc., Experimental pharmacology, University of Tübingen). Statistics: Two-way ANOVA with Sidak's multiple comparison test. All bar diagrams presented as means  $\pm$  SEM. See also **Table 12: Values and statistics for Figure 17**. Adapted from (Pham et al., 2023).

#### 4.8. BK supports neuronal K<sup>+</sup> outflow during cLTP induction

Establishing cLTP in electrophysiological and biochemical experiments as a viable model to study synaptic plasticity, particularly LTP, now allows its use to understand more about the role of BK during LTP at the molecular level. To this end we performed K<sup>+</sup>-sensitive single cell measurements in dissociated neuron cultures. Single-cell real time measurements were carried out in hippocampal neurons isolated from P0 mice with BK<sup>+/+</sup> and BK<sup>-/-</sup> genotypes. Neurons were transduced at DIV 7 with a virus containing the genetic information for a FRET-based K<sup>+</sup> ion sensor (Bischof et al., 2017) under control of the CAG promoter and measured at DIV 9. The sensor was efficiently expressed in neurons and is clearly distinguishable from the background (**Figure 18A**). The sensor construct consists of the K<sup>+</sup>-binding protein C- and N-terminally fused to cyan and yellow fluorescent protein

variants (CFP and YFP) mseCFP and cpV, respectively.  $K^+$  binding induces a conformational change in the sensor which brings the two fluorophores in close proximity. This allows the FRET effect to occur, decreasing CFP- and increasing YFP-fluorescence intensity. Accordingly, the ratio of FRET/CFP fluorescence intensity is proportional to  $[K^+]_i$ . To confirm and validate the functionality of the sensor in this experimental setup, neurons were twice perfused with 20  $\mu$ M glutamate. This leads to a decrease of the FRET ratio, correlating to  $K^+$  efflux. This is expected, as glutamate-induced activation of ligand-gated ion channels leads to strong neuronal depolarization, which, in turn, causes the opening of voltage-gated  $K^+$  channels to allow repolarization. After glutamate washout,  $[K^+]_i$  quickly normalizes. Additionally, this experiment confirms the validity of the observed FRET signals because the individual intensities of FRET and CFP are antiparallel due to the conformational change in the sensor (**Figure 18B**).

To examine  $[K^+]_i$  during cLTP induction, baseline  $K^+$  was first established for 5 minutes. Then,  $BK^{+/+}$  neurons were stimulated with FRP for 10 min to induce cLTP. Finally, the FRP cocktail was washed off for another 10 min. During and after cLTP application, a strong and sustained  $K^+$  efflux was observed in the wild-type neurons (black trace, **Figure 18C**). This could be observed in all neurons (light grey traces). The extent to which this process is BK-dependent was investigated in global  $BK^{-/-}$  neurons not in cKO neurons to ensure BK ablation from all hippocampal neurons (**4.1**). Moreover, the exact genotype of individual neuronal cultures deriving from cKO hippocampi remains unknown. Since male  $BK^{-/-}$  mice are not fertile and homozygous  $BK^{-/-}$  can therefore not be bred,  $BK^{-/-}$  mice were obtained by heterozygous mating of  $BK^{+/-}$  mice. Since the probability of  $BK^{-/-}$  mice is only 25%, neurons from different offspring were not pooled, but prepared and inoculated individually. After seeding, biopsies from donor animals were genotyped and only cells from  $BK^{+/+}$  and  $BK^{-/-}$  animals were used in subsequent experiments. Surprisingly, FRP application in  $BK^{-/-}$  (**Figure 18D**) resulted in significantly less  $K^+$  efflux than in  $BK^{+/+}$  (**Figure 18H**), suggesting that BK channels are usually active during cLTP. To support these results, measurements were again performed in  $BK^{+/+}$  neurons during pharmacological BK channel block using PAX. For this purpose, neurons were incubated with 5  $\mu$ M PAX 10 min before and throughout the actual measurement. In this setup,  $K^+$  efflux was also significantly reduced during cLTP (**Figure 18E**). Thus, the results of  $BK^{-/-}$  could be reproduced by blocking BK with PAX in  $BK^{+/+}$ , suggesting that cLTP-induced  $K^+$  efflux is dependent on the presence of functional BK channels.

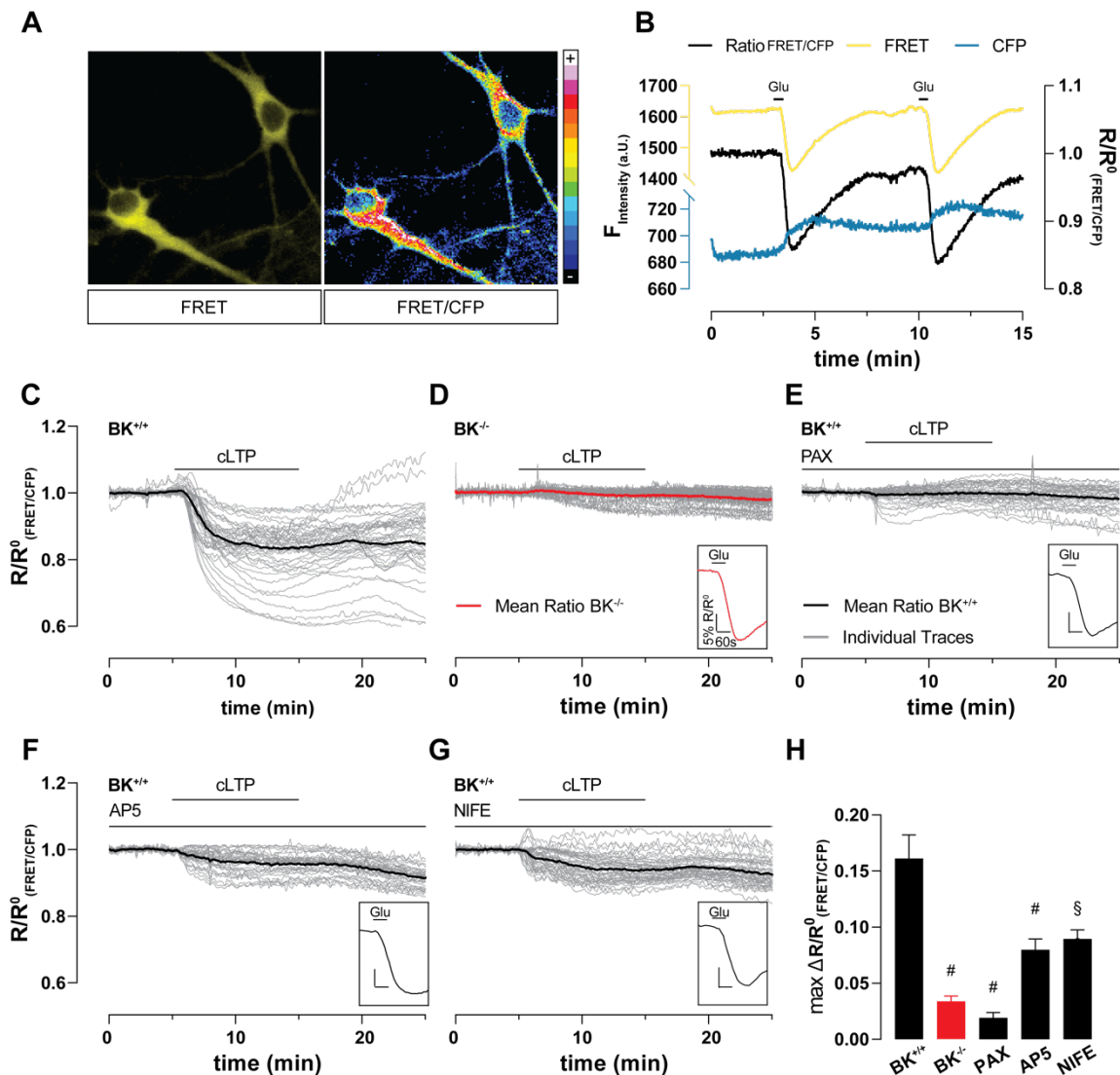


**Figure 18: cLTP provokes a strong and sustained K<sup>+</sup> efflux.** Hippocampal neurons were virally transduced at DIV 7 with a FRET-based genetically encoded K<sup>+</sup> ion indicator, which, at DIV 9 allowed single-cell live imaging of intracellular K<sup>+</sup> concentrations [K<sup>+</sup>]<sub>i</sub> in response to external stimuli. **(A)** Representative FRET image (left) and FRET/CFP ratio image (right). Pseudo-colored image showing [K<sup>+</sup>]<sub>i</sub> from black (lowest) to purple (highest). **(B)** Representative K<sup>+</sup>-sensitive FRET measurement of a neuron. Perfusion with 20 μM glutamate decreased the FRET/CFP ratio (black), which is proportional to [K<sup>+</sup>]<sub>i</sub> of the neuron. The individual fluorescence intensities of FRET and CFP are shown in yellow and blue, respectively. **(C-G)** Individual (grey) and averaged FRET/CFP ratios (black, red in D) after 5 min of baseline, 10 min cLTP induction and 10 min washout under different conditions. If other drugs were used in addition to the cLTP cocktail, they were administered to the neurons 10 min before the actual recording and maintained throughout the measurement as indicated. At the end, 20 μM glutamate was perfused (bottom right) to verify neuronal viability. **(C)** cLTP induction by 10 min perfusion of BK<sup>+/+</sup> (n = 11 independent experiments from a total of n = 54 neurons obtained from N = 6 preparations) with FRP results in a massive reduction of [K<sup>+</sup>]<sub>i</sub>. In both **(D)** BK<sup>-/-</sup> (n = 9 independent experiments with a total of n = 48 neurons obtained from N = 5 preparations) as well as in **(E)** BK<sup>+/+</sup> with pharmacological blockade of BK by paxilline (PAX) (n = 9 independent experiments from a total of n = 43 neurons obtained from from N = 5 preparations), the K<sup>+</sup> efflux was prevented. Each, inhibition of **(F)** NMDAR with 100 μM DL-AP5 (AP5, n = 9 independent experiments with a total of n = 37 neurons obtained from N = 5 preparations) and **(G)** LTCC with 5 μM Nifedipine (NIFE, n = 6 independent experiments with a total of n = 52 neurons obtained from N = 4 preparations) diminished the [K<sup>+</sup>]<sub>i</sub> reduction by approximately 50%. **(H)**

Quantification of C-G. Maximum difference between minimum ratio after cLTP induction and averaged 5-min baseline ratio. Statistics: One-way ANOVA with Dunnett's multiple comparison test. All bar diagrams presented as means  $\pm$  SEM. See also **Table 13: Values and statistics for Figure 18**. Adapted from (Pham et al., 2023).

#### 4.9. BK sustains neuronal $\text{Ca}^{2+}$ oscillations during cLTP induction

The next question was how cLTP provokes BK-dependent  $\text{K}^+$  efflux. One obvious hypothesis is that  $\text{Ca}^{2+}$  influx during cLTP leads to BK channel activation. The most common mechanism for how  $\text{Ca}^{2+}$  dynamics relate to changes in synaptic efficiency is the so-called  $\text{Ca}^{2+}$  control hypothesis, which states that large amplitude  $\text{Ca}^{2+}$  transients trigger LTP (Lisman, 1989). In the CA1 region of the hippocampus, induction of LTP requires increased postsynaptic  $\text{Ca}^{2+}$  levels (Malenka, 1991). Although several  $\text{Ca}^{2+}$ -dependent biochemical processes are involved in LTP, determining their precise role remains a difficult experimental problem. This problem was solved by using cultured hippocampal neurons loaded with 2.5  $\mu\text{M}$  Fura-2-AM at DIV 9, which allowed real-time measurement of  $\text{Ca}^{2+}$  dynamics during LTP induction. The ratio of Fura-2 fluorescence emission intensities at 340 and 380 nm  $R_{(F340/F380)}$  is proportional to  $[\text{Ca}^{2+}]_i$  and thus allows its relative quantification. Analogous to experiments in **Figure 18A**, basal  $[\text{Ca}^{2+}]_i$  was measured over 5 min. Surprisingly, spontaneous  $\text{Ca}^{2+}$  oscillations already occurred under basal conditions. This is consistent with previous reports that already found such spontaneous  $\text{Ca}^{2+}$  oscillations in cultured hippocampal neurons (Huang et al., 2013). These  $\text{Ca}^{2+}$  oscillations are fluctuations in  $[\text{Ca}^{2+}]_i$ , so-called  $\text{Ca}^{2+}$  transients, which contribute to the regulation of neuronal development (**Figure 19A**). They have already been linked to neuronal proliferation, migration, differentiation, and survival. Neuronal networks of the hippocampus in culture show all the characteristics of neuronal activity, such as the formation of synchronous activity through spontaneous  $\text{Ca}^{2+}$  oscillations (Sokolov & Mukhina, 2022). It therefore stands to reason that synaptic plasticity influences spontaneous  $\text{Ca}^{2+}$  oscillations. To evaluate the influence of LTP on  $[\text{Ca}^{2+}]_i$ , cLTP was induced with FRP. As expected, cLTP induction resulted in a significant increase in  $\text{Ca}^{2+}$  oscillations in  $\text{BK}^{+/+}$  (**Figure 19A**). The same measurement in  $\text{BK}^{-/-}$  neurons showed significantly reduced network activity of the neurons compared to  $\text{BK}^{+/+}$  (**Figure 19B**). While application of FRP induced  $\text{Ca}^{2+}$  oscillations, its frequency however was significantly reduced compared to CTRL. When the measurements were repeated in  $\text{BK}^{+/+}$ , but with specific blockade of BK by PAX, spontaneous  $\text{Ca}^{2+}$  oscillations could be observed in the first 5 min, but the frequency remained at the same level despite cLTP induction (**Figure 19C**). These measurements suggest a BK-dependent effect both in spontaneous  $\text{Ca}^{2+}$  oscillations and in the frequency increase after cLTP. This observation suggests that  $\text{Ca}^{2+}$  oscillations might induce  $\text{K}^+$  efflux, which is consistent with the  $\text{K}^+$ -sensitive FRET measurements shown in **Figure 18C-E**. Importantly, when BK is genetically or pharmacologically inactivated, this  $\text{K}^+$  efflux is absent. In summary, spontaneous  $\text{Ca}^{2+}$  oscillation already occur in hippocampal neurons. After LTP induction,  $\text{Ca}^{2+}$  oscillation frequency increased significantly. This effect seems to depend on BK activity.

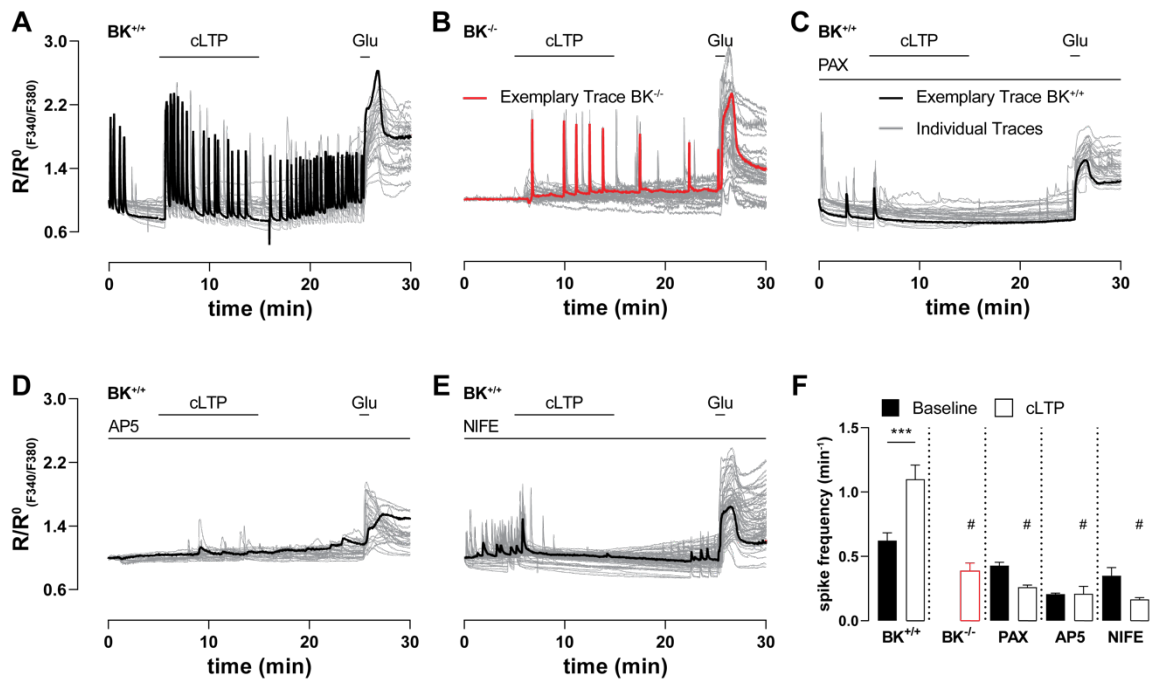


**Figure 19: cLTP increases  $\text{Ca}^{2+}$  oscillation frequencies depending on BK, NMDAR and LTCC.** DIV 9 hippocampal neurons were loaded with  $2.5 \mu\text{M}$  Fura to enable  $\text{Ca}^{2+}$ -sensitive single-cell live imaging. Individual curves (grey) and representative curves (black, red in B) of 5 min baseline, 10 min cLTP induction and 10 min washout phase. At the end of the measurement, stimulation with  $20 \mu\text{M}$  glutamate was performed for 1 min to test the viability of the neurons. If other drugs were used in addition to cLTP induction, they were applied to the neurons 10 min beforehand and maintained throughout the measurement as shown. **(A)** Spontaneous  $\text{Ca}^{2+}$  spike frequency was significantly increased after cLTP induction ( $n = 4$  independent experiments with a total of  $n = 31$  neurons obtained from 4 preparations). **(B)** In  $\text{BK}^{-/-}$  neurons, spontaneous  $\text{Ca}^{2+}$  spikes were completely absent and only occasionally present after cLTP induction ( $n = 4$  independent experiments with a total of  $n = 35$  neurons obtained from 3 preparations). Blockade of BK, NMDAR and LTCC by **(C)**  $5 \mu\text{M}$  paxilline (PAX,  $n = 4$  independent experiments with a total of  $n = 29$  neurons obtained from 3 preparations), **(D)**  $100 \mu\text{M}$  DL-AP5 (AP5,  $n = 4$  independent experiments with a total of  $n = 29$  neurons obtained from 3 preparations) and **(E)**  $5 \mu\text{M}$  Nifedipine (NIFE;  $n = 4$  independent experiments with a total of  $n = 69$  neurons obtained from 5 preparations), respectively, reduced spontaneous  $\text{Ca}^{2+}$  spike frequencies and prevented their increase after cLTP induction. **(F)** Quantification of spike frequency from A-E. To be considered as spike, the event's AUC must be at least 10 % of the glutamate-induced AUC. Statistics: One-way ANOVA with Tukey's multiple comparison test. All bar diagrams presented as means  $\pm$  SEM. See also **Table 14: Values and statistics for Figure 19**. Adapted from (Pham et al., 2023).

#### 4.10. cLTP-associated, BK-mediated neuronal $\text{Ca}^{2+}$ oscillations depend on NMDAR and LTCC

Next, we tried to establish, which  $\text{Ca}^{2+}$  sources might play a role for the observed  $\text{Ca}^{2+}$  oscillations and also for BK channel activation. BK channels are generally considered to be high threshold channels for activation by voltage and  $\text{Ca}^{2+}$ . Within the physiological range of membrane voltages (less than or equal to  $+40 \text{ mV}$ ), the  $[\text{Ca}^{2+}]_i$  concentration required for significant BK channel activation is generally much higher than the cellular global  $[\text{Ca}^{2+}]_i$  level at rest (less than or equal to  $\sim 0.1 \mu\text{M}$ ) and in the excited state (less

than or equal to  $\sim 1 \mu\text{M}$ ) (Rothberg & Magleby, 1999). Therefore, native BK channels must be localized within a nanodomain together with suitable  $\text{Ca}^{2+}$  sources. Recent studies have shown by co-immunopurification and colocalization analyzes that BK channels form complexes with NMDAR, both in the rodent brain and in a heterologous expression system (Zhang et al., 2018). To test whether inhibition of NMDARs leads to a reduced frequency of  $\text{Ca}^{2+}$  oscillations, cLTP was induced under continuous application of the NMDAR channel blocker AP5. As expected, the application of AP5 significantly prevented the cLTP-induced increase of  $\text{Ca}^{2+}$  oscillation frequencies compared to CTRL (**Figure 19D and F**).

In addition to NMDAR, we could also demonstrate functional coupling between BK and LTCC. LTCC can create sufficiently high local  $\text{Ca}^{2+}$  concentrations to activate BK. Under different circumstances, LTCC have also been shown to be important for synaptic activity. The role of LTCC in learning and memory has been studied in many contexts, including hippocampus-dependent spatial memory (Batuecas et al., 1998; Ingram et al., 1994; Quevedo et al., 1998). In these settings, administration of LTCC agonists have been shown to improve memory (Jerome et al., 2012) while antagonists can disrupt memory (Davis & Bauer, 2012). Continuous inhibition of LTCC by NIFE did also significantly prevent increase of  $\text{Ca}^{2+}$  oscillation frequencies in comparison to CTRL (**Figure 19E and F**).

After the signaling partners of BK and the mediators of the  $\text{Ca}^{2+}$  oscillations had been identified, we checked whether a lack of  $\text{Ca}^{2+}$  influx also leads to a lack of  $\text{K}^+$  efflux through cLTP, since lack of  $\text{Ca}^{2+}$  influx should reduce BK activation. For this purpose, real-time measurements were again performed in cultured hippocampal neurons expressing GEPII. Blockade of both NMDAR and LTCC by AP5 and NIFE, respectively, led to a significant reduction in  $\text{K}^+$  efflux by 50% in each case (**Figure 18F, G and H**).

The results suggest that induction of cLTP provokes an increased  $\text{Ca}^{2+}$  oscillation frequencies. The inhibition of  $\text{Ca}^{2+}$  oscillation frequency increase by either PAX, AP5 or NIFE, it is suggested that the oscillations are mediated by NMDAR and LTCC. BK is activated by the functional coupling to the  $\text{Ca}^{2+}$  channels by the high local concentrations and acts as a positive feedback mechanism.

#### **4.11. Unaltered membrane potential during cLTP**

It is surprising that the drop in  $[\text{K}^+]_i$  persisted for so long, even after 10 minutes of FRP washout (**Figure 18C**). Since the neurons respond to 20  $\mu\text{L}$  glutamate at the end of the measurement, the neurons are still viable despite strong and persistent  $\text{K}^+$  efflux. However, the sustained  $\text{K}^+$  efflux raises questions about the membrane potential, as this would have a strong influence on the resting potential of the neurons. To address this question, we chose to measure the neurons loaded with DiBAC<sub>4</sub>(3) using a fluorescence microscope. DiBAC<sub>4</sub>(3) is a voltage-sensitive dye that accumulates in the cytoplasm of the cell after depolarization and therefore increases the fluorescence intensity. Upon hyperpolarization,

the dye is removed from the membrane out to extracellular (Kwan et al., 2009), which corresponds to a decrease in fluorescence intensity. This also means that DiBAC<sub>4</sub>(3), after loading the neurons, must also be present in all buffers throughout the measurements. In summary, DiBAC<sub>4</sub>(3) allows relative quantification of membrane potential by fluorescence microscopy. Surprisingly, cLTP induction did not alter the resting membrane potential in either BK<sup>+/+</sup> (**Figure 20A**) or PAX-inhibited neurons (**Figure 20B**). The quantification, which was an average of 5 min each from baseline (first 5 min), cLTP (5.01 - 15 min) and postcLTP (15.01 - 25 min), showed a slight tendency towards more depolarized membrane potential in the BK<sup>+/+</sup> during cLTP and postcLTP, which was not statistically significant (**Figure 20C**). This could be because after depolarization of the rise in [Ca<sup>2+</sup>]<sub>i</sub>, a rapid K<sup>+</sup> efflux followed, which quickly repolarized the membrane. Since DiBAC<sub>4</sub>(3) responds rather slowly to the membrane potential change, this could mean that i.) the net membrane potential remains unchanged, or ii.) changes that occur are too rapid to be detected by this probe.

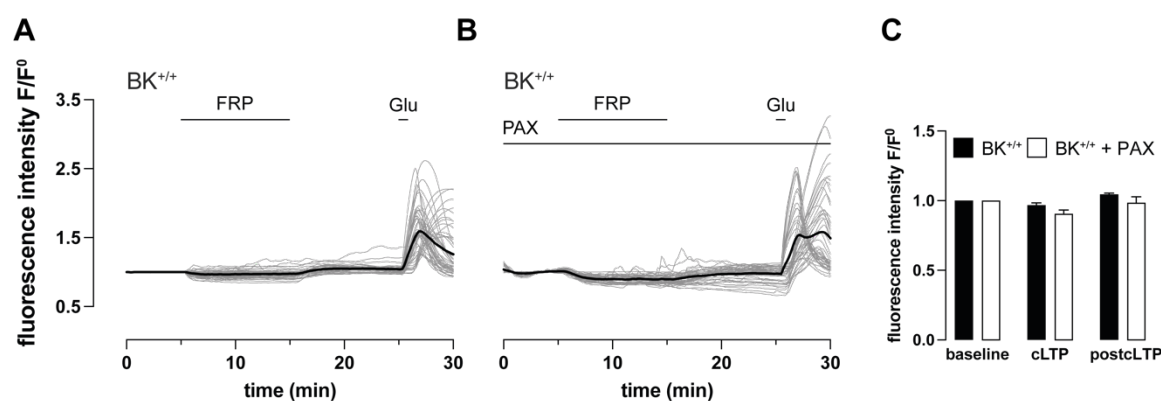


**Figure 20: cLTP does not influence membrane potential.** (A and B) Time course of fluorescence intensity at 493 nm in 9 DIV hippocampal neuronal cultures loaded with the potential-sensitive probe, DiBAC<sub>4</sub>(3). According to manufacturer's instruction DiBAC<sub>4</sub>(3) was present during the whole recording. Traces from individual neurons are plotted in grey, averaged traces in black. Glutamate (20  $\mu$ M) application at the end of each measurement verified cell viability and served as positive control. (A) cLTP induction via FRP did not change membrane potential neither in BK<sup>+/+</sup> (n = 4 independent experiments from a total of n = 49 neurons obtained from N = 3 preparations) nor (B) after BK inhibition by PAX (5  $\mu$ M) (n = 4 independent experiments from a total of n = 46 neurons obtained from N = 3 preparations). (C) Comparison of normalized fluorescence intensity during baseline (first 5 min), cLTP (5.01 – 15 min) and postcLTP (15.01 – 25 min) revealed comparable membrane potential between BK<sup>+/+</sup> and BK<sup>+/+</sup> with PAX. DiBAC<sub>4</sub>(3) measurement was performed by Tamara Hussein (M.Sc., Pharmacology, Toxicology and Clinical pharmacy, University of Tübingen). Statistics: One-way ANOVA with Tukey's multiple comparison test. All bar diagrams presented as means  $\pm$  SEM. See also **Table 15: Values and statistics for Figure 20**. Adapted from (Pham et al., 2023).



## 5. Discussion

### 5.1. T29.1-Cre-mediated hippocampal CA1 pyramidal neuron-restricted conditional BK knockout

The importance of BK channels for synaptic plasticity was already demonstrated before. Pharmacological activation of BK channels rescued limited inducibility of LTP in neurons isolated from 3xTg AD mouse model. In the same mouse model pharmacological BK activation improved memory acquisition assessed by MWM *in vivo* (Wang et al., 2015). By then, it was well established that A $\beta$  inhibits BK activity. In an alternative approach, Typlt et al. (2013) were able to provide additional insight into BK's function in synaptic plasticity by examining BK function in a healthy mouse model. Compared to BK<sup>+/+</sup>, BK<sup>-/-</sup> displayed significantly impaired memory acquisition in the MWM.

Although the studies mentioned above as well as many others strongly implicate an important function of BK in synaptic plasticity, the underlying molecular mechanisms as well as the BK expressing cells involved in the neuronal activity during memory formation remained unknown. An additional caveat stems from the fact that increased latency in the MWM observed in BK<sup>-/-</sup> is possibly influenced by their ataxia (Sausbier et al., 2004) which might interfere with the animal's ability to swim and thus lead to an underestimation of its memory performance.

The cerebellar ataxia in BK<sup>-/-</sup> was demonstrated to originate from cerebellar purkinje cells (Chen et al., 2010). There, the lack of rapid BK-mediated afterhyperpolarization prolongs the inactive closed state of voltage-gated Na<sup>+</sup> channels. This results in a prolonged depolarization phase and subsequently reduced AP frequency ultimately disrupting the olivo-cerebellar feedback mechanism to cause ataxia. To prevent this process in cerebellar Purkinje cells, the T29.1-Cre driver mouse was used to create a hippocampal CA1 pyramidal cell-specific cKO of BK (3.1.2). These mice do not display atactic behavior which might limit their locomotor abilities and possibly confound the results of the behavioral learning experiments (4.2).

### 5.2. *In vivo* characterization of the BK channel

#### 5.2.1. Characterization of BK in anxiety behavior and locomotor activity

In addition to the behavioral learning experiment, experiments testing the fear behavior as well as the locomotor activity of the mice were performed to ensure that the results from the learning experiment were not distorted by differences in the animals' motor abilities. Accordingly, no differences between genotypes were found in fear behavior as tested by the time spent in the center of the arena or the latency to the 1<sup>st</sup> border zone entry during the OFT (Figure 9A and B). Neither were there any distinctions in locomotor activity and ability tested by the activity parameters during the OFT (Figure 9C – E) or beam walk (Figure 10). Furthermore, no differences in motor coordination were found during beam walk in either falls per trial, slips per trial and latency (Figure 6A-C). This is consistent with

expectations, as BK was knocked out exclusively in the hippocampus and not in the Purkinje cells, where BK is responsible for motor coordination. Thus, results of the MWM are genuinely based on impaired cognitive performance.

### **5.2.2. Function of BK in memory acquisition and retrieval**

Western blot and immunofluorescence analysis confirmed specific and effective recombination efficiency of BK in the cKO (4.1). To test the learning behavior of the mice, the MWM was employed. The increased latency of the cKO during the acquisition phase as well as the increased time spent in the quadrant opposed to the target indicated significantly impaired memory acquisition and memory retrieval, respectively (**Figure 11A and B**). This is consistent with the findings of Typlt et al. (2013) who also observed increased latency in global BK<sup>-/-</sup>. Therefore, this data confirms a key role of postsynaptic BK channel in the hippocampus for physiological memory acquisition. Since the MWM is a hippocampus-dependent test (Vorhees & Williams, 2006) and the hippocampus is the most important brain region for spatial learning, this observation is consistent with our expectations.

BK is not the only K<sup>+</sup> channel in the Slo family that is associated with synaptic plasticity. The absence of Slack, which, as the name suggests, has protein sequence homologous to BK, namely a part of the pore domain as well as the downstream TM6, also leads to altered learning behavior. In contrast to cKO, Slack<sup>-/-</sup> showed normal memory acquisition but failed in the reversal phase indicating a lack in memory flexibility (Bausch et al., 2015). Accordingly, adult Slack<sup>-/-</sup> display normal hippocampal LTP, but lack LTD (Matt et al., 2021). This disability to remove memory engrams might be explained by Slack acting like an activity sensor, providing a link between neuronal activity and activity-dependent protein synthesis, maybe through its interaction with the mRNA-binding protein FMRP which is involved in the control of local translation (Ferron, 2016; Zhang et al., 2012). Activity-dependent protein synthesis is particularly important for the gene expression of proteins, which is required for functioning memory extinction (Vianna et al., 2003). A connection with gene expression has also been reported for BK (Li et al., 2016), although in contrast to Slack, this seems to take place directly in the nucleus (Li et al., 2014; Li et al., 2020). On this basis, the different contributions of BK and Slack to the synapse are attributable to the fact that BK is capable of rapid hyperpolarization, affecting the acquisition phase, whereas Slack additionally involves gene expression, being more important for memory flexibility.

### **5.2.3. Impact of BK on learning and memory in aged mice**

Aging of the brain leads to a reduction in synaptic function resulting in memory loss. With age, the number of glutamatergic neurons does not decrease significantly (Morrison & Hof, 1997). Therefore, age-related deficits in memory are likely due to impaired synaptic

plasticity originating from reduced postsynaptic response to neurotransmitters and decreased neuronal excitability (Kempsell & Fieber, 2015). It has already been shown that expression of  $K^+$  channels decrease with age (Brown & Kaczmarek, 2011; Eatock, 2003; Gates et al., 1999; Jung & Lambon Ralph, 2021). Such age-related decline was also observed for BK activity in neurons of the SCN (Farajnia et al., 2015) and dorsal spinal ganglia (Yu et al., 2015). Hence, there maybe also an age-dependent reduction in BK activity in hippocampal neurons. As seen in **Figure 11A** and **Figure 15A**, reduced BK function led to worsened memory acquisition and non-inducible LTP, respectively. These deficits are also expected to be observed in older individuals. For this reason, in addition to the young animals at 2 - 4 months of age, 12-month-old CTRL and cKO were tested for a BK-dependent effect on possible cognitive decline. An age-dependent reduction in cognition can be assumed in this age (Wong and Brown, 2007). Surprisingly, no difference was found between CTRL and cKO in memory acquisition and flexibility in the MWM (**4.3**). The reason for the similar performance of both genotypes may be that BK activity in the CTRL has age-dependently decreased to such an extent where the cognitive performance of the CTRL matches that of cKO. This important aspect was unfortunately not further addressed in the present work. Surprisingly, however, the decline in latency is much faster in the young mice than in the aged mice. This observation is supported by the last day of the acquisition phase, on which the aged mice have a latency of approximately 25 s, whereas it is less than 20 s in young animals. A lower cognitive performance of the old mice compared to the young mice is a more likely explanation than deteriorated swimming ability, because at the age of 12 months, no limitations of motor characteristics can be assumed yet (Gower & Lamberty, 1993). Another reason could be that the older mice performed only two swimming sessions per day, while the younger ones did four and therefore were better able to learn platform placement. To identify the reason between the cognitive performance between young and aged mice, they should have been evaluated side-by-side within the same experimental cohort. Unfortunately, due to the young and aged groups being examined individually at different times, they cannot be compared to each other by stringent statistics. It would also be interesting to examine whether aged CTRL vs. cKO or young vs. aged showed altered LTP. In addition to cognition, anxiety behavior and locomotor characteristics of the mice were tested and did not differ between genotypes and the groups of mice with different ages. This is consistent with present data, as age does not appear to have a negative effect on these traits (Gower & Lamberty, 1993).

### **5.3. Ex vivo characterization of synaptic plasticity in cKO**

#### **5.3.1. Lack of LTP in BK-deficient mice**

It is generally well accepted that LTP is the molecular correlate to the acquisition phase (Bannerman et al., 1995; Jeffery & Morris, 1993; Morris et al., 1986; Moser et al., 1998). To confirm the findings again on *ex vivo* level, LTP was induced by HFS and FRP in acute

brain slices of cKO and CTRL mice. Consistent with increased latency of cKO, potentiation fell back to baseline levels after 60 minutes post-HFS and GluA1-S845 phosphorylation was reduced, respectively, which therefore leads to the conclusion that LTP could not be expressed.

In Matt et al. (2021) LTD in *Slack*<sup>-/-</sup> could not be induced either, which matches the finding of defective memory flexibility in the reversal phase of the MWM (Bausch et al., 2015). The relationship between the reversal phase and LTD is well studied and established. Usually, findings in the reversal phase of the MWM could be confirmed equally in the LTD and vice versa (Collingridge et al., 2010; Nicholls et al., 2008). This was the reason why LTD was not examined in cKO in this study, as the performance in the reversal phase was comparable between genotypes (**Figure 11E**).

## **5.4. *In vitro* characterization of BK in synaptic plasticity**

### **5.4.1. In search of BK's molecular contribution to LTP induction**

In search of the molecular mechanism behind the learning deficit of cKO, the following three strategies were employed. First, presynaptic as well as postsynaptic functions were analyzed. This was done to rule out the possibility that it is not a constraint of the molecular machinery for LTP, but rather reduced basal synaptic transmission or reduced presynaptic glutamate release probability that leads to a defective potentiation in cKO. In the NEX-Cre<sup>tg/+</sup> *Swell1*<sup>fl/fl</sup> mouse model, for instance, in which *Swell1*, an obligatory subunit of the glutamate-permeable volume-regulated anion channel VRAC, is absent in all neurons including the hippocampus, increased PPF ratio was observed (Yang et al., 2019). Because increased PPF ratio indicates a basal, lower glutamate release probability, this indicated defective presynaptic function, which was also reflected in reduced LTP and poorer memory retrieval in the NEX-Cre *Swell1*<sup>fl/fl</sup> (Yang et al., 2019). PPF ratios in cKO, however, suggest normal presynaptic function (**Figure 15B**). Due to BK knockout in cKO being constricted to the (postsynaptic) CA1 region, this was in accordance with expectations.

Second, a reduction in basal synaptic transmission may also lead to defective LTP formation, as this may indicate a reduced density or altered subunit composition of postsynaptic AMPAR (Christie et al., 2010; Cisternas et al., 2019). We could, however, not detect any discrepancies in IOR between genotypes. This was despite the fact that IOR is a readout of postsynaptic function, the location where BK is knocked out in the cKO model. This finding can probably be explained by the fact that under conditions of basal synaptic transmission,  $[Ca^{2+}]_i$  is not sufficient to activate BK.  $K^+$  conductance and transport for plasma membrane repolarization during regular synaptic transmission is most likely carried out by other molecules that require lower or no  $Ca^{2+}$  to function. Corresponding candidates might be SK (Sun et al., 2020) or  $K_v$  (Kim & Nimigeon, 2016) channels. Moreover, in the subsequent live imaging experiments, it was observed that without

stimulus, neuronal activity is already present, but is not sufficient to provoke measurable  $K^+$  efflux (see first 5 minutes of **Figure 19A** and **Figure 18C**).

Despite normal IOR indicating unaltered basal synaptic transmission and consequently normal iGluR expression and composition, iGluR expression and its subunit composition were nevertheless tested. The decision was influenced by findings in Matt et al. (2021), where infantile *Slack*<sup>-/-</sup> also displayed deficient LTP. Biochemical analysis, however, found significantly reduced postsynaptic GluN2B content, while total NMDAR expression was unchanged. This finding implicated GluN2B being important for physiological LTP (Matt et al., 2021). This is likely since GluN2B-containing NMDARs have lower  $Mg^{2+}$  sensitivity than GluN2A-containing NMDARs and are therefore more easily activated. In addition, their conductivity is higher (Wyllie et al., 2013). Related to this, the expression of AMPAR and NMDAR and their subunit composition were additionally analyzed in whole hippocampal lysates of cKO as a second strategy. No altered expression or subunit composition of NMDAR and AMPAR was observed in either learn-naive mice or mice that completed the MWM.

As a third and final approach, phosphorylation of AMPAR at the GluA1 subunit was tested at phosphorylation site S845 after cLTP induction, showing a significantly higher increase in CTRL compared to cKO. Exocytosis probability and thus incorporation into the postsynaptic membrane of intrasynaptic GluA1 contained in postsynaptic vesicles is favored by phosphorylation at GluA1-S845 (Roche et al., 1996). This mechanism does not appear to work in cKO.

In summary, it became clear that the phosphorylation mechanism of GluA1, and thereby its incorporation into the postsynaptic membrane, was no longer occurring because of the lack of BK function. However, the exact connection between phosphorylation and AMPAR incorporation and the mechanism behind it could not be determined by this experiment. However, Forskolin, a PKA activator, and Rolipram, a PDE4 inhibitor, both present in the cLTP-inducing cocktail, increase intracellular cAMP levels, resulting in enhanced PKA activity. The enhanced PKA activity could therefore phosphorylate both BK and AMPAR. In this case, BK phosphorylation could lead to higher voltage and  $Ca^{2+}$  sensitivity and thus to an increased open probability (Schubert & Nelson, 2001). This would contribute to an increased  $Ca^{2+}$  influx through LTCC and NMDAR via a positive feedback mechanism (5.4.2) and promotes LTP expression. In the case of AMPAR, the PKA-dependent phosphorylation of GluA1-S845 also leads to a higher open probability and favors the incorporation of AMPAR into the postsynaptic membrane. (Fernandez-Monreal et al., 2012; He et al., 2009; Yang et al., 2008; Yang et al., 2010).

#### **5.4.2. BK-mediated effects on $Ca^{2+}$ and $K^+$ dynamics during cLTP induction**

$K^+$  sensitive real-time measurements in cultured hippocampal neurons revealed a strong, BK-mediated  $K^+$  efflux occurring during cLTP induction (**Figure 18C**). As expected, this strong  $K^+$  efflux appears to be a response to the increased  $Ca^{2+}$  oscillation frequency

during cLTP as compared to the basal state (**Figure 19A**). This is unsurprising, because in addition to depolarized membrane potentials, BK requires a high local  $\text{Ca}^{2+}$  concentration in its microdomain to open (Shah et al., 2021) (**Figure 21A**). Prior to cLTP, the basal spiking frequency is probably not sufficient to support BK activation, as no  $\text{K}^+$  efflux is observed with GEPH. The doubling of spike frequency by cLTP induction, however, seemed to be sufficient to provoke strong  $\text{K}^+$  efflux. The oscillation frequencies in **Figure 19** are not absolute indicators for the intracellular spike frequency which is assumed to correlate with AP frequency.  $\text{Ca}^{2+}$  spikes at AP frequencies ( $>10$  Hz) are too fast to be measured by Fura-2 and the microscope used, but they still give a good relative measure. No  $\text{Ca}^{2+}$  oscillations or  $\text{K}^+$  efflux were observed after BK blockade by PAX or in  $\text{BK}^{-/}$  cells (**Figure 19B, C and Figure 18D, E, respectively**). This indicates how important  $\text{K}^+$  efflux is for neuronal excitability as well as firing frequencies and  $\text{Ca}^{2+}$  signaling. Initially, this appears counterintuitive since  $\text{K}^+$  efflux is expected to hyperpolarize the cell membrane and therefore inhibit  $\text{Ca}^{2+}$  influx. It is not, however, the first finding which would prove BK to be responsible for increased excitability of the cell (Gittis et al., 2010; Gu et al., 2007; Perez et al., 2013). The literature describes BK as a dynamic fine tuner, helping to amplify small electrical signals and to weaken too strong electrical signals (Contet et al., 2016). This apparent contradiction can be better understood if the timing of BK activation is understood. Usually, the AP is divided into the following three phases: First, depolarization is mediated by voltage-gated  $\text{Na}^+$  and  $\text{Ca}^{2+}$  channels, followed by a second phase of repolarization by rapidly activating voltage-gated  $\text{K}^+$  channels. Finally, mainly slow activating and deactivating voltage-gated  $\text{K}^+$  channels provide the AHP phase. BK can dynamically fine tune these events because it can both repolarize through its fast-activating ability but can also participate in the AHP. As a result, BK can either accelerate or decelerate spontaneous firing by participating in fast repolarization through fAHP and slower AHP, respectively (Faber & Sah, 2002; Gu et al., 2007; Montgomery & Meredith, 2012).

The  $\text{Ca}^{2+}$  oscillations supported by BK during cLTP, remained completely absent when either AP5 or NIFE were additionally applied (**Figure 19D and E**) suggesting both NMDAR and LTCC as  $\text{Ca}^{2+}$  sources for the observed oscillations. Indeed, functional and molecular interactions of BK with both NMDAR and LTCC was previously reported (Gomez et al., 2021; Marcantoni et al., 2010; Zhang et al., 2018) and would therefore support the observation. In the case of LTCC, as described briefly before, BK is assumed to support  $\text{Ca}^{2+}$  oscillations through  $\text{K}^+$  efflux in a positive feedback manner via the fAHP mechanism (**Figure 21B**). Explaining how BK activity is related to NMDAR activity is more difficult. NMDARs are activated by simultaneous binding of glutamate and a co-agonist (usually glycine or D-serine). The ion conducting pore, however, is only permeable when the  $\text{Mg}^{2+}$  block is released by postsynaptic depolarization (Kampa et al., 2004). Based on that information, BK-mediated hyperpolarization would be expected to inactivate NMDAR by strengthening the  $\text{Mg}^{2+}$  or by pulling an  $\text{Mg}^{2+}$  ion back into the pore. Surprisingly, the opposite has been observed in this study. This may be mainly due to the peculiarity of the NMDAR being blocked by an  $\text{Mg}^{2+}$  ion. After the  $\text{Mg}^{2+}$  is ejected by depolarization, e.g., by

AMPA, the  $Mg^{2+}$  unblocking breaks down into a fast and a subsequent slow component. A physiological consequence is that short depolarizations occurring at an earlier time point after glutamate application are better able to open NMDAR channels (Kampa et al., 2004). Because BK in hippocampal neurons is responsible for rapid firing frequency and thus for frequency regulation (Gittis et al., 2010; Gu et al., 2007; Perez et al., 2013), it can maximally open NMDAR channels with short and rapid successive depolarizations, leading to well-functioning plasticity.

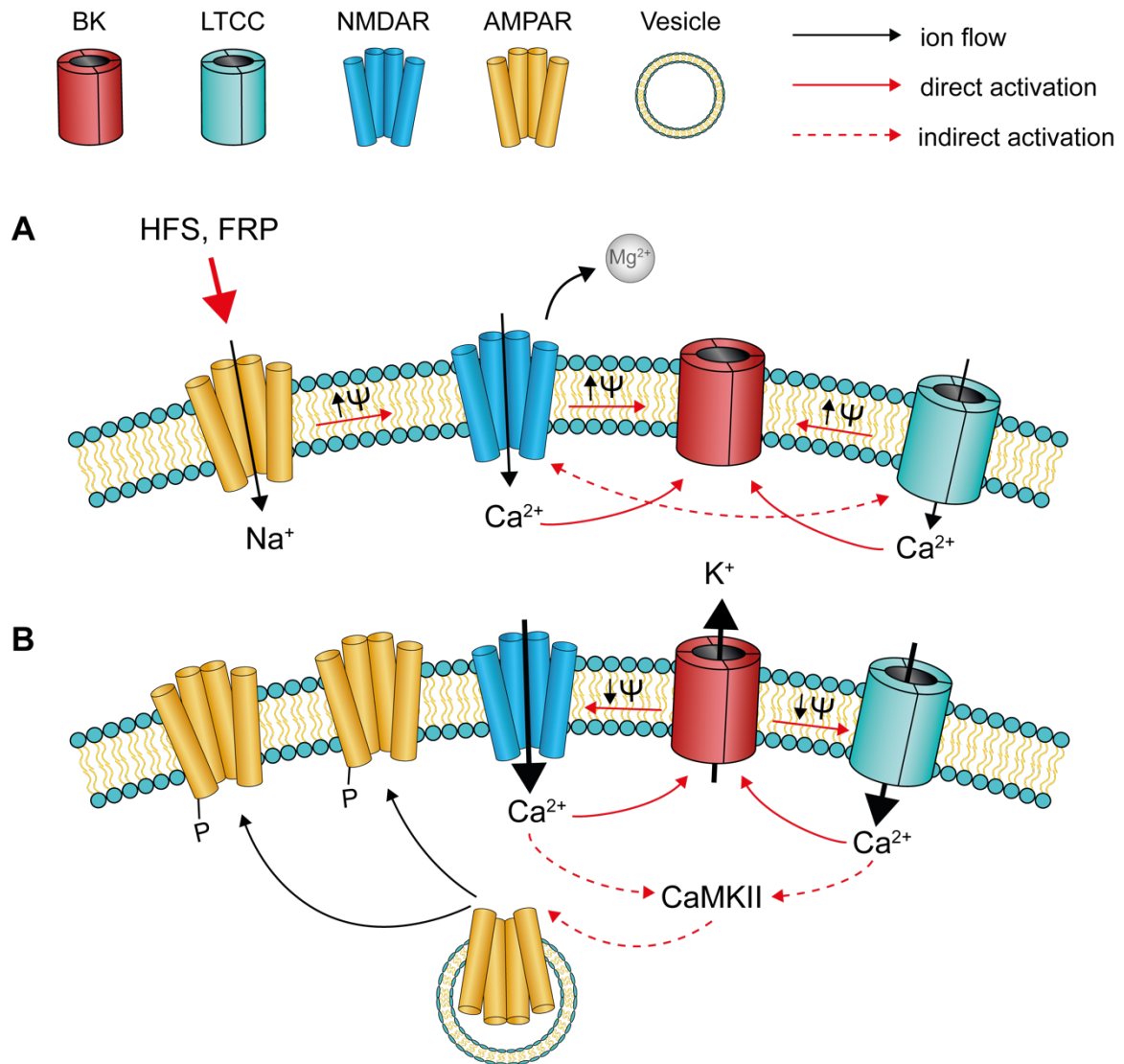


**Figure 21: Proposed mechanism of BK's contribution to synaptic plasticity. (A)** LTP induction through HFS or FRP activates (AMPA) allowing  $Na^+$  influx to depolarize the postsynaptic membrane. The more positive membrane potential increases  $[Ca^{2+}]_i$  through two mechanisms: First, releasing the  $Mg^{2+}$  block of the NMDAR conducting pore to allow its opening and second, by activating LTCC. Furthermore, NMDAR and LTCC synergize, with NMDAR aiding in membrane depolarization and thereby enhancing the activation of LTCC. Upon activation, LTCC undergoes a conformational alteration causing an increase in the conductance of both LTCC and NMDAR. BK is activated by both depolarization and high local  $[Ca^{2+}]_i$ . **(B)** Due to the high conductance for  $K^+$  and its rapid kinetics, BK-mediated fAHP promotes rapid reactivation of NMDAR and LTCC, which subsequently facilitate synaptic plasticity through increased  $Ca^{2+}$  oscillations.  $Ca^{2+}$  binds to CaMKII, which activates signaling pathway to promote AMPAR phosphorylation to promote its incorporation into the postsynaptic membrane.

Both inhibition of LTCC or NMDAR by NIFE or by AP5, respectively, completely abolishes  $\text{Ca}^{2+}$  influx (**Figure 19D and E**). At first sight, this is slightly surprising, since the other protein could theoretically compensate for the  $\text{Ca}^{2+}$  influx and  $\text{Ca}^{2+}$  would still enter the cell to initiate LTP. Our findings are supported by the fact that both application of AP5 and NIFE alone can result in complete inhibition of LTP (Cavus & Teyler, 1996). It appears that NMDAR and LTCC act synergistically, in a way that NMDAR released from  $\text{Mg}^{2+}$  blockade by the AMPA/kainate receptor are responsible for the opening of LTCCs (Rajadhyaksha et al., 1999). Conversely, TBS-induced NMDAR-dependent LTP could no longer be induced in a  $\text{Ca}_v1.2$  LTCC KO mouse model (Sridharan et al., 2020).  $\text{Ca}_v1.2$  LTCC can commit a conformational change after activation, not only increasing their own conductance, but also that of NMDAR (Li et al., 2016) (**Figure 21A**). This would explain why a complete loss of  $\text{Ca}^{2+}$  influx is observed regardless of whether LTCC or NMDAR are blocked.

### **5.4.3. BK and other $\text{K}^+$ channels in synaptic plasticity**

Despite the high sequence homology between Slack and BK, both channels differently contribute to synaptic plasticity in the hippocampus as previously described. Another  $\text{K}^+$  channel that has already been linked to synaptic plasticity is SK. Pharmacological inhibition of SK by apamin enhances LTP and improves spatial learning by abolishing SK-mediated AHP, which otherwise contributes to inhibition of NMDAR (Faber et al., 2005). It seems to be paradoxical that pharmacological inhibition of SK, in contrast to BK, leads to enhanced LTP, after all, both are  $\text{K}^+$  channels and also contribute to AHP. However, BK has been shown to be involved in rapid repolarization after APs. Consistent with our observations, BK inhibition was previously shown to slow the firing rate of hippocampal CA1 pyramidal cells, GABAergic neurons, and cardiac autonomic neurons (Gittis et al., 2010; Gu et al., 2007; Pérez et al., 2013). The reason why SK channels respond differently could be that SK activation decreases expression of CaMKII (Shrestha et al., 2019), which no longer phosphorylates AMPAR. This, in turn, reduces the probability of AMPAR exocytosis, which would favor postsynaptic potentiation.

## **5.5. Putative role of BK in pathologies of the CNS**

### **5.5.1. BK in epilepsy**

In addition to its fundamental role in synaptic plasticity, BK was also assigned an important role in epilepsy. Epilepsy is a chronic neuropathological condition in which neurons are easily excitable and excitation is abnormally synchronous, resulting in pathological brain activity, also called seizures (Milligan, 2021). This leads to the assumption that BK hyperactivity causes faster recovery of  $\text{Na}^+$  channels from their inactivated state which shortens the refractory period and therefore provokes higher neuronal excitation due to faster repolarization and higher AHP amplitude. This is in accordance with the data

observed in this study, as BK is required in the hippocampus to drive at least LTCC to a faster recovery from the refractory period. In BK  $\beta 4$  KO mice, increased spontaneous seizures were observed to originate in the hippocampus and spread throughout the neocortex (Brenner et al., 2005). Therefore, it might make sense to investigate the composition of hippocampal BK channel complexes in healthy and epileptic people, to investigate if the abundance of  $\beta 4$  subunits negatively correlates with seizure susceptibility and whether the hippocampus expresses more  $\beta 4$  than other brain areas.

### **5.5.2. Synaptic plasticity as an early marker of impaired cognitive performance**

AD is the most common form of dementia and the prognosis worsens with advancing age (Querfurth & LaFerla, 2010). A breakthrough in AD research occurred when A $\beta$  was discovered to play a major pathogenic role in familial clustering of AD cases. It is controversially discussed that mutations of genes encoding APP or presenilin can result into pathological accumulation of A $\beta$  at the translational level, in an early form of AD (Chapman et al., 2001; Selkoe, 2002; Wang et al., 2006). As a result, the amyloid cascade hypothesis was proposed, in which mutations can increase synaptotoxic A $\beta$ , triggering structural brain damage, associated synaptic dysfunction and memory loss in disease progression.

AD research and testing of potential therapeutics has focused primarily on the 3xTg mouse model, which incorporates, as already stated (1.3), mutated human APP, Tau and PS genes to elicit AD-like deposition (Ashe, 2001; Janus & Westaway, 2001; Zaks & Ashe, 2010). However, evidence suggests that the A $\beta$  hypothesis is inadequate to explain AD pathogenesis, especially since studies trying to prevent A $\beta$  depletion as therapeutic strategy have all been unsuccessful (De Strooper & Karran, 2016; Herrup, 2015; Small & Duff, 2008). Although aducanumab has long been found to be a promising therapy, it has not been convincing in phase III clinical trials because successful removal of A $\beta$  plaques by aducanumab did not correlate with improved cognitive performance (Budd Haeberlein et al., 2022). Lecanemab, a further antibody targeting A $\beta$ , which was approved by the FDA in 2023, also achieved a significant reduction in A $\beta$  to below 30 centiloids (van Dyck et al., 2023) in the verum group of patients with early AD, which is considered the cut-off for elevated A $\beta$  levels (Fleisher et al., 2011). Nonetheless, this only resulted in limited success regarding improved cognition. The Clinical Dementia Rating-Sum of Boxes (CDR-SB) score was utilized to evaluate cognitive and functional capabilities. In the verum group, the score demonstrated a significant difference of merely 0.45, which falls below the 0.5 threshold indicating clinical relevance as per the consensus (Borland et al., 2022). The problem is that the A $\beta$  hypothesis only applies to heritable FAD, however AD is also characterized by other mechanisms of pathogenesis. The decline in cognitive performance in AD, as well as in other ND associated with a decline in cognition, however, is consistent with impaired synaptic plasticity.

Interestingly, several studies suggest a period before plaque deposition in early AD, when cognitive impairment is not yet observed, but synaptic plasticity has already decreased. This probably comes from soluble A $\beta$  that is harmful to neurons through synaptotoxicity and hampers synaptic plasticity (Haass & Selkoe, 2007; Querfurth & LaFerla, 2010). In the future, reduced LTP may thus be considered an early clinical marker for AD (Jacobsen et al., 2006; Ma et al., 2010; Oddo et al., 2003). As soon as plaques formation can be diagnosed, neuronal decline has already happened and the disease has manifested. Even results attesting normal cognitive function might thus come too late, because the reduction in plasticity might already have started. As a result, individuals with a higher risk state for AD or other ND should be tested for plasticity (Hill et al., 2011).

### 5.5.3. BK as a therapy for impaired synaptic plasticity

The *in vivo* MWM and *ex vivo* LTP experiments in **Figure 11A** and **Figure 15A**, respectively, suggest that BK is necessary for physiological memory consolidation. Although the study did not test whether BK activation leads to improved cognition, the body of studies suggests that it may. For example, in the 3xtg AD mouse model, intraneuronal deposition of A $\beta$  was shown to reduce BK currents to unmeasurable levels (Rowan et al., 2005; Yamamoto et al., 2011). When BK was activated by electroconvulsive shock, BK currents were present again (Sakagami et al., 2005; Yamamoto et al., 2011). These findings were confirmed when decreased BK activity was observed after the injection of A $\beta$  peptide into neocortical pyramidal cells of in healthy mice (Yamamoto et al., 2011). These studies together with the present findings suggest BK channels as potential therapeutic target to improve cognitive performance, not only in AD, but also in other ND associated with cognition decline. Potential clinical therapeutics might include BK channel activators like BMS-204352, NS1619, and NS11021, which have previously been used in clinical trials but were never approved for their intended use. For example, BMS-204352 was originally used for the acute neuroprotective treatment of ischemic stroke (Jensen, 2002). Ischemic stroke occurs when a detached thrombus prevents blood flow into cerebral arteries causing rapid neuronal cell death from anoxia and the ensuing neurotoxic Ca<sup>2+</sup> uptake due to excessive hyperexcitation (Moskowitz et al., 2010).

The well-tolerated BMS-204352 is thought to limit Ca<sup>2+</sup> influx by amplification of BK-mediated AHP, thereby protecting neurons from demise. In the case of reduced cognition, analogous to the data in **Figure 11A**, BMS-204352 would support the reciprocal activation of NMDAR and LTCC, leading to more Ca<sup>2+</sup> oscillations, which might in turn improve cognitive performance. That BMS-204352 should lead to reduced Ca<sup>2+</sup> influx in stroke and more Ca<sup>2+</sup> influx for improved cognition is again not a contradiction but owing to BK's ability to fine-tune. While stroke provokes a tonically high Ca<sup>2+</sup> influx, Ca<sup>2+</sup> influx during LTP is of oscillating nature. One can therefore assume that in this case, Ca<sup>2+</sup> only reaches high concentrations in BK-containing nanodomains. Before the occurrence of Ca<sup>2+</sup>-mediated excitotoxicity, Ca<sup>2+</sup> influx is limited by rapid BK activation. In rats, BMS-204352 could significantly reduce cortical infarct volume 2 hours after TMCAO (Jensen, 2002).

Nevertheless, research on BMS-204352 was discontinued, as in phase III trials no reduction of infarct tissue was achieved in treated stroke patients compared to the placebo group (Jensen, 2002). Although it did not lead to any improvement in stroke outcome, could BMS-204352 lead to future treatment of reduced synaptic plasticity and thus improve cognitive performance? This is rather unlikely, as BMS-204352 not only activates BK, but also inhibits glutamate release by 25-30% (Gribkoff et al., 2001). This is of course good for inhibiting excitotoxicity, which is what BMS-204352 was designed for in the first place. This mechanism of action, however, would result in reduced synaptic transmission and probably exert negative influence on synaptic plasticity. Consequently, this would result in a reduced postsynaptic  $Ca^{2+}$  influx, which would at least substantially inhibit LTP. Another possibility is to use the BK activator NS1619 and the approx. 10x more potent and more specific NS11021. NS11021 seems to be the most suitable. Although inhibition of glutamate release is not described in the literature for NS1619, its occurrence has nevertheless to be expected, since NS1619 is described to inhibit SERCA (Wrzosek, 2014). This would be particularly evident in the presynapse, as the  $Ca^{2+}$  induced  $Ca^{2+}$  release (CICR) from the ER triggered by LTCC is crucial for glutamate release. After CICR, SERCA inhibition may result in a prevention in re-uptake of the released  $Ca^{2+}$  from the ER, leading to an increase in cytosolic  $[Ca^{2+}]_i$ . In fact, direct SERCA inhibition by Thapsigargin reduced the increase in  $[Ca^{2+}]_i$  after tetanic stimulation. This leads to the assumption that the ER cannot be replenished by SERCAs once emptied, due to the inhibition caused by Thapsigargin and probably NS1619. This lack of replenishment causes CICR to cease. Reduced cytosolic  $[Ca^{2+}]_i$  prevents the fusion of glutamate containing vesicles with the presynaptic membrane and consequently glutamate release. Presumably, this is the same mechanism by which BMS-204352 inhibits glutamate release. It would also be conceivable to use drugs that are already available on the market and might indirectly modulate BK channel activity by altering its phosphorylation state which could be NO-GC/cGMP modulating drugs. The cGKI-dependent phosphorylation of BK leads to an increased voltage and  $Ca^{2+}$  sensitivity (**see 1.5**) (Schubert & Nelson, 2001). This would suggest that cGKI-dependent activation of BK may lead to even higher  $Ca^{2+}$  oscillations, which might in turn facilitate learning processes. There are already many approved cGMP elevating drugs such as Riociguat and Vericiguat, both of which are NO-GC stimulators, Sildenafil and Vardenafil, PDE5 inhibitors and Sacubitril, a neprilysin inhibitor, all of which can lead to cGKI activation. This approach would have the advantage that the risk profile of these drugs is already known (Armstrong et al., 2020; Galie et al., 2005; Ghofrani et al., 2013; McMurray et al., 2014). The disadvantage is that none of these drugs penetrates the blood-brain barrier (BBB). For this purpose, the NO-GC stimulators BAY-747 and CY6463 and the NO-GC activator Runcaciguat were developed as BBB penetrating candidates, which look promising in the first pre-clinical studies (Correia et al., 2021; Nelissen et al., 2022). However, it remains to be seen whether these effects are BK dependent.

## 5.6. Limitations and subsequent experiments

The findings in this present study provide clear evidence that BK plays an important role in synaptic plasticity, both *in vivo* and *in vitro*. Several paradigms were used to initiate memory formation. *In vivo*, memory acquisition was induced by the MWM, whereas *ex vivo* and *in vitro* LTP was induced in acute brain slices and cultured hippocampal cells by electrical HFS and chemically by cLTP, respectively.

One of the main criticisms against the MWM is that the learning behavior of the mouse may possibly be affected by the stress induced from fear of drowning (Moreira et al., 2016; Wong et al., 2007). As a stress-free alternative to the MWM, the hippocampus-dependent Barnes Maze was proposed, in which mice have to find, among many escape options, the one escape option where shelter from predators could be found (Pitts, 2018). In turn, the disadvantage of the method is that the subject's motivation is low and many mice do not complete the test but remain on the spot. The conclusions this study draws from MWM data, however, should not be affected by this particular bias, as stress is assumed to affect both CTRL and cKO in the same way. In addition, the results on reduced cognitive performance in cKO could be corroborated by electrically and chemically induced LTP.

It is very well established that synaptic plasticity during MWM as well as electrical LTP, relies on the same molecular principles, thus allowing the translation of findings within one experiment to the other (Vorhees & Williams, 2006). Although there are also reports for such similarities between cLTP and conventional LTP, this connection is not fully understood yet. GluA1-S845 and S831, for example, are thought to be important for LTP expression as they promote AMPAR incorporation into the postsynapse as well as higher AMPAR conductance. For example, increased phosphorylation at GluA1-S831 was detected after HFS-LTP (Lee et al., 2000), whereas increased pS845-GluA1 was not. Indeed, a higher and sustained potentiation of fEPSP was also observed after perfusion with FRP (Otmakhov et al., 2004). Also in our hands, cLTP leads to a highly significant potentiation of fEPSP recordings in slices (**Figure 15A**). Together with the fact that cLTP reliably induces phosphorylation at GluA1-S845, this suggests that results from cLTP can be transferred to electrical LTP and vice versa.

Another criticism could regard the mechanisms of cLTP induction by FRP. Although FRP was shown to induce LTP, the presence of the cAMP-inducing Forskolin suggests that PKA activation might just induce a kind of NMDAR-independent LTP. This possible drawback to the FRP cocktail was addressed by Otmakhov et al. (2004). In that study, NMDAR inhibition prevented potentiation of fEPSP during cLTP. Also, direct PKA activation by the cAMP analog Sp-cAMPS did not potentiate synapses when NMDAR are blocked (Bozdagi et al., 2000). This suggests that increased cAMP levels are not sufficient to induce LTP, despite the PKA signaling pathway's clear contributions to synaptic plasticity, which still requires an active NMDAR. Other studies found similar results (Barco et al., 2002; Huang & Kandel, 1995; Ma et al., 1999). A possible explanation for this unexpected finding is the two components concept of LTP. This hypothesis characterizes LTP first as the increased incorporation of AMPAR into the post synapse (LTPN) and

second as the increase of AMPAR conductance through elevated numbers of Ca<sup>2+</sup>-permeable AMPAR (LTP<sub>γ</sub>). To induce LTPN, CaMKII activation is sufficient, while LTP<sub>γ</sub> additionally requires active PKA signaling (Park et al., 2021). Since CaMKII activation requires NMDAR-mediated Ca<sup>2+</sup> influx, NMDAR inhibition prevents CaMKII activation and autophosphorylation and consequently the initiation of LTP. Ca<sup>2+</sup> influx would not be compensated by LTCC either (**Figure 19D**). Although it is relatively clear that FRP induces NMDAR-dependent LTP, cLTP experiments could also be performed using a more obvious NMDAR-mediated induction paradigm like low or no Mg<sup>2+</sup> in combination with its allosteric modulator glycine.

Next, the question arises whether phosphorylation at GluA1-S845 is indeed important for postsynaptic AMPAR incorporation and is therefore the correct readout for the cLTP experiment? Since phosphorylation of GluA1-S845 represents an important experimental readout of experiments using acute brain slices (**Figure 17**), this would be important to check. There recently was some controversy in the literature about the fraction of total AMPAR that gets phosphorylated at GluA1-S845 after cLTP induction. Using Phos-tag SDS-PAGE, one study reported to find only between 0.1 to 1 % of S831 and S845 to be basally phosphorylated (Hosokawa et al., 2015). After neuronal stimulation or *in vivo* learning, the proportion increased only insignificantly. This suggested that most AMPAR are not phosphorylated at all and consequently questions the importance of phosphorylation for incorporation into the postsynaptic membrane and enhancement of conductance. However, this result argues against many studies that have previously attested an importance of the s845 and S831 phosphorylation site (Huganir & Nicoll, 2013). Additionally, studies using phosphodeficient and phosphomimetic GluA1 and GluA2 knockin mice showed that AMPAR phosphorylation is indeed essential for synaptic plasticity. LTP/LTD in the cortex, cerebellum, and hippocampus require AMPAR phosphorylation to function (Lee et al., 2003; Steinberg et al., 2006). The regulation of excitability for LTP induction as well as the process to reinforce fear learning, are blocked in mice, in which the LTP associated phosphorylation sites of GluA1 are mutated from S831 and S845 to alanine (Hu et al., 2007; Lee et al., 2003; Seol et al., 2007).

The study from Hosokawa et al. (2015) was thus widely criticized and refuted. Shortly after its publication, Diering et al. (2016), in direct answer demonstrated that the basal phosphorylation of GluA1 is around 10-15% and even increases up to 50% after LTP induction. Thus, S845 can be regarded as a valid readout for the study of synaptic plasticity.

Once established, the cLTP protocol was subsequently used with dissociated neurons, where a strong K<sup>+</sup> efflux and increased Ca<sup>2+</sup> oscillation frequencies could be observed (**Figure 18 and Figure 19**). Interestingly, sustained K<sup>+</sup> outflow did not affect the membrane potential (**Figure 20**). This finding was so far not verified using current clamp recordings during cLTP induction. However, this would be technically difficult if the neurons were patched in a manner analogous to live imaging experiments, as they would have to remain in this state for up to half an hour. More feasible would be the quantification of the

membrane potential by a fluorescence microscope, enabled by DiBAC<sub>4</sub>(3). The advantage is that DiBAC<sub>4</sub>(3) is non-toxic at the concentration recommended by the manufacturer and therefore well tolerated by the cell. The disadvantage is that the dye is intensimetric and thus very susceptible to variable microscope settings and resulting artifacts. No large net change in membrane potential was found, likely due to the strong K<sup>+</sup> efflux occurring rapidly after depolarization as a result of the increase in [Ca<sup>2+</sup>]<sub>i</sub>, which rapidly repolarized the membrane potential. In addition, DiBAC<sub>4</sub>(3) images the membrane potential too slowly compared to the frequency that is needed to image the FURA-2 oscillations. In this case, however, it was sufficient to compare the basement membrane potential with the potential during and after cLTP induction, because depolarization after glutamate perfusion was nevertheless indicated to be relatively fast and DiBAC<sub>4</sub>(3) responded more promptly than the manufacturer's instructions may suggest.

Another aspect in need of future attention is the role of the NO/cGMP/cGKI pathway in synaptic plasticity. This is of particular interest, because the cGKI is known to activate BK channels by phosphorylation at S691 and S873. Since there are already numerous cGMP-based drugs on the market whose risk profile is already known, their applicability to support cognitive performance would be particularly valuable. cGMP is either generated by membrane-bound particulate guanylate cyclase (pGC) or by cytoplasmic soluble nitric oxide sensitive guanylate cyclase (NO-GC). The NO-GC was shown to be of particular importance for learning behavior. In contrast to the pGC, the NO-GC is expressed in many different regions of the brain such as hippocampus, striatum, cerebral cortex and locus coeruleus (Matsuoka et al., 1992). Exploiting NO-GC as pharmacological target to improve cognitive performance is a rather recent strategy, so there is little literature in this field of NO-GC drug development. However, the importance of NO-GC in learning behavior is beyond doubt. ODQ, an inhibitor of NO-GC was shown in a wide variety of studies to inhibit LTP (Arancio et al., 1995; Boulton et al., 1995; Chien et al., 2003; Zhuo et al., 1994).

Furthermore, bilateral intrahippocampal administration of the NO-GC inhibitor LY 83,583 induced complete amnesia in experimental animals (Bernabeu et al., 1997). In reverse, activation of NO-GC was shown to improve memory by two weeks application of the NO-GC activator Yc-1 in 24-month-old rats, which significantly improved memory acquisition (Komsuoglu Celikyurt et al., 2014). The positive NO-GC effect on memory appears to be mediated by cGKI, as its activation or inhibition, analogous to NO-GC, contributes to improved or worsened memory performance, respectively (Arancio et al., 1995; Izquierdo et al., 2002; Zhuo et al., 1994). Since BK is a substrate of cGKI and important for synaptic plasticity as well, it can be postulated that BK as an effector mediates these positive effects on memory performance. Thus, the NO-GC activator Cinaciguat (or a BBB penetrant derivate) should increase potentiation or phosphorylation at GluA1-S845 after HFS-LTP and cLTP, respectively, which should not be observed in cKO. Indeed, for the two BBB penetrating NO-GC stimulator BAY-747 and activator Runcaciguat a higher GluA1-S845 phosphorylation after cLTP induction could be observed (Nelissen et al., 2022). Consistently, this should also lead to increased K<sup>+</sup> efflux and Ca<sup>2+</sup> oscillation frequency at

the cellular level. While some NO-GC stimulators and activators are approved drugs and available on the market, so far none of them is blood brain barrier penetrant. Therefore, they cannot be easily applied *in vivo*. Recently developed blood brain barrier penetrant NO-GC stimulators, however, are in the clinical trial phase. Experimentally, these activators could be fed to mice for a certain period before the experimental procedure and subsequently the memory performance could be determined by MWM. This should result in a reduced latency during the acquisition phase in the BK CTRL and a longer residence time in the target quadrant during the probe trial.



## 6. Summary

Impaired synaptic plasticity is one cause for cognitive decline in ND like AD (Baudouin et al., 2012; Wang et al., 2004; Zoghbi & Bear, 2012). While BK mutations have been linked to cognitive impairment (Deng et al., 2013; Du et al., 2020; Higgins et al., 2008; Zhang et al., 2006), their exact impact on synaptic plasticity remains elusive.

BK's role in synaptic plasticity was investigated using hippocampal pyramidal neuron-specific conditional BK knockout mice cKO mediated by T29.1-Cre (Tsien, Huerta, & Tonegawa, 1996) and littermate controls CTRL.

Western-blot and immunofluorescence identified effective and hippocampus-specific BK depletion in cKO. BWT and OFT verified the ability of these mice to perform behavioral memory tasks. cKO consistently displayed delayed learning during MWM acquisition phase and limited memory retrieval during probe trials. In animals with advanced age, learning deficits could no longer be detected, probably because the smaller difference is masked by declining cognition. *In vivo* findings in young mice were additionally corroborated by the lack of electrically and chemically induced LTP measured by the initial slope of fEPSPs and the absence of increased AMPAR phosphorylation at S845-GluA1, a surrogate parameter for physiological LTP. Furthermore, cLTP induction in primary hippocampal neurons led to BK-mediated reduction in  $[K^+]_i$  as observed using GEPII. Decreased  $[K^+]_i$  was accompanied by increased frequencies of neuronal  $Ca^{2+}$  oscillations, as detected by FURA-2. Both,  $[K^+]_i$  reduction and  $Ca^{2+}$  oscillations were sensitive to DL-AP5 and Nifedipine, indicating potential functional interactions between NMDAR, LTCC and BK during LTP. Despite a strong and prolonged  $K^+$  efflux during cLTP, no change in membrane potential was observed via DiBAC<sub>4</sub>(3) in either BK<sup>+/+</sup> neurons or PAX-inhibited BK<sup>+/+</sup> neurons. This is probably due to the rapid repolarization by the  $Ca^{2+}$  oscillations.

The data suggest BK-dependent  $K^+$  efflux as critical to support hippocampal synaptic plasticity by maintaining  $Ca^{2+}$  influx through NMDA receptors and LTCC during LTP. This suggests BK modulation as a potential therapeutic option to treat cognitive impairment.



## 7. Zusammenfassung

Eine beeinträchtigte synaptische Plastizität ist eine der Ursachen für den kognitiven Abbau bei neurodegenerativen Erkrankungen wie Alzheimer (Baudouin et al., 2012; Wang et al., 2004; Zoghbi & Bear, 2012). Während BK-Mutationen mit kognitiven Beeinträchtigungen in Verbindung gebracht werden (Deng et al., 2013; Du et al., 2020; Higgins et al., 2008; Zhang et al., 2006), ist ihre genaue Auswirkung auf die synaptische Plastizität nach wie vor ungeklärt.

Die Rolle von BK bei der synaptischen Plastizität wurde mithilfe von konditionalen, hippocampalen, Pyramidenneuronen-spezifischen BK-Knockout-Mäusen cKO, vermittelt durch die T29.1-Cre und ihren Wurfgeschwisterkontrollen CTRL untersucht.

Western-Blot und Immunfluoreszenz zeigten eine effektive und hippocampuspezifische BK-Depletion in cKO. BWT und OFT bestätigten die Fähigkeit dieser Mäuse, verhaltensbasierte Lernversuche auszuführen. cKO zeigte durchweg verzögertes Lernen während der MWM-Erwerbsphase und eingeschränkten Gedächtnisabruf während der Prüfversuche. Bei Tieren mit fortgeschrittenem Alter konnten keine Lerndefizite mehr nachvollzogen werden, was wahrscheinlich daran liegt, dass die kleineren Unterschiede durch die abnehmende Kognition maskiert wurden. *In vivo* Befunde in den jungen Mäusen wurden zusätzlich durch das Fehlen einer elektrisch und chemisch induzierten LTP, gemessen an der anfänglichen Steigung der fEPSPs und durch das Fehlen einer erhöhten AMPAR-Phosphorylierung an S845-GluA1, einem Surrogatparameter für physiologische LTP, bestätigt. Außerdem führte die cLTP-Induktion in primären Hippocampus-Neuronen zu einer BK-vermittelten Verringerung von  $[K^+]_i$ , wie mit GEPII beobachtet wurde. Die Verringerung von  $[K^+]_i$  ging mit einer erhöhten Frequenz neuronaler  $Ca^{2+}$ -Oszillationen einher, wie mit FURA-2 ermittelt wurde. Sowohl die  $[K^+]_i$ -Reduktion als auch die  $Ca^{2+}$ -Oszillationen reagierten empfindlich auf DL-AP5 und Nifedipin, was auf mögliche funktionelle Interaktionen zwischen NMDAR, LTCC und BK während LTP hinweist. Trotz eines starken und anhaltenden  $K^+$ -Effluxes während cLTP wurde weder in  $BK^{+/+}$  Neuronen noch in PAX-inhibierten  $BK^{+/+}$  Neuronen eine Veränderung des Membranpotentials durch DiBAC<sub>4</sub>(3) beobachtet. Dies ist wahrscheinlich auf die schnelle Repolarisierung durch die  $Ca^{2+}$ -Oszillationen zurückzuführen.

Die Daten deuten darauf hin, dass der BK-abhängige  $K^+$ -Efflux entscheidend für die Unterstützung der synaptischen Plastizität im Hippocampus ist, indem er den  $Ca^{2+}$ -Einstrom durch NMDAR und LTCC während LTP aufrechterhält. Dies deutet darauf hin, dass die BK-Modulation eine potenzielle therapeutische Option zur Behandlung kognitiver Beeinträchtigungen darstellen könnte.



## 8. References

- Alioua, A., Tanaka, Y., Wallner, M., Hofmann, F., Ruth, P., Meera, P., & Toro, L. (1998). The large conductance, voltage-dependent, and calcium-sensitive K<sup>+</sup> channel, Hslo, is a target of cGMP-dependent protein kinase phosphorylation in vivo. *J Biol Chem*, 273(49), 32950-32956. <https://doi.org/10.1074/jbc.273.49.32950>
- Arancio, O., Kandel, E. R., & Hawkins, R. D. (1995). Activity-dependent long-term enhancement of transmitter release by presynaptic 3',5'-cyclic GMP in cultured hippocampal neurons. *Nature*, 376(6535), 74-80. <https://doi.org/10.1038/376074a0>
- Armstrong, P. W., Pieske, B., Anstrom, K. J., Ezekowitz, J., Hernandez, A. F., Butler, J., Lam, C. S. P., Ponikowski, P., Voors, A. A., Jia, G., McNulty, S. E., Patel, M. J., Roessig, L., Koglin, J., O'Connor, C. M., & Group, V. S. (2020). Vericiguat in Patients with Heart Failure and Reduced Ejection Fraction. *N Engl J Med*, 382(20), 1883-1893. <https://doi.org/10.1056/NEJMoa1915928>
- Ashe, K. H. (2001). Learning and memory in transgenic mice modeling Alzheimer's disease. *Learn Mem*, 8(6), 301-308. <https://doi.org/10.1101/lm.43701>
- Baez, M. V., Cercato, M. C., & Jerusalinsky, D. A. (2018). NMDA Receptor Subunits Change after Synaptic Plasticity Induction and Learning and Memory Acquisition. *Neural Plast*, 2018, 5093048. <https://doi.org/10.1155/2018/5093048>
- Banke, T. G., Bowie, D., Lee, H., Huganir, R. L., Schousboe, A., & Traynelis, S. F. (2000). Control of GluR1 AMPA receptor function by cAMP-dependent protein kinase. *J Neurosci*, 20(1), 89-102. <https://doi.org/10.1523/JNEUROSCI.20-01-00089.2000>
- Bannerman, D. M., Good, M. A., Butcher, S. P., Ramsay, M., & Morris, R. G. (1995). Distinct components of spatial learning revealed by prior training and NMDA receptor blockade. *Nature*, 378(6553), 182-186. <https://doi.org/10.1038/378182a0>
- Barco, A., Alarcon, J. M., & Kandel, E. R. (2002). Expression of constitutively active CREB protein facilitates the late phase of long-term potentiation by enhancing synaptic capture. *Cell*, 108(5), 689-703. [https://doi.org/10.1016/s0092-8674\(02\)00657-8](https://doi.org/10.1016/s0092-8674(02)00657-8)
- Bard, L., Sainlos, M., Bouchet, D., Cousins, S., Mikasova, L., Breillat, C., Stephenson, F. A., Imperiali, B., Choquet, D., & Groc, L. (2010). Dynamic and specific interaction between synaptic NR2-NMDA receptor and PDZ proteins. *Proc Natl Acad Sci U S A*, 107(45), 19561-19566. <https://doi.org/10.1073/pnas.1002690107>
- Barnes, J., Bartlett, J. W., van de Pol, L. A., Loy, C. T., Scahill, R. I., Frost, C., Thompson, P., & Fox, N. C. (2009). A meta-analysis of hippocampal atrophy rates in Alzheimer's disease. *Neurobiol Aging*, 30(11), 1711-1723. <https://doi.org/10.1016/j.neurobiolaging.2008.01.010>
- Barria, A., Muller, D., Derkach, V., Griffith, L. C., & Soderling, T. R. (1997). Regulatory phosphorylation of AMPA-type glutamate receptors by CaM-KII during long-term potentiation. *Science*, 276(5321), 2042-2045. <https://doi.org/10.1126/science.276.5321.2042>
- Batuecas, A., Pereira, R., Centeno, C., Pulido, J. A., Hernandez, M., Bollati, A., Bogonez, E., & Satrustegui, J. (1998). Effects of chronic nimodipine on working memory of old rats in relation to defects in synaptosomal calcium homeostasis. *Eur J Pharmacol*, 350(2-3), 141-150. [https://doi.org/10.1016/s0014-2999\(98\)00250-7](https://doi.org/10.1016/s0014-2999(98)00250-7)
- Baudouin, S. J., Gaudias, J., Gerharz, S., Hatstatt, L., Zhou, K., Punnakkal, P., Tanaka, K. F., Spooren, W., Hen, R., De Zeeuw, C. I., Vogt, K., & Scheiffele, P. (2012). Shared synaptic pathophysiology in syndromic and nonsyndromic rodent models of autism. *Science*, 338(6103), 128-132. <https://doi.org/10.1126/science.1224159>
- Bauer, E. P., Schafe, G. E., & LeDoux, J. E. (2002). NMDA receptors and L-type voltage-gated calcium channels contribute to long-term potentiation and different components of fear memory formation in the lateral amygdala. *J Neurosci*, 22(12), 5239-5249. <https://doi.org/10.1523/JNEUROSCI.22-12-05239.2002>
- Bausch, A. E., Dieter, R., Nann, Y., Hausmann, M., Meyerderks, N., Kaczmarek, L. K., Ruth, P., & Lukowski, R. (2015). The sodium-activated potassium channel Slack is required for optimal cognitive flexibility in mice. *Learn Mem*, 22(7), 323-335. <https://doi.org/10.1101/lm.037820.114>
- Beecham, G. W., Hamilton, K., Naj, A. C., Martin, E. R., Huentelman, M., Myers, A. J., Corneveaux, J. J., Hardy, J., Vonsattel, J. P., Younkin, S. G., Bennett, D. A., De Jager, P. L., Larson, E. B., Crane, P. K., Kamboh, M. I., Kofler, J. K., Mash, D. C., Duque, L., Gilbert, J. R., . . . Montine, T. J. (2014). Genome-wide association meta-analysis of neuropathologic features of Alzheimer's disease and related dementias. *PLoS Genet*, 10(9), e1004606. <https://doi.org/10.1371/journal.pgen.1004606>
- Beecham, G. W., Martin, E. R., Li, Y. J., Slifer, M. A., Gilbert, J. R., Haines, J. L., & Pericak-Vance, M. A. (2009). Genome-wide association study implicates a chromosome 12 risk locus for late-onset Alzheimer disease. *Am J Hum Genet*, 84(1), 35-43. <https://doi.org/10.1016/j.ajhg.2008.12.008>
- Bentzen, B. H., Olesen, S. P., Ronn, L. C., & Grunnet, M. (2014). BK channel activators and their therapeutic perspectives. *Front Physiol*, 5, 389. <https://doi.org/10.3389/fphys.2014.00389>
- Berkefeld, H., & Fakler, B. (2008). Repolarizing responses of BKCa-Cav complexes are distinctly shaped by their Cav subunits. *J Neurosci*, 28(33), 8238-8245. <https://doi.org/10.1523/JNEUROSCI.2274-08.2008>

- Berkefeld, H., & Fakler, B. (2013). Ligand-gating by Ca<sup>2+</sup> is rate limiting for physiological operation of BK(Ca) channels. *J Neurosci*, 33(17), 7358-7367. <https://doi.org/10.1523/JNEUROSCI.5443-12.2013>
- Berkefeld, H., Fakler, B., & Schulte, U. (2010). Ca<sup>2+</sup>-activated K<sup>+</sup> channels: from protein complexes to function. *Physiol Rev*, 90(4), 1437-1459. <https://doi.org/10.1152/physrev.00049.2009>
- Bernabeu, R., Schroder, N., Quevedo, J., Cammarota, M., Izquierdo, I., & Medina, J. H. (1997). Further evidence for the involvement of a hippocampal cGMP/cGMP-dependent protein kinase cascade in memory consolidation. *NeuroReport*, 8(9), 2221-2224. [https://journals.lww.com/neuroreport/Fulltext/1997/07070/Further\\_evidence\\_for\\_the\\_involvement\\_of\\_a.26.aspx](https://journals.lww.com/neuroreport/Fulltext/1997/07070/Further_evidence_for_the_involvement_of_a.26.aspx)
- Bischof, H., Rehberg, M., Stryeck, S., Artinger, K., Eroglu, E., Waldeck-Weiermair, M., Gottschalk, B., Rost, R., Deak, A. T., Niedrist, T., Vujic, N., Lindermuth, H., Prassl, R., Pelzmann, B., Groschner, K., Kratky, D., Eller, K., Rosenkranz, A. R., Madl, T., . . . Malli, R. (2017). Novel genetically encoded fluorescent probes enable real-time detection of potassium in vitro and in vivo. *Nat Commun*, 8(1), 1422. <https://doi.org/10.1038/s41467-017-01615-z>
- Bliss, T. V., & Lomo, T. (1973). Long-lasting potentiation of synaptic transmission in the dentate area of the anaesthetized rabbit following stimulation of the perforant path. *J Physiol*, 232(2), 331-356. <https://doi.org/10.1113/jphysiol.1973.sp010273>
- Borland, E., Edgar, C., Stomrud, E., Cullen, N., Hansson, O., & Palmqvist, S. (2022). Clinically Relevant Changes for Cognitive Outcomes in Preclinical and Prodromal Cognitive Stages: Implications for Clinical Alzheimer Trials. *Neurology*, 99(11), e1142-e1153. <https://doi.org/10.1212/WNL.000000000000200817>
- Boulton, C. L., Southam, E., & Garthwaite, J. (1995). Nitric oxide-dependent long-term potentiation is blocked by a specific inhibitor of soluble guanylyl cyclase. *Neuroscience*, 69(3), 699-703. [https://doi.org/10.1016/0306-4522\(95\)00349-n](https://doi.org/10.1016/0306-4522(95)00349-n)
- Bozdagi, O., Shan, W., Tanaka, H., Benson, D. L., & Huntley, G. W. (2000). Increasing numbers of synaptic puncta during late-phase LTP: N-cadherin is synthesized, recruited to synaptic sites, and required for potentiation. *Neuron*, 28(1), 245-259. [https://doi.org/10.1016/s0896-6273\(00\)00100-8](https://doi.org/10.1016/s0896-6273(00)00100-8)
- Brenner, R., Chen, Q. H., Vilaythong, A., Toney, G. M., Noebels, J. L., & Aldrich, R. W. (2005). BK channel beta4 subunit reduces dentate gyrus excitability and protects against temporal lobe seizures. *Nat Neurosci*, 8(12), 1752-1759. <https://doi.org/10.1038/nn1573>
- Brenner, R., Perez, G. J., Bonev, A. D., Eckman, D. M., Kosek, J. C., Wiler, S. W., Patterson, A. J., Nelson, M. T., & Aldrich, R. W. (2000). Vasoregulation by the beta1 subunit of the calcium-activated potassium channel. *Nature*, 407(6806), 870-876. <https://doi.org/10.1038/35038011>
- Brooks, D. M., Patel, S. A., Wohlgelegen, E. D., Semmens, E. O., Pearce, A., Sorich, E. A., & Rau, T. F. (2017). Multiple mild traumatic brain injury in the rat produces persistent pathological alterations in the brain. *Exp Neurol*, 297, 62-72. <https://doi.org/10.1016/j.expneurol.2017.07.015>
- Brown, M. R., & Kaczmarek, L. K. (2011). Potassium channel modulation and auditory processing. *Hear Res*, 279(1-2), 32-42. <https://doi.org/10.1016/j.heares.2011.03.004>
- Budd Haeberlein, S., Aisen, P. S., Barkhof, F., Chalkias, S., Chen, T., Cohen, S., Dent, G., Hansson, O., Harrison, K., von Hehn, C., Iwatsubo, T., Mallinckrodt, C., Mummery, C. J., Muralidharan, K. K., Nestorov, I., Nisenbaum, L., Rajagovindan, R., Skordos, L., Tian, Y., . . . Sandrock, A. (2022). Two Randomized Phase 3 Studies of Aducanumab in Early Alzheimer's Disease. *J Prev Alzheimers Dis*, 9(2), 197-210. <https://doi.org/10.14283/jpad.2022.30>
- Burns, L. C., Minster, R. L., Demirci, F. Y., Barmada, M. M., Ganguli, M., Lopez, O. L., DeKosky, S. T., & Kamboh, M. I. (2011). Replication study of genome-wide associated SNPs with late-onset Alzheimer's disease. *Am J Med Genet B Neuropsychiatr Genet*, 156B(4), 507-512. <https://doi.org/10.1002/ajmg.b.31194>
- Butler, A., Tsunoda, S., McCobb, D. P., Wei, A., & Salkoff, L. (1993). mSlo, a complex mouse gene encoding "maxi" calcium-activated potassium channels. *Science*, 261(5118), 221-224. <https://doi.org/10.1126/science.7687074>
- Canas, P. M., Duarte, J. M., Rodrigues, R. J., Kofalvi, A., & Cunha, R. A. (2009). Modification upon aging of the density of presynaptic modulation systems in the hippocampus. *Neurobiol Aging*, 30(11), 1877-1884. <https://doi.org/10.1016/j.neurobiolaging.2008.01.003>
- Capera, J., Serrano-Novillo, C., Navarro-Perez, M., Cassinelli, S., & Felipe, A. (2019). The Potassium Channel Odyssey: Mechanisms of Traffic and Membrane Arrangement. *Int J Mol Sci*, 20(3), 734. <https://doi.org/10.3390/ijms20030734>
- Carter, R. J., Morton, J., & Dunnett, S. B. (2001). Motor coordination and balance in rodents. *Curr Protoc Neurosci*, Chapter 8(1), Unit 8 12. <https://doi.org/10.1002/0471142301.ns0812s15>
- Cavus, I., & Teyler, T. (1996). Two forms of long-term potentiation in area CA1 activate different signal transduction cascades. *J Neurophysiol*, 76(5), 3038-3047. <https://doi.org/10.1152/jn.1996.76.5.3038>
- Ceprian, M., & Fulton, D. (2019). Glial Cell AMPA Receptors in Nervous System Health, Injury and Disease. *Int J Mol Sci*, 20(10), 2450. <https://doi.org/10.3390/ijms20102450>
- Chapman, P. F., Falinska, A. M., Knevet, S. G., & Ramsay, M. F. (2001). Genes, models and Alzheimer's disease. *Trends Genet*, 17(5), 254-261. [https://doi.org/10.1016/s0168-9525\(01\)02285-5](https://doi.org/10.1016/s0168-9525(01)02285-5)
- Chen, X., Kovalchuk, Y., Adelsberger, H., Henning, H. A., Sausbier, M., Wietzorrek, G., Ruth, P., Yarom, Y., & Konnerth, A. (2010). Disruption of the olivo-cerebellar circuit by Purkinje neuron-specific ablation

- of BK channels. *Proc Natl Acad Sci U S A*, 107(27), 12323-12328. <https://doi.org/10.1073/pnas.1001745107>
- Chien, W. L., Liang, K. C., Teng, C. M., Kuo, S. C., Lee, F. Y., & Fu, W. M. (2003). Enhancement of long-term potentiation by a potent nitric oxide-guanylyl cyclase activator, 3-(5-hydroxymethyl-2-furyl)-1-benzyl-indazole. *Mol Pharmacol*, 63(6), 1322-1328. <https://doi.org/10.1124/mol.63.6.1322>
- Christie, L. A., Russell, T. A., Xu, J., Wood, L., Shepherd, G. M., & Contractor, A. (2010). AMPA receptor desensitization mutation results in severe developmental phenotypes and early postnatal lethality. *Proc Natl Acad Sci U S A*, 107(20), 9412-9417. <https://doi.org/10.1073/pnas.0908206107>
- Cisternas, P., Oliva, C. A., Torres, V. I., Barrera, D. P., & Inestrosa, N. C. (2019). Presymptomatic Treatment With Andrographolide Improves Brain Metabolic Markers and Cognitive Behavior in a Model of Early-Onset Alzheimer's Disease. *Front Cell Neurosci*, 13, 295. <https://doi.org/10.3389/fncel.2019.00295>
- Collingridge, G. L., Peineau, S., Howland, J. G., & Wang, Y. T. (2010). Long-term depression in the CNS. *Nat Rev Neurosci*, 11(7), 459-473. <https://doi.org/10.1038/nrn2867>
- Colom-Cadena, M., Spires-Jones, T., Zetterberg, H., Blennow, K., Caggiano, A., DeKosky, S. T., Fillit, H., Harrison, J. E., Schneider, L. S., Scheltens, P., de Haan, W., Grundman, M., van Dyck, C. H., Izzo, N. J., Catalano, S. M., & Synaptic Health Endpoints Working, G. (2020). The clinical promise of biomarkers of synapse damage or loss in Alzheimer's disease. *Alzheimers Res Ther*, 12(1), 21. <https://doi.org/10.1186/s13195-020-00588-4>
- Contet, C., Goulding, S. P., Kuljis, D. A., & Barth, A. L. (2016). BK Channels in the Central Nervous System. *Int Rev Neurobiol*, 128, 281-342. <https://doi.org/10.1016/bs.irn.2016.04.001>
- Contreras, G. F., Castillo, K., Enrique, N., Carrasquel-Ursulaez, W., Castillo, J. P., Milesi, V., Neely, A., Alvarez, O., Ferreira, G., Gonzalez, C., & Latorre, R. (2013). A BK (Slo1) channel journey from molecule to physiology. *Channels (Austin)*, 7(6), 442-458. <https://doi.org/10.4161/chan.26242>
- Coon, A. L., Wallace, D. R., Mactutus, C. F., & Booze, R. M. (1999). L-type calcium channels in the hippocampus and cerebellum of Alzheimer's disease brain tissue. *Neurobiol Aging*, 20(6), 597-603. [https://doi.org/10.1016/s0197-4580\(99\)00068-8](https://doi.org/10.1016/s0197-4580(99)00068-8)
- Correia, S. S., Iyengar, R. R., Germano, P., Tang, K., Bernier, S. G., Schwartzkopf, C. D., Tobin, J., Lee, T. W., Liu, G., Jacobson, S., Carvalho, A., Rennie, G. R., Jung, J., Renhowe, P. A., Lonie, E., Winrow, C. J., Hadcock, J. R., Jones, J. E., & Currie, M. G. (2021). The CNS-Penetrant Soluble Guanylate Cyclase Stimulator CY6463 Reveals its Therapeutic Potential in Neurodegenerative Diseases. *Front Pharmacol*, 12, 656561. <https://doi.org/10.3389/fphar.2021.656561>
- Cull-Candy, S. G., & Farrant, M. (2021). Ca<sup>2+</sup>-permeable AMPA receptors and their auxiliary subunits in synaptic plasticity and disease. *J Physiol*, 599(10), 2655-2671. <https://doi.org/10.1113/JP279029>
- Danbolt, N. C. (2001). Glutamate uptake. *Prog Neurobiol*, 65(1), 1-105. [https://doi.org/10.1016/s0301-0082\(00\)00067-8](https://doi.org/10.1016/s0301-0082(00)00067-8)
- Davis, S. E., & Bauer, E. P. (2012). L-type voltage-gated calcium channels in the basolateral amygdala are necessary for fear extinction. *J Neurosci*, 32(39), 13582-13586. <https://doi.org/10.1523/JNEUROSCI.0809-12.2012>
- De Strooper, B., & Karran, E. (2016). The Cellular Phase of Alzheimer's Disease. *Cell*, 164(4), 603-615. <https://doi.org/10.1016/j.cell.2015.12.056>
- Dell'Orco, J. M., Wasserman, A. H., Chopra, R., Ingram, M. A., Hu, Y. S., Singh, V., Wulff, H., Opal, P., Orr, H. T., & Shakkottai, V. G. (2015). Neuronal Atrophy Early in Degenerative Ataxia Is a Compensatory Mechanism to Regulate Membrane Excitability. *J Neurosci*, 35(32), 11292-11307. <https://doi.org/10.1523/JNEUROSCI.1357-15.2015>
- Deng, P. Y., Rotman, Z., Blundon, J. A., Cho, Y., Cui, J., Cavalli, V., Zakharenko, S. S., & Klyachko, V. A. (2013). FMRP regulates neurotransmitter release and synaptic information transmission by modulating action potential duration via BK channels. *Neuron*, 77(4), 696-711. <https://doi.org/10.1016/j.neuron.2012.12.018>
- Diering, G. H., Gustina, A. S., & Haganir, R. L. (2014). PKA-GluA1 coupling via AKAP5 controls AMPA receptor phosphorylation and cell-surface targeting during bidirectional homeostatic plasticity. *Neuron*, 84(4), 790-805. <https://doi.org/10.1016/j.neuron.2014.09.024>
- Diering, G. H., Heo, S., Hussain, N. K., Liu, B., & Haganir, R. L. (2016). Extensive phosphorylation of AMPA receptors in neurons. *Proc Natl Acad Sci U S A*, 113(33), E4920-4927. <https://doi.org/10.1073/pnas.1610631113>
- Diering, G. H., & Haganir, R. L. (2018). The AMPA Receptor Code of Synaptic Plasticity. *Neuron*, 100(2), 314-329. <https://doi.org/10.1016/j.neuron.2018.10.018>
- Dorszewska, J., Kozubski, W., Waleszczyk, W., Zabel, M., & Ong, K. (2020). Neuroplasticity in the Pathology of Neurodegenerative Diseases. *Neural Plast*, 2020, 4245821. <https://doi.org/10.1155/2020/4245821>
- Du, X., Carvalho-de-Souza, J. L., Wei, C., Carrasquel-Ursulaez, W., Lorenzo, Y., Gonzalez, N., Kubota, T., Staisch, J., Hain, T., Petrossian, N., Xu, M., Latorre, R., Bezanilla, F., & Gomez, C. M. (2020). Loss-of-function BK channel mutation causes impaired mitochondria and progressive cerebellar ataxia. *Proc Natl Acad Sci U S A*, 117(11), 6023-6034. <https://doi.org/10.1073/pnas.1920008117>
- Dudem, S., Large, R. J., Kulkarni, S., McClafferty, H., Tikhonova, I. G., Sergeant, G. P., Thornbury, K. D., Shipston, M. J., Perrino, B. A., & Hollywood, M. A. (2020). LINGO1 is a regulatory subunit of large conductance, Ca<sup>2+</sup>-activated potassium channels. *Proc Natl Acad Sci U S A*, 117(4), 2194-2200. <https://doi.org/10.1073/pnas.1916715117>

- Eatock, R. A. (2003). Auditory physiology: listening with K<sup>+</sup> channels. *Curr Biol*, 13(19), R767-769. <https://doi.org/10.1016/j.cub.2003.09.018>
- Ehinger, R., Kuret, A., Matt, L., Frank, N., Wild, K., Kabagema-Bilan, C., Bischof, H., Malli, R., Ruth, P., Bausch, A. E., & Lukowski, R. (2021). Slack K(+) channels attenuate NMDA-induced excitotoxic brain damage and neuronal cell death. *FASEB J*, 35(5), e21568. <https://doi.org/10.1096/fj.202002308RR>
- Elkins, T., Ganetzky, B., & Wu, C. F. (1986). A *Drosophila* mutation that eliminates a calcium-dependent potassium current. *Proc Natl Acad Sci U S A*, 83(21), 8415-8419. <https://doi.org/10.1073/pnas.83.21.8415>
- Ennaceur, A. (2014). Tests of unconditioned anxiety - pitfalls and disappointments. *Physiol Behav*, 135, 55-71. <https://doi.org/10.1016/j.physbeh.2014.05.032>
- Faber, E. S., Delaney, A. J., & Sah, P. (2005). SK channels regulate excitatory synaptic transmission and plasticity in the lateral amygdala. *Nat Neurosci*, 8(5), 635-641. <https://doi.org/10.1038/nn1450>
- Faber, E. S., & Sah, P. (2002). Physiological role of calcium-activated potassium currents in the rat lateral amygdala. *J Neurosci*, 22(5), 1618-1628. <https://doi.org/10.1523/JNEUROSCI.22-05-01618.2002>
- Farajnia, S., Meijer, J. H., & Michel, S. (2015). Age-related changes in large-conductance calcium-activated potassium channels in mammalian circadian clock neurons. *Neurobiol Aging*, 36(6), 2176-2183. <https://doi.org/10.1016/j.neurobiolaging.2014.12.040>
- Fenyves, B. G., Arnold, A., Gharat, V. G., Haab, C., Tishinov, K., Peter, F., de Quervain, D., Papassotiropoulos, A., & Stetak, A. (2021). Dual Role of an mps-2/KCNE-Dependent Pathway in Long-Term Memory and Age-Dependent Memory Decline. *Curr Biol*, 31(3), 527-539 e527. <https://doi.org/10.1016/j.cub.2020.10.069>
- Fernandez-Monreal, M., Brown, T. C., Royo, M., & Esteban, J. A. (2012). The balance between receptor recycling and trafficking toward lysosomes determines synaptic strength during long-term depression. *J Neurosci*, 32(38), 13200-13205. <https://doi.org/10.1523/JNEUROSCI.0061-12.2012>
- Ferraguti, F., Klausberger, T., Cobden, P., Baude, A., Roberts, J. D., Szucs, P., Kinoshita, A., Shigemoto, R., Somogyi, P., & Dalezios, Y. (2005). Metabotropic glutamate receptor 8-expressing nerve terminals target subsets of GABAergic neurons in the hippocampus. *J Neurosci*, 25(45), 10520-10536. <https://doi.org/10.1523/JNEUROSCI.2547-05.2005>
- Ferron, L. (2016). Fragile X mental retardation protein controls ion channel expression and activity. *J Physiol*, 594(20), 5861-5867. <https://doi.org/10.1113/JP270675>
- Fleisher, A. S., Chen, K., Liu, X., Roontiva, A., Thiyyagura, P., Ayutyanont, N., Joshi, A. D., Clark, C. M., Mintun, M. A., Pontecorvo, M. J., Doraiswamy, P. M., Johnson, K. A., Skovronsky, D. M., & Reiman, E. M. (2011). Using positron emission tomography and florbetapir F18 to image cortical amyloid in patients with mild cognitive impairment or dementia due to Alzheimer disease. *Arch Neurol*, 68(11), 1404-1411. <https://doi.org/10.1001/archneurol.2011.150>
- Förster, T. (2006). Zwischenmolekulare Energiewanderung und Fluoreszenz. *Annalen der Physik*, 437(1-2), 55-75. <https://doi.org/10.1002/andp.19484370105>
- Frontiers in Neuroscience. (2009). In J. J. Buccafusco (Ed.), *Methods of Behavior Analysis in Neuroscience* (2nd ed.). CRC Press/Taylor & Francis
- Copyright © 2009, Taylor & Francis Group, LLC. <https://www.ncbi.nlm.nih.gov/pubmed/21204335>
- Galie, N., Ghofrani, H. A., Torbicki, A., Barst, R. J., Rubin, L. J., Badesch, D., Fleming, T., Parpia, T., Burgess, G., Branzi, A., Grimminger, F., Kurzyna, M., Simonneau, G., & Sildenafil Use in Pulmonary Arterial Hypertension Study, G. (2005). Sildenafil citrate therapy for pulmonary arterial hypertension. *N Engl J Med*, 353(20), 2148-2157. <https://doi.org/10.1056/NEJMoa050010>
- Gardoni, F., Picconi, B., Ghiglieri, V., Polli, F., Bagetta, V., Bernardi, G., Cattabeni, F., Di Luca, M., & Calabresi, P. (2006). A critical interaction between NR2B and MAGUK in L-DOPA induced dyskinesia. *J Neurosci*, 26(11), 2914-2922. <https://doi.org/10.1523/JNEUROSCI.5326-05.2006>
- Gates, G. A., Couropmitree, N. N., & Myers, R. H. (1999). Genetic associations in age-related hearing thresholds. *Arch Otolaryngol Head Neck Surg*, 125(6), 654-659. <https://doi.org/10.1001/archotol.125.6.654>
- Gehring, T. V., Luksys, G., Sandi, C., & Vasilaki, E. (2015). Detailed classification of swimming paths in the Morris Water Maze: multiple strategies within one trial. *Sci Rep*, 5(1), 14562. <https://doi.org/10.1038/srep14562>
- Ghofrani, H. A., Galie, N., Grimminger, F., Grunig, E., Humbert, M., Jing, Z. C., Keogh, A. M., Langleben, D., Kilama, M. O., Fritsch, A., Neuser, D., Rubin, L. J., & Group, P.-S. (2013). Riociguat for the treatment of pulmonary arterial hypertension. *N Engl J Med*, 369(4), 330-340. <https://doi.org/10.1056/NEJMoa1209655>
- Giese, K. P., Fedorov, N. B., Filipkowski, R. K., & Silva, A. J. (1998). Autophosphorylation at Thr286 of the alpha calcium-calmodulin kinase II in LTP and learning. *Science*, 279(5352), 870-873. <https://doi.org/10.1126/science.279.5352.870>
- Gittis, A. H., Moghadam, S. H., & du Lac, S. (2010). Mechanisms of sustained high firing rates in two classes of vestibular nucleus neurons: differential contributions of resurgent Na, Kv3, and BK currents. *J Neurophysiol*, 104(3), 1625-1634. <https://doi.org/10.1152/jn.00378.2010>
- Goebbels, S., Bormuth, I., Bode, U., Hermanson, O., Schwab, M. H., & Nave, K. A. (2006). Genetic targeting of principal neurons in neocortex and hippocampus of NEX-Cre mice. *Genesis*, 44(12), 611-621. <https://doi.org/10.1002/dvg.20256>

- Goldstein, S. A., Bayliss, D. A., Kim, D., Lesage, F., Plant, L. D., & Rajan, S. (2005). International Union of Pharmacology. LV. Nomenclature and molecular relationships of two-P potassium channels. *Pharmacol Rev*, 57(4), 527-540. <https://doi.org/10.1124/pr.57.4.12>
- Gomez, R., Maglio, L. E., Gonzalez-Hernandez, A. J., Rivero-Perez, B., Bartolome-Martin, D., & Giraldez, T. (2021). NMDA receptor-BK channel coupling regulates synaptic plasticity in the barrel cortex. *Proc Natl Acad Sci U S A*, 118(35), e2107026118. <https://doi.org/10.1073/pnas.2107026118>
- Gomez-Isla, T., Price, J. L., McKeel, D. W., Jr., Morris, J. C., Growdon, J. H., & Hyman, B. T. (1996). Profound loss of layer II entorhinal cortex neurons occurs in very mild Alzheimer's disease. *J Neurosci*, 16(14), 4491-4500. <https://doi.org/10.1523/JNEUROSCI.16-14-04491.1996>
- Gould, T. D., Dao, D. T., & Kovacsics, C. E. (2009). The Open Field Test. *Mood and Anxiety Related Phenotypes in Mice: Characterization Using Behavioral Tests*, 42, 1-20. [https://doi.org/10.1007/978-1-60761-303-9\\_1](https://doi.org/10.1007/978-1-60761-303-9_1)
- Gower, A. J., & Lamberty, Y. (1993). The aged mouse as a model of cognitive decline with special emphasis on studies in NMRI mice. *Behav Brain Res*, 57(2), 163-173. [https://doi.org/10.1016/0166-4328\(93\)90132-a](https://doi.org/10.1016/0166-4328(93)90132-a)
- Greger, I. H., Watson, J. F., & Cull-Candy, S. G. (2017). Structural and Functional Architecture of AMPA-Type Glutamate Receptors and Their Auxiliary Proteins. *Neuron*, 94(4), 713-730. <https://doi.org/10.1016/j.neuron.2017.04.009>
- Gribkoff, V. K., Starrett, J. E., Jr., Dworetzky, S. I., Hewawasam, P., Boissard, C. G., Cook, D. A., Frantz, S. W., Heman, K., Hibbard, J. R., Huston, K., Johnson, G., Krishnan, B. S., Kinney, G. G., Lombardo, L. A., Meanwell, N. A., Molinoff, P. B., Myers, R. A., Moon, S. L., Ortiz, A., . . . Yeola, S. W. (2001). Targeting acute ischemic stroke with a calcium-sensitive opener of maxi-K potassium channels. *Nat Med*, 7(4), 471-477. <https://doi.org/10.1038/86546>
- Groc, L., Heine, M., Cousins, S. L., Stephenson, F. A., Lounis, B., Cognet, L., & Choquet, D. (2006). NMDA receptor surface mobility depends on NR2A-2B subunits. *Proc Natl Acad Sci U S A*, 103(49), 18769-18774. <https://doi.org/10.1073/pnas.0605238103>
- Grunnet, M., & Kaufmann, W. A. (2004). Coassembly of big conductance Ca<sup>2+</sup>-activated K<sup>+</sup> channels and L-type voltage-gated Ca<sup>2+</sup> channels in rat brain. *J Biol Chem*, 279(35), 36445-36453. <https://doi.org/10.1074/jbc.M402254200>
- Gu, N., Vervaeke, K., & Storm, J. F. (2007). BK potassium channels facilitate high-frequency firing and cause early spike frequency adaptation in rat CA1 hippocampal pyramidal cells. *J Physiol*, 580(Pt.3), 859-882. <https://doi.org/10.1113/jphysiol.2006.126367>
- Gustafsson, B., Wigstrom, H., Abraham, W. C., & Huang, Y. Y. (1987). Long-term potentiation in the hippocampus using depolarizing current pulses as the conditioning stimulus to single volley synaptic potentials. *J Neurosci*, 7(3), 774-780. <https://doi.org/10.1523/JNEUROSCI.07-03-00774.1987>
- Gutman, G. A., Chandy, K. G., Grissmer, S., Lazdunski, M., McKinnon, D., Pardo, L. A., Robertson, G. A., Rudy, B., Sanguinetti, M. C., Stuhmer, W., & Wang, X. (2005). International Union of Pharmacology. LIII. Nomenclature and molecular relationships of voltage-gated potassium channels. *Pharmacol Rev*, 57(4), 473-508. <https://doi.org/10.1124/pr.57.4.10>
- Haass, C., & Selkoe, D. J. (2007). Soluble protein oligomers in neurodegeneration: lessons from the Alzheimer's amyloid beta-peptide. *Nat Rev Mol Cell Biol*, 8(2), 101-112. <https://doi.org/10.1038/nrm2101>
- Hamill, O. P., Marty, A., Neher, E., Sakmann, B., & Sigworth, F. J. (1981). Improved patch-clamp techniques for high-resolution current recording from cells and cell-free membrane patches. *Pflugers Arch*, 391(2), 85-100. <https://doi.org/10.1007/BF00656997>
- Hanley, J. G. (2018). The Regulation of AMPA Receptor Endocytosis by Dynamic Protein-Protein Interactions [Review]. *Front Cell Neurosci*, 12, 362. <https://doi.org/10.3389/fncel.2018.00362>
- Harada, C. N., Natelson Love, M. C., & Triebel, K. L. (2013). Normal cognitive aging. *Clin Geriatr Med*, 29(4), 737-752. <https://doi.org/10.1016/j.cger.2013.07.002>
- Hayashi, Y. (2022). Molecular mechanism of hippocampal long-term potentiation - Towards multiscale understanding of learning and memory. *Neurosci Res*, 175, 3-15. <https://doi.org/10.1016/j.neures.2021.08.001>
- He, K., Song, L., Cummings, L. W., Goldman, J., Haganir, R. L., & Lee, H. K. (2009). Stabilization of Ca<sup>2+</sup>-permeable AMPA receptors at perisynaptic sites by GluR1-S845 phosphorylation. *Proc Natl Acad Sci U S A*, 106(47), 20033-20038. <https://doi.org/10.1073/pnas.0910338106>
- Hebert, B., Pietropaolo, S., Meme, S., Laudier, B., Laugeray, A., Doisne, N., Quartier, A., Lefevre, S., Got, L., Cahard, D., Laumonier, F., Crusio, W. E., Pichon, J., Menuet, A., Perche, O., & Briault, S. (2014). Rescue of fragile X syndrome phenotypes in Fmr1 KO mice by a BKCa channel opener molecule. *Orphanet J Rare Dis*, 9(1), 124. <https://doi.org/10.1186/s13023-014-0124-6>
- Hell, J. W., Westenbroek, R. E., Warner, C., Ahijanian, M. K., Prystay, W., Gilbert, M. M., Snutch, T. P., & Catterall, W. A. (1993). Identification and differential subcellular localization of the neuronal class C and class D L-type calcium channel alpha 1 subunits. *J Cell Biol*, 123(4), 949-962. <https://doi.org/10.1083/jcb.123.4.949>
- Hendry, S. H., Schwark, H. D., Jones, E. G., & Yan, J. (1987). Numbers and proportions of GABA-immunoreactive neurons in different areas of monkey cerebral cortex. *J Neurosci*, 7(5), 1503-1519. <https://doi.org/10.1523/JNEUROSCI.07-05-01503.1987>

- Heo, S., Diering, G. H., Na, C. H., Nirujogi, R. S., Bachman, J. L., Pandey, A., & Haganir, R. L. (2018). Identification of long-lived synaptic proteins by proteomic analysis of synaptosome protein turnover. *Proc Natl Acad Sci U S A*, 115(16), E3827-E3836. <https://doi.org/10.1073/pnas.1720956115>
- Herron, C. E., Lester, R. A., Coan, E. J., & Collingridge, G. L. (1986). Frequency-dependent involvement of NMDA receptors in the hippocampus: a novel synaptic mechanism. *Nature*, 322(6076), 265-268. <https://doi.org/10.1038/322265a0>
- Herrup, K. (2015). The case for rejecting the amyloid cascade hypothesis. *Nat Neurosci*, 18(6), 794-799. <https://doi.org/10.1038/nn.4017>
- Hibino, H., Inanobe, A., Furutani, K., Murakami, S., Findlay, I., & Kurachi, Y. (2010). Inwardly rectifying potassium channels: their structure, function, and physiological roles. *Physiol Rev*, 90(1), 291-366. <https://doi.org/10.1152/physrev.00021.2009>
- Higgins, J. J., Hao, J., Kosofsky, B. E., & Rajadhyaksha, A. M. (2008). Dysregulation of large-conductance Ca<sup>2+</sup>-activated K<sup>+</sup> channel expression in nonsyndromal mental retardation due to a cereblon p.R419X mutation. *neurogenetics*, 9(3), 219-223. <https://doi.org/10.1007/s10048-008-0128-2>
- Hill, N. L., Kolanowski, A. M., & Gill, D. J. (2011). Plasticity in Early Alzheimer's Disease: An Opportunity for Intervention. *Top Geriatr Rehabil*, 27(4), 257-267. <https://doi.org/10.1097/tgr.0b013e31821e588e>
- Hodgkin, A. L., & Huxley, A. F. (1952). Currents carried by sodium and potassium ions through the membrane of the giant axon of Loligo. *J Physiol*, 116(4), 449-472. <https://doi.org/10.1113/jphysiol.1952.sp004717>
- Hollmann, M., & Heinemann, S. (1994). Cloned glutamate receptors. *Annu Rev Neurosci*, 17, 31-108. <https://doi.org/10.1146/annurev.ne.17.030194.000335>
- Honer, W. G., Barr, A. M., Sawada, K., Thornton, A. E., Morris, M. C., Leurgans, S. E., Schneider, J. A., & Bennett, D. A. (2012). Cognitive reserve, presynaptic proteins and dementia in the elderly. *Transl Psychiatry*, 2(5), e114. <https://doi.org/10.1038/tp.2012.38>
- Hoshi, T., Tian, Y., Xu, R., Heinemann, S. H., & Hou, S. (2013). Mechanism of the modulation of BK potassium channel complexes with different auxiliary subunit compositions by the omega-3 fatty acid DHA. *Proc Natl Acad Sci U S A*, 110(12), 4822-4827. <https://doi.org/10.1073/pnas.1222003110>
- Hosokawa, T., Mitsushima, D., Kaneko, R., & Hayashi, Y. (2015). Stoichiometry and phosphoisotypes of hippocampal AMPA-type glutamate receptor phosphorylation. *Neuron*, 85(1), 60-67. <https://doi.org/10.1016/j.neuron.2014.11.026>
- Hu, H., Real, E., Takamiya, K., Kang, M. G., Ledoux, J., Haganir, R. L., & Malinow, R. (2007). Emotion enhances learning via norepinephrine regulation of AMPA-receptor trafficking. *Cell*, 131(1), 160-173. <https://doi.org/10.1016/j.cell.2007.09.017>
- Huang, L., Liu, Y., Zhang, P., Kang, R., Liu, Y., Li, X., Bo, L., & Dong, Z. (2013). In vitro dose-dependent inhibition of the intracellular spontaneous calcium oscillations in developing hippocampal neurons by ketamine. *PLOS ONE*, 8(3), e59804. <https://doi.org/10.1371/journal.pone.0059804>
- Huang, Y. Y., & Kandel, E. R. (1995). D1/D5 receptor agonists induce a protein synthesis-dependent late potentiation in the CA1 region of the hippocampus. *Proc Natl Acad Sci U S A*, 92(7), 2446-2450. <https://doi.org/10.1073/pnas.92.7.2446>
- Haganir, R. L., & Nicoll, R. A. (2013). AMPARs and synaptic plasticity: the last 25 years. *Neuron*, 80(3), 704-717. <https://doi.org/10.1016/j.neuron.2013.10.025>
- Hull, C. A., Chu, Y., Thanawala, M., & Regehr, W. G. (2013). Hyperpolarization induces a long-term increase in the spontaneous firing rate of cerebellar Golgi cells. *J Neurosci*, 33(14), 5895-5902. <https://doi.org/10.1523/JNEUROSCI.4052-12.2013>
- Indriati, D. W., Kamasawa, N., Matsui, K., Meredith, A. L., Watanabe, M., & Shigemoto, R. (2013). Quantitative localization of Cav2.1 (P/Q-type) voltage-dependent calcium channels in Purkinje cells: somatodendritic gradient and distinct somatic coclustering with calcium-activated potassium channels. *J Neurosci*, 33(8), 3668-3678. <https://doi.org/10.1523/JNEUROSCI.2921-12.2013>
- Ingram, D. K., Joseph, J. A., Spangler, E. L., Roberts, D., Hengemihle, J., & Fanelli, R. J. (1994). Chronic nimodipine treatment in aged rats: analysis of motor and cognitive effects and muscarinic-induced striatal dopamine release. *Neurobiol Aging*, 15(1), 55-61. [https://doi.org/10.1016/0197-4580\(94\)90144-9](https://doi.org/10.1016/0197-4580(94)90144-9)
- Izquierdo, L. A., Barros, D. M., Vianna, M. R., Coitinho, A., deDavid e Silva, T., Choi, H., Moletta, B., Medina, J. H., & Izquierdo, I. (2002). Molecular pharmacological dissection of short- and long-term memory. *Cell Mol Neurobiol*, 22(3), 269-287. <https://doi.org/10.1023/a:1020715800956>
- Jacobsen, J. S., Wu, C. C., Redwine, J. M., Comery, T. A., Arias, R., Bowlby, M., Martone, R., Morrison, J. H., Pangalos, M. N., Reinhart, P. H., & Bloom, F. E. (2006). Early-onset behavioral and synaptic deficits in a mouse model of Alzheimer's disease. *Proc Natl Acad Sci U S A*, 103(13), 5161-5166. <https://doi.org/10.1073/pnas.0600948103>
- Jafari, A., Noursadeghi, E., Khodaghali, F., Saghiri, R., Sauve, R., Aliaghaei, A., & Eliassi, A. (2015). Brain mitochondrial ATP-insensitive large conductance Ca<sup>(+)</sup>(2)-activated K<sup>(+)</sup> channel properties are altered in a rat model of amyloid-beta neurotoxicity. *Exp Neurol*, 269, 8-16. <https://doi.org/10.1016/j.expneurol.2014.12.024>
- Jan, L. Y., & Jan, Y. N. (2012). Voltage-gated potassium channels and the diversity of electrical signalling. *J Physiol*, 590(11), 2591-2599. <https://doi.org/10.1113/jphysiol.2011.224212>
- Janus, C., & Westaway, D. (2001). Transgenic mouse models of Alzheimer's disease. *Physiol Behav*, 73(5), 873-886. [https://doi.org/10.1016/s0031-9384\(01\)00524-8](https://doi.org/10.1016/s0031-9384(01)00524-8)

- Jeffery, K. J., & Morris, R. G. (1993). Cumulative long-term potentiation in the rat dentate gyrus correlates with, but does not modify, performance in the water maze. *Hippocampus*, 3(2), 133-140. <https://doi.org/10.1002/hipo.450030205>
- Jensen, B. S. (2002). BMS-204352: a potassium channel opener developed for the treatment of stroke. *CNS Drug Rev*, 8(4), 353-360. <https://doi.org/10.1111/j.1527-3458.2002.tb00233.x>
- Jerome, D., Hou, Q., & Yuan, Q. (2012). Interaction of NMDA receptors and L-type calcium channels during early odor preference learning in rats. *Eur J Neurosci*, 36(8), 3134-3141. <https://doi.org/10.1111/j.1460-9568.2012.08210.x>
- Jiang, Y., Lee, A., Chen, J., Cadene, M., Chait, B. T., & MacKinnon, R. (2002). Crystal structure and mechanism of a calcium-gated potassium channel. *Nature*, 417(6888), 515-522. <https://doi.org/10.1038/417515a>
- Johnston, D., & Amaral, D. G. (2004). Hippocampus. In G. M. Shepherd (Ed.), *The Synaptic Organization of the Brain* (pp. 455-498). Oxford University Press. <https://doi.org/10.1093/acprof:oso/9780195159561.003.0011>
- Jung, J., & Lambon Ralph, M. A. (2021). The immediate impact of transcranial magnetic stimulation on brain structure: Short-term neuroplasticity following one session of cTBS. *NeuroImage*, 240, 118375. <https://doi.org/10.1016/j.neuroimage.2021.118375>
- Kaczmarek, L. K., Aldrich, R. W., Chandy, K. G., Grissmer, S., Wei, A. D., & Wulff, H. (2017). International Union of Basic and Clinical Pharmacology. C. Nomenclature and Properties of Calcium-Activated and Sodium-Activated Potassium Channels. *Pharmacol Rev*, 69(1), 1-11. <https://doi.org/10.1124/pr.116.012864>
- Kampa, B. M., Clements, J., Jonas, P., & Stuart, G. J. (2004). Kinetics of Mg<sup>2+</sup> unblock of NMDA receptors: implications for spike-timing dependent synaptic plasticity. *J Physiol*, 556(Pt 2), 337-345. <https://doi.org/10.1113/jphysiol.2003.058842>
- Kempsell, A. T., & Fieber, L. A. (2015). Age-related deficits in synaptic plasticity rescued by activating PKA or PKC in sensory neurons of *Aplysia californica* [Original Research]. *Front Aging Neurosci*, 7, 173. <https://doi.org/10.3389/fnagi.2015.00173>
- Kim, D. M., & Nimigean, C. M. (2016). Voltage-Gated Potassium Channels: A Structural Examination of Selectivity and Gating. *Cold Spring Harb Perspect Biol*, 8(5). <https://doi.org/10.1101/cshperspect.a029231>
- Kim, M. J., Futai, K., Jo, J., Hayashi, Y., Cho, K., & Sheng, M. (2007). Synaptic accumulation of PSD-95 and synaptic function regulated by phosphorylation of serine-295 of PSD-95. *Neuron*, 56(3), 488-502. <https://doi.org/10.1016/j.neuron.2007.09.007>
- Kimm, T., Khaliq, Z. M., & Bean, B. P. (2015). Differential Regulation of Action Potential Shape and Burst-Frequency Firing by BK and Kv2 Channels in Substantia Nigra Dopaminergic Neurons. *J Neurosci*, 35(50), 16404-16417. <https://doi.org/10.1523/JNEUROSCI.5291-14.2015>
- Komsuoglu Celikyurt, I., Utkan, T., Ozer, C., Gacar, N., & Aricioglu, F. (2014). Effects of YC-1 on learning and memory functions of aged rats. *Med Sci Monit Basic Res*, 20, 130-137. <https://doi.org/10.12659/MSMBR.891064>
- Kondo, T., Shirasawa, T., Itoyama, Y., & Mori, H. (1996). Embryonic genes expressed in Alzheimer's disease brains. *Neurosci Lett*, 209(3), 157-160. [https://doi.org/10.1016/0304-3940\(96\)12618-5](https://doi.org/10.1016/0304-3940(96)12618-5)
- Kubo, Y., Adelman, J. P., Clapham, D. E., Jan, L. Y., Karschin, A., Kurachi, Y., Lazdunski, M., Nichols, C. G., Seino, S., & Vandenberg, C. A. (2005). International Union of Pharmacology. LIV. Nomenclature and molecular relationships of inwardly rectifying potassium channels. *Pharmacol Rev*, 57(4), 509-526. <https://doi.org/10.1124/pr.57.4.11>
- Kwan, H. Y., Shen, B., Ma, X., Kwok, Y. C., Huang, Y., Man, Y. B., Yu, S., & Yao, X. (2009). TRPC1 associates with BK(Ca) channel to form a signal complex in vascular smooth muscle cells. *Circ Res*, 104(5), 670-678. <https://doi.org/10.1161/CIRCRESAHA.108.188748>
- Kyle, B. D., & Braun, A. P. (2014). The regulation of BK channel activity by pre- and post-translational modifications. *Front Physiol*, 5, 316. <https://doi.org/10.3389/fphys.2014.00316>
- Langwieser, N., Christel, C. J., Kleppisch, T., Hofmann, F., Wotjak, C. T., & Moosmang, S. (2010). Homeostatic switch in hebbian plasticity and fear learning after sustained loss of Cav1.2 calcium channels. *J Neurosci*, 30(25), 8367-8375. <https://doi.org/10.1523/JNEUROSCI.4164-08.2010>
- Latorre, R., Castillo, K., Carrasquel-Ursulaez, W., Sepulveda, R. V., Gonzalez-Nilo, F., Gonzalez, C., & Alvarez, O. (2017). Molecular Determinants of BK Channel Functional Diversity and Functioning. *Physiol Rev*, 97(1), 39-87. <https://doi.org/10.1152/physrev.00001.2016>
- Lau, A., & Tymianski, M. (2010). Glutamate receptors, neurotoxicity and neurodegeneration. *Pflugers Arch*, 460(2), 525-542. <https://doi.org/10.1007/s00424-010-0809-1>
- Laumonier, F., Roger, S., Guerin, P., Molinari, F., M'Rad, R., Cahard, D., Belhadj, A., Halayem, M., Persico, A. M., Elia, M., Romano, V., Holbert, S., Andres, C., Chaabouni, H., Colleaux, L., Constant, J., Le Guennec, J. Y., & Briault, S. (2006). Association of a functional deficit of the BKCa channel, a synaptic regulator of neuronal excitability, with autism and mental retardation. *Am J Psychiatry*, 163(9), 1622-1629. <https://doi.org/10.1176/ajp.2006.163.9.1622>
- Lee, H. K., Barbarosie, M., Kameyama, K., Bear, M. F., & Haganir, R. L. (2000). Regulation of distinct AMPA receptor phosphorylation sites during bidirectional synaptic plasticity. *Nature*, 405(6789), 955-959. <https://doi.org/10.1038/35016089>

- Lee, H. K., Takamiya, K., Han, J. S., Man, H., Kim, C. H., Rumbaugh, G., Yu, S., Ding, L., He, C., Petralia, R. S., Wenthold, R. J., Gallagher, M., & Huganir, R. L. (2003). Phosphorylation of the AMPA receptor GluR1 subunit is required for synaptic plasticity and retention of spatial memory. *Cell*, 112(5), 631-643. [https://doi.org/10.1016/s0092-8674\(03\)00122-3](https://doi.org/10.1016/s0092-8674(03)00122-3)
- Lei, S., Pelkey, K. A., Topolnik, L., Congar, P., Lacaille, J. C., & McBain, C. J. (2003). Depolarization-induced long-term depression at hippocampal mossy fiber-CA3 pyramidal neuron synapses. *J Neurosci*, 23(30), 9786-9795. <https://doi.org/10.1523/JNEUROSCI.23-30-09786.2003>
- Li, B., Jie, W., Huang, L., Wei, P., Li, S., Luo, Z., Friedman, A. K., Meredith, A. L., Han, M. H., Zhu, X. H., & Gao, T. M. (2014). Nuclear BK channels regulate gene expression via the control of nuclear calcium signaling. *Nat Neurosci*, 17(8), 1055-1063. <https://doi.org/10.1038/nn.3744>
- Li, B., Sutari, B. S., Sun, S. D., Luo, Z., Wei, C., Chenouard, N., Mandelberg, N. J., Zhang, G., Wamsley, B., Tian, G., Sanchez, S., You, S., Huang, L., Neubert, T. A., Fishell, G., & Tsien, R. W. (2020). Neuronal Inactivity Co-opts LTP Machinery to Drive Potassium Channel Splicing and Homeostatic Spike Widening. *Cell*, 181(7), 1547-1565 e1515. <https://doi.org/10.1016/j.cell.2020.05.013>
- Li, B., Tadross, M. R., & Tsien, R. W. (2016). Sequential ionic and conformational signaling by calcium channels drives neuronal gene expression. *Science*, 351(6275), 863-867. <https://doi.org/10.1126/science.aad3647>
- Li, Q., & Yan, J. (2016). Modulation of BK Channel Function by Auxiliary Beta and Gamma Subunits. *Int Rev Neurobiol*, 128, 51-90. <https://doi.org/10.1016/bs.irm.2016.03.015>
- Lim, I. A., Hall, D. D., & Hell, J. W. (2002). Selectivity and promiscuity of the first and second PDZ domains of PSD-95 and synapse-associated protein 102. *J Biol Chem*, 277(24), 21697-21711. <https://doi.org/10.1074/jbc.M112339200>
- Liman, E. R., Hess, P., Weaver, F., & Koren, G. (1991). Voltage-sensing residues in the S4 region of a mammalian K<sup>+</sup> channel. *Nature*, 353(6346), 752-756. <https://doi.org/10.1038/353752a0>
- Lipscombe, D., Helton, T. D., & Xu, W. (2004). L-type calcium channels: the low down. *J Neurophysiol*, 92(5), 2633-2641. <https://doi.org/10.1152/jn.00486.2004>
- Lisman, J. (1989). A mechanism for the Hebb and the anti-Hebb processes underlying learning and memory. *Proc Natl Acad Sci U S A*, 86(23), 9574-9578. <https://doi.org/10.1073/pnas.86.23.9574>
- Liu, B., Liao, M., Mielke, J. G., Ning, K., Chen, Y., Li, L., El-Hayek, Y. H., Gomez, E., Zukin, R. S., Fehlings, M. G., & Wan, Q. (2006). Ischemic insults direct glutamate receptor subunit 2-lacking AMPA receptors to synaptic sites. *J Neurosci*, 26(20), 5309-5319. <https://doi.org/10.1523/JNEUROSCI.0567-06.2006>
- Liu, P., Smith, P. F., & Darlington, C. L. (2008). Glutamate receptor subunits expression in memory-associated brain structures: regional variations and effects of aging. *Synapse*, 62(11), 834-841. <https://doi.org/10.1002/syn.20563>
- Lodge, D. (2009). The history of the pharmacology and cloning of ionotropic glutamate receptors and the development of idiosyncratic nomenclature. *Neuropharmacology*, 56(1), 6-21. <https://doi.org/10.1016/j.neuropharm.2008.08.006>
- Logothetis, D. E., Kammen, B. F., Lindpaintner, K., Bisbas, D., & Nadal-Ginard, B. (1993). Gating charge differences between two voltage-gated K<sup>+</sup> channels are due to the specific charge content of their respective S4 regions. *Neuron*, 10(6), 1121-1129. [https://doi.org/10.1016/0896-6273\(93\)90060-5](https://doi.org/10.1016/0896-6273(93)90060-5)
- Lopez, G. A., Jan, Y. N., & Jan, L. Y. (1991). Hydrophobic substitution mutations in the S4 sequence alter voltage-dependent gating in Shaker K<sup>+</sup> channels. *Neuron*, 7(2), 327-336. [https://doi.org/10.1016/0896-6273\(91\)90271-z](https://doi.org/10.1016/0896-6273(91)90271-z)
- Lu, W., Man, H., Ju, W., Trimble, W. S., MacDonald, J. F., & Wang, Y. T. (2001). Activation of synaptic NMDA receptors induces membrane insertion of new AMPA receptors and LTP in cultured hippocampal neurons. *Neuron*, 29(1), 243-254. [https://doi.org/10.1016/s0896-6273\(01\)00194-5](https://doi.org/10.1016/s0896-6273(01)00194-5)
- Lu, W., & Roche, K. W. (2012). Posttranslational regulation of AMPA receptor trafficking and function. *Curr Opin Neurobiol*, 22(3), 470-479. <https://doi.org/10.1016/j.conb.2011.09.008>
- Luscher, C., & Malenka, R. C. (2012). NMDA receptor-dependent long-term potentiation and long-term depression (LTP/LTD). *Cold Spring Harb Perspect Biol*, 4(6). <https://doi.org/10.1101/cshperspect.a005710>
- Ma, L., Zablow, L., Kandel, E. R., & Siegelbaum, S. A. (1999). Cyclic AMP induces functional presynaptic boutons in hippocampal CA3-CA1 neuronal cultures. *Nat Neurosci*, 2(1), 24-30. <https://doi.org/10.1038/4525>
- Ma, T., Hoefler, C. A., Capetillo-Zarate, E., Yu, F., Wong, H., Lin, M. T., Tampellini, D., Klann, E., Blitzer, R. D., & Gouras, G. K. (2010). Dysregulation of the mTOR pathway mediates impairment of synaptic plasticity in a mouse model of Alzheimer's disease. *PLOS ONE*, 5(9). <https://doi.org/10.1371/journal.pone.0012845>
- Malenka, R. C. (1991). The role of postsynaptic calcium in the induction of long-term potentiation. *Mol Neurobiol*, 5(2-4), 289-295. <https://doi.org/10.1007/BF02935552>
- Malenka, R. C. (2003). Synaptic plasticity and AMPA receptor trafficking. *Ann N Y Acad Sci*, 1003, 1-11. <https://doi.org/10.1196/annals.1300.001>
- Malinow, R., & Malenka, R. C. (2002). AMPA receptor trafficking and synaptic plasticity. *Annu Rev Neurosci*, 25, 103-126. <https://doi.org/10.1146/annurev.neuro.25.112701.142758>
- Malinow, R., & Miller, J. P. (1986). Postsynaptic hyperpolarization during conditioning reversibly blocks induction of long-term potentiation. *Nature*, 320(6062), 529-530. <https://doi.org/10.1038/320529a0>

- Malinska, D., Mirandola, S. R., & Kunz, W. S. (2010). Mitochondrial potassium channels and reactive oxygen species. *FEBS Lett*, 584(10), 2043-2048. <https://doi.org/10.1016/j.febslet.2010.01.013>
- Manabe, T. (2017). NMDA receptor-independent long-term potentiation in hippocampal interneurons. *J Physiol*, 595(11), 3263-3264. <https://doi.org/10.1113/JP274093>
- Marcantoni, A., Vandael, D. H., Mahapatra, S., Carabelli, V., Sinnegger-Brauns, M. J., Striessnig, J., & Carbone, E. (2010). Loss of Cav1.3 channels reveals the critical role of L-type and BK channel coupling in pacemaking mouse adrenal chromaffin cells. *J Neurosci*, 30(2), 491-504. <https://doi.org/10.1523/JNEUROSCI.4961-09.2010>
- Marijic, J., Li, Q., Song, M., Nishimaru, K., Stefani, E., & Toro, L. (2001). Decreased expression of voltage- and Ca(2+)-activated K(+) channels in coronary smooth muscle during aging. *Circ Res*, 88(2), 210-216. <https://doi.org/10.1161/01.res.88.2.210>
- Martin, S. J., Grimwood, P. D., & Morris, R. G. (2000). Synaptic plasticity and memory: an evaluation of the hypothesis. *Annu Rev Neurosci*, 23, 649-711. <https://doi.org/10.1146/annurev.neuro.23.1.649>
- Marty, A. (1981). Ca-dependent K channels with large unitary conductance in chromaffin cell membranes. *Nature*, 291(5815), 497-500. <https://doi.org/10.1038/291497a0>
- Matsuoka, I., Giullini, G., Poyard, M., Stengel, D., Parma, J., Guellaen, G., & Hanoune, J. (1992). Localization of adenylyl and guanylyl cyclase in rat brain by in situ hybridization: comparison with calmodulin mRNA distribution. *J Neurosci*, 12(9), 3350-3360. <https://doi.org/10.1523/JNEUROSCI.12-09-03350.1992>
- Matt, L., Pham, T., Skrabak, D., Hoffmann, F., Eckert, P., Yin, J., Gisevius, M., Ehinger, R., Bausch, A., Ueffing, M., Boldt, K., Ruth, P., & Lukowski, R. (2021). The Na(+)-activated K(+) channel Slack contributes to synaptic development and plasticity. *Cell Mol Life Sci*, 78(23), 7569-7587. <https://doi.org/10.1007/s00018-021-03953-0>
- McKinney, B. C., & Murphy, G. G. (2006). The L-Type voltage-gated calcium channel Cav1.3 mediates consolidation, but not extinction, of contextually conditioned fear in mice. *Learn Mem*, 13(5), 584-589. <https://doi.org/10.1101/lm.279006>
- McMurray, J. J., Packer, M., Desai, A. S., Gong, J., Lefkowitz, M. P., Rizkala, A. R., Rouleau, J. L., Shi, V. C., Solomon, S. D., Swedberg, K., Zile, M. R., Investigators, P.-H., & Committees. (2014). Angiotensin-neprilysin inhibition versus enalapril in heart failure. *N Engl J Med*, 371(11), 993-1004. <https://doi.org/10.1056/NEJMoa1409077>
- Meech, R. W. (1972). Intracellular calcium injection causes increased potassium conductance in Aplysia nerve cells. *Comp Biochem Physiol A Comp Physiol*, 42(2), 493-499. [https://doi.org/10.1016/0300-9629\(72\)90128-4](https://doi.org/10.1016/0300-9629(72)90128-4)
- Meech, R. W. (1974). The sensitivity of Helix aspersa neurones to injected calcium ions. *J Physiol*, 237(2), 259-277. <https://doi.org/10.1113/jphysiol.1974.sp010481>
- Meech, R. W. (1978). Calcium-dependent potassium activation in nervous tissues. *Annu Rev Biophys Bioeng*, 7(1), 1-18. <https://doi.org/10.1146/annurev.bb.07.060178.000245>
- Megias, M., Emri, Z., Freund, T. F., & Gulyas, A. I. (2001). Total number and distribution of inhibitory and excitatory synapses on hippocampal CA1 pyramidal cells. *Neuroscience*, 102(3), 527-540. [https://doi.org/10.1016/s0306-4522\(00\)00496-6](https://doi.org/10.1016/s0306-4522(00)00496-6)
- Meredith, A. L., Thorneloe, K. S., Werner, M. E., Nelson, M. T., & Aldrich, R. W. (2004). Overactive bladder and incontinence in the absence of the BK large conductance Ca2+-activated K+ channel. *J Biol Chem*, 279(35), 36746-36752. <https://doi.org/10.1074/jbc.M405621200>
- Micheva, K. D., Busse, B., Weiler, N. C., O'Rourke, N., & Smith, S. J. (2010). Single-synapse analysis of a diverse synapse population: proteomic imaging methods and markers. *Neuron*, 68(4), 639-653. <https://doi.org/10.1016/j.neuron.2010.09.024>
- Miller, S. G., & Kennedy, M. B. (1986). Regulation of brain type II Ca2+/calmodulin-dependent protein kinase by autophosphorylation: a Ca2+-triggered molecular switch. *Cell*, 44(6), 861-870. [https://doi.org/10.1016/0092-8674\(86\)90008-5](https://doi.org/10.1016/0092-8674(86)90008-5)
- Milligan, T. A. (2021). Epilepsy: A Clinical Overview. *Am J Med*, 134(7), 840-847. <https://doi.org/10.1016/j.amjmed.2021.01.038>
- Mohr, C. J., Schroth, W., Murdter, T. E., Gross, D., Maier, S., Stegen, B., Dragoi, A., Steudel, F. A., Stehling, S., Hoppe, R., Madden, S., Ruth, P., Huber, S. M., Brauch, H., & Lukowski, R. (2022). Subunits of BK channels promote breast cancer development and modulate responses to endocrine treatment in preclinical models. *Br J Pharmacol*, 179(12), 2906-2924. <https://doi.org/10.1111/bph.15147>
- Montgomery, J. R., & Meredith, A. L. (2012). Genetic activation of BK currents in vivo generates bidirectional effects on neuronal excitability. *Proc Natl Acad Sci U S A*, 109(46), 18997-19002. <https://doi.org/10.1073/pnas.1205573109>
- Monyer, H., Burnashev, N., Laurie, D. J., Sakmann, B., & Seeburg, P. H. (1994). Developmental and regional expression in the rat brain and functional properties of four NMDA receptors. *Neuron*, 12(3), 529-540. [https://doi.org/10.1016/0896-6273\(94\)90210-0](https://doi.org/10.1016/0896-6273(94)90210-0)
- Moosmang, S., Haider, N., Klugbauer, N., Adelsberger, H., Langwieser, N., Muller, J., Stiess, M., Marais, E., Schulla, V., Lacinova, L., Goebbels, S., Nave, K. A., Storm, D. R., Hofmann, F., & Kleppisch, T. (2005). Role of hippocampal Cav1.2 Ca2+ channels in NMDA receptor-independent synaptic plasticity and spatial memory. *J Neurosci*, 25(43), 9883-9892. <https://doi.org/10.1523/JNEUROSCI.1531-05.2005>

- Moreira, P. S., Almeida, P. R., Leite-Almeida, H., Sousa, N., & Costa, P. (2016). Impact of Chronic Stress Protocols in Learning and Memory in Rodents: Systematic Review and Meta-Analysis. *PLOS ONE*, 11(9), e0163245. <https://doi.org/10.1371/journal.pone.0163245>
- Morris, R. G. (1999). D.O. Hebb: The Organization of Behavior, Wiley: New York; 1949. *Brain Res Bull*, 50(5-6), 437. [https://doi.org/10.1016/s0361-9230\(99\)00182-3](https://doi.org/10.1016/s0361-9230(99)00182-3)
- Morris, R. G., Anderson, E., Lynch, G. S., & Baudry, M. (1986). Selective impairment of learning and blockade of long-term potentiation by an N-methyl-D-aspartate receptor antagonist, AP5. *Nature*, 319(6056), 774-776. <https://doi.org/10.1038/319774a0>
- Morrison, J. H., & Hof, P. R. (1997). Life and death of neurons in the aging brain. *Science*, 278(5337), 412-419. <https://doi.org/10.1126/science.278.5337.412>
- Moser, E. I., Krobort, K. A., Moser, M. B., & Morris, R. G. (1998). Impaired spatial learning after saturation of long-term potentiation. *Science*, 281(5385), 2038-2042. <https://doi.org/10.1126/science.281.5385.2038>
- Moskowitz, M. A., Lo, E. H., & Iadecola, C. (2010). The science of stroke: mechanisms in search of treatments. *Neuron*, 67(2), 181-198. <https://doi.org/10.1016/j.neuron.2010.07.002>
- Mulkey, R. M., Herron, C. E., & Malenka, R. C. (1993). An essential role for protein phosphatases in hippocampal long-term depression. *Science*, 261(5124), 1051-1055. <https://doi.org/10.1126/science.8394601>
- Nascimento, E. B., Dierschnabel, A. L., Lima, R. H., Sousa, M. B. C., Suchecki, D., Silva, R. H., & Ribeiro, A. M. (2022). Stress-related impairment of fear memory acquisition and disruption of risk assessment behavior in female but not in male mice. *Behav Processes*, 199, 104660. <https://doi.org/10.1016/j.beproc.2022.104660>
- Nelissen, E., Possemis, N., Van Goethem, N. P., Schepers, M., Mulder-Jongen, D. A. J., Dietz, L., Janssen, W., Gerisch, M., Huser, J., Sandner, P., Vanmierlo, T., & Prickaerts, J. (2022). The sGC stimulator BAY-747 and activator runcaciguat can enhance memory in vivo via differential hippocampal plasticity mechanisms. *Sci Rep*, 12(1), 3589. <https://doi.org/10.1038/s41598-022-07391-1>
- Nicholls, R. E., Alarcon, J. M., Malleret, G., Carroll, R. C., Grody, M., Vronskaya, S., & Kandel, E. R. (2008). Transgenic mice lacking NMDAR-dependent LTD exhibit deficits in behavioral flexibility. *Neuron*, 58(1), 104-117. <https://doi.org/10.1016/j.neuron.2008.01.039>
- Nishimaru, K., Eghbali, M., Lu, R., Marijic, J., Stefani, E., & Toro, L. (2004). Functional and molecular evidence of MaxiK channel beta1 subunit decrease with coronary artery ageing in the rat. *J Physiol*, 559(Pt 3), 849-862. <https://doi.org/10.1113/jphysiol.2004.068676>
- Nowak, L., Bregestovski, P., Ascher, P., Herbet, A., & Prochiantz, A. (1984). Magnesium gates glutamate-activated channels in mouse central neurones. *Nature*, 307(5950), 462-465. <https://doi.org/10.1038/307462a0>
- Obermair, G. J., Szabo, Z., Bourinet, E., & Flucher, B. E. (2004). Differential targeting of the L-type Ca<sup>2+</sup> channel alpha 1C (CaV1.2) to synaptic and extrasynaptic compartments in hippocampal neurons. *Eur J Neurosci*, 19(8), 2109-2122. <https://doi.org/10.1111/j.0953-816X.2004.03272.x>
- Oddo, S., Caccamo, A., Shepherd, J. D., Murphy, M. P., Golde, T. E., Kaye, R., Metherate, R., Mattson, M. P., Akbari, Y., & LaFerla, F. M. (2003). Triple-transgenic model of Alzheimer's disease with plaques and tangles: intracellular Abeta and synaptic dysfunction. *Neuron*, 39(3), 409-421. [https://doi.org/10.1016/s0896-6273\(03\)00434-3](https://doi.org/10.1016/s0896-6273(03)00434-3)
- Olsson, B., Zetterberg, H., Hampel, H., & Blennow, K. (2011). Biomarker-based dissection of neurodegenerative diseases. *Prog Neurobiol*, 95(4), 520-534. <https://doi.org/10.1016/j.pneurobio.2011.04.006>
- Opazo, P., Labrecque, S., Tigaret, C. M., Frouin, A., Wiseman, P. W., De Koninck, P., & Choquet, D. (2010). CaMKII triggers the diffusional trapping of surface AMPARs through phosphorylation of stargazin. *Neuron*, 67(2), 239-252. <https://doi.org/10.1016/j.neuron.2010.06.007>
- Otmakhov, N., Khibnik, L., Otmakhova, N., Carpenter, S., Riahi, S., Asrican, B., & Lisman, J. (2004). Forskolin-induced LTP in the CA1 hippocampal region is NMDA receptor dependent. *J Neurophysiol*, 91(5), 1955-1962. <https://doi.org/10.1152/jn.00941.2003>
- Pallanck, L., & Ganetzky, B. (1994). Cloning and characterization of human and mouse homologs of the Drosophila calcium-activated potassium channel gene, slowpoke. *Hum Mol Genet*, 3(8), 1239-1243. <https://doi.org/10.1093/hmg/3.8.1239>
- Pannese, E. (2011). Morphological changes in nerve cells during normal aging. *Brain Struct Funct*, 216(2), 85-89. <https://doi.org/10.1007/s00429-011-0308-y>
- Papazian, D. M., Schwarz, T. L., Tempel, B. L., Jan, Y. N., & Jan, L. Y. (1987). Cloning of genomic and complementary DNA from Shaker, a putative potassium channel gene from Drosophila. *Science*, 237(4816), 749-753. <https://doi.org/10.1126/science.2441470>
- Park, D. C., & Festini, S. B. (2017). Theories of Memory and Aging: A Look at the Past and a Glimpse of the Future. *J Gerontol B Psychol Sci Soc Sci*, 72(1), 82-90. <https://doi.org/10.1093/geronb/gbw066>
- Park, P., Georgiou, J., Sanderson, T. M., Ko, K. H., Kang, H., Kim, J. I., Bradley, C. A., Bortolotto, Z. A., Zhuo, M., Kaang, B. K., & Collingridge, G. L. (2021). PKA drives an increase in AMPA receptor unitary conductance during LTP in the hippocampus. *Nat Commun*, 12(1), 413. <https://doi.org/10.1038/s41467-020-20523-3>

- Perez, G. J., Desai, M., Anderson, S., & Scornik, F. S. (2013). Large-conductance calcium-activated potassium current modulates excitability in isolated canine intracardiac neurons. *Am J Physiol Cell Physiol*, 304(3), C280-286. <https://doi.org/10.1152/ajpcell.00148.2012>
- Pérez, G. J., Desai, M., Anderson, S., & Scornik, F. S. (2013). Large-conductance calcium-activated potassium current modulates excitability in isolated canine intracardiac neurons. *American Journal of Physiology-Cell Physiology*, 304(3), C280-C286. <https://doi.org/10.1152/ajpcell.00148.2012>
- Pham, T., Hussein, T., Calis, D., Bischof, H., Skrabak, D., Cruz Santos, M., Maier, S., Spähn, D., Kalina, D., Simonsig, S., Ehinger, R., Groschup, B., Knipper, M., Plesnila, N., Ruth, P., Lukowski, R., & Matt, L. (2023). BK channels sustain neuronal Ca(2+) oscillations to support hippocampal long-term potentiation and memory formation. *Cell Mol Life Sci*, 80(12), 369. <https://doi.org/10.1007/s00018-023-05016-y>
- Piechotta, P. L., Rapedius, M., Stansfeld, P. J., Bolleballi, M. K., Ehrlich, G., Andres-Enguix, I., Fritzenschaft, H., Decher, N., Sansom, M. S., Tucker, S. J., & Baukrowitz, T. (2011). The pore structure and gating mechanism of K2P channels. *EMBO J*, 30(17), 3607-3619. <https://doi.org/10.1038/emboj.2011.268>
- Pitts, M. W. (2018). Barnes Maze Procedure for Spatial Learning and Memory in Mice. *Bio Protoc*, 8(5). <https://doi.org/10.21769/bioprotoc.2744>
- Platzer, J., Engel, J., Schrott-Fischer, A., Stephan, K., Bova, S., Chen, H., Zheng, H., & Striessnig, J. (2000). Congenital deafness and sinoatrial node dysfunction in mice lacking class D L-type Ca<sup>2+</sup> channels. *Cell*, 102(1), 89-97. [https://doi.org/10.1016/s0092-8674\(00\)00013-1](https://doi.org/10.1016/s0092-8674(00)00013-1)
- Querfurth, H. W., & LaFerla, F. M. (2010). Alzheimer's disease. *N Engl J Med*, 362(4), 329-344. <https://doi.org/10.1056/NEJMra0909142>
- Quevedo, J., Vianna, M., Daroit, D., Born, A. G., Kuyven, C. R., Roesler, R., & Quillfeldt, J. A. (1998). L-type voltage-dependent calcium channel blocker nifedipine enhances memory retention when infused into the hippocampus. *Neurobiol Learn Mem*, 69(3), 320-325. <https://doi.org/10.1006/nlme.1998.3822>
- Rajadhyaksha, A., Barczak, A., Macias, W., Leveque, J. C., Lewis, S. E., & Konradi, C. (1999). L-Type Ca(2+) channels are essential for glutamate-mediated CREB phosphorylation and c-fos gene expression in striatal neurons. *J Neurosci*, 19(15), 6348-6359. <https://doi.org/10.1523/JNEUROSCI.19-15-06348.1999>
- Raymond, C. R., & Redman, S. J. (2002). Different calcium sources are narrowly tuned to the induction of different forms of LTP. *J Neurophysiol*, 88(1), 249-255. <https://doi.org/10.1152/jn.2002.88.1.249>
- Reiner, A., & Levitz, J. (2018). Glutamatergic Signaling in the Central Nervous System: Ionotropic and Metabotropic Receptors in Concert. *Neuron*, 98(6), 1080-1098. <https://doi.org/10.1016/j.neuron.2018.05.018>
- Reuter, H. (1996). Diversity and function of presynaptic calcium channels in the brain. *Curr Opin Neurobiol*, 6(3), 331-337. [https://doi.org/10.1016/s0959-4388\(96\)80116-4](https://doi.org/10.1016/s0959-4388(96)80116-4)
- Richardson, K., Schoen, M., French, B., Umscheid, C. A., Mitchell, M. D., Arnold, S. E., Heidenreich, P. A., Rader, D. J., & deGoma, E. M. (2013). Statins and cognitive function: a systematic review. *Ann Intern Med*, 159(10), 688-697. <https://doi.org/10.7326/0003-4819-159-10-201311190-00007>
- Roberts, R., & Knopman, D. S. (2013). Classification and epidemiology of MCI. *Clin Geriatr Med*, 29(4), 753-772. <https://doi.org/10.1016/j.cger.2013.07.003>
- Roche, K. W., O'Brien, R. J., Mammen, A. L., Bernhardt, J., & Huganir, R. L. (1996). Characterization of multiple phosphorylation sites on the AMPA receptor GluR1 subunit. *Neuron*, 16(6), 1179-1188. [https://doi.org/10.1016/s0896-6273\(00\)80144-0](https://doi.org/10.1016/s0896-6273(00)80144-0)
- Rothberg, B. S., & Magleby, K. L. (1999). Gating kinetics of single large-conductance Ca<sup>2+</sup>-activated K<sup>+</sup> channels in high Ca<sup>2+</sup> suggest a two-tiered allosteric gating mechanism. *J Gen Physiol*, 114(1), 93-124. <https://doi.org/10.1085/jgp.114.1.93>
- Rowan, M. J., Klyubin, I., Wang, Q., & Anwyl, R. (2005). Synaptic plasticity disruption by amyloid beta protein: modulation by potential Alzheimer's disease modifying therapies. *Biochem Soc Trans*, 33(Pt 4), 563-567. <https://doi.org/10.1042/BST0330563>
- Sakagami, Y., Yamamoto, K., Sugiura, S., Inokuchi, K., Hayashi, T., & Kato, N. (2005). Essential roles of Homer-1a in homeostatic regulation of pyramidal cell excitability: a possible link to clinical benefits of electroconvulsive shock. *Eur J Neurosci*, 21(12), 3229-3239. <https://doi.org/10.1111/j.1460-9568.2005.04165.x>
- Sakimura, K., Kutsuwada, T., Ito, I., Manabe, T., Takayama, C., Kushiya, E., Yagi, T., Aizawa, S., Inoue, Y., Sugiyama, H., & et al. (1995). Reduced hippocampal LTP and spatial learning in mice lacking NMDA receptor epsilon 1 subunit. *Nature*, 373(6510), 151-155. <https://doi.org/10.1038/373151a0>
- Sako, W., Murakami, N., Izumi, Y., & Kajii, R. (2014). MRI can detect nigral volume loss in patients with Parkinson's disease: evidence from a meta-analysis. *J Parkinsons Dis*, 4(3), 405-411. <https://doi.org/10.3233/JPD-130332>
- Sanz-Clemente, A., Nicoll, R. A., & Roche, K. W. (2013). Diversity in NMDA receptor composition: many regulators, many consequences. *Neuroscientist*, 19(1), 62-75. <https://doi.org/10.1177/1073858411435129>
- Sausbier, M., Hu, H., Arntz, C., Feil, S., Kamm, S., Adelsberger, H., Sausbier, U., Sailer, C. A., Feil, R., Hofmann, F., Korth, M., Shipston, M. J., Knaus, H. G., Wolfer, D. P., Pedroarena, C. M., Storm, J. F., & Ruth, P. (2004). Cerebellar ataxia and Purkinje cell dysfunction caused by Ca<sup>2+</sup>-activated K<sup>+</sup> channel deficiency. *Proc Natl Acad Sci U S A*, 101(25), 9474-9478. <https://doi.org/10.1073/pnas.0401702101>

- Schubert, R., & Nelson, M. T. (2001). Protein kinases: tuners of the BKCa channel in smooth muscle. *Trends Pharmacol Sci*, 22(10), 505-512. [https://doi.org/10.1016/s0165-6147\(00\)01775-2](https://doi.org/10.1016/s0165-6147(00)01775-2)
- Selkoe, D. J. (2002). Alzheimer's disease is a synaptic failure. *Science*, 298(5594), 789-791. <https://doi.org/10.1126/science.1074069>
- Seoh, S. A., Sigg, D., Papazian, D. M., & Bezanilla, F. (1996). Voltage-sensing residues in the S2 and S4 segments of the Shaker K<sup>+</sup> channel. *Neuron*, 16(6), 1159-1167. [https://doi.org/10.1016/s0896-6273\(00\)80142-7](https://doi.org/10.1016/s0896-6273(00)80142-7)
- Seol, G. H., Ziburkus, J., Huang, S., Song, L., Kim, I. T., Takamiya, K., Huganir, R. L., Lee, H. K., & Kirkwood, A. (2007). Neuromodulators control the polarity of spike-timing-dependent synaptic plasticity. *Neuron*, 55(6), 919-929. <https://doi.org/10.1016/j.neuron.2007.08.013>
- Shah, K. R., Guan, X., & Yan, J. (2021). Structural and Functional Coupling of Calcium-Activated BK Channels and Calcium-Permeable Channels Within Nanodomain Signaling Complexes. *Front Physiol*, 12, 796540. <https://doi.org/10.3389/fphys.2021.796540>
- Sharman, J. L., Mpamhanga, C. P., Spedding, M., Germain, P., Staels, B., Dacquet, C., Laudet, V., Harmar, A. J., & Nc, I. (2011). IUPHAR-DB: new receptors and tools for easy searching and visualization of pharmacological data. *Nucleic Acids Res*, 39(Database issue), D534-538. <https://doi.org/10.1093/nar/gkq1062>
- Shen, K., & Meyer, T. (1999). Dynamic control of CaMKII translocation and localization in hippocampal neurons by NMDA receptor stimulation. *Science*, 284(5411), 162-166. <https://doi.org/10.1126/science.284.5411.162>
- Sheng, M., Cummings, J., Roldan, L. A., Jan, Y. N., & Jan, L. Y. (1994). Changing subunit composition of heteromeric NMDA receptors during development of rat cortex. *Nature*, 368(6467), 144-147. <https://doi.org/10.1038/368144a0>
- Shepherd, J. D., & Huganir, R. L. (2007). The cell biology of synaptic plasticity: AMPA receptor trafficking. *Annu Rev Cell Dev Biol*, 23(1), 613-643. <https://doi.org/10.1146/annurev.cellbio.23.090506.123516>
- Shi, J., Krishnamoorthy, G., Yang, Y., Hu, L., Chaturvedi, N., Harilal, D., Qin, J., & Cui, J. (2002). Mechanism of magnesium activation of calcium-activated potassium channels. *Nature*, 418(6900), 876-880. <https://doi.org/10.1038/nature00941>
- Shieh, C. C., Coghlan, M., Sullivan, J. P., & Gopalakrishnan, M. (2000). Potassium channels: molecular defects, diseases, and therapeutic opportunities. *Pharmacol Rev*, 52(4), 557-594. <https://www.ncbi.nlm.nih.gov/pubmed/11121510>
- Shipston, M. J., & Armstrong, D. L. (1996). Activation of protein kinase C inhibits calcium-activated potassium channels in rat pituitary tumour cells. *J Physiol*, 493 ( Pt 3)(Pt 3), 665-672. <https://doi.org/10.1113/jphysiol.1996.sp021413>
- Shrestha, A., Sultana, R., Lee, C. C., & Ogundele, O. M. (2019). SK Channel Modulates Synaptic Plasticity by Tuning CaMKIIalpha/beta Dynamics [Original Research]. *Front Synaptic Neurosci*, 11, 18. <https://doi.org/10.3389/fnsyn.2019.00018>
- Sladeczek, F., Pin, J. P., Recasens, M., Bockaert, J., & Weiss, S. (1985). Glutamate stimulates inositol phosphate formation in striatal neurones. *Nature*, 317(6039), 717-719. <https://doi.org/10.1038/317717a0>
- Small, S. A., & Duff, K. (2008). Linking Aβeta and tau in late-onset Alzheimer's disease: a dual pathway hypothesis. *Neuron*, 60(4), 534-542. <https://doi.org/10.1016/j.neuron.2008.11.007>
- Sokolov, R. A., & Mukhina, I. V. (2022). Spontaneous Ca(2+) events are linked to the development of neuronal firing during maturation in mice primary hippocampal culture cells. *Arch Biochem Biophys*, 727, 109330. <https://doi.org/10.1016/j.abb.2022.109330>
- Sridharan, P. S., Lu, Y., Rice, R. C., Pieper, A. A., & Rajadhyaksha, A. M. (2020). Loss of Cav1.2 channels impairs hippocampal theta burst stimulation-induced long-term potentiation. *Channels (Austin)*, 14(1), 287-293. <https://doi.org/10.1080/19336950.2020.1807851>
- Steinberg, J. P., Takamiya, K., Shen, Y., Xia, J., Rubio, M. E., Yu, S., Jin, W., Thomas, G. M., Linden, D. J., & Huganir, R. L. (2006). Targeted in vivo mutations of the AMPA receptor subunit GluR2 and its interacting protein PICK1 eliminate cerebellar long-term depression. *Neuron*, 49(6), 845-860. <https://doi.org/10.1016/j.neuron.2006.02.025>
- Stoyas, C. A., Bushart, D. D., Switonski, P. M., Ward, J. M., Alaghatta, A., Tang, M. B., Niu, C., Wadhwa, M., Huang, H., Savchenko, A., Gariani, K., Xie, F., Delaney, J. R., Gaasterland, T., Auwerx, J., Shakkottai, V. G., & La Spada, A. R. (2020). Nicotinamide Pathway-Dependent Sirt1 Activation Restores Calcium Homeostasis to Achieve Neuroprotection in Spinocerebellar Ataxia Type 7. *Neuron*, 105(4), 630-644 e639. <https://doi.org/10.1016/j.neuron.2019.11.019>
- Styren, S. D., Bowser, R., & Dekosky, S. T. (1997). Expression of fetal ALZ-50 reactive clone 1 (FAC1) in dentate gyrus following entorhinal cortex lesion. *J Comp Neurol*, 386(4), 555-561. <https://www.ncbi.nlm.nih.gov/pubmed/9378851>
- Su, F., Guo, A. C., Li, W. W., Zhao, Y. L., Qu, Z. Y., Wang, Y. J., Wang, Q., & Zhu, Y. L. (2017). Low-Dose Ethanol Preconditioning Protects Against Oxygen-Glucose Deprivation/Reoxygenation-Induced Neuronal Injury By Activating Large Conductance, Ca(2+)-Activated K(+) Channels In Vitro. *Neurosci Bull*, 33(1), 28-40. <https://doi.org/10.1007/s12264-016-0080-3>
- Sugiyama, H., Ito, I., & Hirono, C. (1987). A new type of glutamate receptor linked to inositol phospholipid metabolism. *Nature*, 325(6104), 531-533. <https://doi.org/10.1038/325531a0>

- Sugunan, S., Nampoothiri, S. S., Garg, T., & Krishnamurthy, R. G. (2016). Role of KCa3.1 Channels in CNS Diseases: A Concise Review. *CNS Neurol Disord Drug Targets*, 15(10), 1299-1305. <https://doi.org/10.2174/1871527315666160822111913>
- Summers, K. C., Bogard, A. S., & Tavalin, S. J. (2019). Preferential generation of Ca(2+)-permeable AMPA receptors by AKAP79-anchored protein kinase C proceeds via GluA1 subunit phosphorylation at Ser-831. *J Biol Chem*, 294(14), 5521-5535. <https://doi.org/10.1074/jbc.RA118.004340>
- Sun, J., Liu, Y., Baudry, M., & Bi, X. (2020). SK2 channel regulation of neuronal excitability, synaptic transmission, and brain rhythmic activity in health and diseases. *Biochim Biophys Acta Mol Cell Res*, 1867(12), 118834. <https://doi.org/10.1016/j.bbamcr.2020.118834>
- Sweet, T. B., & Cox, D. H. (2009). Measuring the influence of the BKCa beta1 subunit on Ca2+ binding to the BKCa channel. *J Gen Physiol*, 133(2), 139-150. <https://doi.org/10.1085/jgp.200810129>
- Tao, X., Hite, R. K., & MacKinnon, R. (2017). Cryo-EM structure of the open high-conductance Ca(2+)-activated K(+) channel. *Nature*, 541(7635), 46-51. <https://doi.org/10.1038/nature20608>
- Tomita, S., Adesnik, H., Sekiguchi, M., Zhang, W., Wada, K., Howe, J. R., Nicoll, R. A., & Brecht, D. S. (2005). Stargazin modulates AMPA receptor gating and trafficking by distinct domains. *Nature*, 435(7045), 1052-1058. <https://doi.org/10.1038/nature03624>
- Traynelis, S. F., Wollmuth, L. P., McBain, C. J., Menniti, F. S., Vance, K. M., Ogden, K. K., Hansen, K. B., Yuan, H., Myers, S. J., & Dingledine, R. (2010). Glutamate receptor ion channels: structure, regulation, and function. *Pharmacol Rev*, 62(3), 405-496. <https://doi.org/10.1124/pr.109.002451>
- Traynelis, S. F., Wollmuth, L. P., McBain, C. J., Menniti, F. S., Vance, K. M., Ogden, K. K., Hansen, K. B., Yuan, H., Myers, S. J., & Dingledine, R. (2010). Glutamate Receptor Ion Channels: Structure, Regulation, and Function. *Pharmacological Reviews*, 62(3), 405-496. <https://doi.org/10.1124/pr.109.002451>
- Trimmer, J. S. (2015). Subcellular localization of K+ channels in mammalian brain neurons: remarkable precision in the midst of extraordinary complexity. *Neuron*, 85(2), 238-256. <https://doi.org/10.1016/j.neuron.2014.12.042>
- Tseng-Crank, J., Foster, C. D., Krause, J. D., Mertz, R., Godinot, N., DiChiara, T. J., & Reinhart, P. H. (1994). Cloning, expression, and distribution of functionally distinct Ca(2+)-activated K+ channel isoforms from human brain. *Neuron*, 13(6), 1315-1330. [https://doi.org/10.1016/0896-6273\(94\)90418-9](https://doi.org/10.1016/0896-6273(94)90418-9)
- Tsien, J. Z., Chen, D. F., Gerber, D., Tom, C., Mercer, E. H., Anderson, D. J., Mayford, M., Kandel, E. R., & Tonegawa, S. (1996). Subregion- and cell type-restricted gene knockout in mouse brain. *Cell*, 87(7), 1317-1326. [https://doi.org/10.1016/s0092-8674\(00\)81826-7](https://doi.org/10.1016/s0092-8674(00)81826-7)
- Tsien, J. Z., Huerta, P. T., & Tonegawa, S. (1996). The essential role of hippocampal CA1 NMDA receptor-dependent synaptic plasticity in spatial memory. *Cell*, 87(7), 1327-1338. [https://doi.org/10.1016/s0092-8674\(00\)81827-9](https://doi.org/10.1016/s0092-8674(00)81827-9)
- Typlt, M., Mirkowski, M., Azzopardi, E., Ruettiger, L., Ruth, P., & Schmid, S. (2013). Mice with deficient BK channel function show impaired prepulse inhibition and spatial learning, but normal working and spatial reference memory. *PLOS ONE*, 8(11), e81270. <https://doi.org/10.1371/journal.pone.0081270>
- van Dyck, C. H., Swanson, C. J., Aisen, P., Bateman, R. J., Chen, C., Gee, M., Kanekiyo, M., Li, D., Reyderman, L., Cohen, S., Froelich, L., Katayama, S., Sabbagh, M., Vellas, B., Watson, D., Dhadda, S., Irizarry, M., Kramer, L. D., & Iwatsubo, T. (2023). Lecanemab in Early Alzheimer's Disease. *N Engl J Med*, 388(1), 9-21. <https://doi.org/10.1056/NEJMoa2212948>
- VanGuilder, H. D., Yan, H., Farley, J. A., Sonntag, W. E., & Freeman, W. M. (2010). Aging alters the expression of neurotransmission-regulating proteins in the hippocampal synaptome. *J Neurochem*, 113(6), 1577-1588. <https://doi.org/10.1111/j.1471-4159.2010.06719.x>
- Veng, L. M., Mesches, M. H., & Browning, M. D. (2003). Age-related working memory impairment is correlated with increases in the L-type calcium channel protein alpha1D (Cav1.3) in area CA1 of the hippocampus and both are ameliorated by chronic nimodipine treatment. *Brain Res Mol Brain Res*, 110(2), 193-202. [https://doi.org/10.1016/s0169-328x\(02\)00643-5](https://doi.org/10.1016/s0169-328x(02)00643-5)
- Vianna, M. R., Igaz, L. M., Coitinho, A. S., Medina, J. H., & Izquierdo, I. (2003). Memory extinction requires gene expression in rat hippocampus. *Neurobiol Learn Mem*, 79(3), 199-203. [https://doi.org/10.1016/s1074-7427\(03\)00003-0](https://doi.org/10.1016/s1074-7427(03)00003-0)
- Voglis, G., & Tavernarakis, N. (2006). The role of synaptic ion channels in synaptic plasticity. *EMBO Rep*, 7(11), 1104-1110. <https://doi.org/10.1038/sj.embor.7400830>
- Vorhees, C. V., & Williams, M. T. (2006). Morris water maze: procedures for assessing spatial and related forms of learning and memory. *Nat Protoc*, 1(2), 848-858. <https://doi.org/10.1038/nprot.2006.116>
- Walikonis, R. S., Jensen, O. N., Mann, M., Provance, D. W., Jr., Mercer, J. A., & Kennedy, M. B. (2000). Identification of proteins in the postsynaptic density fraction by mass spectrometry. *J Neurosci*, 20(11), 4069-4080. <https://doi.org/10.1523/JNEUROSCI.20-11-04069.2000>
- Wallner, M., Meera, P., & Toro, L. (1999). Chapter 8 Calcium-Activated Potassium Channels in Muscle and Brain. In Y. Kurachi, L. Y. Jan, & M. Lnzdunski (Eds.), *Potassium Ion Channels Molecular Structure, Function, and Diseases* (Vol. 46, pp. 117-140). Academic Press. [https://doi.org/10.1016/s0070-2161\(08\)60924-7](https://doi.org/10.1016/s0070-2161(08)60924-7)
- Wang, B., Hu, Q., Hearn, M. G., Shimizu, K., Ware, C. B., Liggitt, D. H., Jin, L. W., Cool, B. H., Storm, D. R., & Martin, G. M. (2004). Isoform-specific knockout of FE65 leads to impaired learning and memory. *J Neurosci Res*, 75(1), 12-24. <https://doi.org/10.1002/jnr.10834>

- Wang, B., Rothberg, B. S., & Brenner, R. (2006). Mechanism of beta4 subunit modulation of BK channels. *J Gen Physiol*, 127(4), 449-465. <https://doi.org/10.1085/jgp.200509436>
- Wang, L., Kang, H., Li, Y., Shui, Y., Yamamoto, R., Sugai, T., & Kato, N. (2015). Cognitive recovery by chronic activation of the large-conductance calcium-activated potassium channel in a mouse model of Alzheimer's disease. *Neuropharmacology*, 92, 8-15. <https://doi.org/10.1016/j.neuropharm.2014.12.033>
- Ward, E. V., Berry, C. J., & Shanks, D. R. (2013). Age effects on explicit and implicit memory [Hypothesis and Theory]. *Front Psychol*, 4, 639. <https://doi.org/10.3389/fpsyg.2013.00639>
- Wei, A. D., Gutman, G. A., Aldrich, R., Chandry, K. G., Grissmer, S., & Wulff, H. (2005). International Union of Pharmacology. LII. Nomenclature and molecular relationships of calcium-activated potassium channels. *Pharmacol Rev*, 57(4), 463-472. <https://doi.org/10.1124/pr.57.4.9>
- Wenthold, R. J., Petralia, R. S., Blahos, J., II, & Niedzielski, A. S. (1996). Evidence for multiple AMPA receptor complexes in hippocampal CA1/CA2 neurons. *J Neurosci*, 16(6), 1982-1989. <https://doi.org/10.1523/JNEUROSCI.16-06-01982.1996>
- West, M. J., Coleman, P. D., Flood, D. G., & Troncoso, J. C. (1994). Differences in the pattern of hippocampal neuronal loss in normal ageing and Alzheimer's disease. *Lancet*, 344(8925), 769-772. [https://doi.org/10.1016/s0140-6736\(94\)92338-8](https://doi.org/10.1016/s0140-6736(94)92338-8)
- Wong, J. M., & Gray, J. A. (2018). Long-Term Depression Is Independent of GluN2 Subunit Composition. *J Neurosci*, 38(19), 4462-4470. <https://doi.org/10.1523/JNEUROSCI.0394-18.2018>
- Wong, T. P., Howland, J. G., Robillard, J. M., Ge, Y., Yu, W., Titterness, A. K., Brebner, K., Liu, L., Weinberg, J., Christie, B. R., Phillips, A. G., & Wang, Y. T. (2007). Hippocampal long-term depression mediates acute stress-induced spatial memory retrieval impairment. *Proc Natl Acad Sci U S A*, 104(27), 11471-11476. <https://doi.org/10.1073/pnas.0702308104>
- Wrzosek, A. (2014). The potassium channel opener NS1619 modulates calcium homeostasis in muscle cells by inhibiting SERCA. *Cell Calcium*, 56(1), 14-24. <https://doi.org/10.1016/j.ceca.2014.03.005>
- Wyllie, D. J., Livesey, M. R., & Hardingham, G. E. (2013). Influence of GluN2 subunit identity on NMDA receptor function. *Neuropharmacology*, 74, 4-17. <https://doi.org/10.1016/j.neuropharm.2013.01.016>
- Xia, X. M., Zeng, X., & Lingle, C. J. (2002). Multiple regulatory sites in large-conductance calcium-activated potassium channels. *Nature*, 418(6900), 880-884. <https://doi.org/10.1038/nature00956>
- Xie, J., & McCobb, D. P. (1998). Control of alternative splicing of potassium channels by stress hormones. *Science*, 280(5362), 443-446. <https://doi.org/10.1126/science.280.5362.443>
- Yamamoto, K., Ueta, Y., Wang, L., Yamamoto, R., Inoue, N., Inokuchi, K., Aiba, A., Yonekura, H., & Kato, N. (2011). Suppression of a neocortical potassium channel activity by intracellular amyloid-beta and its rescue with Homer1a. *J Neurosci*, 31(31), 11100-11109. <https://doi.org/10.1523/JNEUROSCI.6752-10.2011>
- Yan, J., & Aldrich, R. W. (2010). LRRC26 auxiliary protein allows BK channel activation at resting voltage without calcium. *Nature*, 466(7305), 513-516. <https://doi.org/10.1038/nature09162>
- Yang, J., Vitery, M. D. C., Chen, J., Osei-Owusu, J., Chu, J., & Qiu, Z. (2019). Glutamate-Releasing SWELL1 Channel in Astrocytes Modulates Synaptic Transmission and Promotes Brain Damage in Stroke. *Neuron*, 102(4), 813-827 e816. <https://doi.org/10.1016/j.neuron.2019.03.029>
- Yang, Y., Wang, X. B., Frerking, M., & Zhou, Q. (2008). Delivery of AMPA receptors to perisynaptic sites precedes the full expression of long-term potentiation. *Proc Natl Acad Sci U S A*, 105(32), 11388-11393. <https://doi.org/10.1073/pnas.0802978105>
- Yang, Y., Wang, X. B., & Zhou, Q. (2010). Perisynaptic GluR2-lacking AMPA receptors control the reversibility of synaptic and spines modifications. *Proc Natl Acad Sci U S A*, 107(26), 11999-12004. <https://doi.org/10.1073/pnas.0913004107>
- Yankner, B. A., Lu, T., & Loerch, P. (2008). The aging brain. *Annu Rev Pathol*, 3(1), 41-66. <https://doi.org/10.1146/annurev.pathmechdis.2.010506.092044>
- Yazejian, B., Sun, X. P., & Grinnell, A. D. (2000). Tracking presynaptic Ca<sup>2+</sup> dynamics during neurotransmitter release with Ca<sup>2+</sup>-activated K<sup>+</sup> channels. *Nat Neurosci*, 3(6), 566-571. <https://doi.org/10.1038/75737>
- Yu, W., Lin, X., Gao, S., & Li, C. (2015). Age-related changes of inactivating BK channels in rat dorsal root ganglion neurons. *J Neurol Sci*, 358(1-2), 138-145. <https://doi.org/10.1016/j.jns.2015.08.1526>
- Zahs, K. R., & Ashe, K. H. (2010). 'Too much good news' - are Alzheimer mouse models trying to tell us how to prevent, not cure, Alzheimer's disease? *Trends Neurosci*, 33(8), 381-389. <https://doi.org/10.1016/j.tins.2010.05.004>
- Zhang, J., Guan, X., Li, Q., Meredith, A. L., Pan, H. L., & Yan, J. (2018). Glutamate-activated BK channel complexes formed with NMDA receptors. *Proc Natl Acad Sci U S A*, 115(38), E9006-E9014. <https://doi.org/10.1073/pnas.1802567115>
- Zhang, L., Li, X., Zhou, R., & Xing, G. (2006). Possible role of potassium channel, big K in etiology of schizophrenia. *Med Hypotheses*, 67(1), 41-43. <https://doi.org/10.1016/j.mehy.2005.09.055>
- Zhang, Y., Brown, M. R., Hyland, C., Chen, Y., Kronengold, J., Fleming, M. R., Kohn, A. B., Moroz, L. L., & Kaczmarek, L. K. (2012). Regulation of neuronal excitability by interaction of fragile X mental retardation protein with slack potassium channels. *J Neurosci*, 32(44), 15318-15327. <https://doi.org/10.1523/JNEUROSCI.2162-12.2012>
- Zhou, X. B., Arntz, C., Kamm, S., Motejlek, K., Sausbier, U., Wang, G. X., Ruth, P., & Korth, M. (2001). A molecular switch for specific stimulation of the BKCa channel by cGMP and cAMP kinase. *J Biol Chem*, 276(46), 43239-43245. <https://doi.org/10.1074/jbc.M104202200>

- Zhou, X. B., Wulfsen, I., Utku, E., Sausbier, U., Sausbier, M., Wieland, T., Ruth, P., & Korth, M. (2010). Dual role of protein kinase C on BK channel regulation. *Proc Natl Acad Sci U S A*, *107*(17), 8005-8010. <https://doi.org/10.1073/pnas.0912029107>
- Zhu, J. J., Esteban, J. A., Hayashi, Y., & Malinow, R. (2000). Postnatal synaptic potentiation: delivery of GluR4-containing AMPA receptors by spontaneous activity. *Nat Neurosci*, *3*(11), 1098-1106. <https://doi.org/10.1038/80614>
- Zhuo, M., Hu, Y., Schultz, C., Kandel, E. R., & Hawkins, R. D. (1994). Role of guanylyl cyclase and cGMP-dependent protein kinase in long-term potentiation. *Nature*, *368*(6472), 635-639. <https://doi.org/10.1038/368635a0>
- Zoghbi, H. Y., & Bear, M. F. (2012). Synaptic dysfunction in neurodevelopmental disorders associated with autism and intellectual disabilities. *Cold Spring Harb Perspect Biol*, *4*(3). <https://doi.org/10.1101/cshperspect.a009886>



## 9. Supplemental Tables

Table 3: Values and statistics for Figure 8

Panel					
B	<b>genotype</b>	<b>relative expression</b>	<b>n</b>	<b>statistics</b>	<b>p</b>
	CTRL	0.258 ± 0.015	3	unpaired t-test	0.045 vs. CTRL
	cKO	0.200 ± 0.014	3		

Table 4: Values and statistics for Figure 9

Panel							
A	<b>genotype</b>	<b>interval (min)</b>	<b>time in center (%)</b>	<b>n</b>	<b>statistics</b>	<b>p</b>	
	CTRL	0 - 5	16.568 ± 1.759	14	F <sub>1,78</sub> = 0.23 p = 0.87		
		5 - 25	17.674 ± 2.848	14			
		0 - 30	17.491 ± 2.425	14			
	cKO	0 - 5	13.092 ± 1.720	14			0.53 vs. CTRL
		5 - 25	19.445 ± 1.469	14			0.90 vs. CTRL
		0 - 30	18.373 ± 1.347	14			0.99 vs. CTRL
	B	<b>genotype</b>	<b>latency 1<sup>st</sup> entry to border (s)</b>	<b>n</b>	<b>statistics</b>	<b>p</b>	
		CTRL	17.49 ± 2.42	8	unpaired t-test	0.80 vs. CTRL	
cKO		18.37 ± 1.35	8				
C	<b>genotype</b>	<b>interval (min)</b>	<b>time in rest (%)</b>	<b>n</b>	<b>statistics</b>	<b>p</b>	
	CTRL	0 - 5	12.494 ± 2.360	14	F <sub>1,27</sub> = 2.029 p = 0.17		
		5 - 25	23.756 ± 2.840	14			
		0 - 30	22.050 ± 2.693	14			
	cKO	0 - 5	10.400 ± 1.248	15			0.83 vs. CTRL
		5 - 25	18.572 ± 1.890	15			0.37 vs. CTRL
		0 - 30	17.584 ± 1.840	15			0.46 vs. CTRL
	D	<b>genotype</b>	<b>interval (min)</b>	<b>distance (m)</b>	<b>n</b>	<b>statistics</b>	<b>p</b>
		CTRL	0 - 5	34.365 ± 2.255	14	F <sub>1,27</sub> = 2.221 p = 0.15	
5 - 25			138.673 ± 10.014	14			
0 - 30			173.038 ± 12.024	14			
cKO		0 - 5	35.191 ± 2.515	15			0.99 vs. CTRL
		5 - 25	163.679 ± 11.352	15			0.30 vs. CTRL
		0 - 30	198.870 ± 12.429	15			0.38 vs. CTRL
E		<b>genotype</b>	<b>interval (min)</b>	<b>rearings</b>	<b>n</b>	<b>statistics</b>	<b>p</b>
		CTRL	0 - 5	12.643 ± 2.422	14	F <sub>1,81</sub> = 1.863 p = 0.18	
	5 - 25		38.714 ± 5.543	14			
	0 - 30		51.357 ± 7.779	14			
	cKO	0 - 5	8.400 ± 1.298	15			0.87 vs. CTRL
		5 - 25	35.667 ± 2.939	15			0.95 vs. CTRL
		0 - 30	44.067 ± 3.427	15			0.56 vs. CTRL
	F	<b>genotype</b>	<b>interval (min)</b>	<b>mean speed</b>	<b>n</b>	<b>statistics</b>	<b>p</b>
		CTRL	0 - 5	11.454 ± 0.751	14	F <sub>1,81</sub> = 3.831 p = 0.05	
5 - 25			9.245 ± 0.667	14			
0 - 30			9.614 ± 0.668	14			
cKO		0 - 5	11.729 ± 0.838	15			0.99 vs. CTRL
		5 - 25	10.970 ± 0.735	15			0.26 vs. CTRL
		0 - 30	11.101 ± 0.671	15			0.39 vs. CTRL

**Table 5: Values and statistics for Figure 10**

Panel	genotype	beam	falls per trial	n	statistics	p
A	CTRL	28 mm square	0.133 ± 0.077	15	F <sub>1,168</sub> = 0.08 p = 0.77	
		12 mm square	0.100 ± 0.053	15		
		5 mm square	0.133 ± 0.059	15		
		28 mm round	0.100 ± 0.053	15		
		17 mm round	0.167 ± 0.080	15		
		11 mm round	0.167 ± 0.080	15		
	cKO	28 mm square	0.333 ± 0.105	15		0.1902 vs. CTRL
		12 mm square	0.033 ± 0.033	15		0.9799 vs. CTRL
		5 mm square	0.067 ± 0.045	15		0.9799 vs. CTRL
		28 mm round	0.067 ± 0.045	15		0.9795 vs. CTRL
		17 mm round	0.100 ± 0.053	15		0.9799 vs. CTRL
		11 mm round	0.133 ± 0.077	15		0.9995 vs. CTRL
B	CTRL	28 mm square	0.125 ± 0.049	12	F <sub>1,124</sub> = 0.08 p = 0.77	
		12 mm square	0.271 ± 0.072	12		
		5 mm square	0.477 ± 0.086	11		
		28 mm round	0.146 ± 0.048	12		
		17 mm round	0.325 ± 0.175	10		
		11 mm round	0.600 ± 0.163	10		
	cKO	28 mm square	0.031 ± 0.031	8		0.9911 vs. CTRL
		12 mm square	0.304 ± 0.079	14		0.9999 vs. CTRL
		5 mm square	1.038 ± 0.157	13		0.0005 vs. CTRL
		28 mm round	0.096 ± 0.035	13		0.9995 vs. CTRL
		17 mm round	0.125 ± 0.056	10		0.7140 vs. CTRL
		11 mm round	0.250 ± 0.112	11		0.1107 vs. CTRL
C	CTRL	28 mm square	15.098 ± 2.494	12	F <sub>1,136</sub> = 1.442 p = 0.23	
		12 mm square	9.470 ± 1.733	12		
		5 mm square	13.529 ± 2.109	14		
		28 mm round	12.253 ± 2.697	12		
		17 mm round	8.861 ± 1.492	13		
		11 mm round	9.529 ± 2.142	10		
	cKO	28 mm square	11.343 ± 4.081	12		0.7842 vs. CTRL
		12 mm square	8.254 ± 1.085	14		0.9990 vs. CTRL
		5 mm square	13.719 ± 1.965	13		0.9999 vs. CTRL
		28 mm round	8.898 ± 1.811	13		0.8477 vs. CTRL
		17 mm round	6.274 ± 1.034	12		0.9504 vs. CTRL
		11 mm round	11.267 ± 1.770	11		0.9959 vs. CTRL
D	CTRL	square	0.144 ± 0.038	15	F <sub>1,354</sub> = 0.14 p = 0.70	
		round	0.100 ± 0.051	15		
		square & round	0.122 ± 0.030	15		
	cKO	square	0.144 ± 0.048	15		0.98 vs. CTRL
		round	0.100 ± 0.048	15		0.84 vs. CTRL
		square & round	0.122 ± 0.032	15		0.997 vs. CTRL

<b>E</b>	<b>genotype</b>	<b>beam</b>	<b>latency per trial</b>	<b>n</b>	<b>statistics</b>	<b>p</b>
	CTRL	square	12.321 ± 1.517	14	F <sub>1,290</sub> = 2.88 p = 0.09	
		round	9.601 ± 1.008	13		
		square & round	11.073 ± 0.937	14		
	cKO	square	10.826 ± 1.751	14		0.77 vs. CTRL
		round	8.631 ± 0.795	13		0.93 vs. CTRL
		square & round	9.690 ± 0.947	14		0.81 vs. CTRL

<b>F</b>	<b>genotype</b>	<b>beam</b>	<b>slips per trial</b>	<b>n</b>	<b>statistics</b>	<b>p</b>
	CTRL	square	0.281 ± 0.038	12	F <sub>1,180</sub> = 0.18 p = 0.68	
		round	0.306 ± 0.082	12		
		square & round	0.302 ± 0.046	12		
	cKO	square	0.539 ± 0.082	14		0.0092 vs. CTRL
		round	0.147 ± 0.041	13		0.19 vs. CTRL
		square & round	0.353 ± 0.047	14		0.91 vs. CTRL

**Table 6: Values and statistics for Figure 11**

<b>Panel</b>	<b>genotype</b>	<b>days of training</b>	<b>latency (s)</b>	<b>n</b>	<b>statistics</b>	<b>p</b>
<b>A</b>	CTRL	<b>1</b>	52.408 ± 1.795	20	F <sub>1,234</sub> = 16.74 p < 0.001	
	cKO		54.171 ± 2.032	21		0.0017 vs. CTRL
	CTRL	<b>2</b>	21.833 ± 2.246	20		
	cKO		30.868 ± 3.281	21		0.03 vs. CTRL
	CTRL	<b>3</b>	16.804 ± 2.025	20		
	cKO		23.382 ± 3.116	21		0.09 vs. CTRL
	CTRL	<b>4</b>	11.351 ± 1.244	20		
	cKO		18.178 ± 2.522	21		0.02 vs. CTRL
	CTRL	<b>5</b>	9.019 ± 0.651	20		
	cKO		13.352 ± 1.831	21		0.03 vs. CTRL
	CTRL	<b>Probe</b>	9.919 ± 1.124	20		
	cKO		12.846 ± 2.796	21		0.57 vs. CTRL

<b>B</b>	<b>genotype</b>	<b>quadrant</b>	<b>latency (s)</b>	<b>n</b>	<b>statistics</b>	<b>p</b>
	CTRL	<b>NE</b>	38.907 ± 2.630	20	F <sub>1,156</sub> = 0.03 p < 0.85	
	cKO		30.825 ± 1.875	21		0.047 vs. CTRL
	CTRL	<b>NW</b>	19.754 ± 1.617	20		
	cKO		20.841 ± 1.701	21		
	CTRL	<b>SW</b>	15.864 ± 1.527	20		0.03 vs. CTRL
	cKO		22.389 ± 1.669	21		
	CTRL	<b>SE</b>	21.411 ± 2.294	20		
	cKO		22.879 ± 1.827	21		

<b>C</b>	<b>genotype</b>	<b>latency (s)</b>	<b>n</b>	<b>statistics</b>	<b>p</b>
	CTRL	11.98 ± 1.454	20	Mann-Whitney test	
	cKO	14.81 ± 3.271	21		0.8614 vs. CTRL
	<b>genotype</b>	<b>target crossings</b>	<b>n</b>	<b>statistics</b>	<b>p</b>
	CTRL	4.650 ± 0.5159	20	Mann-Whitney test	
	cKO	3.571 ± 0.5051	21		0.1218 vs. CTRL
	<b>genotype</b>	<b>thigmotaxis (%)</b>	<b>n</b>	<b>statistics</b>	<b>p</b>
	CTRL	2.617 ± 0.7422	20	Mann-Whitney test	
	cKO	3.509 ± 0.9292	21		0.3685 vs. CTRL

Panel						
<b>E</b>	<b>genotype</b>	<b>days of training</b>	<b>latency (s)</b>	<b>n</b>	<b>statistics</b>	<b>p</b>
	CTRL	<b>7</b>	19.87 ± 2.24	20	$F_{1,241} = 1.250$  $p = 0.2648$	
	cKO		24.09 ± 2.69	21		0.8095 vs. CTRL
	CTRL	<b>8</b>	15.42 ± 1.66	20		
	cKO		15.58 ± 2.05	21		0.9999 vs. CTRL
	CTRL	<b>9</b>	14.45 ± 2.25	20		
	cKO		17.13 ± 2.85	21		0.9742 vs. CTRL
	CTRL	<b>10</b>	14.43 ± 2.36	20		
	cKO		16.10 ± 2.16	21		0.9979 vs. CTRL
	CTRL	<b>11</b>	13.20 ± 2.58	20		
	cKO		14.72 ± 2.14	21		0.9988 vs. CTRL
	CTRL	<b>Probe</b>	14.50 ± 3.04	20		
cKO	13.97 ± 3.04		21	0.9999 vs. CTRL		
<b>F</b>	<b>genotype</b>	<b>quadrant</b>	<b>latency (s)</b>	<b>n</b>	<b>statistics</b>	<b>p</b>
	CTRL	<b>NE</b>	13.90 ± 1.66	20	$F_{1,39} = 0.00$  $p = 0.98$	
	cKO		16.69 ± 2.41	21		
	CTRL	<b>NW</b>	20.32 ± 1.85	20		
	cKO		20.53 ± 1.68	21		
	CTRL	<b>SW</b>	31.74 ± 2.75	20		
	cKO		27.77 ± 2.56	21		<0.001 vs. CTRL NE
	CTRL	<b>SE</b>	25.93 ± 3.01	20		
cKO	26.80 ± 2.96		21	0.02 vs. cKO NE		
<b>G</b>	<b>genotype</b>	<b>latency (s)</b>	<b>n</b>	<b>statistics</b>	<b>p</b>	
	CTRL	10.64 ± 1.259	20	Student's T-test		
	cKO	9.913 ± 1.068	21		0.6607 vs. CTRL	
	<b>genotype</b>	<b>target crossings</b>	<b>n</b>	<b>statistics</b>	<b>p</b>	
	CTRL	4.450 ± 0.4615	20	Student's T-test		
	cKO	4.333 ± 0.5133	21		0.8671 vs. CTRL	
	<b>genotype</b>	<b>thigmotaxis (%)</b>	<b>n</b>	<b>statistics</b>	<b>p</b>	
CTRL	2.802 ± 0.7619	20	Mann-Whitney test			
cKO	3.610 ± 0.9051	21		0.2793 vs. CTRL		

**Table 7: Values and statistics for Figure 12**

Panel	genotype	interval (min)	time in center (%)	n	statistics	p
<b>A</b>	CTRL	0 - 5	9.986 ± 1.041	10	F <sub>1,39</sub> = 0.251  p = 0.62	
		5 - 25	9.580 ± 1.584	10		
		0 - 30	9.647 ± 1.434	10		
	cKO	0 - 5	12.274 ± 1.463	5		0.65 vs. CTRL
		5 - 25	9.142 ± 1.143	5		0.99 vs. CTRL
		0 - 30	9.660 ± 1.045	5		0.99 vs. CTRL
<b>B</b>	genotype	latency 1 <sup>st</sup> entry to border (s)	n	statistics	p	
	CTRL	4.26 ± 1.350	10	unpaired t-test		
	cKO	7.042 ± 2.658	5		0.31 vs. CTRL	
<b>C</b>	CTRL	0 - 5	18.539 ± 1.30	10	F <sub>1,39</sub> = 0.841  p = 0.3645	
		5 - 25	37.252 ± 2.77	10		
		0 - 30	34.136 ± 2.38	10		
	cKO	0 - 5	18.612 ± 3.58	5		0.99 vs. CTRL
		5 - 25	33.988 ± 2.13	5		0.77 vs. CTRL
		0 - 30	31.422 ± 2.20	5		0.85 vs. CTRL
<b>D</b>	CTRL	0 - 5	34,04446 ± 1.73	10	F <sub>1,39</sub> = 3.5  p = 0.0677	
		5 - 25	108,161 ± 6.97	10		
		0 - 30	142,2055 ± 8.33	10		
	cKO	0 - 5	37,1106 ± 3.89	5		0.99 vs. CTRL
		5 - 25	123,1425 ± 9.85	5		0.46 vs. CTRL
		0 - 30	160,2531 ± 11.96	5		0.30 vs. CTRL
<b>E</b>	CTRL	0 - 5	12.643 ± 2.422	10	F <sub>1,81</sub> = 1.863  p = 0.18	
		5 - 25	38.714 ± 5.543	10		
		0 - 30	51.357 ± 7.779	10		
	cKO	0 - 5	8.400 ± 1.298	5		0.87 vs. CTRL
		5 - 25	35.667 ± 2.939	5		0.95 vs. CTRL
		0 - 30	44.067 ± 3.427	5		0.56 vs. CTRL
<b>F</b>	CTRL	0 - 5	11.35 ± 0.58	10	F <sub>1,13</sub> = 3.464  p = 0.09	
		5 - 25	6.41 ± 0.43	10		
		0 - 30	7.07 ± 0.43	10		
	cKO	0 - 5	12.37 ± 1.30	5		0.88 vs. CTRL
		5 - 25	8.21 ± 0.66	5		0.15 vs. CTRL
		0 - 30	8.90 ± 0.67	5		0.15 vs. CTRL

**Table 8: Values and statistics for Figure 13**

Panel	genotype	beam	falls per trial	n	statistics	p
A	CTRL	28 mm square	0.05 ± 0.05	11	F <sub>1,78</sub> = 0.544 p = 0.46	
		12 mm square	0.09 ± 0.06	11		
		5 mm square	0.05 ± 0.05	11		
		28 mm round	0.05 ± 0.05	11		
		17 mm round	0 ± 0	11		
		11 mm round	0 ± 0	11		
	cKO	28 mm square	0.25 ± 0.14	4		0.0835 vs. CTRL
		12 mm square	0.13 ± 0.13	4		0.9989 vs. CTRL
		5 mm square	0 ± 0	4		0.9945 vs. CTRL
		28 mm round	0 ± 0	4		0.9945 vs. CTRL
		17 mm round	0 ± 0	4		>0.9999 vs. CTRL
		11 mm round	0 ± 0	4		>0.9999 vs. CTRL
	B	CTRL	28 mm square	0.05 ± 0.05		11
12 mm square			0.05 ± 0.05	11		
5 mm square			1.05 ± 0.26	11		
28 mm round			0.05 ± 0.05	11		
17 mm round			0.18 ± 0.08	11		
11 mm round			0.32 ± 0.15	11		
cKO		28 mm square	0 ± 0	4	>0.9999 vs. CTRL	
		12 mm square	0.25 ± 0.14	4	0.9551 vs. CTRL	
		5 mm square	0.63 ± 0.24	4	0.426 vs. CTRL	
		28 mm round	0.30 ± 0.20	4	0.838 vs. CTRL	
		17 mm round	0 ± 0	4	0.9626 vs. CTRL	
		11 mm round	0.90 ± 0.24	4	0.0674 vs. CTRL	
C		CTRL	28 mm square	12.00 ± 1.88	11	F <sub>1,78</sub> = 3.778 p = 0.06
	12 mm square		6.77 ± 1.30	10		
	5 mm square		10.82 ± 1.76	10		
	28 mm round		12.50 ± 2.32	11		
	17 mm round		6.51 ± 1.14	11		
	11 mm round		8.15 ± 1.32	11		
	cKO	28 mm square	6.12 ± 1.44	4	0.2983 vs. CTRL	
		12 mm square	4.76 ± 1.23	4	0.9873 vs. CTRL	
		5 mm square	9.99 ± 1.68	5	0.9999 vs. CTRL	
		28 mm round	9.60 ± 2.40	5	0.8885 vs. CTRL	
		17 mm round	3.48 ± 0.67	3	0.9405 vs. CTRL	
		11 mm round	8.46 ± 2.86	5	>0.9999 vs. CTRL	
	D	CTRL	square	0.061 ± 0.029	11	
round			0.015 ± 0.015	11		
square & round			0.038 ± 0.016	11		
cKO		square	0.125 ± 0.065	4	0.45 vs. CTRL	
		round	0.000 ± 0.000	4	0.98 vs. CTRL	
		square & round	0.063 ± 0.034	4	0.85 vs. CTRL	

<b>E</b>	<b>genotype</b>	<b>beam</b>	<b>latency per trial</b>	<b>n</b>	<b>statistics</b>	<b>p</b>
	CTRL	square	9.931 ± 1.022	11	F <sub>1,174</sub> = 2.88 p = 0.09	
		round	9.053 ± 1.038	11		
		square & round	9.48 ± 0.725	11		
	cKO	square	7.189 ± 1.034	4		0.35 vs. CTRL
		round	7.751 ± 1.510	4		0.85 vs. CTRL
		square & round	7.470 ± 0.898	4		0.32 vs. CTRL

<b>F</b>	<b>genotype</b>	<b>beam</b>	<b>slips per trial</b>	<b>n</b>	<b>statistics</b>	<b>p</b>
	CTRL	square	0.379 ± 0.119	11	F <sub>1,180</sub> = 0.56 p = 0.46	
		round	0.182 ± 0.061	11		
		square & round	0.280 ± 0.068	11		
	cKO	square	0.292 ± 0.114	4		0.95 vs. CTRL
		round	0.400 ± 0.140	4		0.46 vs. CTRL
		square & round	0.352 ± 0.092	4		0.91 vs. CTRL

**Table 9: Values and statistics for Figure 14**

<b>Panel</b>	<b>genotype</b>	<b>days of training</b>	<b>latency (s)</b>	<b>n</b>	<b>statistics</b>	<b>p</b>
<b>A</b>	CTRL	<b>1</b>	52.76 ± 2.87	14	F <sub>1,128</sub> = 2.116 p = 0.1482	
	cKO		55.33 ± 1.66	16		
	CTRL	<b>2</b>	43.28 ± 2.55	14		
	cKO		37.61 ± 3.00	15		
	CTRL	<b>3</b>	35.36 ± 3.75	11		
	cKO		28.14 ± 4.47	13		
	CTRL	<b>4</b>	29.82 ± 4.76	11		
	cKO		26.52 ± 3.91	15		
	CTRL	<b>5</b>	24.74 ± 4.19	13		
	cKO		22.54 ± 3.03	16		

<b>B</b>	<b>genotype</b>	<b>quadrant</b>	<b>latency (s)</b>	<b>n</b>	<b>statistics</b>	<b>p</b>
	CTRL	<b>NE</b>	34.77 ± 4.10	14	F <sub>1,156</sub> = 0.03 p = 0.85	
	cKO		33.40 ± 4.07	16		
	CTRL	<b>NW</b>	26.77 ± 3.17	14		
	cKO		23.30 ± 3.23	16		
	CTRL	<b>SW</b>	16.65 ± 1.97	14		0.0007 vs. CTRL NE
	cKO		18.24 ± 1.96	16		0.0032 vs. cKO NE
	CTRL	<b>SE</b>	20.11 ± 2.86	14		
	cKO		22.67 ± 2.68	16		

<b>C</b>	<b>genotype</b>	<b>latency (s)</b>	<b>n</b>	<b>statistics</b>	<b>p</b>
	CTRL	27.73 ± 5.199	13	Student's t-test	
	cKO	26.92 ± 4.744	15		0.9091 vs. CTRL
	<b>genotype</b>	<b>target crossings</b>	<b>n</b>	<b>statistics</b>	<b>p</b>
	CTRL	1.071 ± 0.1951	14	Student's t-test	
	cKO	1.438 ± 0.2410	16		0.2563 vs. CTRL
	<b>genotype</b>	<b>thigmotaxis (%)</b>	<b>n</b>	<b>statistics</b>	<b>p</b>
CTRL	6.086 ± 1.623	14	Mann-Whitney test		
cKO	11.24 ± 5.328	14		0.5021 vs. CTRL	

Panel						
<b>E</b>	<b>genotype</b>	<b>days of training</b>	<b>latency (s)</b>	<b>n</b>	<b>statistics</b>	<b>p</b>
	CTRL	<b>7</b>	35.31 ± 4.33	13	F <sub>1,132</sub> = 0.075 p = 0.7844	
	cKO		25.99 ± 3.90	15		0.3063 vs. CTRL
	CTRL	<b>8</b>	26.65 ± 3.67	14		
	cKO		29.22 ± 5.34	14		0.9916 vs. CTRL
	CTRL	<b>9</b>	19.95 ± 2.82	14		
	cKO		20.82 ± 3.54	15		0.9999 vs. CTRL
	CTRL	<b>10</b>	18.18 ± 2.11	14		
	cKO		23.43 ± 3.61	15		0.8280 vs. CTRL
	CTRL	<b>11</b>	17.43 ± 2.69	14		
	cKO		21.17 ± 2.72	14		0.9563 vs. CTRL
<b>F</b>	<b>genotype</b>	<b>quadrant</b>	<b>latency (s)</b>	<b>n</b>		<b>statistics</b>
	CTRL	<b>NE</b>	24.54 ± 1.50	13	F <sub>1,108</sub> = 0.00 p = 0.95	
	cKO		25.58 ± 2.06	16		
	CTRL	<b>NW</b>	22.34 ± 1.54	13		
	cKO		20.90 ± 1.23	16		
	CTRL	<b>SW</b>	26.66 ± 1.96	12		
	cKO		28.11 ± 1.85	16		
	CTRL	<b>SE</b>	23.28 ± 2.03	14		
	cKO		22.57 ± 2.01	16		
	<b>G</b>	<b>genotype</b>	<b>latency (s)</b>	<b>n</b>		<b>statistics</b>
CTRL		18.53 ± 2.90	13	Student's T-test		
cKO		22.53 ± 4.81	15		0.5183 vs. CTRL	
<b>genotype</b>		<b>target crossings</b>	<b>n</b>	<b>statistics</b>	<b>p</b>	
CTRL		1.50 ± 29	14	Student's T-test		
cKO		1.88 ± 0.29	16		0.37 vs. CTRL	
<b>genotype</b>		<b>thigmotaxis (%)</b>	<b>n</b>	<b>statistics</b>	<b>p</b>	
CTRL		6.85 ± 3.51	14	Mann-Whitney test		
cKO		10.44 ± 5.70	16		0.59 vs. CTRL	

**Table 10: Values and statistics for Figure 15**

Panel								
A	genotype	minute	falls per trial	n	statistics	p		
CTRL		46	136.53 ± 8.24	7	F <sub>1,195</sub> = 83.31 p < 0.0001			
		47	136.71 ± 8.34	7				
		48	137.28 ± 7.91	7				
		49	136.19 ± 6.98	7				
		50	142.11 ± 7.47	7				
		51	139.29 ± 8.18	7				
		52	139.10 ± 8.20	7				
		53	139.12 ± 8.40	7				
		54	141.38 ± 9.30	7				
		55	139.55 ± 8.56	7				
		56	137.92 ± 8.99	7				
		57	138.13 ± 9.48	7				
		58	136.73 ± 8.41	7				
		59	138.85 ± 7.88	7				
		60	140.37 ± 9.07	7				
	cKO	genotype	minute	slips per trial		n		p
			46	111.48 ± 7.46		8		0.48 vs. CTRL
			47	111.49 ± 8.63		8		0.47 vs. CTRL
			48	114.38 ± 9.07		8		0.63 vs. CTRL
			49	107.48 ± 8.04		8		0.27 vs. CTRL
		50	110.71 ± 9.04	8		0.16 vs. CTRL		
		51	108.58 ± 8.13	8		0.18 vs. CTRL		
		52	113.37 ± 7.85	8		0.44 vs. CTRL		
		53	110.54 ± 7.53	8		0.27 vs. CTRL		
		54	107.94 ± 7.72	8		0.10 vs. CTRL		
		55	107.69 ± 8.71	8		0.14 vs. CTRL		
		56	106.44 ± 8.95	8		0.16 vs. CTRL		
		57	111.54 ± 9.94	8		0.38 vs. CTRL		
		58	108.70 ± 10.18	8		0.30 vs. CTRL		
	59	107.01 ± 9.79	8		0.14 vs. CTRL			
	60	107.39 ± 10.77	8		0.11 vs. CTRL			

<b>B</b>	<b>genotype</b>	<b>minute</b>	<b>falls per trial</b>	<b>n</b>	<b>statistics</b>	<b>p</b>	
	CTRL	46	207.88 ± 33.66	10	F <sub>1,276</sub> = 72.41 p < 0.0001		
		47	202.98 ± 36.15	10			
		48	207.69 ± 35.63	10			
		49	212.27 ± 34.45	10			
		50	199.19 ± 35.28	10			
		51	213.81 ± 34.14	10			
		52	213.16 ± 35.40	10			
		53	217.47 ± 37.06	10			
		54	208.78 ± 34.57	10			
		55	203.02 ± 29.18	10			
		56	204.03 ± 31.57	9			
	57	205.93 ± 29.57	10				
	58	200.95 ± 27.38	10				
	59	205.21 ± 27.17	10				
	60	222.03 ± 34.65	8				
	cKO	46	140.32 ± 9.43	10			0.55 vs. CTRL
		47	139.34 ± 8.48	10			0.65 vs. CTRL
		48	135.12 ± 9.45	10			0.43 vs. CTRL
		49	139.36 ± 9.07	10			0.42 vs. CTRL
		50	137.62 ± 9.39	10			0.70 vs. CTRL
51		131.86 ± 10.83	10		0.24 vs. CTRL		
52		141.63 ± 9.50	10		0.45 vs. CTRL		
53		132.30 ± 9.93	10		0.19 vs. CTRL		
54		124.69 ± 9.34	10		0.21 vs. CTRL		
55		124.82 ± 6.57	10		0.31 vs. CTRL		
56		135.59 ± 4.92	10		0.57 vs. CTRL		
57	135.36 ± 10.65	10		0.48 vs. CTRL			
58	129.75 ± 12.93	10		0.46 vs. CTRL			
59	135.38 ± 12.44	10		0.49 vs. CTRL			
60	133.95 ± 11.09	10		0.22 vs. CTRL			

<b>C</b>	<b>genotype</b>	<b>interstimulus interval (ms)</b>	<b>paired-pulse ratio</b>	<b>n</b>	<b>statistics</b>	<b>p</b>
	CTRL	10	0.98 ± 0.05	6	F <sub>1,60</sub> = 0.05 p = 0.81	
		20	1.29 ± 0.10	6		
		50	1.21 ± 0.07	6		
		100	1.30 ± 0.06	6		
		200	1.17 ± 0.06	6		
		500	1.00 ± 0.07	6		
	cKO	10	0.98 ± 0.13	6		>0.9999 vs. CTRL
		20	1.03 ± 0.12	6		0.2666 vs. CTRL
		50	1.20 ± 0.10	6		>0.9999 vs. CTRL
		100	1.27 ± 0.13	6		>0.9999 vs. CTRL
		200	1.28 ± 0.08	6		0.9601 vs. CTRL
		500	1.13 ± 0.06	6		0.9223 vs. CTRL

D	genotype	stimulation ( $\mu$ A)	paired-pulse ratio	n	statistics	p	
	CTRL	25	$0,00 \pm 0,01$	8	$F_{1,90} = 1,35$ $p = 0,25$		
		50	$-0,15 \pm 0,03$	8			
		75	$-0,37 \pm 0,10$	8			
		100	$-0,54 \pm 0,15$	8			
		125	$-0,68 \pm 0,19$	8			
		150	$-0,83 \pm 0,23$	8			
	cKO	25	$-0,01 \pm 0,00$	9			0,9806 vs. CTRL
		50	$-0,10 \pm 0,02$	9			0,9806 vs. CTRL
		75	$-0,26 \pm 0,04$	9			0,9806 vs. CTRL
		100	$-0,44 \pm 0,06$	9			0,9806 vs. CTRL
		125	$-0,59 \pm 0,10$	9			0,9806 vs. CTRL
		150	$-0,73 \pm 0,12$	9			0,9806 vs. CTRL

Table 11: Values and statistics for Figure 16

Panel	genotype	protein	relative expression	n	statistics	p
A	CTRL	GluA1	$0,79 \pm 0,16$	3	Student's t-test	0,9257 vs. CTRL
	cKO		$0,81 \pm 0,11$	3		
	CTRL	GluA2	$0,59 \pm 0,20$	3	Student's t-test	0,6512 vs. CTRL
	cKO		$0,50 \pm 0,04$	3		
	CTRL	GluN1	$0,14 \pm 0,10$	3	Student's t-test	0,9560 vs. CTRL
	cKO		$0,13 \pm 0,08$	3		
	CTRL	GluN2A	$0,09 \pm 0,04$	3	Student's t-test	0,9204 vs. CTRL
	cKO		$0,08 \pm 0,03$	3		
	CTRL	GluN2B	$0,22 \pm 0,08$	3	Student's t-test	0,6093 vs. CTRL
	cKO		$0,17 \pm 0,06$	3		
B	CTRL	GluA1	$0,45 \pm 0,08$	5	Student's t-test	0,7452 vs. CTRL
	cKO		$0,41 \pm 0,08$	7		
	CTRL	GluN2A	$0,07 \pm 0,01$	5	Student's t-test	0,4550 vs. CTRL
	cKO		$0,10 \pm 0,03$	7		
	CTRL	GluN2B	$0,17 \pm 0,02$	5	Student's t-test	0,5363 vs. CTRL
	cKO		$0,21 \pm 0,05$	7		

**Table 12: Values and statistics for Figure 17**

Panel						
<b>A</b>	genotype	stimulated / unstimulated	pS845 / GluA1	n	statistics	p
	CTRL	unstimulated	1.000 ± 0.223	4	F <sub>1,11</sub> = 31.85	0.0006 vs. unstim. CTRL
	cKO		1.250 ± 0.141	4		
	CTRL	stimulated	4.376 ± 0.772	3	p < 0.0002	0.02 vs. stim. CTRL
	cKO		2.216 ± 0.365	4		
<b>B</b>	genotype	stimulated / unstimulated	pS831 / GluA1	n	statistics	p
	CTRL	unstimulated	1.216 ± 0.170	4	F <sub>1,12</sub> = 0.002	>0.99 vs. unstim. CTRL
	cKO		1.000 ± 0.344	4		
	CTRL	stimulated	1.120 ± 0.363	4	p < 0.97	>0.9999 vs. stim. CTRL
	cKO		1.069 ± 0.334	4		
<b>C</b>	genotype	stimulated / unstimulated	pS845 / GluA1	n	statistics	p
	CTRL x PAX	unstimulated	1.000 ± 0.294	3	F <sub>1,8</sub> = 0.17	0.9972 vs. unstim. CTRL
	cKO x PAX		0.848 ± 0.215	3		
	CTRL x PAX	stimulated	0.827 ± 0.220	3	p < 0.69	0.8649 vs. stim. CTRL
	cKO x PAX		1.218 ± 0.225	3		
<b>D</b>	genotype	stimulated / unstimulated	pS831 / GluA1	n	statistics	p
	CTRL x PAX	unstimulated	1.000 ± 0.700	3	F <sub>1,8</sub> = 0.04	>0.9999 vs. unstim. CTRL
	cKO x PAX		0.962 ± 0.803	3		
	CTRL x PAX	stimulated	0.766 ± 0.452	3	p < 0.86	>0.9999 vs. stim. CTRL
	cKO x PAX		0.953 ± 0.581	3		

**Table 13: Values and statistics for Figure 18**

Panel					
<b>H</b>	condition	R/R <sup>0</sup> <sub>FRET/CFP</sub>	n	statistics	p
	BK <sup>+/+</sup>	0.161 ± 0.021	11	F <sub>4,42</sub> = 4.28	<0.001 vs. BK <sup>+/+</sup>
	BK <sup>-/-</sup>	0.034 ± 0.005	11		<0.001 vs. BK <sup>+/+</sup>
	PAX	0.019 ± 0.005	10		<0.001 vs. BK <sup>+/+</sup>
	AP5	0.080 ± 0.010	9		<0.001 vs. BK <sup>+/+</sup>
	NIFE	0.090 ± 0.008	6		0.002 vs. BK <sup>+/+</sup>
			p < 0.005		

**Table 14: Values and statistics for Figure 19**

Panel						
<b>F</b>	stimulated / unstimulated	cond.	R/R <sup>0</sup> <sub>FRET/CFP</sub>	n	statistics	p
	unstimulated	CTRL	0.6232 ± 0.059	4	F <sub>5,23</sub> = 2.52	p < 0.06
		KO	0 ± 0	4		
		PAX	0.4278 ± 0.027	4		
		AP5	0.2071 ± 0.007	4		
		NIFE	0.3498 ± 0.062	9		
	stimulated	CTRL	1.099 ± 0.111	4	F <sub>9,39</sub> = 2.71	<0.0001 vs. CTRL baseline
		KO	0.3967 ± 0.063	4		<0.0001 vs. CTRL cLTP
		PAX	0.2603 ± 0.016	4		<0.0001 vs. CTRL cLTP
		AP5	0.2089 ± 0.058	3		<0.0001 vs. CTRL cLTP
		NIFE	0.1659 ± 0.014	9		<0.0001 vs. CTRL cLTP

**Table 15: Values and statistics for Figure 20**

Panel	stimulated / unstimulated	cond.	R/R <sup>0</sup>	n	statistics	p
F	BK <sup>+/+</sup>	baseline	1.00 ± 0.00	4		
		cLTP	0.97 ± 0.02	4		
		postcLTP	1.05 ± 0.01	4		
	BK <sup>+/+</sup> + PAX	baseline	1.00 ± 0.00	4		>0.9999 vs. BK <sup>+/+</sup>
		cLTP	0.91 ± 0.03	4		0.1691 vs. BK <sup>+/+</sup>
		postcLTP	0.99 ± 0.04	4		0.1914 vs. BK <sup>+/+</sup>



## 10. Publications and congress contributions

### 10.1. Publications

Cruz Santos M., Birkenfeld L., Pham T., Maier M., Paulus K., Ullemeyer L., Knauer A., Kabagema-Bilan C., Längst N., Offermanns S., Wettschureck N., Roslan A., Gawaz M., Ichinose F., Lukowski R. (202x). Angiotensin II-induced cardiac fibrosis and systolic dysfunction are attenuated by myofibroblast-specific cGKI. **(in preparation)**

Pham T., Hussein T., Calis D., Bischof H., Skrabak D., Cruz Santos M., Maier S., Spähn D., Kalina D., Simonsig, S., Ehinger R., Bernhard G., Knipper M., Plesnila N., Ruth P., Lukowski R., Matt L. (2023). BK channels sustain neuronal  $Ca^{2+}$  oscillations to support hippocampal long-term potentiation and memory formation. *Cell Mol Life Sci*; doi: 10.1007/s00018-023-05016-y

Skrabak D., Bischof H., Pham T., Ruth P., Ehinger R., Matt L., Lukowski R. (2023). Slack  $K^+$  channels limit kainic acid-induced seizure severity by modulating neuronal excitability and firing. *Commun Biol*.; doi: 10.1038/s42003-023-05387-9

Matt L., Pham T., Skrabak D., Hoffmann F., Eckert P., Yin J., Gisevius M., Ehinger R., Bausch A., Ueffing M., Boldt K., Ruth P., Lukowski R. (2021). The  $Na^+$ -activated  $K^+$  channel Slack contributes to synaptic development and plasticity. *Cell Mol Life Sci*; doi: 10.1007/s00018-021-03953-0.

## 10.2. Congress contributions

Pham T., Hussein T., Bischof H., Simonsig S., Kalina D., Ehinger R., Ruth P., Lukowski R., Matt L.: „BK channels sustain neuronal Ca<sup>2+</sup> oscillations to support hippocampal long-term potentiation and memory formation“; Annual meeting of the German Pharmaceutical Society (DPhG), 07.10. – 10.10.2023, Tübingen, Germany

Pham T., Hussein T., Bischof H., Simonsig S., Kalina D., Ehinger R., Ruth P., Lukowski R., Matt L.: „cGKI/BK interactions may be crucial for Schaffer Collateral LTP and hippocampus-dependent memory formation“; 10<sup>th</sup> International Conference on cGMP, 17.06. – 19.06.2022, Augsburg, Germany

Pham T., Bischof H., Hussein T., Simonsig S., Kalina D., Ehinger R., Ruth P., Lukowski R., Matt L.: „Postsynaptic BK contributes critically to Schaffer collateral LTP and promotes hippocampus dependent memory formation“; CanCaN2021 – International Conference organized by the trainees of the RTG 2381, 17.11. – 19.11.2021, Tübingen, Germany

Pham T., Bischof H., Simonsig S., Kalina D., Ehinger R., Ruth P., Lukowski R., Matt L.: „Postsynaptic BK is crucial for Schaffer collateral LTP and promotes hippocampal memory formation“; Annual meeting of the German Pharmaceutical Society (DPhG), 28.09. – 01.10.2021, Online

**Lesmüller Poster Prize** for best poster in the category “Pharmacology”

Pham T., Bischof H., Simonsig S., Kalina D., Ehinger R., Ruth P., Lukowski R., Matt L.: „Postsynaptic BK channels promote schaffer collateral LTP and hippocampal memory formation in the Morris Water Maze“; 87th Annual Meeting of the German Society for Experimental and Clinical Pharmacology and Toxicology (DGPT), 02. – 05.03.2021, Online

**Award** for best poster in the category “Experimental and Clinical Pharmacology”

Pham T., Cruz Santos M., Roeßing M., Böttcher A., Barresi M., Marchetta P., Gonschorek D., Rodriguez J., Kremser M., Lukowski R., Feil R.: “International PhD Program in Biomedicine. cGMP: From Bedside to Bench (GRK 2381)“; cGMP Forum, Boston, USA, 11/2019

## **11. Curriculum Vitae**



## **12. Acknowledgements**

